# POLITECNICO DI TORINO

Master's degree in Civil Engineering

MASTER'S DEGREE THESIS

# Construction-based optimization criteria for steel trusses


Supervisor:

**Prof. Giuseppe Carlo Marano**

Co-supervisors:

**Dott. Eng. Raffaele Cucuzza**
**Dott. Eng. Gabriele Rosi**

Candidates:

**Antonio Sforza**

**Arianna Zamagna**


---

APRIL 2023 - A.Y. 2022/2023

**Abstract**

In this Thesis, a grouping strategy for the simultaneous size, shape and topology optimization of steel truss structures has been presented. The novelty of our study relies in the definition of the objective function, not intended to a simple weight minimization, but accounting also for constructability issues. More precisely, based on practical and cost considerations, the optimum number of distinct cross-sections used has been sought. We have also addressed the complexity of fabrication and assembly phases, discouraging too much truss's subdivisions. In addition, structural buckling verification has been included in the OF, due to the fact that this kind of instability is the most challenging for trusses.
The dissertation has started from the introduction of the basic concepts of structural optimization techniques, their relevance in civil engineering and the most common target functions tackled. In Chapter 2, we have reported the review of a great number of papers, available in the Literature, concerning structural performance optimizations. In Chapter 3, we have moved to the definition of constructability in civil engineering problems, stressing the importance of early involvement of such considerations in a project. Once the basic theoretical concepts have been explained, in Chapter 4 the main case study has been illustrated, i.e. the one related to the simple truss. At first, a brief introduction to this class of structures has been introduced, highlighting the main features, problems and applications in civil engineering. Then we have also mentioned the power of parametric design technique and the software used to gain such models. Moving towards the core of our case study, an overview of the design variables considered has been listed and described in details. Specifically, CHS profiles, five truss types, heights and number of subdivisions of the truss have been varied at each iteration of the optimization. The dynamic grouping strategy, as well as the assembly of the model have been illustrated. Then, in the Subsection 4.6, the objective function formulation has been finally proposed, with the careful calibration of all the parameters involved. The parametric modelling, the FEM structural analysis and the optimization have been carried out with Rhinoceros plug-ins, Grasshopper, Karamba3D and Octopus, respectively. In Chapter 5, the performance of the proposed objective function has been examined in different conditions, namely the simple size optimization, the combined size and shape ones and

finally accounting also for the topology case. Results have been reported, where the influence of each penalty function has been studied and analyzed with great detail. Once tested the procedure at the truss level, we have moved to a larger scale, studying the case of a single storey industrial building, in Chapter 6. The applicability of our method has been demonstrated for the larger building in order to understand how the theoretic analysis can suit a more practical problem. Once again, the parametric design has been exploited, always in Rhinoceros environment. Now, for a more realistic representation, both gravitational and lateral loadings have been accounted. The additional design variables have been listed and the objective function has been remodeled to fit the new problem. At the end, the numerical results for the size, shape and topology optimization of the industrial building have been reported. In Chapter 7, possible future developments for such analysis have been highlighted to show how the outcomes of our study could stimulate further innovations.

# Contents

# List of Figures

# Chapter 1

# Introduction

Several disciplines, including engineering, science and economy, have been greatly impacted by the advent of optimization techniques. In general terms, optimization is a method aimed at changing an existing process in order to increase the occurrence of favorable outcomes and it is done by finding the best values of the elements, or variables, from the set of available alternatives. In the field of civil engineering, structural optimization based on mathematical computing has gained increasing interest as a way for efficient and sustainable designs, due to the development of many computational tools. Optimization can support civil engineering work in each step of a project life cycle, such as design, construction, operation and maintenance [75]. Moreover, it involves many fields of application, such as transportation, geotechnical as well as hydraulic environments, construction management problems, together with structural ones. In the present Thesis, we are going to focus specifically on this last topic. Structural optimization refers to an optimization that seeks to determine the ideal configuration of structures, or structural elements, to accomplish certain goals, under predetermined conditions. In particular, the most common types of structure being analyzed are trusses and frames, along with shells and bridges. Among others, structural performance is an important topic in the civil optimization field, in fact many researchers have focused their attention at enhancing specific structural skills, such as mechanical behavior, ductility capacity as well as dynamic seismic capability, in order to adapt the structures to various environments. In civil engineering, most of the optimization objectives are related to a minimization of the total cost that, in turn, is related to a minimum weight or volume design. This task is fundamental due to the growth of building material prices. However, many studies have investigated the cost function in more details, with the purpose of considering not only the expense for the elements' material, but also accounting for construction, erection, maintenance and many other factors affecting the overall cost of a structure. Another important topic involving structural optimization is related to the environmental sphere. In fact, due to the enormous quantity of CO2 emissions in the civil engineering sector and the growing focus on environmental issues, sustainability has recently become one of the main goals of structural optimization. The goal is to create structures that are not only efficient in terms of material use and energy consumption but also have a minimal impact on the environment throughout their entire life cycle. This may involve material optimization, thus selecting materials that are renewable, recycled, or have a low environmental impact during their production and disposal, but also energy optimization or life cycle assessment. All these aspects can be explored and analyzed one at a time or can be addressed together in the same optimization procedure.

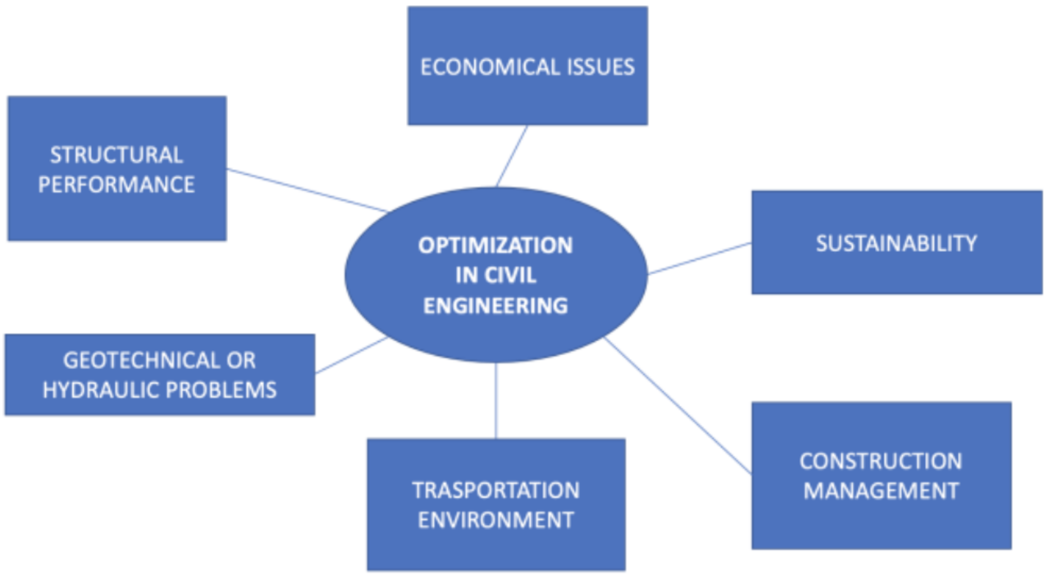


Figure 1.1: Optimazion problems in Civil Engineering

An optimization problem starts with the definition of three main components, namely the Objective Function (OF), the design variables and the constraints. The former one, also called Merit Function, is the quantity that is going to be minimized or maximized by changing the set of design variables. During the procedure, the structure under study has to satisfy some constraints which in general are referred to stresses, displacements, natural frequencies or geometric requirements. They can be in the form of inequalities or equalities, however generally the second ones are converted into the other formulation by means of a tolerance value. For example, $h(\boldsymbol{X}) = 0$ can be transformed in $|h(\boldsymbol{X})| \leq \varepsilon$, where $\varepsilon$ is the small tolerance allowed. In addition, constraints could be combined into the objective function as penalty functions to convert the constrained problem to an unconstrained one. The optimizations, based on the nature of the decision variables, can be classified into discrete or continuous problems. The values of continuous design variables fluctuate within a certain range, while discrete ones can assume only certain values in a finite set of available candidates. When possible, discrete problems are treated as continuous ones and only at the end round-off procedure is performed. The range of design variables is called search space or design space, which could be further divided into feasible and infeasible domains. Therefore, the constraints are limiting the design space, with the so-called "constraint surface". Nevertheless, not all of them contribute to the surface definition, thus they will be divided into active and inactive ones. The general formulation of the optimization can be written as follows 1.1:

$$\begin{aligned} Min \quad or \quad Max &: f(\boldsymbol{X}) \\ subjected \quad to \quad &: g_i(\boldsymbol{X}) \leq 0, \quad i = 1, 2, 3...m \\ &h_j(\boldsymbol{X}) = 0, \quad j = 1, 2, 3...p \\ &\boldsymbol{X} \in S \end{aligned} \tag{1.1}$$

Where $\boldsymbol{X}$ is the vector of the $n$ design variable $\boldsymbol{X}=\{x_1, x_2, ...x_n\}$; $f(\boldsymbol{X})$ is the objective function and $g_i(\boldsymbol{X})$ and $h_j(\boldsymbol{X})$ are the $m$ inequalities and $p$ equality constrains, respectively; and $S$ is the search space of the optimization problem. Moreover, based on the number of objective functions we want to achieve, we can have single-OF or multi-OF problems. Obviously, in multi-objective optimizations all the considered merit functions may not be optimized simultaneously, because they may conflict with each other. In general, we refer to the concept, formulated by Vilfredo Pareto in 1896, of Pareto front that represent the best trade-offs between different objectives. It is a curve that is made by the set of non-dominated solutions, which means that no solution on the curve is better than another in all objectives. So the important property characterizing any point on such curve is not to be dominated by any other. In fact, the points on the Pareto front are optimal in the sense that they cannot be improved in one objective without sacrificing the performance in another goal. Thus, the Pareto front is a powerful tool in multi-objective optimizations, as it allows designers to make informed decisions about the best trade-offs between different objectives. By exploring the Pareto front, designers can identify the optimal solution that meets their design requirements and preferences, and understand the impact and importance of the different objectives. The non-dominated solutions forming the Pareto front can be visualized, for example, using scatter plots. To help decision maker in finding the best solution, we can identify the so-called Utopia point, defined as the ideal point that minimizes all the OFs and it can be found by considering its distance from the front. For example, if we want to minimize two functions, $f_1$ and $f_2$, we can see graphically the Pareto front and Utopia point in the following image 1.2:

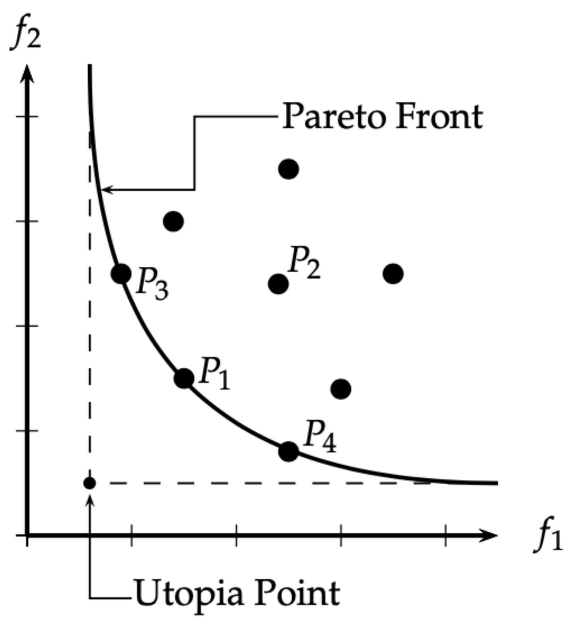


Figure 1.2: Representation of the Pareto optimal front and Utopia point

In the field of structural optimization, three main approaches can be followed to obtain the optimal layout of the considered building:

1. ***Size optimization*** is aimed to find the optimal cross-section of the structural elements, which in general applications are taken from a discrete list of available cross-sections. Typically, this involves finding the smallest possible size that can still meet the required performance specifications, while minimizing weight and material usage.

2. ***Shape optimization***, also called configuration optimization, treats the nodal coordinates of the structure as design variables. By doing so, the distribution of the solicitation is changing accordingly, therefore the optimal structural shape would minimize stress concentrations.

3. ***Topology optimization*** involves the best spatial arrangement of the structural elements and determining the optimal material distribution within a structure. Thus, it focuses on how nodes or joints are connected and supported, deleting unnecessary structural members or material portions.

These three procedures can be also coupled together, generating mixed optimization approaches with combined variables and purposes.

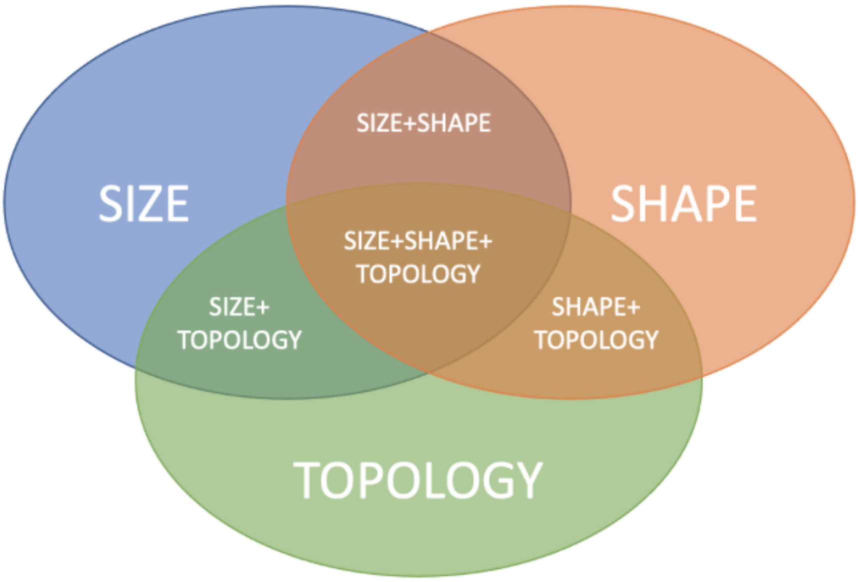


Figure 1.3: General scheme of the different optimization approaches

# Chapter 2

# Paper Review on Structural Performance Optimizations

## 2.1 Algorithms historical excursus

Nowadays, structural optimization problems are solved with the so-called Meta-heuristic algorithms, however they started to appear only from the 1975. The existence of optimization methods can be traced back to the days of Newton, Lagrange and Cauchy. In particular, the development of differential calculus methods of optimization was provided by the studies of Newton and Leibniz, and the fundamentals to the calculus of variations were laid by Bernoulli, Euler, Lagrange and Weistrass. Joseph-Louis Lagrange was also the inventor of the method of optimization for constrained problems, which involve the inclusion of unknown multipliers. Augustine-Louis Cauchy, instead, investigated the solution procedure by direct substitution and made the first application of the steepest descent method to solve unconstrained optimization problems. From the occurrence of the computers, faster implementations of optimization problems were possible, stimulating the interest of many researchers in the developing of improved methods. The classical approaches, now collected in the Operational Research field, can be distinguished into mathematical programming techniques, stochastic methods and statistical approaches. They are also referred as gradient-based or mathematical methods. However, as the optimizers became more and more ambitious, the limitations of these methods resulted to be too constrictive for practical applications. In fact, although these gradient-based algorithms had good performance in some applications, the convergence to the global optimum was difficult to be ensured and the algorithms could be trapped in one local optimum if the initial design and the search direction were not well defined. Moreover, they were quite difficult to be implemented and resulted to be inefficient to handle optimization problems of large structures. To overcome these limitations, heuristic methods were introduced at first, but then they were upgraded to metaheuristic algorithms. Metaheuristics uses strategies to guide the process that are inspired by evolutionary principles, physics phenomena, swarm rules, as well as natural and man-made processes.

### 2.1.1 Metaheuristic Algorithms

The most famous metaheuristic algorithm is for sure the Genetic Algorithm, formulated by J. Holland in 1975 at the University of Michigan, developed and improved further by his student David E. Goldberg. Like the name implies, GA takes inspiration from the genetic field, recalling the survival-of-the-fittest principle of nature. In genetics, the characteristics of an individual are transmitted to the offspring through the chromosomes, which contain a series of information called alleles. The Genotype is the set of such alleles, thus the set of information collected in the chromosomes. The Phenotype, instead, is the observable physical characteristics traduced from the genotype. Based on the Darwin's theory of evolution and natural selection, only the best individuals will evolve in the next generations. Thus, GA tries to mimic this procedure, starting from the initialization phase and then moving towards fitness evaluation, selection, crossover and mutation operators, looped until a convergence criterion is met.

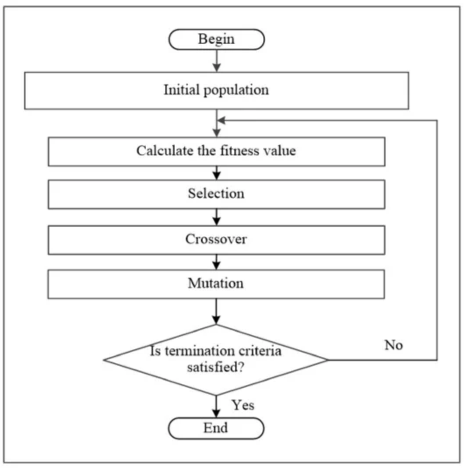


Figure 2.1: Flowchart of the standard genetic algorithm [3]

In the first phase, a population of N individuals is randomly generated, where each individual is coded by strings of binary variables that corresponds to the chromosomes; each bit represents an allele. In particular, the dimension N of the population should be taken at least two or four times the value of the number n of design variables. Then the fitness evaluation is performed on the first population, meaning that the objective function value for each individual is calculated. So, the fitness evaluation measures how well the individual meets the stated objective. Then the selection operator is the phase in which individuals are chosen, based on their fitness value, to generate the members of the next population. There are different selection schemes like "Roulette Wheel Selection", where the probability of being selected is proportional to the fitness value of the individual, "Tournament Selection", where a predefined number of individuals (tournament set) are drawn randomly and only the one with the highest fitness out of the tournament set is selected, and many others which are available in the Literature.

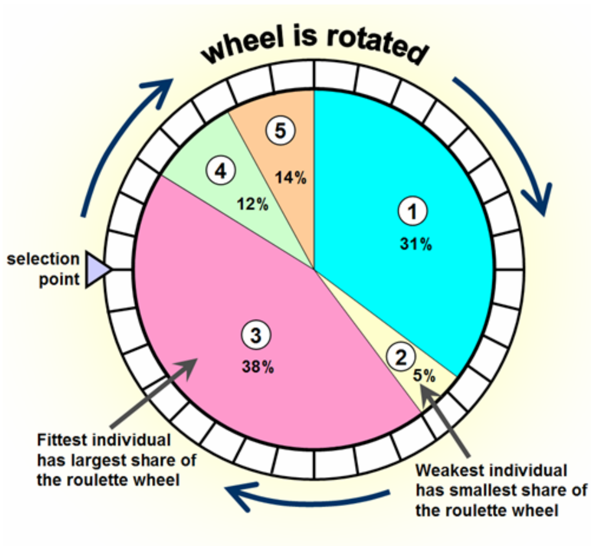


Figure 2.2: Roulette wheel selection

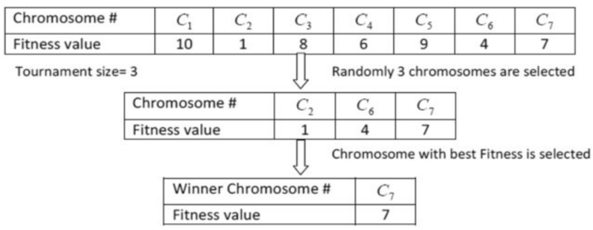


Figure 2.3: Tournament selection [14]

Then from the selected parents the actual reproduction and generation of the offspring is carried out by means of crossover and mutation operators. They are just giving the recombination rules of the information given by the parents to the offspring, preserving integrity, avoiding loss of information and ensuring a little bit of diversity. As for the selection operator, also crossover and mutation can be performed following different techniques.

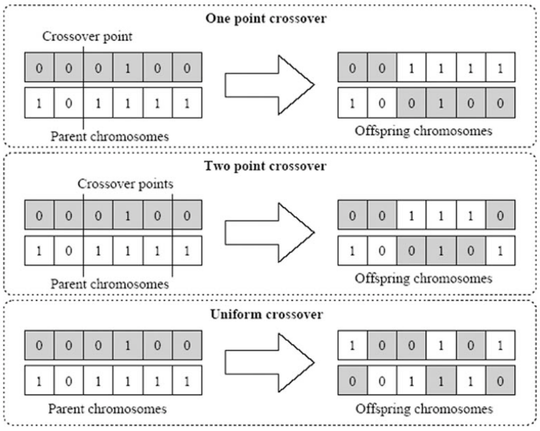


Figure 2.4: Three examples of crossover operator [104]

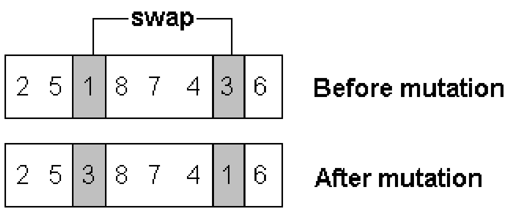


Figure 2.5: Mutation operator example [28]

For example Adeli, Hojjat, and Nai-Tsang Cheng. in [1] have tested different crossover schemes for the weight-minimization of large steel truss structures, namely single-point and double-points crossovers, as well as both 20% and 50%-uniform crossovers. In this research, they have demonstrated not only the efficacy of genetic algorithm in such applications, but also that the best outcomes have been provided by using the 20%-uniform crossover.
Another stimulating application of GA algorithm has been proposed by Cheng, J. in [19]. In this article a steel truss arch bridge has been optimized to achieve the minimum weight, considering the members' cross-sections as both continuous and discrete variables. In particular, the proposed algorithm has integrated the concepts of GA for the optimization and the finite element method (FEM) to compute the value of implicit constraint functions. It has shown that, with respect to traditional design, the optimum configuration found by means of the proposed method can be more than 40% lighter, but that this improvement is limited when using discrete variables instead of continuous ones.
In Literature, there are also GA-based optimizations of multi-objective problems, like the work done by Dhingra, Anoop K., and B. H. Lee. in [26]. Here the optimization of truss structures has been carried out considering single and multi-objective functions, namely maximization of fundamental frequency of vibration, weight minimization and minimization of the deflection of free nodes. In particular, when dealing with multi-OF, the problem has been solved by combining the fitness indices associated with the three objective functions according to the game theoretic bargaining model. The design variables have been chosen as the cross-sectional ar-

eas of the truss's members, to which lower and upper bounds have been applied together with stresses and Euler buckling constraints. The analysis is particularly appealing because the performance of GA algorithm has been compared with both gradient-based SLP and branch-and-bound algorithms, to show the remarkable advancement.
Another interesting example of GA application on multi-OF optimizations has been illustrated by Coello, C. A., and Alan D. Christiansen. in [22]. In this study, min-max optimum technique transformed the multi-objective optimization problem, aimed at the weight, stress and displacement minimizations of truss structures, into several single objective optimizations, easier and faster to be solved.
It is worth mentioning also other powerful metaheuristic algorithms, such as Simulating Annealing, Particle Swarm Optimization, Teaching-Learning-Based, Eagle Strategy, Cuckoo Search, Moth-flame as well as Improved Firework algorithms.
For instance, the Simulated Annealing strategy, introduced by Kirkpatrick et al. in 1983, has been compared with the linearized branch-and-bound method by Balling, Richard J. in [13]. As the name suggests, the algorithm is simulating the annealing procedure. It recalls the ability of a metal that in its cooling phase, after heating, can break out of local minima stages, i.e. glass states, and eventually converge upon the global minimum stage, i.e. pure crystal. In the paper, the applicability of such procedure has been tested on three-dimensional steel frames in a size optimization, aimed at the minimum weight design. From the outputs, the annealing strategy analysis, although slower than the linearized branch-and-bound method, resulted to be more robust.
Kaveh, A., Abbasgholiha, H., in [56] have performed a steel frame optimization using the Big Bang-Big Crunch (BB-BC) algorithm. The minimum weight design has been obtained from the size optimization, while satisfying both serviceability and strength requirements. As regards the BB-BC optimization algorithm, it consists of two steps: a Big Bang, where candidate solutions are randomly distributed over the search space, and a Big Crunch, where a contraction operation estimates a weighted average of the randomly distributed candidate solutions. This method is reconducted and relies on the theories of the evolution of the universe, according to which in the Big Bang phase energy dissipation produces disorder, whereas in the Big Crunch phase, randomly distributed particles are drawn into an order. The BB–BC optimization method similarly generates random points in the Big Bang phase and shrinks these points to a single representative point via a center of mass

in the Big Crunch phase. After several sequential Big Bang and Big Crunch phases, the distribution of randomness within the search space becomes smaller and the algorithm converges to a solution. In the specific paper here reported, four frame structures have been optimized using the BB-BC algorithm, making a comparison between procedures following different codes.

Gandomi, A.H., Talatahari, S., Yang, X.-S., Deb, S., in [34] proposed a novel technique, known as Cuckoo Search (CS), to identify the truss structure designs with the lowest weight. The initial motivation of developing the CS algorithm was the intent to combine the advantages of existing algorithms such as Particle Swarm Optimization (PSO) and Differential Evolution (DE) but with the reminding of the cuckoos' breeding behavior. Cuckoo search metaheuristic algorithm was developed in 2009 by Xin-She Yang and Suash Deb and it is based on the idealized rule according to which each cuckoo lays one egg at a time, dumps it in a randomly chosen nest and then the best nests, with high quality of eggs (solutions), will carry over to the next generations. The best solution is carried over to the next iteration, which is essentially elitism. The outperformance of CS over PSO and GA has been demonstrated by several examples of different structure types, such as 25-bar transient truss structure, 56-bar dome truss structure, 64-bar planar truss structure, 200-bar planar truss structure and finally a 942-bar tower truss structure.

In the swarm-inspired algorithm environment, the Particle Swarm Optimization (PSO) is one of the best known. Subsequently, some variants have been generated, like the Quantum Particle Swarm Optimization (QPSO) algorithm. However, as highlighted by Gholizadeh, S., Moghadas, R. in [40], such method has displayed some drawbacks related to not balanced global and local searching abilities and inefficient capacity for tackling large-scale or complex problems. Thus in the reported research, improved solution has been implemented and tested on the minimum weight optimization of steel frame structures. The Improved Quantum Particle Swarm Optimization (IQPSO) algorithm has exhibited a good balance between exploration and exploitation. Moreover, from the numerical results on a three-bay, six-story and a four-bay, twelve-story steel frames, it has shown that IQPSO is able to provide lighter systems than QPSO ones, with a faster analysis.

Later on, Kaveh, A., Ilchi Ghazaan, M. in [60] have carried out a comparison between the Colliding Bodies Optimization (CBO) and the Enhanced Colliding Bodies Optimization (ECBO), applied to both trusses and frames. The objective of the discrete size optimization was to minimize the weight of the structure while satisfying some constraints on strength, displacement and cross-sections limits. Regarding CBO, it is a metaheuristic algorithm, introduced by Kaveh and Mahdavi, in which several colliding bodies (CB) collide with each other, exploring the search space. After, the colliding bodies are sorted in increasing order, according to their objective function values, and two equal groups are created: stationary group and moving group. Moving objects collide to stationary objects to improve their positions and push stationary objects towards better positions. Instead, in ECBO, a memory that saves several historically best CBs is utilized to improve the performance of the CBO and reduce the computational cost. Furthermore, ECBO changes some components of CBs randomly to prevent premature convergence. Four benchmark structural examples have been considered, namely 25-bar space truss, 72-bar space truss, 3-bay 15-story frame and 3-bay 24-story frame. Results have indicated that the convergence speed of CBO was better than ECBO for truss problems, due to their simplicity; however, the reliability of search and solution accuracy of the ECBO was superior. In frame examples, the ECBO had remarkably better performance than CBO and other methods in terms of accuracy, reliability, and speed of convergence. Overall, the comparison of the results with some other well-known meta-heuristics has shown the suitability and efficiency of the proposed algorithms.

An interesting combination of metaheuristic algorithms, namely Eagle Strategy (ES) algorithm with Differential Evolution (DE), has been developed by Talatahari, S., Gandomi, A.H., Yang, X.-S., Deb, S., in [108]. Those two algorithms have been combined to obtain a new one, denoted as the ES–DE. Its performance has been tested, for weight minimizations, on several frame structures and it has been proven that the new strategy allowed to reach a good balance between global diversification and local intensification. In fact, optimization results have illustrated the superiority of ES–DE over standard DE. Furthermore, the proposed algorithm was very competitive with other state-of-art metaheuristic optimization methods, almost always finding the best designs at the lowest computational cost.

Another example of nature-inspired metaheuristic algorithm is the Grey Wolf Algorithm (GWA), explored by Gholizadeh, S., Fattahi, F., in [37]. It has been applied, once again, to derive the minimum weight design of frame structures, under earthquake loadings. In particular, in this study the GWA has been compared with GA and Harmony Search Algorithm (HSA). GWA is a metaheuristic algorithm proposed by Mirjalili et. al., based on the leadership hierarchy and hunting mechanism of grey wolves in nature. Two numerical examples, including a 6-story 1-bay planar steel frame and a 12- story 3-bay planar steel frame have been illustrated to demonstrate the efficiency of the GWA.

Also the Moth-Flame Optimization (MFO) algorithm is nature-inspired, recalling the navigation technique of moths. An enhanced version has been tested by Gholizadeh, Saeed, Hamed Davoudi, and Fayegh Fattahi in [36]. In fact, since MFO meta-heuristic algorithm has shown some difficulties in solving discrete optimization problems of steel frame structures with large design space, an Enhanced Moth-Flame Optimization (EMFO) algorithm has been proposed to tackle this class of problems. In the new formulation, a new term in the position updating equation has been employed, which contains information about the best position attained so far during the procedure. In such equation, a scaling factor, determined by performing a sensitivity analysis, has been introduced too. Furthermore, a mutation operator has been added to the algorithm to decrease the probability of trapping into local optimal designs. The power of the proposed EMFO algorithm has been illustrated by presenting three benchmark size optimization problems of steel frame structures, subjected to gravity loads and wind action. The results obtained by EMFO in all examples have been compared with the optimum designs found by MFO and other algorithms, such as GA, Ant Colony Optimization (ACO), Harmony Search (HS), Improved Ant Colony Optimization (IACO), Evolution Strategy (ES), Teaching-learning Based Optimization (TLBO) and Modified Particle Swarm Optimization (MPSO). The numerical results have demonstrated that the proposed EMFO meta-heuristic algorithm not only converged to better optimal solutions, compared to the mentioned meta-heuristic algorithms, but it also required fewer structural analyses. Consequently, it can be stated that the proposed EMFO meta-heuristic can address the discrete optimization problem of steel moment resisting frame and steel braced frame structures with large number of design variables.

Even though EMFO has proven its efficacy against many algorithms, also TLBO has shown good results in a number of researches. It was developed by R.V. Rao et al. in 2011 and exploits and simulates the environment of a classroom, in particular the teaching-learning procedures between teacher and students, to optimize a given objective function. The teacher is considered as a person having the highest information and will imparts his/her knowledge to the students in the class. Then the learners will interact with each others to further modify and improve their gained knowledge. So, TLBO method starts from the initial class population creation and then it follows two phases: teaching and learning. Artar, Musa in [7] have solved the minimum weight optimization problem of different braced (non-swaying) planar problems, applying such algorithm. Several benchmark tests taken from literature were adopted, as the 162-member X-braced planar steel frame and a 304-member K-braced planar steel frame. The results showed the robustness and applicability of TLBO method for structural problems, in comparison with GA, HS, ACO and Tabu Search (TS) algorithm.

Instead Camp, C.V., Farshchin, M., in [16] illustrated a modified version of the algorithm applied to fixed geometry space truss structures. With regards to the algorithm utilized in the current study, the modified TLBO algorithm used a fitness-based weighted mean in the teaching phase and a refined student updating process. Three common benchmark truss design problems have been presented, such as a 25-bar transmission tower, a 10-bar cantilever truss, and a 72-bar multi-story truss. The improved performance of the modified TLBO can be attributed to the use of a fitness-weighted mean during the Teacher Phase that assigned more influence on qualified individuals in the population.

Gholizadeh, Saeed, and Arman Milany in [39] have proposed a new version of the Firework Algorithm (FWA), called Improved Firework Algorithm (IFWA), to deal with discrete structural optimization problems of steel trusses and frames. The optimization problem has been formulated in terms of minimization of the weight of the steel structures, in which the cross-sectional areas of the members were chosen as discrete design variables. The constraints applied on truss structures involved stresses and nodal displacement limitations, while stresses and both lateral and inter-story drifts constraints were considered in the analysis of frame structures. As the name suggests, FWA has been developed based on the phenomena of a firework explosion, where the fireworks, i.e. the search agents, are randomly generated in the design space during the first phase. Their fitness values are evaluated, as well as the number of sparks and the explosion amplitude, for each firework. In the second phase, different types of sparks are generated in the surrounding local area of each firework in the design space. In the last phase, a new population of fireworks is selected among the original ones and the generated sparks. The algorithm terminates when one of the stopping conditions is met. In particular, the explosion amplitude plays an important role, because a larger value is associated with a bad firework. The main drawback of the original FWA was that there was no direct interaction among the solutions found during the optimization process. Moreover, the slow convergence speed was another disadvantage. To deal with these problems, a new equation has

been proposed for explosion sparks generation, in which information about previous fireworks is included. Numeric examples have been illustrated to show the validity of the proposed method, not only by comparing the results of the proposed IFWA with the original FWA, but also with the results attained by a variety of well-known metaheuristic algorithms in the literature, such as Improved Mine Blast Algorithm (IMBA), DE, Adaptive Elitist Differential Evolution (AEDE) and others.
The Adaptive Dimensional Search (ADS) algorithm, proposed by Hasançebi and Kazemzadeh Azad for discrete sizing optimization of truss structures in [46], has been reformulated to tackle discrete sizing optimization problems of real-size steel frames by the same authors in [47]. Five examples, taken from the literature, have been analyzed using ADS algorithm to prove its reliability and efficiency in optimum design of steel frames.

## 2.2 Size Optimization

In the present section we have collected all the considered papers regarding size optimization problems, focused on structural performances. In particular, they are mainly concerned about frame applications and, due to the great attention that they have raised among researchers, it has been proposed a division in main topics rather than a simple chronological ordered list. By means of the following chart 2.6, it is possible to appreciate the amount of studies dealing with each of the 5 presented themes, i.e. non-linear behavior of structures, optimization under seismic loadings, connection flexibility considerations of frames, soil-structure interaction investigation, large roof structures and multi-bays, multi-storeys frames.

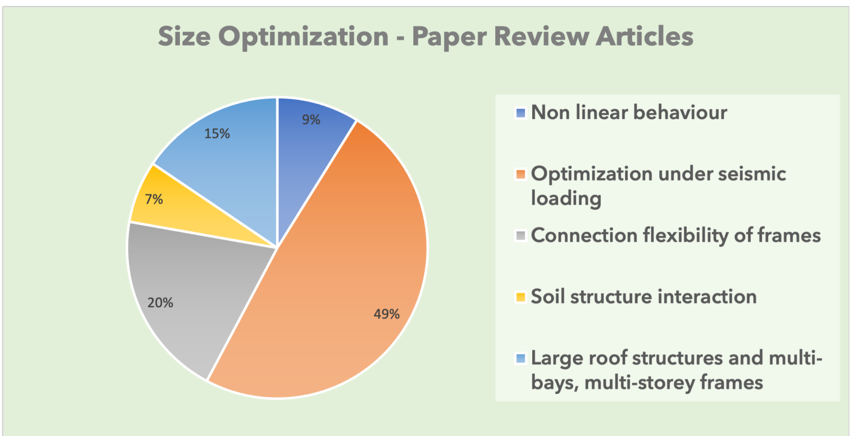


Figure 2.6: Collected papers on size optimization

### 2.2.1 Non-linear behaviour of structures

Many researches on frames or truss structures have been primarily concentrated on their linear-elastic behavior, entirely neglecting their resistance capacity to loads outside the elastic domain. However, there have been also some authors that have investigated exactly this aspect. Non-linearities in terms of both geometry and materials has been explored for example in the study [102] provided by Saka, M. P., and M. S. Hayalioglu in 1991. Specifically, in this paper, the minimum weight design of a non-linear elastic-plastic frame with displacement limitations has been investigated. These limits were kept big enough in order to allow the frame to undergo large deformations. In any case, structural checks have been performed at every cycle of the optimization in order to guarantee the overall stability of the frame. The design variables were chosen as the cross-sections of the frame's members and a lower bound to their sizes was applied. As said, the problem accounted for both geometric and material non-linearities of the structure, whose response was obtained by employing a Newton-Raphson-type iteration technique. Small load increments were imposed, allowing the members to reach yielding, so that plastic hinges could be developed accordingly. The iterations stopped when a prescribed load factor was reached. Numerical examples of portal frames, pitch roof frames and both multi-storey and multi-bays frames were reported to show how the algorithm works. Moreover, a comparison with linear elastic frames was carried out for the same examples. The study has demonstrated how consideration of geometric and material non-linearities in the optimum design, not only led to a more realistic approach, but also to lighter frames. The reduction in the overall weight varied between 20 and 30% when compared with the optimum designs obtained simply considering linear elastic behaviour. However, most of the computational time has been consumed for the frame's non-linear response prediction.

In another similar paper [50], the same authors of the previously described research have extended the design of geometrically non-linear elastic-plastic steel frames including tapered members, illustrated in figure 2.7.

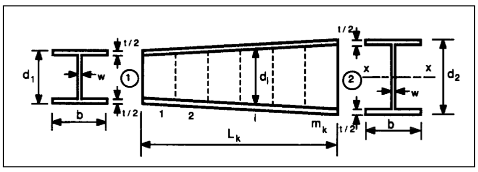

Figure 2.7: Tapered member [50]

Here, each member introduced two variables into the design problem: the first was the cross-sectional area at one end of the beam and the other was the ratio of areas at both ends. In this way, a well-defined reduction function from one edge of the beam to the other was introduced. In particular, the variation of the cross-section has been considered linear for simplicity. The weight minimization was still the target function and the large deformation analysis was carried out as before. In order to demonstrate the applicability of the algorithm presented, three elastic-plastic steel structures with tapered members have been considered. As in the previous research, also here a comparison between the proposed elastic-plastic analysis with the traditional linear elastic one, of the same structures, has been performed. In agreement with the previous results, also in this analysis a greater saving in the mass of structures was possible if geometric and material non-linearities were considered in the formulation of the optimum design problems.

Later on, the authors Se-Hyu Choi, Seung-Eock Kim with [20] proposed a non-linear inelastic analysis for an optimal design of steel frame. A direct search method was employed to reach minimum weight design, that was the Objective Function of the problem. Constraint functions were related to load-carrying capacities and displacements. At first, a non-linear inelastic analysis was performed to check the load-carrying capacity of the structure; then if some columns or beams were not verified, a member with the largest unit value, calculated by Load resistance factor design (LRFD) interaction equations, was replaced one by one with an adjacent larger member selected in the database. The same procedure was done to check displacements and if they were not satisfied, a member with the largest displacement ratio was replaced with a bigger member. The database enclosed wide flange sections (W-sections) listed in the AISC-LRFD (American Institute of Steel Construction - Load Resistance Factor Design) specification. This routine was repeated until the serviceability and loading conditions were satisfied. Ductility requirements were also accounted in the optimization process, in fact adequate rotation capacity was required for members to develop their full plastic moment capacity. The design examples consisted in a planar portal frame and two-story frame, both subjected to dead, live and wind load. The member sizes of the optimal design using the proposed analysis and the convention LRFD were compared. Results showed that the weights can be reduced by 8.0% and 3.7% for the planar portal frame and for the space two-story frame respectively, if compared with those of the conventional design using LRFD specifications. Non-linear inelastic analysis has been demonstrated to be very efficient with respect to previous researches, when only elastic analyses were conducted, assuming a length factor(K) always equal to 1.

Finally, in 2019, an interesting study was provided by Habibi, A., Saffari, H., Izadpanah, M. in [42]. Here it has been developed an unique optimization technique aimed at obtaining a lateral load pattern leading to the smallest possible disparity between the floor displacements of pushover and Non-linear Dynamic Analyses (NDA). The primary goal of this study was to propose an efficient load pattern that best aligned with NDA. To reduce the discrepancy between NDA and pushover results, a reverse engineering strategy has been employed. The lateral floor displacements of the NDA were first calculated and used as a benchmark to achieve the desired outcome. Second, the lateral load pattern that produced the least difference between the lateral floor displacements of the NDA and those of the pushover analysis was identified. The lateral forces of floors were taken into account as design variables while the expression of the OF was simply the ratio between the difference of floor lateral displacements resulting from non-linear time history and pushover analysis, normalized with respect to the floor lateral displacement from the non-linear time history analysis. From the physical and structural dynamic point of view, each optimization problem needed at least two constraints. In this study, based on engineering experience and also on the recommendations of seismic instructions, the base shear of buildings was assumed as a percentage of the total weight (ten percent of total weight in general); another adopted constraint in this study was to adopt the positive values for lateral forces along the height of buildings. 5-story, 2-bay, 10-story, 3-bay and 15-story, 3-bay special moment resisting steel frames has been analysed to validate the applicability of the recommended method, in comparison to current load patterns, such as uniform, linear, and parabolic.

### 2.2.2 Optimization under seismic loading

An important topic faced in structural optimization analyses is the design of steel structures subjected to seismic loadings. It was investigated since the ages when only gradient-based optimization techniques were available. For example, Feng, T-T., J. S. Arora, and E. J. Haug Jr. in [32] presented a simple weight minimization of elastic structures, subjected to dynamic loads, where the elements' cross-sections were taken as design variables. The adopted constraints were applied to the dynamic response, i.e. displacements and stresses, at critical points of the structure. In addition, upper and lower bounds on natural frequencies were imposed, as well as a design parameters boundary. A state space steepest descend method was employed for the optimization, while the structural response was obtained from a finite element model. In parallel, modal analysis techniques were used to solve the dynamic problem. Tubular cantilever beams and planar truss-frames have been studied by means of the proposed procedure.

A similar study has been carried out by Cheng, Franklin Y., and D. S. Juang. in [18], in which the same design variables, constraints and objective function have been defined. In the proposed research, the analysis was focused on two-dimensional steel frameworks, with and without bracing members, subjected to both static and seismic forces. In addition, a cost objective function of the same structures has been compared to the classical weight minimization. Regarding the cost minimization target function, the parameters considered included the cost of structural members, painting, connections (steel plates and welding), together with the damage expense, limited to the repair of non-structural elements. The results have shown that the optimum solution of the minimum weight design was close to that of the minimum cost case; the latter, however, demanded a gradual change of the column stiffnesses.

A step forward in the application of weight minimizations of both braced and unbraced steel frames was proposed by Memari, A. M., and M. Madhkhan in [76]. A comparative study of different types of braced, unbraced, regular and irregular frames, subjected to combined gravity loads and seismic lateral forces, has been carried out by the authors, as shown in 2.8.

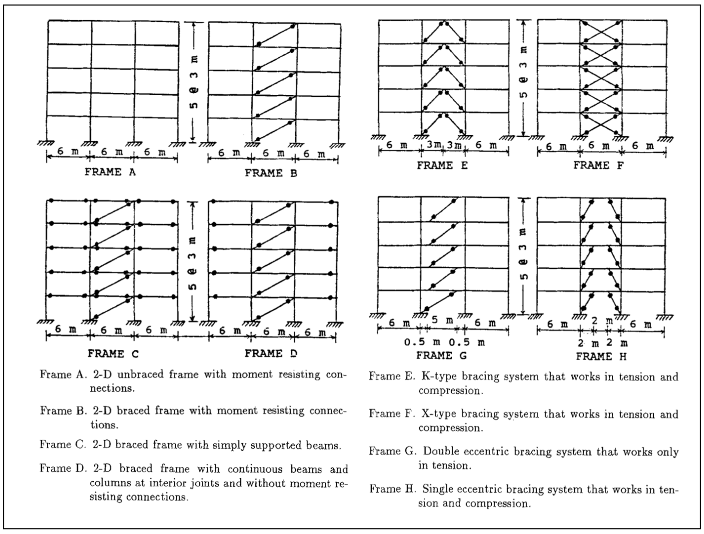


Figure 2.8: Frame structures analyzed [76]

The main scope of the study was to expose the applicability of the proposed design approach and to provide a comprehensive investigation deriving from the comparisons between several structural configurations. The members' cross-sectional areas were chosen as design variables, treated as continuous variables. Only at the end of the optimization, the available sections, taken from the German database and with the closest properties of the chosen design variables, were assigned to the optimum frame members. Of course, the obtained structure was then checked to assure the satisfaction of all the constraints. In particular, the design had to satisfy combined bending and axial stresses, shear stress, compression buckling and tension slenderness criteria, according to the AISC of 1983. Moreover, the maximum allowable relative story displacement was checked, as well as the upper and lower bounds applied to the design variable values. The feasible directions method has been employed as nonlinear constrained minimization algorithm. The structural analysis has been carried out with the finite element approach, while both equivalent static force and response spectrum analysis methods were considered.

A new formulation for discrete and/or continuous variable optimal structural design was implemented by Palizzolo, L., Benfratello, S., Tabbuso, P. in [87]. The best design for elastic plastic frames, under both static and dynamic loads, was achieved by developing a minimum volume optimization. In the static condition, the structure had to remain in the elastic field while subjected to fixed loads, instead for seismic excitations, the elastic shakedown limit in seismic serviceability could not be violated by the plastic frame. Elements buckling was planned to be prevented for both combinations. A practical example, referred to a 4-storeys frame has been solved by considering the design variables at first as discrete and then as continuous. In particular, the thickness of the box-shaped cross-sections was allowed to vary within a specified range. As expected, the structural volume related to the discrete variable design was higher than the continuous variable one.

In the context of structural optimizations under seismic loading conditions, many studies have focused their attention on the uniform distribution of properties throughout the considered building.

A first exploration of such topic was carried out by Kapoor, M. P., and J. V. N. Rao. [54], in which the best stiffness distribution of a multi-storey frame was sought. The objective function of the optimization was tackled as the minimum structural weight, formulated by means of a nonlinear programming technique. In the probabilistic procedure presented, the multi-storey frame has been idealized as a multi-degree “shear beam” subjected to earthquake ground motion treated as a random process. The “shear beam” idealization consisted in replacing the multi-storey frame with a system of masses, shear springs and dashpots, while white noise has been chosen to represent the ground acceleration. This probabilistic formulation of the problem was compared with the deterministic one, which used the response spectra approach, ignoring the randomness of the ground motion. The design variables were chosen as the moments of inertia of the columns of different storeys, expressed as a function of the areas, section dimensions and modulus of all the available I-sections listed in the Indian Standard Institution (ISI) specifications. Actually, the rows of the standard section list represented effectively the set of the Design Variable: once the index of each competence raw of the adopted standard section list was selected by the optimizer, all the geometrical and mechanical properties related to that section were obtained simultaneously. The constraints considered regarded the upper bounds of the probability that the stress in the columns at each storey level, due to earthquake acceleration, exceeds the yield stress. In addition, lower and upper bounds were applied on the maximum and minimum moments of inertia of the I-sections. From the comparison between the probabilistic and deterministic formulations of the optimum design of multi-storey frames, it has been demonstrated that the first one provided more realistic results.

Later on, Moghaddam, H., Hajirasouliha, I., Doostan, A. in [79], proposed a strategy for enhancing the dynamic response of concentrically braced steel frames, subjected to seismic excitation, based on the concept of uniform distribution of deformation. As demonstrated in previous studies, during strong earthquakes the deformation demand in structures does not vary uniformly, but there are some stiffer elements that do not fully exploit their seismic capacity. Therefore, the goal of the proposed iterative optimization technique was to gradually shift inefficient material from strong to weak areas of a structure, by changing its structural features. Thus, the Objective function of the problem can be related to the maximum uniformity of structural properties. Design guidelines such as FEMA 365 (Federal Emergency Management Agency - Prestandard and commentary for the seismic rehabilitation of buildings) and SEAOC Vision 200 ( Structural Engineers Association of California - Performance based seismic engineering for buildings) have identified the inter-story drift as an efficient indicator of damage to nonstructural elements. The proposed practical examples, reported in 2.9, were related to steel concentric braced frames with 5, 10 and 15 stories and members frames were sized to support gravity and lateral load.

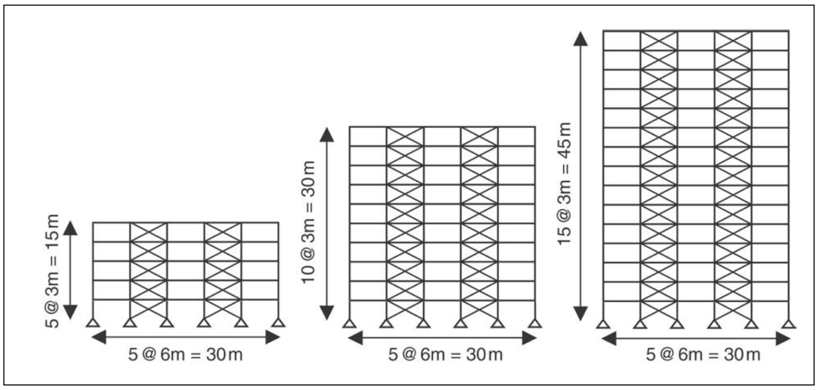


Figure 2.9: Concentrically braced steel frames analyzed in [79]

The cross-sections have been considered as design variables in the optimization. At first, columns and beams were sized to meet the code drift requirements and then the sections of the brace members were defined in order to reach the uniform deformation state. From the analysis, it has been demonstrated that generally there is a unique optimum distribution of structural properties, independent of the seismic load pattern used for the initial design.

The effects of strength distribution pattern on seismic response of tall buildings has been examined again by Moghaddam, H., and I. Hajirasouliha in [78], which proposed an optimization procedure aimed at finding more rational criteria for determining design earthquake forces. In this case, the idea of shifting the inefficient material from strong to weak areas of structure has been applied to shear buildings. In more details, in the shear building models, each floor is assumed to be a lumped mass that is connected by perfect elastic–plastic shear springs. The total mass of the structure is distributed uniformly over its height as can be seen in figure 2.10.

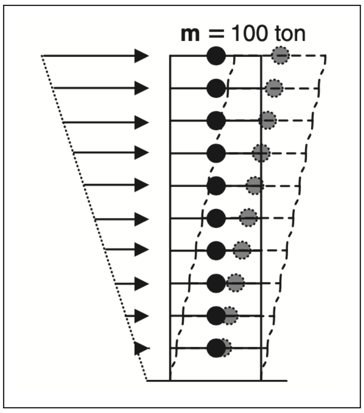


Figure 2.10: Typical 10-story shear building model [78]

Moreover, to evaluate the weight of the seismic resistant system for MDOF structures, it has been assumed that the weight of the lateral-load-resisting system at each story is proportional to the story shear strength. Then the loading pattern corresponding to the minimum required structural weight would be regarded as the optimum loading pattern. To accomplish this, the total weight of the seismic resistant system has been calculated for shear building models with various fundamental period, ranging from 1 to 3 s, and different target ductility demands, from 1 (elastic) to 8. In all MDOF models, lateral stiffness was assumed as proportional to shear strength at each story, obtained in accordance with the selected design lateral load pattern. As noted before, it has been highlighted also in this paper that there is a unique relation between the distribution pattern of lateral seismic forces and the distribution of strength (as the strength at each floor was obtained from the corresponding story shear force). Hence, for shear buildings, it was possible to determine the optimum pattern for distribution of seismic lateral loads instead of strength. Fifteen selected strong ground motion records have been considered and modal analysis has been performed at each iteration to retrieve the building seismic response. The authors also suggest a more adequate load pattern, obtained as a function of the fundamental period of the structure and the target ductility, which has been proved to outperform with respect to conventional loading patterns suggested by most seismic codes.

The uniform deformation theory was also exploited by Mohammadi, R.K., Sharghi A.H., in [81], combined with another important concept when designing in seismic condition, i.e. the Performance-Based Design (PBD) approach. In PBD frameworks, a performance objective is defined as a given level of performance for a specific hazard level. More in details, a performance level is representative of the level of expected loss, while the hazard level of the seismic intensity. In general, three performance levels are considered, such as immediate occupancy (IO), life safety (LS) and collapse prevention (CP) which correspond respectively to a 20%, 10% and 2% probability of exceedance in 50 years period. Specifically, in the considered paper, the authors focused the attention on the optimization of 3, 5 and 10 storeys eccentrically braced steel frames (EBF), subjected to 12 earthquake ground motions. Once again, the weight minimization has been defined as OF, which in this case had to satisfy the Life Safety (LS) performance level according to ASCE 41-06 (Seismic Rehabilitation of Existing Building - American Society of Civil Engineers). Maximum displacements, maximum rotation of plastic hinges and maximum capacity of force-controlled elements were considered as optimization constraints. Regarding the design variables of the problem, they were mainly dependent on the properties of the link beams that basically govern the seismic behavior of EBF. Web shear area of the link beams was considered as the major design variable; based on the concept of Uniform Deformation Theory (UDT) the cross-sectional area of the web had to be increased in zone where more shear deformation was required and reduced in the link-beams that had too high deformation capacity. Once link beams properties had been properly modified, the other frames members were sized based on maximum axial force and bending moment. The optimization process was stopped when the Coefficient of Variation (COV) of the link beams has reached a value small enough as the structure tends to a uniform deformation state. To demonstrate the potential of the proposed method, it has been compared with EBF optimization according to conventional load patterns, showing that in this way such structures suffer less damage.

An enhanced adaptive optimization algorithm based on the idea of Uniform Damage Distribution (UDD) was coupled with the Performance-Based optimization framework by Moghaddam, H., Hajirasouliha, I., Hosseini Gelekolai, S.M., in [80]. The research was intended to assess the seismic design of steel moment resistant frames (MRFs), subjected to dynamic earthquake excitations. In the minimum-weight optimization, the design variables were always the members' cross-sections, while constraints were applied to maximum plastic rotations, to monitor the deformation of the frame, and strength-based demand to capacity ratios, to check the acting forces. The efficiency of the proposed optimization has been demonstrated considering 3, 5, 7, 10 and 15-storey steel MRFs and a set of five strong earthquake records from the Pacific Earthquake Engineering Research Center (PEER) database. It has been shown that the optimal design frames required up to 38% less structural weight than their code-based design (ASCEE) counterparts for the same performance level.

The optimization process for seismic design of steel frames for multiple performance and multiple hazard levels under various performance objectives was described in great details by Qimao Liu and Juha Paavola in [69]. The reported diagram in figure 2.11 explains very well how the targeted damage states under the different hazard level express the performance objectives of the structure. Then, the intersections of the structural capacity diagram (achieved by structural analysis) and demand diagram (obtained by response spectra related to hazard levels) is the performance points we wanted. Comparing the performance points with the performance targets, we can evaluate the performance of the structures under the different hazard levels.

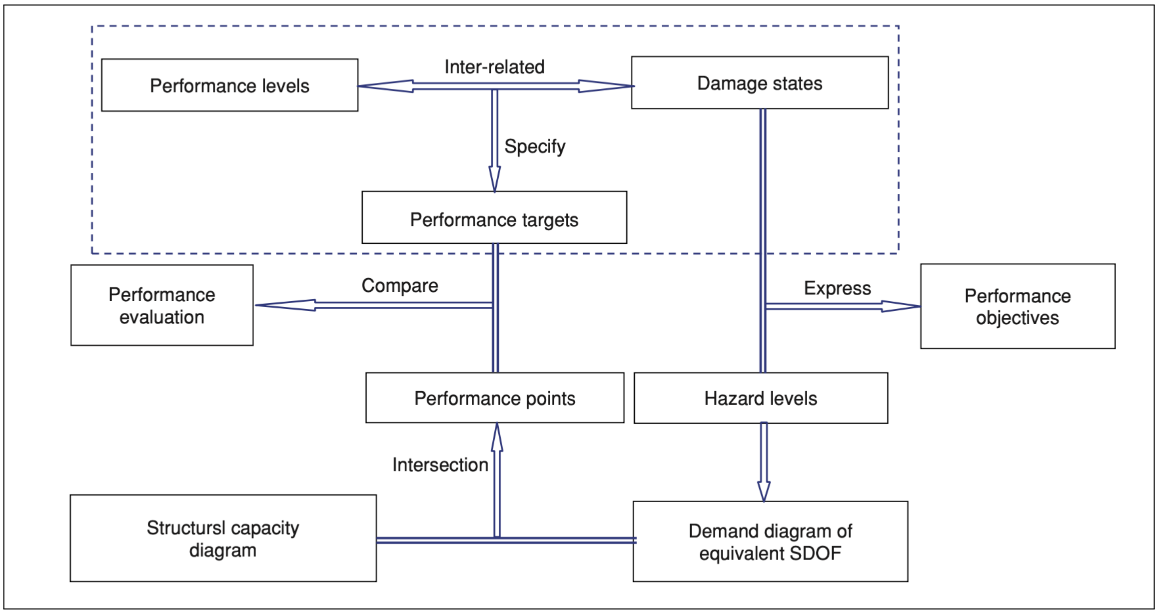


Figure 2.11: Performance-based seismic design concepts [69]

Three particular performance objectives, which may be stated in terms of specific damage versus a set of seismic hazard levels, are expressions of acceptable performance of the structure. In particular, the authors have defined three performance objectives: basic objective, enhanced objective 1 and enhanced objective 2. For example, enhanced objective 1 correspond to serviceability performance levels in an occasional hazard levels, or Life safety, and a rare hazard levels. Specifically, the reported graph 2.12 illustrates well the seismic environment in which the performance objectives were evaluated.

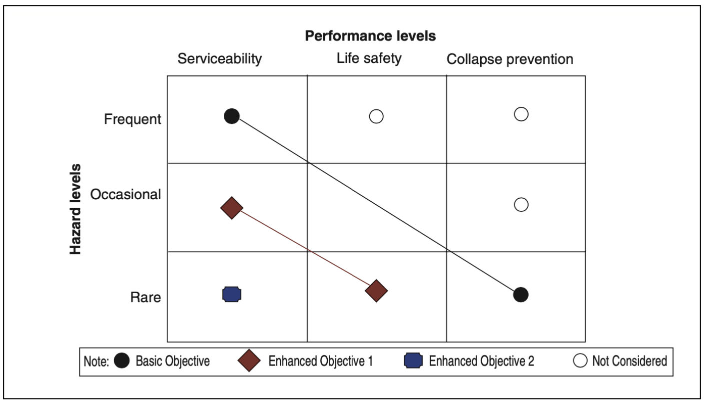


Figure 2.12: Performance objectives in [69]

The authors of the paper have been focused in finding the inelastic drifts of the performance points, that was compared with the limits of inelastic drifts of the structure, also called performance targets. In fact, it is common knowledge, that any seismic design of frame buildings must include inter-story drift control as a key component, which is one of the most important part in seismic design regulations. Moreover, residual inter-story drift is a factor in the structure's damage. Practically speaking, the performance points are where the elastic/inelastic response spectrum diagram (also known as the demand diagram) and the structural capacity diagram cross. In the optimization process depicted, a three-story steel frame has been optimized in order to reach a minimum weight design. The considered design variables were the different geometric characteristic of I-shape section, i.e. flange width and thickness and web depth and thickness, of all the beams and columns of the different storeys. As expected, different optimum designs have been obtained in function of different hazard levels. For example, thee mass of the optimum design for Enhanced Objective 1 (2858 kg) is greater than that of the optimum design for Basic Objective (2593 kg).

Also Gholizadeh, S., and A. Milani. in [38], have exploited the concept of Performance-Based optimization seismic design (PBOSD), with specific focus on a comparison of different metaheuristic algorithms, such as Particle Swarm Optimization (PSO), Dolphin Echolocation Optimization (DEO), Enhanced Colliding Bodies Optimization (ECBO) and a slightly modified ECBO called ECBO-II. Considering the above-mentioned performance objectives, in order to assess the structural performance in terms of strength and deformation capacity, globally as well as at the element level, a set of 8 nonlinear time-history analyses were conducted for each hazard level. The constraints applied during the PBOSD procedure regarded the serviceability and ultimate state limit checks. Thus, structural members were checked in terms of strength and displacements. Weight was minimized during the optimization, while the members' cross-sections, chosen as design variables, were taken from the AISC list of W-shaped sections. The applicability of the method has been examined on two steel frames, in which rigid connections and fixed supports were assumed. Results have revealed that for both examples the drift constraint at IO level dominates the optimal solutions.

The PBOSD approach has been also applied by Mansouri, S.F., Maheri, M.R., in [73]. The minimum weight design of steel frames has been implemented using the Constraint Control Method (CCM), in which the design variables have been chosen

as the W-shaped cross-sections of the structural members. Two set of constrain were defined, in which the first one, based on AISC-LRFD specifications, included the stress constraints for members undergoing axial force and bending moments due to gravity loads; instead the second set of constraints was related to the lateral seismic loading in the form of relative lateral story displacements (relative drift) at different performance levels. With the CCM approach, the most conservative member sections were first chosen and by progressively shrinking their size, while managing the problem limitations, the solutions approached toward an ideal design. Three two-dimensional (2D) benchmark steel sway frames were analyzed with the suggested method, including a three-storey four-bay frame and a nine-storey five-bay frame. The CCM drastically reduced the number of structural analyses required to reach a solution, compared to the more commonly used metaheuristic optimization methods, while producing comparable optimum solutions. For this reason, CCM has been found to be particularly suitable as an optimizer for solving solution-extensive problems, such as performance-based optimum design of structures. Moreover, as shown in the previous article, the drift constraint has been prevailing over the force-based stress constraints, strongly determining the final design of the structure.
In the field of steel concrete composite moment-resistant frame, Kaveh A., Mahdipour Moghanni, R., Javadi, S.M., in [64] have developed a Chaotic Optimization Algorithm (COA) based on Chebyshev chaotic map, following a performance-based design. Chaotic map was employed to prevent trapping in local optima and to improve the exploration and exploitation of the algorithm. PBD in combination with COA was illustrated by means of weight minimization of both 8-story and 20-story steel concrete composite moment resisting frames. Regarding the design variables of the optimization problem, I-shape beams and concrete-filled steel tube (CFT) columns were adopted, chosen from a list of available cross-sections. Strength and drift constrain were agreed to design the optimized structure. To achieve the minimum weight, three main steps were followed. In the first step, the five best designs for each frame were obtained based on the results of the pushover analysis, performed twenty times for each performance level. Once fragility curves were plotted for each selected frame, their best optimal design was chosen, based on the corresponding damage margin ratio (DMR) of each damage level. DMR has been used to select the best five design, determined from the outcomes of the pushover analyses. DMR has been defined as the ratio of intensity measure's value (IM) in accordance with 50% probability of collapse to the intensity of the maximum considered earthquake.

In particular, higher values of DMR in a specific damage level indicate more safety conditions. While in the 8-storey frame analysis, DMR values resulted to be almost equal for each damage level, for the 20-storey case a larger scattering of the DMR values has been obtained. Thus, it should be concluded that 20-story's seismic behavior was sensitive to the selected sections and minimum weight was not a good parameter to choose the best optimal design, due to its variable seismic behavior according to DMR values.

A slightly different research has been conducted by Lv, Y., Li, Z.-X., Xu, L.-H., Ding, Y. with [70], in which a different goal of the structural optimization was proposed. In fact, instead of tackling the traditional weight minimization, it faced the maximization of the structural global performance under severe earthquakes. An Equivalent Seismic Performance Optimization (ESPO) has been employed to minimize the difference between the seismic capacities of structural members. In the optimization process, the importance coefficient (IC) and damage index (DI) were defined and correctly balanced in order to identify how different structural elements responded to earthquake ground motion. DI can be defined as the weighted average of the local damage indices or the change of modal parameters of the damaged structures. IC coefficient indicates the elements that may not be damaged during earthquake excitation. Numerical analysis results, on 9-story steel frame, have indicated that structural members with higher importance coefficient (IC) may not be damaged during earthquake, however, the ones with low IC may fail. More in details, an objective function (OF) was set to minimize the seismic performance index (SPI) for every structural member, evaluated from the two previously introduced, IC and DI. The maximum inter-story drift was adopted as the performance criteria for global structure. Optimization of the structure was conducted by changing the section area of steel columns as continuous design variables. From the analysis, it has been shown that IC values were different for columns at the same position belonging to the same story. Moreover, corner columns had the largest IC values and a state of damage with higher tendency to trigger the global damage. By means of the DI value outcomes, it was proven that the damage was largely concentrated at the first story. Therefore, the IC and DI values was intended to provide a guidance in the design of such structures, in order to understand which column needed a stiffer cross-section.

The optimization problems involving structures under seismic loadings were also conducted in the field of multi-objective problems. As briefly mentioned in the Introduction Chapter, multi-objectives optimization procedures are quite challenging if compared to single-objective problems. The main issue is that they work with competing goals, meaning that the design accounting for one target may lead to a decrease in the performance of the other objectives. As a result, rather than a single solution, the so-called Ideal Point, or Utopia Point, that maximizes or minimizes all objective functions simultaneously, there is a set of incomparable optimal solutions, each of which is superior to the others in a particular objective. Decision-makers can choose from a variety of options in this collection of non-dominated or Pareto optimal solutions, in order to best meet the needs of a given project. In the field of multi-objectives optimization of frames subjected to seismic loads, the main target functions addressed can be summarized in the following ones. The weight minimization is still one of the most common goals, mainly used as a parameter to reduce the overall cost of the structure under study. Then other objective functions are defined, such as minimization of inter-story drift, maximization of energy dissipation capacity or minimization of structural damage. Ductility and energy dissipation capacity are addressed as key performance parameters for the seismic damage of frames when some structural parts exceed their elastic limits during strong earthquakes.

An example of multi-objective optimization has been performed by Kaveh, A., Shojaei, I., Gholipour, Y., Rahami, H., in [65]. The objectives out here included minimizing inter-story drift, under applied ground movements, minimizing structural damage, evaluated by a damage index, and minimizing total construction cost, measured by means of sections weight. The structure modeled in the non-linear analysis was an Eccentric Braced Frame (EBF) with 4 spans and 5 storeys. During the GA-based optimization, both strength and slenderness constraints were applied, together with limitations on the maximum relative displacements for each story, governed by the period of the structure. The cross-sections of beams, columns and braces were chosen as design variables, taken from a discrete list of available sections. While for the first objective function they have been simply varied to meet the minimum weight of the structure, for the other two objectives a balance needed to be found on the strength of the material. In fact, high yield strengths could not ensure decreasing damages, especially the non-structural damage. Essentially, when subjected to high strength, the structure will experience high accelerations even during mild excitations that cause great non-structural damages. Specifically, damage index has been defined as the ratio between the maximum deformation of the member under loading and the maximum deformation capacity under one-way loading plus a parameter, related to the dissipated energy during loading, and multiplied by a constant value. The possible values of such index range between 0, when there is no expectation of damage, up to 1, when there is a potential for collapse. Moreover, neural network has been trained and employed for estimating the relation between the input and output variables. Input variables included the standard sections while outputs included drift, dissipated energy, and plastic deformation under ground motions. Results have revealed, as expected, that an increase in volume, led to a decrease in the inter-story drift but also to a damage index larger than a given threshold. Thus, high computation time were required to find a good balance between the three OF, even though neural networks helped in the decrease of the number of calculations.

In the same year, Choi, S.W., Kim, Y., Lee, J., Hong, K., Park, H.S., in [21] focused their analysis on another important topic for seismic design of frames. In fact, according to the capacity design theory, there is a sort of hierarchical design which states that we should have concentration of plastic hinges in the beams before than in columns. Thus, the multi-objective seismic design of special moment resisting frames (SMRF), based on non-linear static analysis, has been proposed and applied to find optimal column-to-beam strength ratios, required for ensuring the so-called beam–hinge mechanism. Consequently, the scope of the work was to minimize not only the structural weight but also the column-to-beam strength ratio. Constraints were imposed to control member strengths, inter-story drift ratio, prevention of formation of plastic hinge at columns connected at joints, and cross-sectional areas of vertically continuous columns. The cross-sections of beams and columns were chosen as design variables, taken from a discrete list of W-shaped sections. In particular, the multi-objective optimization employed the Non-dominated Sorting Genetic Algorithm-II (NSGA-II), based on multiple Pareto-optimal solutions. Predictably, the results on both three-story and nine-story steel moment frames presented decreasing optimal strength ratios for increased structural weights. In more details, the maximum strength ratios among the joints in SMRF has been faced at the external joints, rather than at the internal ones. Based on the investigation, it has been suggested that for a more cost-effective design, the strength ratios may be established while taking into account the positions (internal and exterior) of the joints.

Different objective functions were faced by Xu, L.-H., Xiao, S.-J., Wu, Y.-W., Li, Z.-X., in their article [114], in which the minimization of structural damage and an improvement of energy dissipation capacity were taken as main goals in the design of steel frames. Depending on the optimization strategy requested, both continuous and discontinuous design variables were taken into account, regarding cross-section properties of the members. The structural damage of the structure has been evaluated considering a damage index of the structure for every single member as function of its maximum curvature, yield curvature and ultimate curvature. In the performance-based optimization process used, the incremental dynamic analysis was first conducted on the original structure in order to identify the most unfavorable failure mode, using the failure probability function. The most adverse earthquake, corresponding to the most unfavorable failure mode, was selected as the seismic excitation for the multi-objective optimization. Then based on the values of inter-story drifts, material and sections were properly selected. Taking a 20-story steel frame structure as an example, seismic failure modes has been identified and optimized using this method. Results have indicated that, if compared to the original frame, the global damage of the optimized structure under the considered earthquake excitation was reduced, while its hysteretic energy dissipation capacity was improved. Furthermore, the inter story drift ratio distribution of the optimized structure resulted to be more uniform, leading to a significant improvement of the structural seismic performance.

Another performance-based seismic design has been proposed by Karimi, F., Hoseini Vaez, S.R., in [55]. In the study, the goals were the weight minimization and a uniform distribution of inter-story drift across the structure. In particular, the second objective was pursued to avoid the occurrence of soft-story mechanics during seismic excitation. In the optimization, the cross-sections were representative of the discrete design variables and the applied constraints involved inter-story drift, beam and column rotations, as well as weak beam-strong column mechanism checks, as specified in FEMA 356 (Recommended Seismic Design Criteria for New Steel Moment-Frame Buildings) provisions. The optimization has been carried out considering not only the performance-based design (PBD) method at the Collapse Prevention performance level, but at first accounting for the load and resistance factor design (LRFD) method. In the first step, LRFD method has been exploited to evaluate the structural adequacy of the structure, i.e. controlling demand-to-capacity ratio of beams under dominant load combinations, including factored gravity, service and seismic loads. Once obtained acceptable results, the second step involved the application to the structure of a non-linear pushover analysis with a parabolic load distribution. In this step, structural adequacy has been checked for four target roof displacements, corresponding to four performance levels. This stage involved the verification in terms of rotation of members and inter-story drifts, as specified in FEMA requirements. In conclusion, by means of two examples, it has been proved that an optimization based only on selective and limited rehabilitation criteria, ignoring the resistance-based provisions, may produce lighter designs, but the results will not necessarily be reliable in terms of resistance.

The same objective functions were also considered by Kaveh, A., Farhadmanesh, M., in [57]. In this study, however, they are applied on a different structure typology, namely steel plate shear wall (SPW) systems. A SPW, characterized by an high energy dissipation, is a lateral load resisting system that contains an infill plate attached to the surrounding beams and columns. Basically, it acts like a cantilever wall in the total height of the building. When subjected to high seismic loads, it shows an high initial stiffness and behave in a very ductile manner, absorbing high amounts of energy. The minimization of weight has been accounted by selecting the least-weight cross-sections of the structural member, along with the web plate thickness in the frame panels. For what regards the second objective function, concerning the inter-story drift minimization, it has been formulated in terms of its standard deviation. Stiffness, strength and displacement constraints were checked among the iterations. In particular, many well-known metaheuristic algorithms, such as Particle Swarm Optimization (PSO), Enhanced Colliding Bodies Optimization (ECBO), and Colliding Bodies Optimization (CBO), has been implemented. To demonstrate the efficiency of the SPW a comparison with a similar moment frame was done, taking into account both low and high seismicity regions. The optimization results have shown that the optimized structure is 25% heavier than the optimum SPW.

Another interesting research has been illustrated by Ghasemof, A., Mirtaheri, M., Karami Mohammadi, R., in [35]. The previously explained concept of Uniform Damage Distribution (UDD) has been here used to introduce a new algorithm to multi-objective design of steel moment frames. This algorithm is based on the uniform damage (also known as uniform deformation) theory and starting from that, the so-called multi-objective uniform damage optimization (MUDO) method is presented. Structural weight and maximum inter-story drift ratio (IDR) has been treated as two conflicting objectives, representing economy and safety measures. The design variables handled to reach the minimum values of the weight and IDR were chosen from a discrete list of cross-sections, given by the AISC manual. Two analyses at different levels were implemented: the linear static one to check the de-

sign constraints, while nonlinear static analysis (pushover analysis) to determine the non-linear structural response, such as the maximum IDR. The considered design constraints were including geometric, strength, strong column-weak beam and drift restrictions. Those constraints were related to constructability problems, meaning that the column section of the upper story should not be larger than the column section of the lower story. Moreover, the flexural behavior of beams and columns at the joints level was controlled, in order to avoid strong columns and weak beams effects. To demonstrate the efficiency and robustness of the proposed algorithm, 3-, 6- and 9-story steel moment frames have been compared with those of two well-known multi-objective optimization metaheuristic algorithms, NSGA-II and MOPSO.
In the multi-objective seismic design framework, it is worth mentioning other two studies that in different ways addressed the importance of the connections' role in frames under seismic loads. The first one was illustrated by Mojtabaei, S.M., Hajirasouliha, I., Ye, J. in [82] analysed thin-walled cold-formed steel (CFS) components and connections used in portal frames. This study has made an effort to enhance the seismic parameters of CFS bolted moment connections, including their capacity for energy dissipation and ductility. Due to that, the objective functions of the current problem were intended to maximize the seismic resistance in terms of ductility and energy dissipation. The ductility for the connection was simply defined as the ratio of target and yield rotations, while plastic and bearing deformations, concerning the bolted moment connections, were used to provide the energy dissipation of the moment resisting frame. The cross-sections, the position of the intermediate stiffeners, and the angles of the inclined lips were identified as design factors. A population-based stochastic optimization technique, based on Particle Swarm Optimization (PSO), was used to find the global optimized design solutions.
The second peculiar study has been formulated by Moradi, S., Alam, M.S., in [83]. It explored post-tensioned steel beam-column connections in frame structures, able to significantly reduce long-term seismic damages and the related post-earthquake maintenance costs. The considered objective functions involved the reduction of the size of the beam sections and subsequently enhancing the structural response properties of the PT connections. The goal was to increase the PT connection's initial stiffness, load capacity and final drift. In particular, it was desired to produce a ductile behavior for a PT steel beam-column connection. This aim was incorporated in the optimization problem by maximizing the ultimate drift.Additionally, PT connections were planned to have increased load capacities, thus the second optimization

goal was to increase the maximum load capacity responsiveness. To further minimize lateral displacements under lateral stresses, connections in framed structures needed improved initial stiffness. Therefore, the third goal was to maximize the initial stiffness response. Finally, the cost minimization has been accounted, in terms of amount of material. To pursue these objectives, beam depth, beam flange thickness and beam flange width were taken as design variables. Constrains were defined in terms of upper and lower bound of different quantities, such as span length, PT force, beam depth, beam flange thickness and beam flange width.

### 2.2.3 Connection flexibility of frames

Many authors over the years have investigated the optimization of steel frames by accounting for connections flexibility effects. In fact, most of the time, in the analysis and design of steel frames, beam-to-column connections are generally assumed to be either fully rigid or perfectly pinned. In the former case, bending moment, as well as shear and axial forces are transmitted from one element to another and no relative rotation of the connection is allowed; in the latter case, only shear and axial forces can be transmitted between the joined elements, thus moment of connection is always zero and there is no existing restraint for the rotation. Since experiments have revealed that the real behavior of the frame's joints is in between these extremes, many researchers suggested that they should be modelled as semi-rigid ones. In order to do so, rotational springs are attached to the ends of the elements, allowing comparison of different connections rigidity through the variation of their stiffness. In particular, the spring has zero volume but allows moment transfer. If the spring stiffness is infinite, a fixed connection is achieved with full moment transfer. If the spring stiffness is zero, a pinned connection is realized with no moment transfer. As final case, the semi rigid connection is characterized by some rotational stiffness and thus some moment is transferred. The integration of semi-rigid connections effect into size optimization analyses, mainly aimed at weight minimizations, has led to different results.

For example, one of the earliest studies here examined was illustrated by Machaly, E. S. B. in [71]. They demonstrated the advantages of using semi-rigid connections modelling in several weight-optimizations. Gables, portal frames and multi-bays three-storey frames have been optimized, using a nonlinear programming technique. During the process, I-shaped cross-sections were assumed for the columns and girders and their geometrical properties were chosen as design variables, such as the breath of flange and height of web. Both strength requirements, in terms of stresses, as well as stiffness requirements, in terms of nodal displacements, have been applied in the optimization. Side constraints, regarding physical limitations of the cross-sections and buckling considerations, have been applied too. In the reported examples, the structures have been subjected to dead and live loads. By means of the presented analysis, the authors have proven that the use of semi-rigid connection is able to provide a weight saving from 10% to almost 30%, depending on the structure considered. In particular, such material reduction can be mainly addressed to girders rather than columns. Another conclusion pointed out by the study, is that deflection was not the most stringent factor.

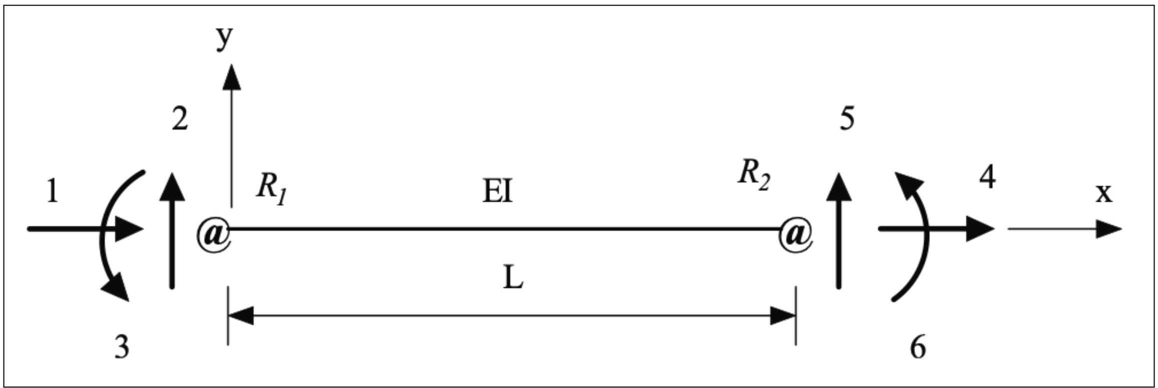


Figure 2.13: Semi-rigid member [23]

In agreement with such results, A. Csébfalvi in [23], presented a study focused on discrete minimal weight design of steel planar frames with semi-rigid beam-to-column connections through the use of a Genetic Algorithm (GA). In the optimization the design variables were chosen as the member sections. The optimization followed the recommendation of Eurocode 3 (EC3) to properly control size, displacements and stress constrains. During the procedure, the connection spring's characteristics had been allowed to vary within a defined range of spring rotational stiffness. Then, semi-rigid joints were adjusted in order to account for both displacements and internal forces distribution. By means of two examples, a simple-bay frame and a two-bay frame, it has been shown how semi-rigid connections modelling improve the design, if compared to the case of rigid or pinned connected frames. However, it's important to underline that the optimal solution highly depended on the loading condition and geometry of the structure.

Also K.A. Korkmaz and M. El-Gafy in [67], have proven that neglecting the effects of beam-to-column connection flexibility in the design would lead to unrealistic predictions of the stiffness and strength of steel structures and to heavier designs. More in details, in the proposed analysis, the target function of the optimization was the weight minimization of structures with geometric non-linear behaviour. The non-linear response had been determined by performing a pushover analysis. The constraints were applied on the stresses and displacements, while the design variables were representative of the members' cross-sections, taken from a list of available sections. Optimal design examples of 3,10 and 20-story rigid and semi rigid connected frames had been reported, pointing out that the designs with rigid connections usually involved over-stressed members and a less level of accuracy in the drift predictions. Moreover, with semi-rigid designs, weights were lower if compared to those of the rigid ones, as reported in the following figure 2.14.

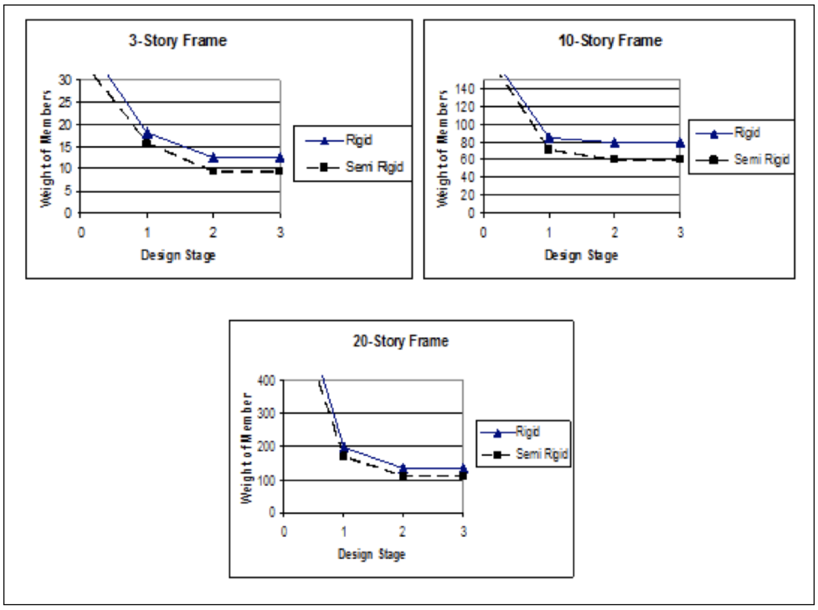


Figure 2.14: Weights comparison of rigid and semi-rigid connected 3-, 10- and 20-story steel structures [67]

Slightly different outcomes has been found by A.Elvin and J. Strydom in their paper [29]. For the purpose of optimizing tall buildings with semi-rigid connections, Elvin and Strydom (2018) created the virtual work optimization method (VWOW). VWOM is an automated method that has the objective to minimizes the weight of the structure while remaining consistent with building code standards for a particular geometry, deflection criteria, and load scenarios. Cross-sections were chosen as the design variables of the optimization, pre-arranged to satisfy strength and deflection criteria. In particular, deflection constrains were checked at critical nodes. An important passage was the determination of how any modification was affecting each critical zone. A section adjustment was considered efficient if it caused a significant decrease in deflection at all critical points for only a tiny mass increase. Moreover, when choosing members to reduce deflections, the most effective adjustments were decided using the virtual work principle. More in details, some steps have been proposed and followed by the authors during the proposed optimization problem. First, a connection stiffness was assigned in the process. Second, candidates were chosen based on their strength. Third, the member that reduced deflections with the least amount of mass increase was identified. To illustrate the method, four case studies of tall building had been presented using the VWOM. Results have shown that buildings with connection stiffnesses that were semi-rigid had either the same weight or heavier than the same structures with rigid connections, with a maximum of 6% of mass increase. This means that in heavier cases, the connection flexibility was compensated by stiffer and hence heavier members. Furthermore, the authors underlined that the cost of semi-rigidconnections is lower than in the case of rigid connections, despite the optimal mass for structures with semi-rigid connections being the same or heavier. Thus, can be concluded that the construction with an optimal price and mass are not always equivalent.

A well detailed analysis concerning the connection flexibility topic has been illustrated by A.V. Oskouei, S.S. Fard and O. Aksogan, in [86]. A genetic algorithm has been employed for the minimum weight optimization, in which the variation of the degree of rigidity of the structure has been carried out by changing the cross-sections of beams and columns. The applied constraints and restraints regarded limits of normal and combined stresses, target displacements and the number and locations of plastic hinges. To demonstrate the main differences of using rigid or semi-rigid connections, nine frames were analyzed. Dead and live loads were considered and for the seismic action the Iranian code was used. Depending on the number of stories, from three to nine, the analyzed frames were divided into three groups. For each frame, both linear static analysis and non-linear static analysis were performed, considering both rigid and semi-rigid connections. In the first group, three-story frames with one bay, two bays and three bays respectively have been investigated. From the results it can be concluded that in frames with semi-rigid connections, the period increased up to 20% and an increment in weight was experienced too, higher for the non-linear analyses. Moreover, the stiffness distribution of the connections resulted to be not uniform in the whole structure, decreasing while moving from the top to the first story. This demonstrated that lower stories are more important to provide resistance to the entire structure. However, it is important to underline that those results depended mainly on the period of the structures and on the design spectrum provided. The next six-story frames analyzed, always characterized by one bay, two bays and three bays, showed that an increase in height leads to an increase in the differences between linear and nonlinear analyses. Even though for the first group of analyses the authors found a weight increase for semi-rigid connections design with respect to the rigid connection case, for both the second and third groups of frames, the weight obtained with semi-rigid connections has been demonstrated to be lower with respect to rigidly connected structures. In particular, the weight of the nine-story frame in the linear analysis case with rigid connections had the maximum value, while the nonlinear analysis with semi-rigid connections had the minimum one. Thus summarizing, in the case of low-rise frames with low periods, where the structure was placed in the constant acceleration section of the design spectrum, the weight increased for a lower stiffness of the connections. On the contrary, the medium- to high-rise frames with long periods, lying in the lower portion of the reflection spectrum (constant velocity part of design spectrum), experienced a weight reduction by lowering the stiffness of the connections. For medium to high structures, it may be argued that employing semi-rigid connections with a nonlinear analytic approach will reduce the structure's weight and cost. However, for short structures with rigid connections, the nonlinear analytical method resulted in a more economically sound design. In any case, the non-linear approach has been proven to be more accurate than the linear one and it led to a significant reduction in the amount of resources consumed.

In contrast to the results exhibited so far, other researchers found out that semi-rigid connections affect the best frame structure design with weight increases.A simplified procedure for the analysis and optimum design of frames with rigid or flexible connections has been illustrated by Y.A. Al-Salloum and T. H. Almusallam in [2]. A volume minimization of frames was carried out by selecting the optimal design variables, chosen as the moment of inertia of the structural members. Stress and displacement constraints were applied to the members of the frame, neglecting buckling verifications. In addition, minimum and maximum values to the design variables were imposed. The elements of the frame were assumed to behave linearly, while the beam-to-column connections with non-linear behaviour. Once again connection flexibility has been modelled as rotational springs attached to the beams.

Two numerical examples have been reported to demonstrate that connection flexibility considerations would lead to heavier designs. Moreover, a further verification has been carried out to check whether or not the best solution obtained considering flexible connections was still feasible if the connections was taken as rigid, and vice versa. It has been demonstrated, for all the examples reported, that unfeasible solutions would be obtained.

A comparison between fully restrained and semi-rigid connected steel frames has been reported also by Doğan, Erkan, Soner Şeker, M. Polat Saka and Celalettin Kozanoğlu in [27]. In particular, this study presented a Hunting Search method-based optimum design algorithm for unbraced steel frames. The non-linear problem, aimed at the weight minimization, has been formulated as a size optimization, hence the W (wide-flange shape) sections of members were treated as design variables, chosen from a discrete steel section list given in LRFD-AISC (Load and Resistance Factor Design, American Institute of Steel Construction). Due to the continuum nature of the hunting search algorithm, the actual design variable considered was the ascending sequence index of the discrete sections list. The design constraints have been implemented following the specifications of AISC code, so displacement limitations, inter-storey drift restrictions of multi-storey frames, as well as strength requirements for beam-columns were considered. Additional constraints, namely geometric ones, were applied too in order to satisfy practical requirements. As design examples, the authors reported three unbraced semi-rigid steel frames, with a comparison with the case of fully restrained structures. According to the observations, since a great amount of horizontal displacement exists in the flexible connections, displacement constraints became dominant in the design, thus stronger sections has been selected. As a result, the weight of the whole structure was greater than the one designed with fully restrained connections. In addition, to demonstrate the efficiency of hunting search algorithm, the same examples were also solved with particle swarm optimizer, which has proven to be robust and efficient in the solution of structural optimization problems, but the former performed better.

Another interesting research has been illustrated by Artar, Musa, and Ayse T. Daloglu, with a further interest in the integration of concrete slabs effect on the behaviour of steel beams in the optimum design of space frames. In [9] the authors introduced the topic of concrete slab effects. Here explained the possible advantages of such considerations, if compared with simple plain steel ones, such as greater stiffness, greater bending strength, less lateral displacements and less mid-span deflection. The optimization process presented employed a Genetic Algorithm (GA) for minimum weight in which suitable standard sections from a specified list, taken from American Institute of Steel Construction (AISC), had to be selected. The stress constraints obeying AISC-LRFD (American Institute of Steel Construction - Load and Resistance Factor Design), lateral displacement constraints, with specific regard to the top and inter-storey drifts, as well as the mid-span deflection constraints for the beams were considered. In addition, the geometric constraints concerning the column-to-column depths and beam-to-column joint sizes were taken into account. Three different numerical examples, taken from the literature, has been solved considering floor beams only made of plain steel and then as composite (steel and concrete) ones. All the outcomes obtained in the study resulted to be in agreement with the ones proved by other authors. Thus, it can be stated that integration of the concrete slabs contribution on the behaviour of steel beams ended up with lighter designs. Then in [8] the same authors incorporated the just explained findings in the optimum design of steel frames with both semi-rigid beam-to-column and column bases connections. Thus, the novelty of such paper is not only in the inclusion of the previous discovery in the connections flexibility analysis, but also in the fact that semi-rigid connections were applied to both beam-to-column joints and column bases. The optimization procedure has been carried out as in the previous study, only adding column-to-column and beam-to-column geometric constraints. Three different plane frames with semi-rigid beam-to-column and column-to-base plate connections were carried out, at first considering only plain steel beams in the finite element analyses. The same optimization procedures were then repeated for the case of frames with composite beams. From the results, it can be noticed that a decrease in the rotational spring stiffness of frames increased the values of the effective length factor K and so the buckling lengths of columns, leading to the selection of larger cross-section profiles for columns. Thus, fully rigid connections promoted lighter designs. Moreover, in the optimum designs of frames with composite beams, consideration of concrete slab effects in finite element analyses significantly reduced the effective length factor of columns and maximum top storey displacements. In fact, in all three frames studied, optimum weight is decreased by about 5-8% when the effect of concrete slab on behaviour of beams is considered.

### 2.2.4 Soil-Structure Interaction

Another factor, influencing size optimizations of steel frames, that has raised interest of some researchers is related to the soil-structure interaction effects. Daloglu, Ayse, et al. in [24], have investigated such topic using metaheuristic algorithms. Three-parameter foundation model has been adopted to incorporate the effect of soil foundation on the behaviour of the frames in the optimum design process. The moduli of subgrade reaction and soil shear parameter have been calculated in terms of vertical deformation profile within subsoil. A computer program was coded in MATLAB (2009) for the optimization processes and connected to SAP2000 (2008) to perform the dedicated analysis of the frames. Both Genetic Algorithm (GA) and Harmony Search (HS) algorithm were used for the minimum weight optimization process. The steel space frames in the study have been subjected to the strength constraints of LRFD-AISC (Load and Resistance Factor Design, American Institute of Steel Construction) specifications, geometric restrictions, as well as maximum lateral displacement limitations exhibited at the top and at the inter-story drifts. Three different space frames taken from literature, for comparison purposes, has been presented: a two story, 21-member irregular space frame, a 4-storey, 84-member space frame and a 20-storey space frame system. The appropriate cross-sections, chosen as design variables, were selected from a predefined list of W-shaped sections. Results have shown that consideration of soil effects increased steel design weight of the frames.

Later on, also Fathizadeh, S.F., Vosoughi, A.R., Banan, M.R. in [31], have explored further this kind on analysis. In this paper, they have described a Performance-based design (PBD) optimization of two-dimensional moment-resisting steel frames (MRSF) that accounted for the effects of the soil-structure interaction(SSI). In particular, an engineering cluster-based genetic algorithm (ECGA) has been employed to run the optimization problem. The minimum weight of structural elements of the frame has been tackled as the objective function and cross-sectional elements profiles has been established as its design variables, taken from the W-shaped American profiles. The optimized structures needed to satisfy different constraints. Geometric limitations were applied to the column sections, meaning that the bottom cross section was assumed to be larger or at least equal to the one on top. In the connection between beam and column, weak beam–strong column constraint was assumed, regulating the amount of plastic moment in the node. In addition, strength and drift constraints were imposed, together with checks on displacements and rotation of the foundations, to control its uplift and settlement. Practical applications of the proposed methods to investigate Soil Structure Interaction (SSI) effects on the PBD Optimizations regarded six and nine-storey MRSF1D, in which different soil types were treated, from very stiff to very loose soil. The influence of different soil typologies on the ideal design of MRSF were investigated, along with their impact on the development of plastic hinges, vertical displacement of foundations, structural period and damping. Results shave shown that with decreasing stiffness of the soil under the MRSF, stronger cross-sections should be selected, which increased the total optimum weight of the frame. Weight of the frame on a type IV soil (loose soil) has been increased of 12.94% in comparison to a frame with fixed foundation. As final example of soil-structure interaction research, we report the multi-objective study carried out by Dehghani, S., A. R. Vosoughi, and Mo R. Banan in [25]. A cluster-based non-dominated sorting genetic algorithm (NSGA II) has been introduced to study the effects of the rehabilitation objectives on multi-objective design optimization of two-dimensional steel X-braced frames, considering soil-structure interaction. The target functions taken into considerations were weight minimization and maximum storey drift minimization. The cross sections of grouped elements of the frames were considered as the discontinuous design variables of the optimization. Geometric constraints have been applied on the cross-sections of columns, as in the precedent paper, such that the bottom columns should be thicker or at least equal to the upper ones. Resistance constraints, in terms of stresses and moments, have been applied under gravity loads, while under serviceability loads, they have been expressed in terms of displacements. Then also resistance constraints for the nonlinear static analysis have been taken into account, according to which shear and axial force limitations had to be verified. Moreover, during the optimization process, rotations and displacements of columns, beams and braces had to be under certain limits. As in the previous study, rotations and displacements of the foundation were checked at three performance levels, such as immediate occupancy (IO), life safety (LS) and collapse prevention (CP). On the other hand, to study the effects of soil- interaction, the substructure method has been employed, according to the procedure of FEMA356 (Federal Emergency Management Agency- Prestandard and commentary for the seismic rehabilitation of buildings) and ATC40 (Applied technology council -Seismic evaluation and retrofit of concrete buildings). The efficiency and accuracy of the proposed method has been demonstrated by way of different examples of frame structures. An important conclusion from this research, in agreement with the previous studies, is that by softening the soil under the frame, minimum weight of the frame has been increased.

### 2.2.5 Large roof structures and multi-bays, multi-storey frames

In this last section we have collected all the articles concerning the application of size optimization on large spans structures and large multi-storeys, multi-bays frames, not mentioned until now.

An interesting research has been proposed by Scholz, H., and G. Faller in [103]. It has been described the computerization of the interaction method, developed by Scholz, applied on a storey-by-storey basis, from top to base, of large multi-storey frames. The goal of the optimization was to obtain a value of the storey failure load factor within a specified range. In the procedure, at first a simplified method has been used to obtain trial member sizes for the whole structure. Then the structure has been analysed using the programmed interaction method. This analysis was carried out in order to obtain the elastic-plastic failure load of each storey, whose members later have been adjusted if the failure load was not within its acceptable threshold limits. In the examples reported to demonstrate the validity of the proposed method, the frame's members was chosen among the American standard sections and the loads applied on the structure were simply the gravity ones, multiplied by given design load factors. Results have shown a good agreement between the proposed method and the rigorous elastic-plastic second-order analysis. It has been argued that the technique can greatly reduce analysis time as well as simplify the optimization of members in the design of such frames.

Later on, multi-bay and multi-storey steel frames have been optimized, in a three-steps numerical procedure, by Thevendran, V., NC Das Gupta, and G. H. Tan. in [111]. Volume minimization has been developed in the optimization, where I-shaped sections have been chosen as design variables, taken from a list of available steel sections. The peculiarity of such analysis was that at the beginning the design variables were considered continuous and then, from the obtained results, the members' cross sections were selected from the database. In fact, in the first stage, both columns and beams have been treated as continuous variables, in the second stage only columns have been approximated with the available sections and finally, in the third stage, also beams sections have been converted into the real ones. The frame was finally re-analysed to check whether any design criteria have been violated. In particular, the frame structure, subjected to dead, live and wind loads, have been designed considering beams' maximum deflection and both shear and moment capacities requirements, as well as stresses and buckling verifications for columns. Moreover, the horizontal deflection of the structure has been checked, along with geometric constraints referred to limiting bounds of the cross-sectional areas and to the variation of columns sizes with levels. The simplicity of the procedure has been shown in a number of examples of such structures.

For industrial, commercial, and leisure buildings, single-story frame structures, also known as large span portal-frames, are frequently employed. Such buildings require the design of a structural system that can cover wide regions without requiring intermediary columns. Moreover, since steel offers a cost-effective alternative, the majority of these buildings are made of it. Pitched roof steel frames belongs to that category of single-story frame and its design has been the subject of M.P. Saka's studies since 2003, with the paper [101].

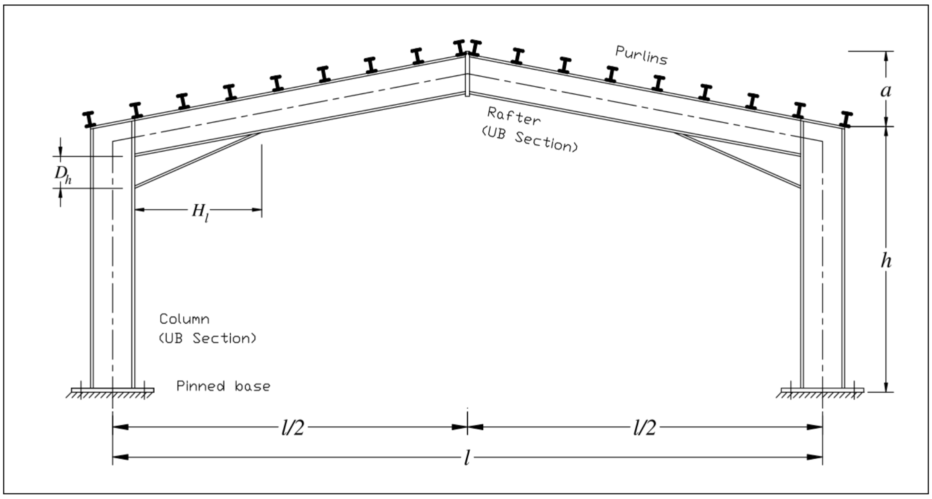


Figure 2.15: Typical pitched roof steel frame with haunched rafters [101]

Although the design of pitched roof steel frames has been compared to simple one-story buildings, it nevertheless had to take into account a number of difficult issues. Design variables, considered to proceed with the optimization, were rafters and columns sections, chosen from the standard universal beam sections set, and depth and length of the haunches. Regarding the design variables, it is important to underline that it is standard practice to use the same universal beam section for both rafters and use other cross section for stanchions, when designing steel portal frames.

Additionally, for economicreasons, the haunches were made from the same section as the rafters. The minimum weight design of the frame was taken as the Objective Function of the problem and different constraints were considered. First, due to serviceability requirements, the horizontal displacement of a column due to unfactored imposed and wind loads was limited to height of the column/300. Similarly, the constraints have restricted the deflection of a beam to its span/360 if it have been carried plaster or other brittle finish. In addition, local capacity check for beam and column with semi-compact or slender cross-section needed to be properly verified against bending and compression(buckling). A genetic algorithm was exploited to find the optimum design and an exterior penalty function was considered during the iterations. To illustrate the procedure, a practical example was reported regarding a frame with 20 meters span and 5 meters in height. Results have revealed that while the displacement and strength constraints didn't approach their upper bounds in the final design, the lateral torsional buckling have reached the allowable value. This had an impact on the ideal depth and length of the haunch among the iterations.
In 2014, McKinstray, R., Lim, J.B.P., Tanyimboh, T.T., Phan, D.T., Sha, W. in [74], focused their attention on the design of large span portal frames with fabricated beams. Fabricated beams were used, in contrast with the most common hot-rolled steel sections for column and rafter members, for weight reduction purposes. In particular, the advantage of employing fabricated steel beams, over the hot-rolled steel section, relies mainly on the maximum span achievable. In fact, using the latter ones, spans can reach only 50 m, while 100m can be achieved by employing the former ones. Fabricated beams were built-up through the welding of steel plates. The dimensions of steel plates were the considered design variables of the optimization. With more details, discrete design variables were adopted for the thickness of the steel plate used to for the web and flange, while continuous design variable for breadth and depth of the section. The overall design optimization goal was to find the portal frame with the least amount material for the main members, while satisfying the design specifications. Columns, rafters and haunches were considered as primary members of the structure and their weight was used to define the objective function. Both ultimate and serviceability limit states were included in the optimization, adopting deflection limits, recommended by the Steel Construction Institute (SCI), and accounting also for the buckling stability of the sections. To optimize the size of the plates used for the columns, rafters, and haunches, a genetic algorithm (GA) was used. For practical purposes, three different frames have been

considered with different spans (40 to 60 meters) and different heights (10 to 12 meters). In order to make a comparison, each of the previously introduced frames were designed and analyzed with both universal beams (UB) and fabricated beams. Four types of UB have been examined, each of which with a different number of design variables, concerning column, rafter and haunch sections, as well as haunch length. Instead, for the fabricated beams cases, the design variables were chosen between height, breadth and thickness of column, haunch, web, flange and rafter. Moreover, in this case they could vary according to geometric constraints. Interesting considerations can be drawn from the results, beginning with an achievable weight saving of 15% in frame weight for large span frames ($> 40$ m). Instead, fabricated beams will be ill-advised for small frames where savings were minimum.

In the design of large span portal-frames, the large span and elements slenderness make them very sensitive to applied loads, especially wind loading. Regarding this last aspect an interesting approach is given by Fu J.Y., Wu, J.R. Dong, C.C. Xu, A. Pi Y.-L. in [33]. In this research, long span portal frames with inclined roofs were designed when subjected to dynamic loads, particularly wind loading. The evaluation of the wind loading on inclined roof was more complex than ordinary rectangular buildings. To overcome these limitations, the load imposed by the wind was evaluated as an Equivalent Wind static Loading (EWSL) by means of Gust Loading Factor (GLF), Load Response Correlation (LRC) and Proper Orthogonal Decomposition (POD) method. Basically, those methods allowed to transform the dynamic loading induced by the wind into a linear static pressure. The objective function was the minimization of the structural weight of all the elements in the portal steel frame, while the design variables were the tapered sections. Sizes needed to be determined for several components of the tapered section, including the web's thickness and height as well as the flanges' width and thickness. Constraints of the optimization problem were based on the drift induced by wind pressure, with particular attention to displacements at the top of columns and vertical displacement at the mid-span of the rafters. In the examples reported, the main focus was on the effects of different combinations of EWSL, on the stiffness of elastic rotational restraints at supports and on the stiffness of semi-rigid connections between rafters and columns. It has been demonstrated that the optimized weight was generally reduced with an increase of the stiffness of both column support and the semi-rigid raft-column connection. The GLF technique yielded the highest optimal weight for ESWLs.

The same type of structure has been analysed also by Kaveh, Ali, Mohammad Zaman Kabir, and Mahdi Bohlool in [62]. In particular, a comparison of different metaheuristic algorithms has been proposed for two different multi-span pitched roof frames with tapered members. Moreover, in the analysis, the apex height of the structures has been investigated, in order to find the best design with minimum weight. The I-shape of the cross-sections of beams and columns was assumed, and specifically, the height and the thickness of the web together with the tapered length ratio have been chosen as design variables in the optimization. Their values was allowed to vary between feasible discrete ranges, as reported in the paper.

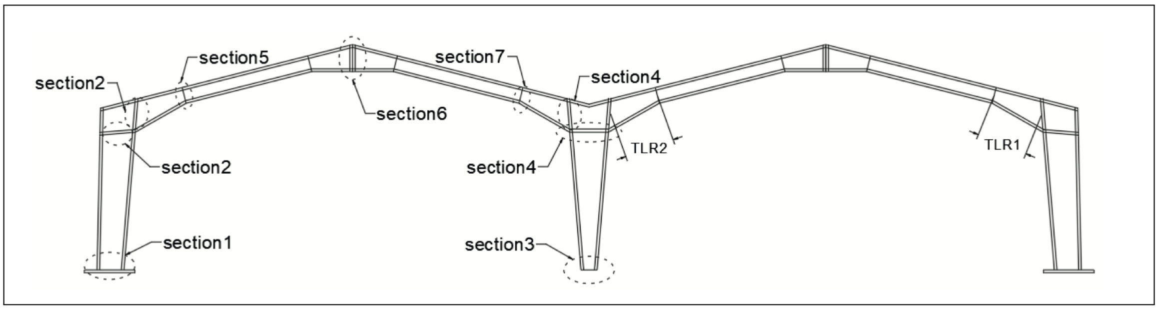


Figure 2.16: Variables of the 2-span frame [62]

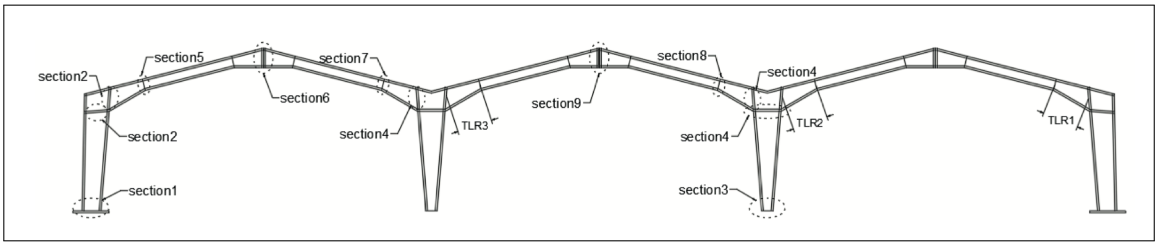


Figure 2.17: Variables of the 3-span frame [62]

The structures under study have been subjected to the load combinations specified in the ASCE7 code (Minimum Design Loads and Associated Criteria for Buildings and Other Structures), in which dead, earthquake, wind, snow and roof live loads were considered. The constraints were applied on the strength of structural members, subjected to compression axial forces and bending. Moreover, displacement limits were imposed, depending on the loading cases, and construction criteria were applied to horizontal and vertical elements of the structure. The optimization algorithms used in the analysis were the following ones: Teaching-Learning Based Optimization, Colliding Bodies Optimization, Enhanced Colliding Bodies Optimization, Vibrating Particles System and Harmony Search. MATLAB software has been used for the algorithm implementation, while SAP200 for the modelling, structural analysis and design of the structures. From the optimization of the two-spans roof frame, the performance of all algorithms resulted to be appropriate, while for the three-spans roof frame, ECBO algorithm has been demonstrated to be the best one. In both examples, the diagram representing the optimized weight as a function of the roof angle has shown that the best weight can be achieved by employing the minimum angle.

Another comparison between metaheuristic algorithms have been depicted by Kaveh, A., Biabani Hamedani, K., Milad Hosseini, S., Bakhshpoori, T., in [61] for multi-storeys and multi-bays structures. Seven population-based meta-heuristic algorithms have been used to optimize the size of two-dimensional steel frame structures. The optimization was aimed at minimizing the weight of rigid-jointed steel frame structures while satisfying some requirements on stress and displacements, according to AISC and Load resistance Factor (LRFD). Minimum weight design has been obtained by selecting appropriate cross-section from a catalogue containing 267 W-shaped section. The well-known penalty approach has been used to handle the constraints of the optimization problem. Specifically, the parameters considered in the penalty were related to the total amount of the constraint that was violated and two constant parameters that had to be properly set in order to achieve a good balance between the intensification and diversification of the algorithm. Three benchmark frame structures have been analyzed, which have a number of story varying from 10 to 24 and 1 or 3 number of bays. Optimized frames have been examined considering Artificial Bee Colony (ABC), Big-Bang Crunch (BBC), Cyclical Parthenogenesis Algorithm (CPA), Cuckoo Search (CS), Thermal Exchange Optimization (TEO), Teaching-Learning-Based Optimization (TLBO), and Water Evaporation Optimization (WEO) metaheuristics techniques. The results of the optimization showed that WEO, CS, and TEO algorithms performed better in terms of the best weight, average weight, and standard deviation on average weight, according to a close examination of the optimization results. In addition, TEO, TLBO, and WEO have exhibited faster convergence rates than other examined algorithms, as shown by convergence curves.

## 2.3 Topology optimization

Topology optimization is a relatively new but rapidly growing area of study, with interesting theoretical implications in many areas of engineering, mathematics, mechanics, multi-physics, and computer science [96]. It has also significant practical applications in the manufacturing sector, particularly in the automotive and aerospace fields, and it is likely to play a significant role in micro-and nanotechnologies. Focusing on the structural design field, topology optimization has been referred to as "an intellectual sparring partner" at the preliminary conceptual design stage (Bendse and Sigmund, 2003). The talented Australian inventor Michell, who developed optimality criteria for the least-weight truss arrangement, wrote the first article on topology optimization more than a century ago (1904). In structural optimization problems, topology optimization can be defined as a design tool which determines the location of the material in a design domain, based on the loads and boundary conditions for a specific objective, i.e. target deflection, compliance, minimum weight design etc. Following this approach, the finite element method (FEM) is applied by splitting a design domain into several small pieces, known as finite elements. Each piece contribute to the creation of the overall structure by having a density that is either solid (black) or empty(white), similar to a pixel in a picture. As shown in the following figure starting from an initial structure with full density material subjected to a concentrated force and specific boundary condition, after the optimization unnecessary material will be removed, as shown in figure 2.18.

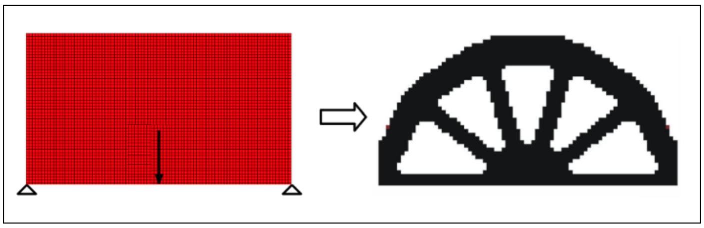

Figure 2.18: Initial design with no voids and final optimized topology design [107]

Topology optimization is generally employed in the conceptual design phase of a high-rise building, in which the main focus is related to the overall stiffness/drift requirements under lateral loads. Therefore, many of the decisions made during this process are related to defining the lateral system that allow to reach an optimal structural design to satisfy certain conditions. The balance between engineering and architecture is another issue that frequently affects the topology optimization industry today. Traditionally, an architect's focus is more on the aesthetics, or "form," of a structure, whereas an engineer's target concerns stability and efficiency, or "function", of the structure [15]. To overcome those conflicting goals, for example, we can think to add some architectural constraints during the optimization process, as reported in figure 2.19.

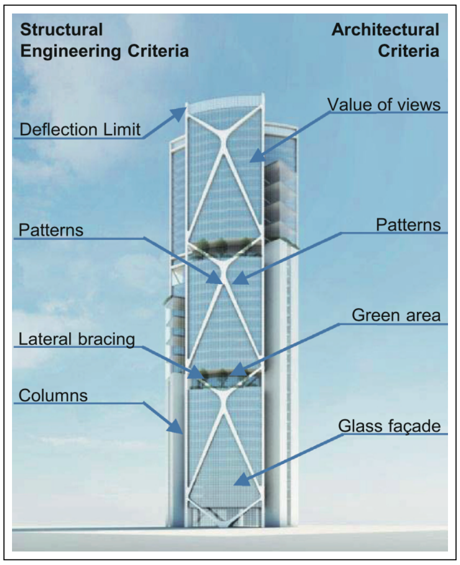


Figure 2.19: Optimized building topology considering both engineering and architectural aspects [15]

Mark J.Jakiela, ColinChapman, JamesDuda, Adenike Adewuya, KazuhiroSaitou, in [53] presented the Genetic Algorithm(GA) for structural topology optimization, through the use of example and reviews. By applying this algorithm, the design domain has been discretized into small rectangular elements, as said before, representative of the presence of material or void by means of a specific code number (respectively number 1 and 0). In this way, the topology has been defined, so the next step was its structural verification through a finite element analysis. Then the fitness of each chromosome, thus of each topology, was computed as a function of the stiffness value, determined as the inverse of the displacement. In fact, the Objective Function was aimed at the minimization of the structure's compliance, by finding the optimal configuration of material and voids within the design, while stress and displacement constraints were applied. An example related to a cantilever plate subjected to vertical load has been provided and discussed.
A classical approach to topology optimization was provided also by Pan Jin; Wang De-yu in 2006, with [88] in which truss structures with 12, 20 and 72 bars were

analyzed using Adaptative Genetic Algorithm(AGA). The objective function of the optimization problem was a minimization of the truss structural weight, when subjected to frequency domain excitations. Minimum weight was achieved by removing extra bars and nodes, classified as removable and non-removable.

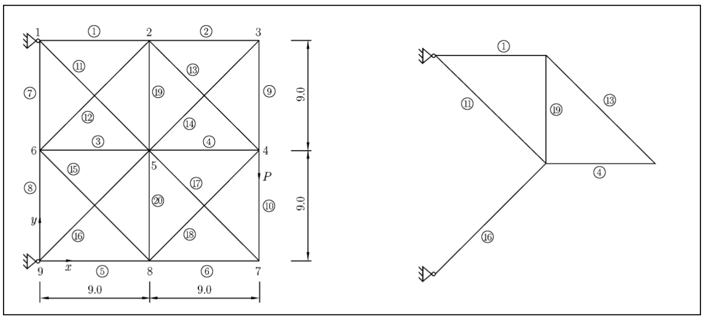

Figure 2.20: Initial truss topology design and final design optimized truss topology after removing extra bars and nodes [88]

The analyzed truss structure was subjected to three kinds of constraints: fundamental frequency, displacement responses and acceleration responses in the frequency domain. Maximum amplitude of displacements and frequency acceleration response had to be lower with respect to an upper bound limit. Those types of constraints have been evaluated from the structural vibration equation, based on finite element method, in which mass, damping and stiffness matrix of the structure needed to be known. Moreover, to obtain the accurate natural frequencies and dynamic responses, it was necessary to renumber every bar and node in the structure and rebuilt the stiffness and mass matrices when some bars or nodes were removed. Running the optimization problem, it is important to underline that AGA could only be applied to maximum unconstrained optimization problems. However, structural topology optimization problems often need considerations of some restrictions and request the objective function to be minimized. Therefore, some handling had to be done to transform the original optimization problems into a form suitable for the genetic algorithm to solve. To overcome this issue, the proposed methodology applied the penalty function method. Such method punished the individuals that violate the optimization constraints, by introducing a penalty into the fitness function. The examples reported in the paper have shown the efficiency of AGA procedure for ground structures, providing a lightest feasible optimized design compared with the original one.

Another important topic addressed in topology optimization techniques deals with the design of conventional moment-resisting steel frames. This type of structure as is well-known, exhibits a good behavior under gravity-induced forces. However, the structure is likely to be ineffective in self-resisting lateral forces promoted by wind and/or earthquake actions. The use of a hybrid system that integrates cross braces to the moment-resisting frames is widely accepted for its cost-efficient and safe performance. Due to that, founding an optimal bracings position is one of the most treated issues in this field. From the studies in 1988 of Bendsøe and Kikuch, topology optimization has been pursued for the design of brace configurations. Cross bracings designs, especially when the braces are added afterward as part of a retrofitting scheme, traditionally use a simple trial-and-error procedure, with the overall goal of minimizing the distance between the floor's mass and stiffness centers and ensuring that the lateral resisting system has a workable load path. A more systematic approach is to set up and solve an optimization problem that automatically computes optimal brace layout and sizes while satisfying the safety of the targeted structural performance.

In the research [99] proposed by D. Safari; Mahmoud R. Maheri a straightforward Genetic Algorithm was used to perform topology optimization of steel braces in 2D steel frames. In this paper, the optimal position of X-braces was explored, with the objective to reduce the weight of steel used in the 2D frame-brace system. The constraints related to the problem included: total drift of the frame, column uplift force, number of braced panel and architectural limitations. Focusing on the latter, it involved limits on the allowable bracing, restricted to some bays only. For example, in the case of the three-bays structure, bracing was first allowed in the two right hand bays and then only in the outer bays. Different examples related to 2D frames, having different numbers of storeys and bays, have shown the efficiency of the proposed algorithm. In fact, over 5% reduction in weight and 8% reduction in drift were achieved by GA topology optimization when compared with conventional frames, in which brace location was admissible horizontal along the same bay or in vertical along the same storey.

Always in the topology optimization environment, since in recent years seismic rehabilitation for existing buildings has been an increasingly important issue, studies on brace systems have been emphasized due to their applicability and effectiveness as reinforcing structure techniques.

An interesting research, targeting seismic assessment of steel frames using braces, was provided by Shengfang Qiao, Xiaolei Han,Kemin Zhou, Jing Ji [94]. This study has been focused on the seismic analysis of steel frame structures with brace configuration, using topology optimization based on truss-like material model. Zhou and Li in 2005 have introduced such method for continuum topology optimizations, which has been further investigated by Zhou and Chen in 2014, by considering natural frequency constraints. In the present paper, the truss-like model has been applied by considering stress constraints and both earthquake and wind loads. Initial truss-like members were used to fill the design domain for topology optimization, based on the original steel frame structure. The final layout of the least-weight structure was obtained by applying a fully-stress criterion and by considering as design variables, in the finite element analysis, both the density and orientation of the truss-like members. The optimized structure obtained by Zhou and Chang in 2014, referred to a 10-storey 2D frame, has been repeated in order to see how the brace configuration could be improved in order not to have braces in the middle of columns but instead in the middle of beams. Thus, the new arrangement was created with diagonal braces or inverted "V" braces. Then engineering requirements about the building function have been considered, further enhancing the optimal brace configuration. To reinforce the advantage of the proposed optimized structure, a comparison with two common optimized brace configurations under different earthquakes intensity was done. Common brace configurations were characterized by “V” brace and single bar brace that were placed vertically along the same bays, a practical example is reported below 2.21.

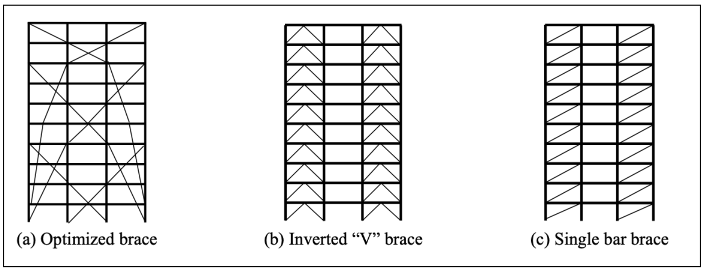


Figure 2.21: Possible braces configuration [94]

Running the analysis for different earthquake intensities, the authors stated that the inverted ‘V’ brace was more acceptable than the single-bar brace when span was twice the storey height. Moreover, in the comparison, two important quantities in seismic design were analyzed: story-drift and first period of the structure. Results have shown that the first period of the optimized structure was reduced by 51.4% with respect the original frame without brace, while around 45% was the reduction of common brace configuration with respect the original one. Regarding the drift, an average reduction of 56.69 among the 10 storeys was obtained, in comparison of 50% average reduction of common braces.

An alternative lateral resisting solution to the common brace system are the Steel plate shear walls (SPSW) described in the paper [12] of Mohammad Hadi Bagherinejadand Abbas Haghollahi. In recent decades, the efficacy of steel plate shear walls (SPSW) as lateral resistance solutions has been proved, even in comparison with brace systems or RC shear walls. In fact, they are characterized by large energy dissipation capability, a stable hysteric behavior along with considerably light and thin configurations, which ensure rapidity in the erection and suitability for seismic retrofitting. In this paper, topology optimization has been exploited to find a new configuration for the perforated steel plate shear wall (PSPSW) based on the maximization of reaction forces as the objective function. Reaction forces were evaluated at fixed nodes when the plate was subjected to a lateral monotonically increased load. The optimization was performed considering an infilled plate using a nonlinear analysis, so geometry and material were taken in account to model the plate under study. As result, the final area of the optimized plate was equal to 50% of the infilled plate. In this optimization analysis, topology optimization could be divided into two parts: the first one was focused on the skeletal or truss structures that had a discontinuous nature, while in the second continuous environment has been considered, with a high volumetric ratio. In fact, in the first discontinuous phase, the volume of the consumed material was very low in relation to the total volume of the structure (problems with a low volumetric ratio), in contrast with the second phase conditions. Moreover, the sensitivity-based method which is a general algorithm that could be used for structural and non-structural problems with large scale. In the sensitivity analysis, the density (design variables) of all elements has been reduced to the predicted volume fraction. In the next step, the FE analysis was done and based on the objective function, the effective elements were recognized using sensitivity analysis. The effective elements had to be retained while the others eliminated. Actually, no element was eliminated, but its density has been decreased to a minimum value set to 0.001, because otherwise in each iteration, the mesh had to be renewed with a very time- consuming procedure. On the other hand, the density of the element could not be equal to zero because it would have caused a singularity in the problem-solving. Finally, another application of topology optimization can be related to optimal location of the connections inside the structure.

This topic was treated by the authors Baghdadi, Abtin and Heristchian, Mahmoud and Kloft, Harald in [11]. The connection placement strategy, also known as the connections-placements approach(CAP), was the subject of this article, which focuses on improving the position of connections in prefabricated buildings. Elements forces and connections properties were evaluated in order to define the optimum type and location of the connections. The methods needs to follow different steps, first of all the results of a structural analysis of the building need to be done and the forces and connections properties should be known. Next a mechanical coefficients was assigned to each connections, after testing the connections under axial, shear and bending forces. Weighted-Indicator-Function was then introduced and it calculates the amount of forces(M,N,T) and the performance of the each connections of the buildings. The minimum amount of WIF indicates the optimal position of the connection under different load combinations. Once defined the optimal locations, also the type of connection based on a set of avalaible and minimum value of WIF, was properly defined.

### 2.3.1 Size and Topology Optimization

In this section all the studies that combined size and topology techniques for structural optimizations have been collected.
A first example was reported by Saka, M. P. with the article [100] in which presented an algorithm for the optimum design of steel frames, studied with both fixed or pinned supports, as well as with and without bracing systems. At first a simple size optimization has been accounted, in which the topic of more or less flexible supports was explored. Then, considering a specific condition, bracing configurations have been analysed in order to find the optimal arrangement. The objective function to be minimized was the weight of the structure, while at first the cross-sectional areas of members have been treated as design variables. In the process, the optimum value of the design parameter was chosen as the one related to the most severe between displacements constraints, combined stress constraints and minimum size constraints. The examples reported for simple portal frames, subjected to a distributed vertical load and an horizontal force, have shown that, with specific regard to pin supports static scheme, displacement limitations were dominant, while fixed-supported frames were governed by the combined stress constraints. Moreover, in the second case the final design was lighter. Then, when the effect of

bracing has been investigated in pin-ended portal frames, the resulting weight was further reduced. Also pitched roof frame examples have been reported, where the structure subjected to distributed vertical loads have been studied with different support conditions, fixed and pinned ones, with and without bracing and, lastly, with the application of an horizontal force too. In the simple vertical load configuration, fixed supports showed lighter weights, but the best design was found with pinned supports and a bracing bar between the eaves. The same conclusions cannot be made with the second load configuration, where the best design was obtained with fixed supports and without bracing. In any case, the dominant constraint was the one regarding the combined stresses. Finally, also multi-storey and multi-bays frames have been analysed, which led to the conclusion that rigidly jointed frames yielded lighter design if they were only subjected to vertical loads. However, in the presence of lateral loads too, frames with simple beam-column connections and bracing produced better designs.

As we have seen in the chapter of size optimization under seismic loadings, addressing the topic of uniform distribution of certain structural properties, an application of such study has been conducted for a simultaneous size and topology procedures by Hajirasouliha I., Pilakoutas, K., Moghaddam, H. [44]. They proposed an efficient method to design nonlinear truss-like structures, subjected to seismic load, in which the objective was to obtain a minimum weight truss by shifting material from strong parts to weak parts, until a uniform distribution of deformation demands was reached. In fact, during strong earthquakes, some structural elements' deformation requirements do not fully utilize the allowable level of seismic capacity; therefore, if the strength of these underused elements was reduced, a status of uniform deformation could be reached, maximizing the dissipation of seismic energy and fully utilizing the material capacity. Assuming that the cost of a member is proportional to its material weight, the least-cost design was interpreted as the least-weight design of the structure. Moreover, indirect considerations about the joints cost have been accounted by the fact that as the algorithm decreased the number of elements, the number of joints was minimized too, thus their overall expense. The minimum cost was achieved by considering as design variables the cross-section areas, specifically their material density and length, while constraints on element buckling and target ductility of each structural member had to be satisfied. The algorithm started from a ground structure with all possible connection members between nodes. Then nodes that was carrying external loads or that was needed to support the truss structure have been maintained in the design, while the ones used just for load sharing have been excluded. In the next step, based on the design load applied, the maximum ductility of each structural member has been computed and iterations proceeded until the maximum ductility demand of all truss elements reached the target ductility. Basically, if the calculated ductility demands were close enough to the target value, the optimization stopped, otherwise inefficient material was reduced. The assumption that the uniform deformation demand led to the full exploitation of material capacity has been previously demonstrated by other studies, such as Hajirasouliha I, Moghaddam H. [43] and Moghaddam H, Hajirasouliha I. [77]. Based on the results of the presented study, the concept of uniform deformation can be used efficiently for topology optimization of nonlinear truss structures subjected to gravity loads and seismic excitations. It has been demonstrated that there is a unique optimum distribution of structural properties, which is independent of the initial cross-sectional area of the ground structure. Moreover, this method was dependent on the variation of target ductility demand, meaning that a fixed arrangement of truss members cannot be appropriate for different performance levels.

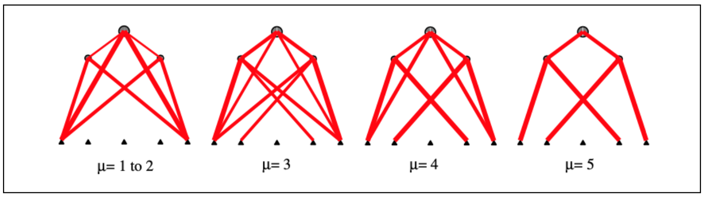


Figure 2.22: Optimum optimized design in fuction of different ductility demands [44]

Additionally, it has shown that using conventional optimization methods based on elastic behavior and equivalent static loads could lead to heavier design, up to an increase of 60% compared to the non-linear dynamic model. It was concluded that non-linear dynamic behavior of truss structures should be considered in the optimum topology design of trusses subjected to seismic excitations. One year later, an application of size and topology optimization has been conducted to model braced frames in lateral design of high-rise buildings, developed by Lauren L. Stromberg, Alessandro Beghini, William F. Baker, Glaucio H. Paulino in [106]. Braced frames have been used in several noteworthy buildings like the John Hancock Center (Chicago, IL), Broadgate Tower (London, UK) and Bank of China Tower (Hong Kong), a picture of the building is reported in figure 2.23.

The design of such systems is traditionally based on diagonal braces arranged to 45°

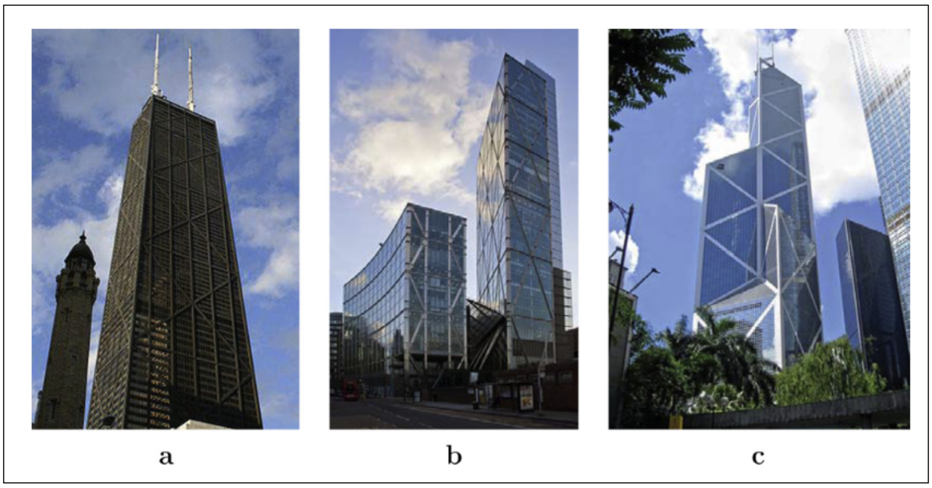


Figure 2.23: Existing buildings featuring remarkable braced frame systems: (a) John Hancock Center in Chicago, IL, (b) Broadgate Tower in London, UK, and (c) Bank of China Tower in Hong Kong . [106]

to 60° angle. In this research, size and topology optimization have been combined to derive the optimal bracing layout of 2D high-rise frames. The energy method in conjunction with the principle of virtual work has been employed in the size optimization. During the process the cross-sectional area of the elements has been changed until the optimal configuration of beams and columns was found, while only gravitational loads were applied. Constraints on maximum allowable material that can be used and maximum stress in structural elements had to be properly checked among the iterations. The structural system was modeled using beam elements and quadrilateral elements(Q4); Q4 represent the region enclosed by two columns and two beams. Beam elements, used for beam and columns, consists of six degrees of freedom (two translation and rotational at each node). While four-node bilinear quadrilateral elements have eight degrees of freedom (two translations per node). To effectively connect the finite elements, the interaction between the rotational and translational degrees of freedom must be considered. Two types of design were explained, where in the first one, beam consisted of simply connecting the beam ends to the extreme corners of the quadrilateral mesh. Thus, the end rotation of the beam had no influence on the quadrilateral finite elements because the rotational degree of freedom was decoupled and all the interior nodes along the length of the beam were free to move independently of the quadrilateral node translations. In the second design case, beams were discretized into beam elements with nodes co-incident with the nodes of the quadrilateral mesh. Consequently, the translational degrees of freedom of both beam and quadrilateral elements were shared throughout the beam's length. Thus, the quadrilateral elements have been constrained to move jointly with the beam elements when the frame deformed.

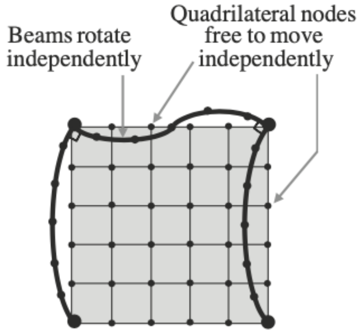


Figure 2.24: Beam free to move

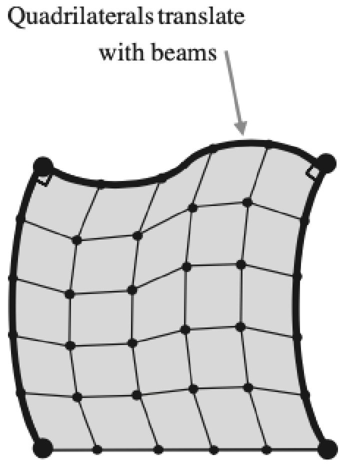


Figure 2.25: Beam and quadrilateral nodes move together

An interesting observation that can be derived from the design example is that minimum compliance led to constant stresses, which was the condition of optimality.
As stated in the section 2.3, retrofitting and rehabilitation of existing building is employed following topology optimization approach in order to find optimal brace locations. Moreover in some studies also the cross section of the braces are considered as a design variable, alongside with brace positions, in order to reduce the amount of volume.
In the paper [109] Tangaramvong and F. Tin-Loi in 2015, presented a mathematical programming–based approach for optimal retrofitting of steel structures with braces, subjected to some system performance criteria. The aim was to ensure the safety of the post-retrofitted structures under applied forces and limited displacement conditions. In the present study, three distinct optimization cases have been addressed, in which the inclusion of non-linear elastoplastic constitutive behavior of materials, considered as traditional complementary constraint, made the optimization problem nonconvex and non-smooth. For all three cases, the objective function was the minimum volume design of braces, while for the last analysis, also the minimization of the number of braces has been accounted. Displacement constraints were applied in all the analyses, whose value has been restricted within a limiting range. The authors started the optimization problem by considering a simple ground structure

concept, in which all possible braces were first generated between direct neighboring predefined nodes within a rehabilitation domain. Once the simple ground structure was known, brace members during the optimization procedure was then retained (non zero brace areas) or eliminated (zero braces area). For all design cases, the structural performance of the repaired structures has been ensured and validated through comparisons with the corresponding exact elastoplastic responses. Specifically, the outcomes of the study have shown that the first practical example provided the least volume, which however resulted to be unpractical because a large number of sections were excessively small. Improvements in the design were obtained for the intermediate analysis, at the cost of larger computational time. Finally, the authors have considered the case with a limitation on the number of braces with the most realistic cost-effective design strategy because it have been incorporated not only the material-related costs but also brace fabrication and erection expenses.

Finally, another contribution to retrofitting of existing frame structure was carried out by Devices Apostolakis with his paper [5]. The goal of this paper is to present an evolutionary computational framework that integrates hierarchical multiscale mega bracing architecture for the seismic design of both regular and irregular three-dimensional multistory structures. Particularly, two steel three-dimensional buildings with moment resisting frame an 8-story irregular and a 14-story regular one is taken into consideration and retrofitted with friction dampers. Friction dampers are added to the structure to improve its seismic performance; in reality, by adding more damping, it absorb some of the seismic energy that is induced in the building. The evaluation criteria used in this paper are based on story drifts and absolute accelerations at each floor. It is possible to build an objective function using relative or predetermined performance target level. In the former, the objective function can be expressed in terms of the ratio of the story drift and absolute acceleration between the un-retrofitted structure and the structure retrofitted with damping devices. In the latter, the objective function can be expressed in terms of the ratio of the previous criteria between the retrofitted structures and prescribed performance target levels. By selecting the latter approach, the objective function of the structure is expressed as the ratio between the maximum and allowable floor displacement plus the same ratio but in terms of floor accelerations. Moreover, in the expression of the OF also a penalty is added, that takes in account the number of X-braces used. The value of the OF is then found for different earthquake and the overall objective function value assigned to the structure is the minimum obtained.

Design variable of the evolutionary framework are the parameters that characterize the frictions dampers: multiscale configuration, or rather “V, inverted “V”, “X” and diagonal braces, section area and slip force. For the design applications presented in this paper, the 25 ground motions with 5% probability of exceedance in 50 years were used as the seismic environment. Three design scenarios were considered for practical applications, the difference was the brace configuration that were allowed to be used, varying from all possible choices to a limitation on X-brace configuration.

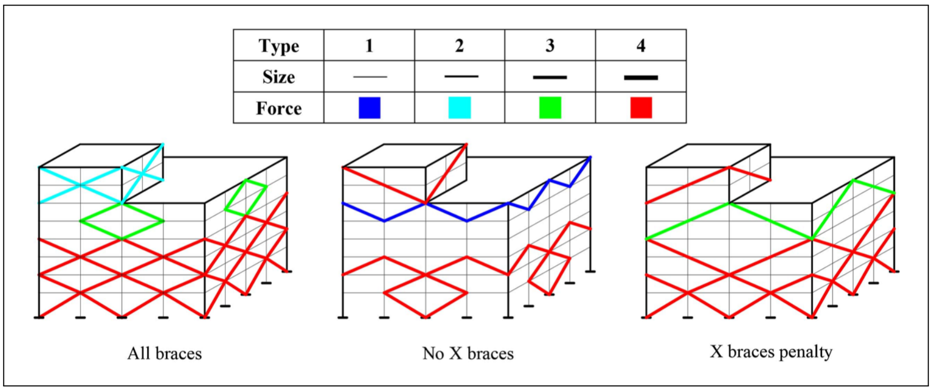


Figure 2.26: Optimal megabrace topologies for the 8-story irregular structure

The ideal design for the 8-story irregular building has the maximum interstory lateral stiffness and slip force values at the bottom levels and gradually decreasing values as you climb the stories. For the 14-story structure, the best designs for all scenarios, however, preferred a layered architecture with vacant stories first, followed by stories with fitted dampening devices.

Duoc T. Phan, James B. P:, Lim Tiku T. Tanymboh, Wei Sha, in [91] explored the performance of combined size and topology optimization for a slightly different type of application. The case study presented is related to low-rise commercial, light industrial, and agricultural buildings made of cold-formed steel portal frames, previously introduced in 2.2.5. This type of construction has been proven to be a competitive alternative to traditional hot-rolled steel portal frames for structures with moderate spans, up to 20 m. Cold-formed sections are lighter than hot-rolled ones, making it possible for semi-skilled workers to bolt and erect the structural members on site without the use of a crane. As a result, the erection costs were significantly lowered if compared to those of hot-rolled steel portal frames, highlighting the importance of this research. Therefore, the authors proposed a combination of size and topology optimizations applied to cold-formed steel portal frame buildings through the use of areal-coded Genetic Algorithm (RC-GA). In place of earlier

GAs, which were known for their slow convergence and lengthy computation times, RC-GA has been employed. A niching technique, that effectively increases the dissimilarity of the solutions in each generation, has been described in an effort to enhance the performance of the traditional GA. The objective of the overall design optimization, including the building topology and section sizes of members, was to determine the portal frame building having the minimum cost, whilst satisfying the design requirements. The design variables were related to some geometric characteristics of the frame, like the span length, height of eaves and the inclination of the pitch, as well as the members cross-sections, which were chosen from a list containing 40 channel-sections. It's important to highlight that the decision variables were both discrete and continuous. A case of a frame with a span of 20 meters and column height of 4 meters has been analyzed in order to demonstrate the efficiency of the proposed method. The algorithm's computational effectiveness and robustness have also been proven and the computational time has been cut in half compared to standard GA.
Another study related to the validation of the application of metaheuristic algorithm for size and topology optimization has been carried out by A.Kaveh, Mahdavi V.R. in [63]. In this paper, steel truss structures have been optimized using a meta-heuristic algorithm called Colliding Bodies Optimization (CBO). In the layout (simultaneous size and topology) optimization problem, two objectives have been taken into account: the best topology or shape for a ground structure and the best cross-sections of that topology. Therefore, the problem began with the ground structure, which was made up of all potential nodes and members. Then, the cross-sectional areas and node layout have been determined to gain the minimum cost. In particular, the cost of the entire structure has been calculated as the sum of the members expense, related to their masses, and of the nodes, evaluated by means of a constant mass value if the node was present. Design variables taken into account to obtain the outcomes included the cross-sectional areas (regarded as a continuous variable) and both the node and member positions. The constraints applied were related to the upper and lower bound of stresses, buckling, displacements and natural frequencies requirements of the structure. The finite element model had to be revised and adjusted when members and nodes were eliminated, which was an important part of topology optimization that needs to be highlighted. This change resulted in a significant amount of useless computing work. Wang and Sun (Wang and Sun 1995) developed a technique in which the members suggested to be removed by the opti-

mization, thus elements with zero cross-sectional value, had to be associated instead with a very small value. The employment of such technique was able to overcome the problem of having elements with null area, that require the re-computation of the stiffness matrix. In this way the computing effort has been reduced while maintaining the finite element model's integrity. Moreover, when a tiny cross-sectional area was chosen, the corresponding stress and local stability constraints were ignored. To compare the effectiveness of the CBO algorithm with other techniques, four numerical examples of various truss designs with increasing numbers of nodes and elements have been taken into consideration. In all the examples tested the cost of the optimized structure was minimum when using the proposed methodology. Moreover, while the majority of meta-heuristic algorithms had some parameters that needed to be carefully adjusted for various types of problems, CBO, being independent from settings, was easy to be implemented.
In another research, conducted by Kaveh, Ali Neda and Farhoudi [58], topology and size optimizations have been exploited to find an economical solution for concentrically structural steel frames. Differential Evolution Algorithm (DE) and Dolphin Echolocation Optimization (DEO) have been applied for structural optimization, to find the best results in terms of minimum weight. Both placement of the bracings and size members have been considered as design variables, while the considered constrain were related to drift, deflection, compaction and strength of the structure.In particular, the structure taken into account was a steel braced frame with dual building system, in which an essentially complete frame provided support for gravity loads, while resistance to lateral loads was provided by a specially detailedmoment-resisting frameand shear walls or braced frames. Three examples of 3 types of frames with different storey heights,have been illustrated to demonstrate that both DE and DEO have good performance in discrete structural topology optimization. Also, DEO leads to better results with less standard deviation in comparison to Genetic Algorithm (GA) and other metaheuristic algorithms.
The same authors in [59], introduced another metaheuristic algorithm, called Dolphin Monitoring (DM) for layout optimization of structures. Actually, the dolphin monitoring ability to control the convergence of the Dolphin Echolocation Optimization (DEO) algorithm has been demonstrated an it has also been applied to other metaheuristic algorithms, such as GA, PSO, BB-BC, CBO and their modified variants. More in details, DM do not change the nature of the algorithms, but it is used only to set the convergence in a predefined number of loops. Specifically in

this paper, the OF was the minimum weight of dual systems, characterized by the best placement of bracings and the best cross sections of the elements of both the moment frames and the X-bracings. The placement of bracings and size of members have been considered simultaneously as optimization variables. The members had to satisfy constraints on the design storey drift, deflection, compaction (limiting width over thickness for compression memebrs), strength, stability coefficients and slenderness ratio limits. The structures taken into account were subjected to both dead load, as well as live loads and earthquake excitations. To evaluate the effectiveness of the suggested strategy, three numerical examples with 3-, 5-, and 10-story braced frames have been provided. The findings of applying DM to numerical examples of GA, ACO, PSO, BB-BC, and CBO demonstrated that DM enhances the minimum, maximum, mean, and standard deviation of the results of all these algorithms. Comparing the results of all the aforementioned algorithms to their modified versions, DM also produced better results in terms of minimum weight.

In the same year also Gholizadeh, S., Poorhoseini, H., performed a layout optimization, illustrated in [41]. Their interest was focused on the process of developing new structures or upgrading existing ones to fulfill specified performance objectives for likely future earthquakes, by applying the seismic performance-based design. Thus, the present paper exploited such method on steel braced frames subjected to earthquake loading. In the SPBD methodology, a nonlinear analysis tool was typically used to determine the seismic demands of structures at predetermined performance levels. According to FEMA-273 (1997), IO, LS, and CP performance levels have been considered in this study. Design variable of the optimization problem included the cross sections of all the structural members: beams, columns and X-bracing, as well as the optimal position of the latter ones. SPBLO process has been applied to five-bay steel braced frames with different number of storeys, with the aim of minimizing structural weight. To ensure that all potential solutions was workable, various design restrictions were examined, among which serviceability and ultimate limit state constraints were considered. In details, geometric and strength assessments were included in the serviceability restrictions. Geometric checks had to be completed in beam-column and column-column framing joints to meet practical requirements. Moreover, a hierarchy of the constrain has been considered, in fact if the serviceability restrictions were not met the design was discarded. Otherwise, a nonlinear pushover analysis was carried out to assess the seismic response of the structure at the desired performance levels. Then, the design criteria and capacity demand levels have been presented in terms of displacements. The constraints of the optimization problem are handled by the exterior penalty function method (EPFM). An enhanced dolphin echolocation meta-heuristic method was suggested to carry out the optimization task. Additionally, as previously mentioned, nonlinear pushover analysis was carried out to analyze the structural responses at the performance levels, which can greatly increase the computing complexity of the layout optimization problem. The adoption of an effective optimization technique is required in order to search the vast design space of the SPBLO problem due to this important issue. An enhanced version of the Dolphin Echolocation (DE) Metaheuristic was suggested in the current study to address this problem. By merging Chaos Theory (CT) and conventional DE, a novel meta-heuristic algorithm dubbed Improved Dolphin echolocation (IDE) is developed. Three examples including 6, 9 and 12 story SBFs were solved in the framework of SPBLO formulation. The numerical results of the SPBLO example revealed that in the framework of SPBSO the optimal solutions attained by IDE were respectively 3.61, 3.20, and 3.32% lighter than those of obtained by DE. The trend of the analysis performed with the two algorithm is shown in the following figure 2.29.

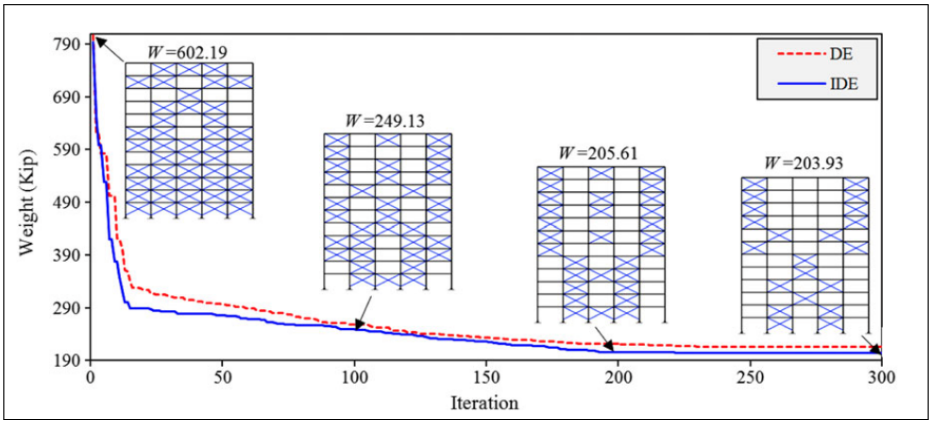


Figure 2.27: Comparison of convergence hystory between DE and IDE in the framework of 12-story SBF [106]

So the results state that the computational performance of IDE was better than that of the DE in terms of optimal structural weight and convergence rate.

Going back to concentrically structural steel frames, an important aspect is related to the fact that braced steel structure's integrity may be compromised by the occurrence of some extremely serious events. This risk had driven researchers to create novel techniques for evaluating structural collapse, among which Jeriniaina Sitarka Tantely, Zhange He in [110] investigated such topic. The introduction of incremental dynamic analysis (IDA), which allows for the creation of a collapse probability curve for the examined structure, was suggested as a technique to understand seismic events. Although the experts agree that the IDA is effective and reliable, they also believe that it is a long process. By using a few series of time history analyses(THA) to approximate the fragility curve, they were able to overcome these limits. It significantly reduced the calculation time for the collapse assessment and provided a reliable approximation of the fragility curve. The use of the fragility curve was extended by proposing a collapse margin ratio (CMR), which become the primary parameter associated with the evaluation of structural safety. The scope of this work was to propose a design optimization of steel structures, using concentric braces, based on collapse safety assessment. Brace locations and sections were the variables of this investigation, while the objective was the maximization of the CMR of the structure. The higher the CMR value, the safer the structure. Constraints were the candidates' non-null vectors, meaning that each level of steel frame structure must had at least one brace. The idea of designable matrix was presented in relation to the best placement for bracing in the structure and derived from the reality that, in actual projects, engineers are not always free to choose where to put the braces because of architectural constraints or owner preferences. So undesignable bay refers to the bay where bracing cannot be installed. An initial matrix describing the building's elevation was created in order to quickly count the number of designable and undesignable bays in a given structure. Sizing brace optimization of seismic steel frame structure aimed to reduce the total steel weight of the braces, which acted as a rough indicator of bracing construction cost. During the procedure, the optimal shape brace section at each story has been evaluated and then the optimal discrete brace section related to that story was identified. The authors advised utilizing a single section of brace for each story since employing several sections might imply the occurrence of weak braces, which would result in unequal lateral force dissipation at that story. Another reason was that premature damage of the structure's frame could be caused by the achievement of the strength limit by the weak brace before the other ones. The algorithm used a database of steel brace sections, selected from commercially available hot-rolled, wide-flange standard steel sections.The authors investigated four steel frame structures, in which the main difference was both the presence of undesignable bays on different sides of the structure and the number of storeys. From the interpretation of the results, the proposed methodology has been proved to be capable of a quick and practical estimation of the collapse margin of several structures in a short time, compared to the prior methods in this field.

Also the study of Aydin Hassanzadeh, Saeed Gholizadeh, illustrated in [49] focused on the collapse-performance-aided optimization of steel concentrically braced frame (SCBF) structures. The interest of the authors had its roots in the evidence that the placement of braces directly affects the seismic performance of SCBF structures, therefore finding an appropriate configuration had become increasingly important. In this analysis, both size and topology optimization have been performed in the framework of the performance-based design (PBD) methodology, using the collapse-margin-ratio (CMR) algorithm. In particular, CMR algorithm has been chosen for its ability to make an appropriate balance between exploration and exploitation. The proposed optimization was aimed at minimizing the structural weight, starting from a fully braced frame and gradually removing unnecessary bracing members. During the procedure, the design variables were representative of the discrete cross-sectional areas of columns, beams and braces, along with the placement of the brace members as topology variables. Moreover, due to practical requirements, the symmetry in the structure was used to group the design variables. The applied constraints regarded practical geometric specifications about column-to-column and beam-to-column framing joints, strength requirements in terms of the elements' demand-capacity ratios (DCR), according to LRFD-AISC code (Load and resistance factor design - American Institute of steel design), and PBD constraints as well. Actually, PBD constraints was not tested until the geometry and strength requirements were met in order to decrease the computational time. However, if PBD constraints were verified, a pushover analysis was performed at each performance level to assess the structural responses, i.e. the maximum inter-story drift and the maximum deformation of columns and braces, which had to be less than their permitted values. After the application of the PBD method, in order to evaluate the collapse potential of the structure, an incremental dynamic analysis (IDA) was carried out according to FEMA-P695 (Federal Emergency Management Agency – Quantification of building seismic performance factors). Consequently, the SCBFs was compared in terms of structural weight and seismic collapse capacity until the best optimal design was found. Three different frames have been analysed with the proposed methodology, which provided optimized structural solutions with simultaneously improved structural weight and collapse performance. The designs with the best bracing topologies were, respectively, 11.59%, 18.68%, and 16.0% lighter than the best SCBFs with fully braced frame in all examples of 5-, 10-, and 15-story SCBFs. Moreover, the best optimized frame was the one with the largest safety factor, that do not necessarily implied heavier weight. Stefanos Sotiropolous, Nick D. Lagaros in [105] tried to identify the structural system's ideal layout and, more specifically, to determine the best lateral brace system configuration in tall buildings subjected to dynamic seismic loadings. Both topology and size optimization have been exploited to reach a minimum value of the objective function (OF), that was tackled as the compliance of the structure. The minimization of the compliance of the structure means the maximization of the building stiffness and it was carried out by varying both the cross-section areas of the structural elements and the building topology. Standardized cross-sectional frame elements have been considered and specifically the European HEA, IPE and CHS sections were used with the aid of regression analysis, while a number of possible brace configurations defined the design domain. Cross-sections were taken from a list, in which minimum and maximum values have been defined to avoid the singularity of the stiffness matrix. During the iterations, the final material volume used was restrained to a limiting value, while stress and strain constraints have been applied to the different frame elements. Two cases of dynamic loading have been examined: harmonic loading and earthquake ground motion excitation. The examples were focused on the optimization of tall structures, like High-rise building and Mega-braced frames.

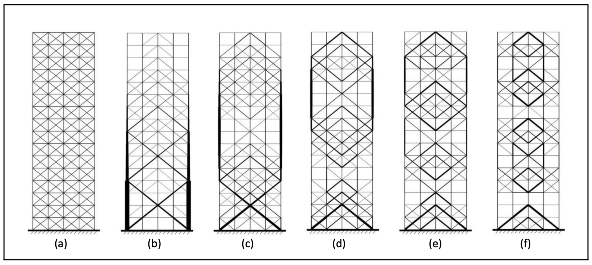


Figure 2.28: (a) Initial Ground Structure of High Rise Building System, optimized structural systems for maximizing the (b) 1st, (c) 2nd, (d) 3rd, (e) 4th, (f) 5th frequency [105]

Morever, they can be divided into three groups, in which the first one addressed the maximization of a specific eigen frequency while the structure was subjected to free vibration; in the second one, time history analysis has been employed and both concentrated harmonic load and ground motion seismic excitation were considered, leading to different formulations of the minimized OF, i.e. dynamic compliance for half-cycle sinusoidal concentrated load and roof deflection (using the sum root of sum squares), respectively; finally, in the third group the response spectrum of EC8 has been implemented for simulating the seismic load. Due to the different nature of the three cases tested, a great variety of observations can be made. More specifically, results from the first case showed how giving more freedom to the initial ground structure, the optimization leads to larger and thus better OF. Then, in the first case of the second group of analyses, it has been observed that when the driving frequency was close to an eigenfrequency, more braces were developed to prevent resonance, while for high driving frequency, the structure had braces only in its upper half. Regarding the minimization of SRSS in which a real earthquake is applied, it has been noticed that the optimized structural system was derived from denser ground structures, more types of braces were produced and so the moment resisting steel frame had smaller tip deflections. In conclusion, relative to the final depicted case, it has been noted that an important role has been played by the number of modes considered. In fact, by the comparison of two different moment resisting frames, the optimized structure had the best structural response if the first three eigenmodes were used for the evaluation of the sum of the compliance.

## 2.4 Shape Optimization

Shape optimization attempts to integrate geometric modelling, structural analysis and optimization into one complete automated computer-aided design [52]. During the entire shape design optimization process, the design domain keeps on changing through design variables updating and subsequent internal and/or external boundary variations. The design variables that characterize a shape optimization are the nodal coordinates of the structure under study, while constraints on geometry and structural responses such as stress, displacements and natural frequencies are generally considered. Throughout a shape optimization process, a change in the coordinates of the elements will lead inevitably to a change in the state of stress. Due to that, a Finite Element Analysis and a mesh refinement is always required at each iteration of the optimization process. Moreover, it is worth mentioning that in most of the studies the shape optimization is generally coupled with size or topology techniques, seldom implemented alone.

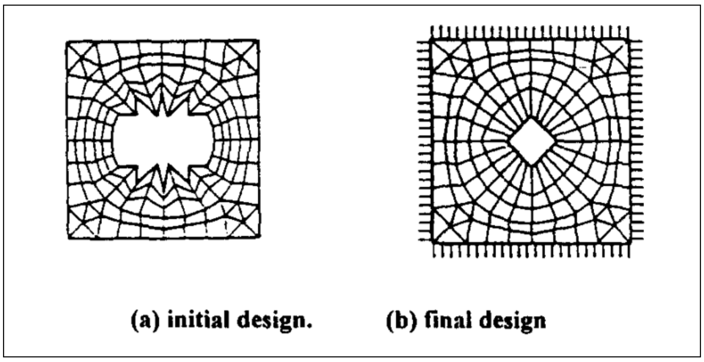


Figure 2.29: Finite element mesh representation for initial design (a) and final design (b) of the optimized hole [52]

### 2.4.1 Size and Shape Optimization

An early coupled optimization of size and shape techniques has been reported by Haque, M.I. in [45]. The design of skeletal geometry of plane rigid frames has been tacked as the paper's aim, by using the modified version of complex method of box. The main advantages of this method are that it does not require time-consuming computations for the gradients of the objective function and the non-linear constraints. The design variables considered in order to obtain a minimum weight of the optimized skeletal structure are simultaneously the cross-section of the structural members and 2D coordinates (x,y) for the position of the joint. Both explicit and implicit constraints have been introduced; the former one defined limiting bounds for the design variable, while the latter imposed restrictions on the behavior of the structure under external loads, following AISC specification. As explained by the authors, to reduce the computational cost is highly desirable to decompose the design space into several subspaces, with each subspace having its own optimization strategy. Following such approach, the entire design space has been decomposed into two subspaces: the geometric design space and the member one. The variables of the first one consisted of unknown joint coordinates, while the ones of the member design space have been defined essentially as the cross-sectional dimensions of the members. Two practical examples have been provided, with variable number of joints free to move. The first one consisted of a plane symmetrical frame with six members and seven joints, among which only 3 were free to move. A plane symmetrical frame has been considered also for the second example, but in this case it had seven joints and six members, with just one joint free to move. In this last case a constraint on the roof inclination has been added, which had to remain fixed at

1:12 slope. Results of the analysis showed that the major improvements in design occurred during the first 10 reflections. The final optimal weight was 4.70 kips, compared with 6.08 kips for the initial input geometry for the first example; while for the second one a final optimum weight of 4.05 kips in contrast with the minimum weight in the initial complex of 5.39 kips. In conclusion, this method has been shown to be very efficient and it's important to underline, again, that the convergence was rapid and no calculations of the gradient of the OF needed to be done.

Later on, Kazemzadeh Azad, S., Bybordiani, M., Kazemzadeh Azad, S., Jawad, F.K.J.,in [10] proposed an application of size and shape optimization on steel truss structures subjected to dynamic excitations. Using the big bang-big crunch algorithm, already mentioned in the metaheuristic algorithm section of the present Chapter, the minimum-weight design has been pursued for 22-members cantilever truss, optimized under sinusoidal excitations, as well as for 44-members truss, designed under rectangular periodic excitations, and a 37-members truss, subjected to step forces with different finite rise time values. The different excitations considered have been chosen to observe the effect of such parameter on the final designs. Moreover, the same structures have been also subjected to a static load in order to make a comparison with the dynamic ones. In size optimization, cross-sectional areas of members have been considered as discrete design variables, selected from a database of 37 hollow core sections. Regarding the geometry or shape optimization, nodal coordinates have been treated as decision variables. The design constraints accounted during the optimization included strength, displacement, and buckling requirements according to AISC-LRFD. Results have shown that by increasing the exciting period of the sinusoidal loading as well as the finite rise time of the non-periodic step force, a minimum weight design was obtained, as shown in figure 2.30. In addition, the achieved lightest design was similar to the one obtained under static loading.

However, different considerations needed to be taken into account for rectangular periodic excitation, for which the reported results detached from the ideal design in the static loading situation even at higher exciting period values.

In 2019, Kaveh, A., Vaez, S.R.H., Hosseini, P., Bakhtiyari, M., in [61] propoesed a design procedure for curved steel roof frames, taken as a part of circular arches, optimized by an Enhanced Vibrating Particles System (EVPS) Algorithm. A combination of size and shape optimization have been employed to find respectively the minimum weight design and the slope angle of the curved roof frames. The cross-

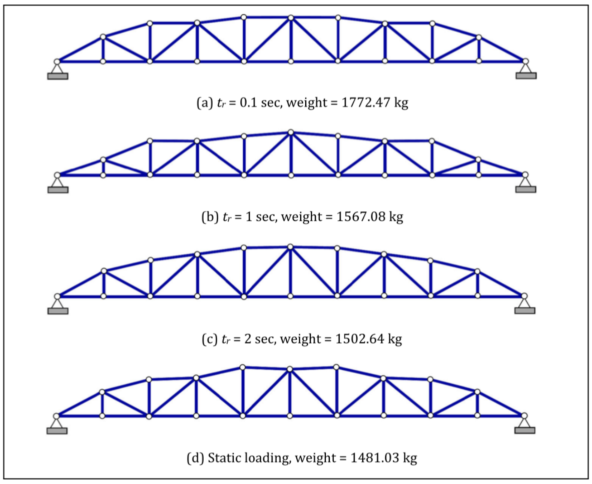


Figure 2.30: Optimal geometries of 37-member truss bridge under: (a, b, c) non-periodic step force with finite rise time (t,); (d) static loading [10]

sections for the web tapered members have been treated as discrete design variables, while the inclination of the slope angle of the curved roof frames has been considered continuous in a defined range (3 to 70 degrees). In particular, straight short elements with tapered members have been used to model the curved roof, where the roof slope angle ($\theta$) has been defined as the slope of the tangent line on the circular arc of the roof with respect to the horizontal line. The coordinates of the points located on the circular arc were allowed to vary to find the best configuration also in accordance with the total amount of loads applied on the frame. In this study, regulations of ASCE have been used for applying the dead, live, snow, wind and seismic loads. The projection of gravity has been applied to the live and snow loads. In particular, the roof slope angle determined the amount of load placed on the frame, which in turn changed during the iterations. The applied constraints were related to maximum vertical and horizontal displacements for serviceability condition, in conjunction with strength and buckling constraints. The optimum results have shown that 65% of roof slope angle values for the steel curved roof frames were between 9 to 22 degrees in total runs. Therefore, this range can be used as an optimal range to design such structures. Moreover, among the selected design constraints, the horizontal displacement of the steel frame supporting the pitched roof hasreached earlierits allowable capacity with respect the other design constraints. As a result, it can be concluded that it is one of the most significant limitations and a determining element in the best design of pitched roof steel frames.
Another stimulating study has been carried out by Phan D.T., Mojtabaei S.M.,

Hajirasouliha I., Ye J., Lim J.B.P., in [92]. In this research, the optimization of cold-formed steel (CFS) structures has been addressed, giving a deeper look to the design of thin-walled CFS sections which are generally affected by various buckling modes. Cold-formed steel sections are employed in constructions because of their great benefits, including a relatively high strength-to-weight ratio, better production flexibility and simplicity in handling, shipping, and installation. Two levels of optimization were faced by the authors, i.e. an element, or section level and then a structure, or frame level, with the objective of minimizing the weight of the CFS portal frame. At the element level, a set of optimized CFS lipped-channel beam sections, with different coil widths and plate thicknesses, has been chosen for the structural members, characterized by various lengths and subjected to different load (UDL) levels. Subsequently, at the frame level, the best cross-sections (with minimum amount of material) have been selected from the optimized sections, which had to satisfy the design constraints related to the internal forces calculated at each iteration. In more details, the structural elements of CFS portal frames have been designed in accordance with EC3, considering ultimate limit state (ULS) and serviceability limit state (SLS) conditions. The frame optimization has been carried out also considering practical ranges for the roof pitch, frame spacing and knee brace configuration (i.e. knee depth and knee angle) to obtain the best design solution. Thus, at the structural level, discrete and continuous design variables have been simultaneously used. In particular, it has been assumed that roof pitch could vary between 6° to 30° and frame spacing has been set in the range of 2 m to 20 m. Such variability implies that also a shape optimization has been implemented. The results have demonstrated that optimizing the cross-sectional geometry of simply supported CFS beams subjected to uniformly distributed vertical or transverse load can substantially improve their flexural capacity, as compared with standard sections. In fact, CFS section reached an higher ultimate flexural capacity (up to 84%) compared to the standard lipped channel section, with the same plate width and thickness. In addition, analyzing the results of structural optimization, also a more cost-effective solution has been achieved, reaching a 20% reduction of structural material. Furthermore, the flexibility of CFS cross-sectional shapes, obtained by varying the relative dimensions of channel sections, provided an excellent opportunity to enhance the load-carrying capacity of available standard sections. This improvement of capacity at the element level, led subsequently to an improvement of the capacity also of the CFS frame system, especially for medium to long-span

CFS portal frame buildings.

### 2.4.2 Size, Shape and Topology Optimization

In the context of simultaneous size, shape and topology optimization was provided by Lagaros et Al in 2008 [68]. In this paper the authors have been applied a combined size, shape and topology optimization in order to reach an optimum design of perforated I-section beams. Web openings in beams are suggested and the major advantages are: reduce the material volume without changing the strength properties of the structures, alleviate stresses in beam columns joints and finally also architectural limitations sometimes impose the necessity of web opening in the building. The considered design variables for size, shape and topology were respectively cross sections, coordinates of the open boundary and number of the web openings. The Objective function of the problem was the weight minimization, however the optimal design was obtained considering some design criteria like shear, bending and Vierendeel bending resistance as well provision for local buckling and web buckling. Regarding the design constraints, were mainly focused on the size of the openings. In fact, it need to be highlighted that any increase in size of the web openings will results in a lower global shear and the global moment resistances of the perforated sections. Due to that some geometric restrictions were implemented to control the size of the openings., in fact all web opening should be located along the center line of the web, maximum diameter of the openings cannot exceed 0.75 times the total height of the beam and the distance between the edges of adjacent openings should not be less than the total height of the beam. Evolutionary Algorithms (EA) has been employed in order to run the optimization problem, practical example is related a frame with different web opening diameters. Results have shown the efficiency of the considered structural system, in fact up to 20% in weight savings was achieved compared to the case with no openings. Another stimulating research has been proposed by Hasançebi, O., Doğan, E., in [48], where several truss bridges have been analyzed. In particular, a comparison based on design weight efficiency of single span steel truss bridge topologies, subjected to gravity load, has been employed. Through a combination of size, shape and topology optimization, nine distinct topological forms of truss bridges (namely, Pratt, Parker, Baltimore, Petit, K-Truss, Warren, Subdivided Warren, Quadrangular Warren and Whipple) have been designed for minimum weight.

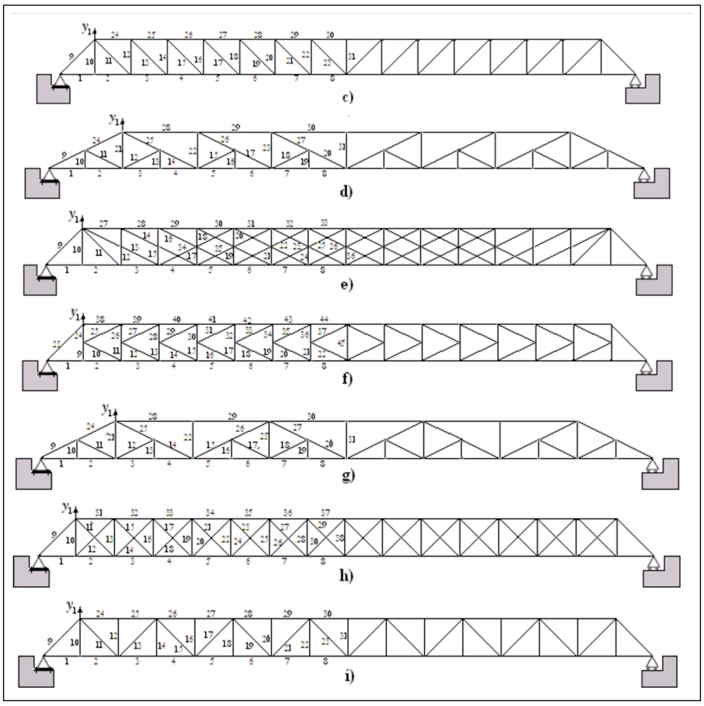

Figure 2.31: The topological forms used to configure long span bridge: a) Parker, b) Petit, c) Pratt, d) Baltimore, e) Whipple, f) K-truss, g) Subdivided Warren, h) Quadrangular Warren, i) Warren

It should be stressed that truss bridges are widely used, especially in the last years, due to their advantages from both a structural and constructional point of views. Moreover, they allow to reach very large spans, using less amount of material. Specifically in this analysis, the bridges were first configured according to these topological forms and the resulting structures have been then optimized considering strength, stability and displacements provisions of ASD-AISC. In the optimum design process, both size (discrete) and shape (continuous) design variables have been employed. In this context, size variables have been used to choose appropriate dimensions for the bridge members, whereas the optimal height and/or shape of the bridge's upper chord have been explored with shape variables. In particular, the number of shape variables used in a model was dependent on the bridge topological form. For example, a single shape variable was used to define the height in bridge models with Pratt, Baltimore, Warren, Subdivided Warren, Quadrangular Warren, Whipple and K-truss forms, since they have a straight upper chord. Moreover, four different span lengths, namely 100, 200, 400 and 600 ft have been considered as separate case studies and for each of these span lengths nine bridges have been generated. In conclusion, it has been found that the topological form selected to create the structural system of a bridge significantly affects the weight of the bridge's final design. For span lengths of 100, 200, 400, and 600, respectively, the design weight disparities between the best (lightest) and worst (heaviest) models was 15%, 30%, 43%, and 55%. Consequently, the selection of economical topological form became more pronounced when span length of the bridge increased. The bridge's ideal forms, created using Petit and Parker trusses, lowered the height of the structure moving from the middle of the span to the ends, reducing the amount of material used in the design. The findings also suggest that, in order to maximize the weight efficiency of the final bridge, some bridge designs, such as Whipple and Pratt, should be avoided for all span lengths. Warren and Quadrangular Warren should also be avoided for relatively large span lengths. Baltimore, Subdivided Warren and K-truss topology led to similar design weights.

Finally, the work done by Ohsaki, M., Iwatsuki, O., Watanabe, H. in [85] gives a clear demonstration of the complexity and at the same time of the power of such procedures. In this research a reverse rocking response was exploited to investigate the behavior of a steel frame structure with a foundation modeled as a flexible base, with the objective to reduce the roof displacements. Due to the foundation's flexibility, the frame had areverserocking when the base beam was rotating against the frame's drift to minimize the displacement of the roof. The foundation beam, on the other hand, if above a stiff base, would been rotating slightly in the same direction as the frame. Topology, size and shape optimization have been carried out to find the best configuration of the base structure, modeled as a truss structure and the OF of the entire optimization was aimed at the reduction of the roof displacement. Running the analysis, unnecessary members have been removed, starting from the highly connected ground structure. Nodal locations have been also considered as variables to comply with shape optimization, while elements with square tube sections have been used as size discrete design variables. Constraints were mainly related to the maximum allowable displacements of the flexible base's elements, as well as to upper and lower boundary of the node coordinates. A practical example of a frame, characterized by 10 meter of span and with a base made of rigidly-jointed frame with square tube sections, has been analyzed. The outputs have shown that the displacement as well as acceleration of the roof of a frame under seismic ground motion can be effectively reduced using a flexible base structure, which exploits rocking of the base in the opposite direction to the drift of the upper frame. Such reverse rocking response is dominated by the 2nd mode rather than the 1st mode. Moreover, in the examples reported, the mean maximum roof displacement, computed using the SRSS method, was successfully minimized compared with the stiff model.

**Table 2 Review of the application of optimization strategies to steel structures**

| Ref. | Year | **S**tatic<br>**D**ynamic | Size | Shape | Topology | **S**ingle/**M**ulti<br>Objective | ID-OF | Design criteria | Design variables |
|---|---|---|---|---|---|---|---|---|---|
| [32] | 1977 | **D** | ☑ | ☐ | ☐ | **S** | (1)-Weight | Stresses<br>Displacement<br>Natural frequency<br>Geometric bounds | Cross-sections |
| [45] | 1985 | **S** | ☑ | ☑ | ☐ | **S** | (1)-Weight | Geometric bounds<br>AISC | Cross-sections<br>Node's<br>coordinates |
| [103] | 1986 | **S** | ☑ | ☐ | ☐ | **S** | (1)-Failure load<br>factor | Failure load<br>factor range | Cross-sections |
| [71] | 1986 | **S** | ☑ | ☐ | ☐ | **S** | (1)-Weight | Stresses<br>Displacements<br>Buckling<br>Geometric bounds | Cross-section's<br>parameters |

| | | | | | | | | | |
|---|---|---|---|---|---|---|---|---|---|
| [72] | 1986 | **S** | ☑ | ☐ | ☐ | **S** | (1)-Weight | Stresses<br>Displacements<br>Buckling<br>Geometric bounds | Cross-section's parameters |
| [54] | 1987 | **D** | ☑ | ☐ | ☐ | **S** | (1)- Weight | Probability of failure<br>Moment of inertia | Columns' moment of inertia |
| [18] | 1989 | **S/D** | ☑ | ☐ | ☐ | **S** | (1)- Weight<br>(2)-Cost | Stresses<br>Displacement<br>Natural frequency | Cross-sections |
| [100] | 1991 | **S** | ☑ | ☐ | ☑ | **S** | (1)-Weight | Stress<br>Displacement | Cross-sections<br>Brace locations |
| [102] | 1991 | **S** | ☑ | ☐ | ☐ | **S** | (1)-Weight | Displacement<br>Geometric bounds | Cross-sections |
| [13] | 1991 | **S** | ☑ | ☐ | ☐ | **S** | (1)-Weight | Stress<br>Displacements | Cross-sections |
| [30] | 1992 | **S** | ☑ | ☐ | ☐ | **S** | (1)-Weight | Stresses<br>Buckling<br>Slenderness<br>Geometric bound | Moment of inertia |

| | | | | | | | | | |
|---|---|---|---|---|---|---|---|---|---|
| [50] | 1992 | **S** | ☑ | ☐ | ☐ | **S** | (1)-Weight | Displacement<br>Geometric bounds | Cross-section<br>at one end<br>of the beam<br>and area ratio<br>at its ends |
| [111] | 1992 | **S** | ☑ | ☐ | ☐ | **S** | (1)-Weight | Stresses<br>Displacements<br>Buckling<br>Geometric bounds | Cross-sections |
| [1] | 1993 | **S** | ☑ | ☐ | ☐ | **S** | (1)-Weight | Stresses<br>Displacements<br>Geometric bounds | Cross-sections |
| [26] | 1994 | **S/D** | ☑ | ☐ | ☐ | **S/M** | (1)-Weight<br>(1)-Displacement<br>(1)-Frequency | Stresses<br>Buckling<br>Geometric bounds | Cross-sections |
| [2] | 1995 | **S** | ☑ | ☐ | ☐ | **S** | (1)-Volume | Stresses<br>Displacements<br>Geometric bounds | Moment<br>of inertia |

| | | | | | | | | | |
|---|---|---|---|---|---|---|---|---|---|
| [76] | 1999 | **S/D** | ☑ | ☐ | ☐ | **S** | (1)-Weight | Stresses<br>Displacement<br>Buckling<br>Slenderness<br>Geometric bounds | Cross-sections |
| [22] | 2000 | **S** | ☑ | ☐ | ☐ | **M** | (1)-Weight<br>(1)-Stress<br>(1)-Displacement | Stresses<br>Displacements | Cross-sections |
| [53] | 2000 | **S** | ☐ | ☐ | ☑ | **S** | (1)-Compliance | Stresses<br>Displacement | Material<br>distribution |
| [20] | 2002 | **S** | ☑ | ☐ | ☐ | **S** | (1)-Weight | AISC-LRFD | Cross-sections |
| [101] | 2003 | **S** | ☑ | ☐ | ☐ | **S** | (1)-Weight | BS 5950<br>Buckling | Cross-section's<br>parameters |
| [79] | 2005 | **S/D** | ☑ | ☐ | ☐ | **S** | (1)-Uniform<br>deformation | UBC<br>FEMA365<br>SEAC2000 | Cross-sections |
| [88] | 2006 | **D** | ☐ | ☐ | ☑ | **S** | (1)-Weight | Frequency<br>Displacement<br>Acceleration | Bars arrangement |

| | | | | | | | | | |
|---|---|---|---|---|---|---|---|---|---|
| [99] | 2006 | **S** | ☐ | ☐ | ☑ | **S** | (1)-Weight | Stresses<br>Displacement<br>Architectural limitations<br>Max number of braced panels | Brace locations |
| [112] | 2006 | **S/D** | ☑ | ☐ | ☐ | **S** | (1)Uniform deformation | UBC<br>FEMA365<br>SEAC2000 | Cross-sections |
| [23] | 2007 | **S** | ☑ | ☐ | ☐ | **S** | (1)-Weight | Stress<br>Displacements | Cross-sections<br>Connection flexibility |
| [68] | 2008 | **S** | ☑ | ☑ | ☑ | **S** | (1)-Weight | Stress<br>Geometric | Cross-sections<br>Coordinates of web openings<br>Number of web openings |

| | | | | | | | | | |
|---|---|---|---|---|---|---|---|---|---|
| [78] | 2010 | **S/D** | ☑ | ☐ | ☐ | **S** | (1)-Uniform deformation | UBC<br>FEMA 365<br>SEAC2000 | Cross-sections |
| [19] | 2010 | **S** | ☑ | ☐ | ☐ | **S** | (1)-Weight | Strenght<br>Deflection | Cross-sections |
| [48] | 2011 | **S** | ☑ | ☑ | ☑ | **S** | (1)-Weight | ASD-AISC | Cross-sections |
| [56] | 2011 | **S** | ☑ | ☐ | ☐ | **S** | (1)-Weight | Strenght<br>Deflection | Cross-sections |
| [44] | 2011 | **S** | ☐ | ☐ | ☑ | **S** | (1)-Weight | Strenght<br>Deflection | Bars arrangement |
| [91] | 2012 | **S** | ☑ | ☐ | ☑ | **S** | (1)-Weight | Stresses<br>Displacements | Cross section<br>Building topology |
| [106] | 2012 | **S** | ☑ | ☐ | ☑ | **S** | (1)-Compliance | Material used<br>Stresses | Cross-sections<br>Material distribution |
| [86] | 2012 | **S/D** | ☑ | ☐ | ☐ | **S** | (1)-Weight | Stresses<br>Displacement<br>Plastic hinges | Cross-sections<br>Connections flexibility |

| | | | | | | | | | |
|---|---|---|---|---|---|---|---|---|---|
| [21] | 2013 | **S/D** | ☑ | ☐ | ☐ | **M** | (1)-Weight<br>(2)-Column-beam<br>strengthratio | Strength<br>Inter-story<br>drift ratio<br>Plastic hinges<br>Geometric bounds | Cross-sections |
| [34] | 2013 | **S** | ☑ | ☐ | ☐ | **S** | (1)-Weight | Stresses<br>Deflections<br>Buckling<br>Geometric bounds | Cross-sections |
| [65] | 2013 | **S/D** | ☑ | ☐ | ☐ | **M** | (1)-Weight<br>(2)-Inter-story<br>drift<br>(3)-Structural<br>damage | Strength<br>Slenderness<br>Displacement<br>Geometric bounds | Cross-sections |
| [16] | 2014 | **S** | ☑ | ☐ | ☐ | **S** | (1)-Weight | Strength<br>Displacement<br>Geometric bounds | Cross-sections |
| [40] | 2014 | **S/D** | ☑ | ☐ | ☐ | **S** | (1)-Weight | Stresses<br>Inter-story drift<br>FEMA356 | Cross-sections |

| | | | | | | | | | |
|---|---|---|---|---|---|---|---|---|---|
| [81] | 2014 | **S/D** | ☑ | ☐ | ☐ | **S** | (1)-Weight | ASCE 41-06<br>Displacement<br>Plastic hinges | Cross-sections |
| [85] | 2014 | **S/D** | ☑ | ☑ | ☑ | S | (1)-Roof<br>displacements | Bounds on<br>nodal coordinates<br>Base displacement | Cross-sections<br>Node's<br>coordinates<br>Members<br>arrangements |
| [69] | 2015 | **S** | ☑ | ☐ | ☐ | **D** | (1)-Weight | Stresses<br>Geometric bounds | Cross-section<br>parameters |
| [74] | 2015 | **S** | ☑ | ☐ | ☐ | **S** | (1)-Weight | Stresses<br>Displacements | Cross-section |
| [60] | 2015 | **S** | ☑ | ☐ | ☐ | **S** | (1)-Weight | Strenght<br>Displacements | Cross-sections |
| [109] | 2015 | **S** | ☑ | ☐ | ☑ | **S** | (1)-Weight<br>(2)-Min number<br>of braces | Stresses<br>Displacements | Cross-sections |
| [108] | 2015 | **S** | ☑ | ☐ | ☐ | **S** | (1)-Weight | AISC | Cross-sections |

| | | | | | | | | | |
|---|---|---|---|---|---|---|---|---|---|
| [37] | 2015 | **S** | ☑ | ☐ | ☐ | **D** | (1)-Weight | Strength<br>Displacements | Cross-sections |
| [9] | 2015 | **S** | ☑ | ☐ | ☐ | **S** | (1)- Weight | AISC-ASD<br>Geometric bounds | Cross-sections<br>Connections<br>rigidity |
| [8] | 2015 | **S** | ☑ | ☐ | ☐ | **S** | (1)- Weight | AISC-ASD<br>Geometric bounds | Cross-sections<br>Connections<br>rigidity<br>Beams material |
| [87] | 2015 | **S** | ☑ | ☐ | ☐ | **S/D** | (1)- Weight | Serviceability<br>for static and<br>seismic load | Cross-sections |
| [70] | 2015 | **S** | ☑ | ☐ | ☐ | **D** | (1)- SPI | FEMA 356<br>FEMA-350 | Cross-sections |
| [58] | 2015 | **S** | ☑ | ☐ | ☑ | **D** | (1)- Weight | FEMA 356<br>FEMA-350 | Cross-sections<br>Brace locations |

| | | | | | | | | | |
|---|---|---|---|---|---|---|---|---|---|
| [63] | 2015 | **S** | ☑ | ☐ | ☑ | **S/D** | (1)- Weight | Stresses<br>Displacements<br>Buckling<br>Natural frequencies | Nodes and members arrangement |
| [7] | 2016 | **S** | ☑ | ☐ | ☐ | **S** | (1)- Weight | AISC-ASD<br>Displacements | Cross-sections |
| [94] | 2016 | **S** | ☐ | ☐ | ☑ | **D** | (1)- Weight | Stresses<br>Displacements | Material distribution |
| [24] | 2016 | **S** | ☑ | ☐ | ☐ | **D** | (1)- Weight | LRFD-AISC | Cross-section |
| [41] | 2016 | **S** | ☑ | ☐ | ☑ | **D** | (1)- Weight | Geometric<br>Strength | Cross-section<br>Brace locations |
| [38] | 2016 | **D** | ☑ | ☐ | ☐ | **S** | (1)-Weight | Strength<br>Displacements<br>Performance objective | Cross-sections<br>Performance objectives |
| [59] | 2016 | **D** | ☑ | ☐ | ☑ | **S** | (1)-Weight | Strength<br>Displacements<br>Stability<br>Buckling | Cross-sections<br>Brace locations |

| | | | | | | | | | |
|---|---|---|---|---|---|---|---|---|---|
| [36] | 2017 | **S** | ☑ | ☐ | ☐ | **S** | (1)-Weight | Stresses<br>Displacements<br>Geometric bounds<br>Fabrication limits | Cross-sections |
| [83] | 2017 | **M** | ☑ | ☐ | ☐ | **D** | (1)-Weight<br>(2)-Ultimate drift<br>(3)-Stiffness response | Stresses<br>Geometric bounds | Cross-sections |
| [10] | 2018 | **S** | ☑ | ☑ | ☐ | **S/D** | (1)-Weight | AISC-LRFD | Cross-sections<br>Nodal Coordinates |
| [12] | 2018 | **S** | ☐ | ☐ | ☑ | **S/D** | (1)-Reaction forces | Stresses | Material distribution |
| [114] | 2018 | **M** | ☑ | ☐ | ☐ | **D** | (1)-Structural damage<br>(2)-Energy Dissipation | Stresses<br>Displacements | Cross-section |
| [67] | 2018 | **S** | ☑ | ☐ | ☐ | **S/D** | (1)-Weight | Stresses<br>Displacements | Cross-section |

| | | | | | | | | | |
|---|---|---|---|---|---|---|---|---|---|
| [39] | 2018 | **S** | ☑ | ☐ | ☐ | **S** | (1)-Weight | Stresses<br>Displacements | Cross-sections |
| [27] | 2018 | **S** | ☑ | ☐ | ☐ | **S** | (1)-Weight | Strength<br>Displacements<br>Geometric bounds | Cross-sections |
| [47] | 2019 | **S/D** | ☑ | ☐ | ☐ | **S** | (1)-Weight | Stress<br>Displacements<br>Slenderness<br>Geometric bounds | Cross-sections |
| [62] | 2019 | **S** | ☑ | ☐ | ☐ | **S** | (1)-Weight | Stress<br>Displacements | Cross-sections |
| [57] | 2019 | **M** | ☑ | ☐ | ☐ | **D** | (1)-Weight<br>(2)-Std deviation<br>inter story<br>drift | Stress<br>Displacements | Cross-sections |
| [55] | 2019 | **M** | ☑ | ☐ | ☐ | **D** | (1)-Weight<br>(2)-Uniform distr.<br>inter story<br>drift | FEMA | Cross-sections |
| [33] | 2019 | **S** | ☑ | ☐ | ☐ | **S** | (1)-Weight | Displacements | Cross-sections |

| | | | | | | | | | |
|---|---|---|---|---|---|---|---|---|---|
| [73] | 2019 | **S** | ☑ | ☐ | ☐ | **D** | (1)-Weight | AISC-LRFD | Cross-sections |
| [25] | 2019 | **M** | ☑ | ☐ | ☐ | **D** | (1)-Weight<br>(2)-Inter story drift | Stresses<br>Displacements<br>Geometric Bounds | Cross-sections |
| [42] | 2019 | **S** | ☑ | ☐ | ☐ | **D** | (1)-Displacements | Base shear<br>Lateral forces | Lateral forces |
| [49] | 2019 | **S** | ☑ | ☐ | ☑ | **D** | (1)-Weight | AISC-LRFD<br>PBD | Cross-sections<br>Brace locations |
| [110] | 2019 | **S** | ☑ | ☐ | ☑ | **S/D** | (1)-CMR | Designable matrix | Cross-sections<br>Brace locations |
| [92] | 2020 | **S** | ☑ | ☑ | ☐ | **S** | (1)-Weight | EC3 | Cross-sections<br>Coordinates of structural elements |
| [61] | 2020 | **S** | ☑ | ☑ | ☐ | **S** | (1)-Weight | ASCE | Cross-sections<br>Elements coordinates |

| | | | | | | | | | |
|---|---|---|---|---|---|---|---|---|---|
| [5] | 2020 | **S** | ☑ | ☐ | ☑ | **D** | (1)-Displacements | Brace configuration | Cross-sections<br>Brace locations<br>Slip force |
| [29] | 2021 | **S** | ☑ | ☐ | ☐ | **S** | (1)-Weight | Strenght<br>Deflection | Cross-sections |
| [11] | 2021 | **M** | ☐ | ☐ | ☑ | **S** | (1)-WIF | Constructability | Element forces |
| [35] | 2021 | **M** | ☑ | ☐ | ☐ | **S/D** | (1)-Weight<br>(2)-IDR | Strenght<br>Geoetric bubds<br>Constructability | Cross-Section |
| [80] | 2021 | **S** | ☑ | ☐ | ☐ | **D** | (1)-Weight | Strenght<br>Deformation<br>Plastic rotations | Cross-Section |
| [82] | 2021 | **M** | ☑ | ☐ | ☐ | **D** | (1)-Ductility<br>(2)-Energy dissipation | Geometric bounds | Cross-Section |
| [64] | 2021 | **S** | ☑ | ☐ | ☐ | **D** | (1)-Weight | Strenght<br>Displacements | Cross-Section |

| | | | | | | | | | |
|---|---|---|---|---|---|---|---|---|---|
| [31] | 2021 | **S** | ☑ | ☐ | ☐ | **D** | (1)-Weight | AISC-FEMA 365<br>Constructability | Cross-Section |
| [105] | 2022 | **S** | ☑ | ☐ | ☑ | **D** | (1)-Compliance | Stress<br>Strain<br>Max. material volume | Cross-Section<br>Brace locations |

# Chapter 3

# Constructability in structural optimization

In order to introduce properly this Chapter we should start by the definition of the term "constructability", which generally speaking is a crucial consideration in civil engineering that can greatly impact the success of a construction project. The Constructability Task Force of the Construction Industry Institute (CII), based at The University of Texas, in 1986, has defined constructability as *"the optimum use of construction knowledge and experience in planning, design, procurement and field operations to achieve overall project objectives"*. In United Kingdom the term "buildability" has been used to define *"the extent to which the design of the building facilitates ease of construction, subject to overall requirements for the completed building"*. Constructability has been identified also as *"the capability of being constructed"* by ASCE 1991, however in the present Thesis we are mainly addressing the meaning of *"integration of construction knowledge, resources, technology and experience into the engineering and design of a project"*, as stated in [4] by Anderson et al. Therefore, the key aspect one should have in mind is that information and experience gained throughout the construction phase must be accounted for and shared in the design in order to improve project objectives. Aimed at accomplish this task, several considerations can be made, ranging from general management organization recommendations to more particular techniques.

O'Connor, James T and Rusch, Stephen E and Schulz, Martin J in [84] started from CII definition and explored seven concepts for improving constructability, stressing the importance of construction-driven schedules, simplified designs, standardization,

preassebly work scoped in advance, easy accessibility, adverse weather facilitation and a careful review of specifications by owner, designer, and constructor personnel. Pulaski, Michael H and Horman, Michael Jin in [93], proposed a model to organize constructability information for design, according to timing and levels of detail, with the intent to link constructability rules to different stages of building design in a step-by-step format. They concluded that "the key to accessing constructability is introducing the right information at the right time and in the right level of detail". Furthermore, also encouragement to innovations, learned lesson from past projects, availability of resources, as well as waste management may all enhance constructability, as highlighted in [66].
Constructability considerations provide several important advantages, many of which are sometimes challenging to understand and evaluate. Russell, Jeffrey S and Swiggum, Kevin E and Shapiro in [98] distinguished such benefits between qualitative and quantitative ones, as reported in 3.1, proposing a way for their estimation. The

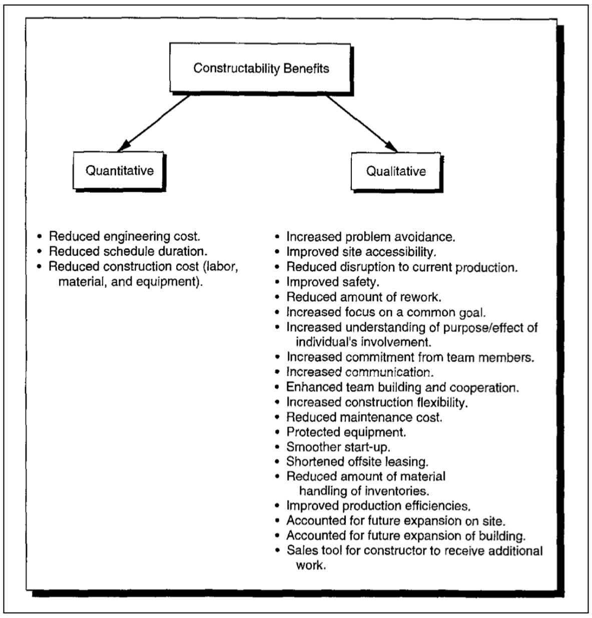


Figure 3.1: Framework for determining constructability benefits [98]

quantitative advantages are the ones that directly reduce cost and schedule duration; their effect can be measured by determining the impact of the change from that of standard practice. The utilization of fewer materials, fewer workers (i.e., reduced labor effort-hours) and fewer fixed pieces of equipment during construction can all help to quantify cost abatement. Also the reduced schedule, in comparison with standard practice, can be translated into cost savings. Instead, substantial qualitative advantages include the prevention of issues through improved collaboration, cooperation, and respect among participants. They also involved more site accessibility and safety, less rework, decreased maintenance costs, intensified focus on common goal, increased construction flexibility, etc. Since it is crucial that any construction project is carried out by the planned completion date, to reduce issues like scheduling conflicts, delays and disagreements that may arise, Arditi et al. in [6] conducted a questionnaire survey of design companies about the adoption of constructability. The benefits, reported in 3.2, are in terms of creating better client and constructors relationship, being involved in fewer lawsuits, a better reputation, professional satisfaction and efficient design. In particular, they have been ranked from 0 to 3, with 0 being the least influential and 3 the most relevant.

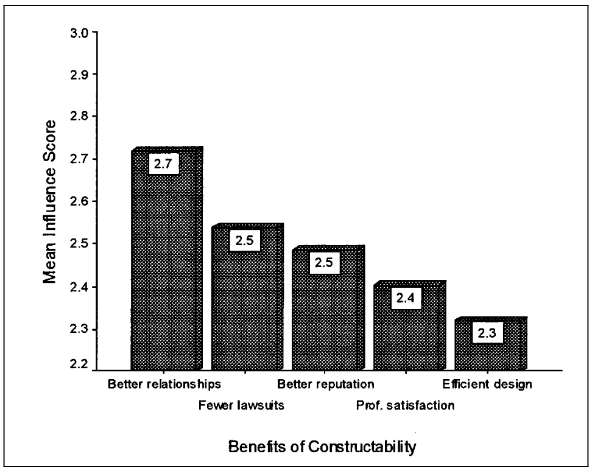


Figure 3.2: Benefits of constructability highlighted by the survey in [6]

Another important aspect, emphasized in [97] is the fact that constructability is a design philosophy that originates from the conceptual design stage, continues through design, and links project planning with design and construction. Therefore, constructability issues have to be identified and analysized at the design phase, not at the end once construction phase starts. Integrating such considerations at the beginning will improve the overall project, the efficiency of construction, as it allows for a more streamlined and cost-effective process. As stated in [66], making use of construction knowledge from the earliest stages of a project, where the ability to influence cost is at greatest, makes sense from both practical and financial viewpoints. Paulson in 1976 [90] described the interrelationships between engineering design, construction and operation costs for a facility, showing how the level of control on those costs decreases as the project evolves. In the reported figure 3.3, the idea of the author is exemplified. In the lower portion, the life of a project, as a function of time, is distinguished into three phases, namely (1) Engineering and design, (2) Procurement and construction, (3) Utilization or operation; in the upper portion, instead, two curves are plotted, always as a function of project time, where the ascending one tracks the cumulative project expenditures, while the descending one shows the decreasing level of influence. In the early phases of design, when the expenditures are relatively small, the project team has the most opportunity to impact the overall cost of the facility. In fact, the decisions and commitments made during this period have an enormously greater impact on future costs; later on, when the cumulative cost of the project increases, the level of influence on such expense will go towards zero. Thus, the initial design phase is crucial and cooperation, together with a high level of details, is required to incorporate basic constructability aspects.

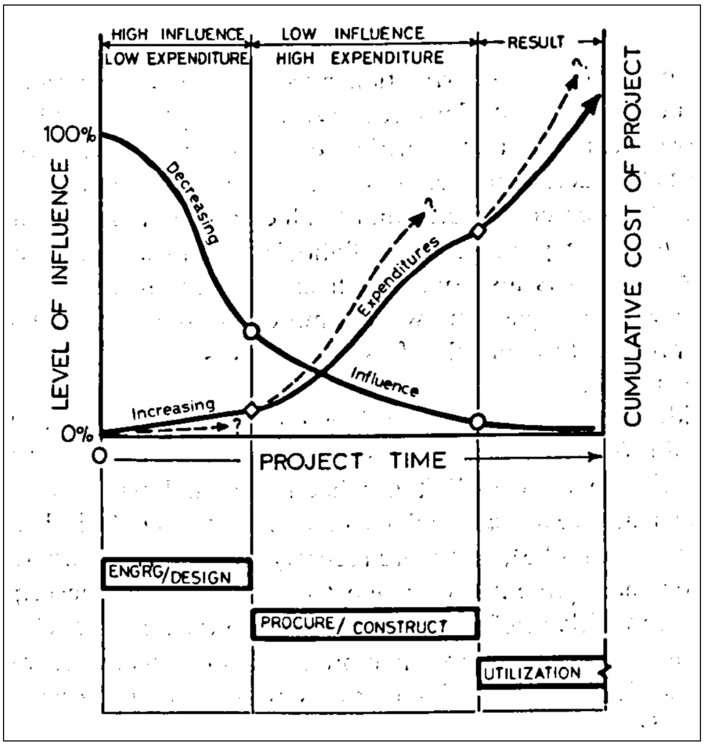


Figure 3.3: Level of influence on project costs by Paulson in [90]

Therefore, constructability in structural optimization can be interpreted as the process of incorporating construction expertise and knowledge into the design and optimization phase. The difficulty of such process is that there are many factors involved. Many of these influencing factors regard the management procedure, thus a good collaboration between all the team members, as well as the importance of having professional and qualified personnel, early involvement of contractor in design and so on. However, in the present Thesis we are more interest in looking at the constructability factors that can be integrated in the structural design choices, and more specifically in the optimization set-up. There are construction techniques that are just intended to simplify the overall production of necessary pieces for the given structure, to reduce the number of elements as well as connections typologies, to standardize sections, to encourage the employment of less diversity, to facilitate the assembly, but also the erection phase and so on. Always from the survey of Arditi et al. in [6], as reported in 3.4, eight factors impacting constructability has been listed and ranked, such as project complexity, design practices, project delivery, project size, project type, client type, project location, and design standards. In the same article, the authors also addressed the factors constraining constructability, as reported in 3.5. Faulty, ambiguous, or defective working drawings, incomplete specifications, and adversarial relationships were found to be the three major factors that cause constructability problems.

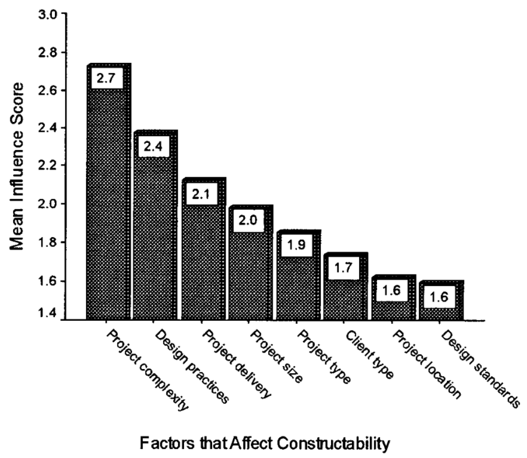


Figure 3.4: Factors affecting constructability [6]

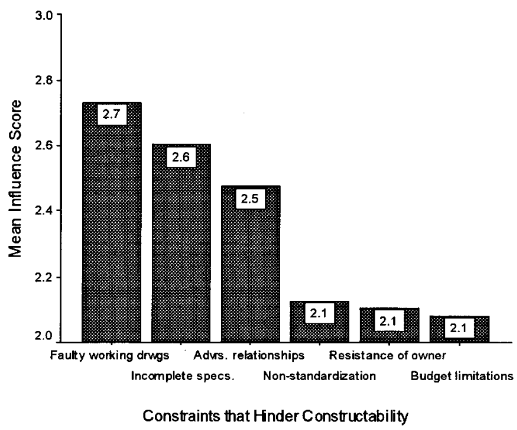


Figure 3.5: Constraints on constructability [6]

Among them, non-standardization of design, which would have a detrimental impact, also plays a significant role. In general, using standardized components and systems can help improve constructability by reducing the need for custom fabrication and assembly. The idea of standardization has been defined, by Pasquire et al. in [89], as "the extensive use of components, methods or processes with regularity, repetition and a successful history" . In [113], Wong et al., also explained how standardization can be translated as the repetition of grids, sizes of components and connection details, stressing the benefits in terms of faster construction, reduced number of mould changes and enhanced productivity. In [66] it has been emphasized the fact that it can be applied to various scenarios from building systems, materials types, construction details and so on, depending also on the economic analysis scale. In fact, the reduction in variety can lead to many benefits such as discounts on more pieces of same material, simplified procedures and so on. Summarizing, standardization is a term that can include different meanings, from the employment of standard elements in the design of a structure, avoiding particular and unique shapes or sections, but also the repetition of members, connections, as well as procedures in the overall project. Furthermore, from a more general point of view, standardization is also paired with modularization and pre-assemble techniques. By looking at the design of a simple truss structure, the structural choices that can be made with a standardization-driven orientation regard the employment of the least amount of different cross-sections, but also the reduction in variation of the connections. In any case, we should always remember the verification of structural and geometric requirements. In Chapter 2 we have seen many examples of side constraints, mainly concerning the joints between beams and columns in frame structures.

An interesting research has been conducted by Abbigayle Horn in [51], where constructability has been defined as the standardization of primary structural elements to balance multi-objective design goals. In particular, the author has introduced non-subjective, quantifiable metrics to measure standardization of structural components. The study focused on two-dimensional steel truss façade structures, subjected to lateral loading with a pinned base, whose scheme is reported in 3.6. Shape optimization has been pursued by allowing node translations in the horizontal and vertical directions, while topology optimization has been completed via Boolean operators that turned diagonal elements on or off. Moreover the number of vertical bays was also a variable in the study, exploring the possibility of having five or six vertical bays. Then, in the structural verification phase, member sizing has been determined based on the minimum area required to satisfy both stress and buckling criteria. The metrics that has been considered to quantify structural performance, which was later compared with constructability performance metrics, regarded the lateral deflection of the façade system at the top of the structure, strain energy and structural weight. The new introduced constructability metrics, formulated to measure design characteristics from a constructability perspective, were:

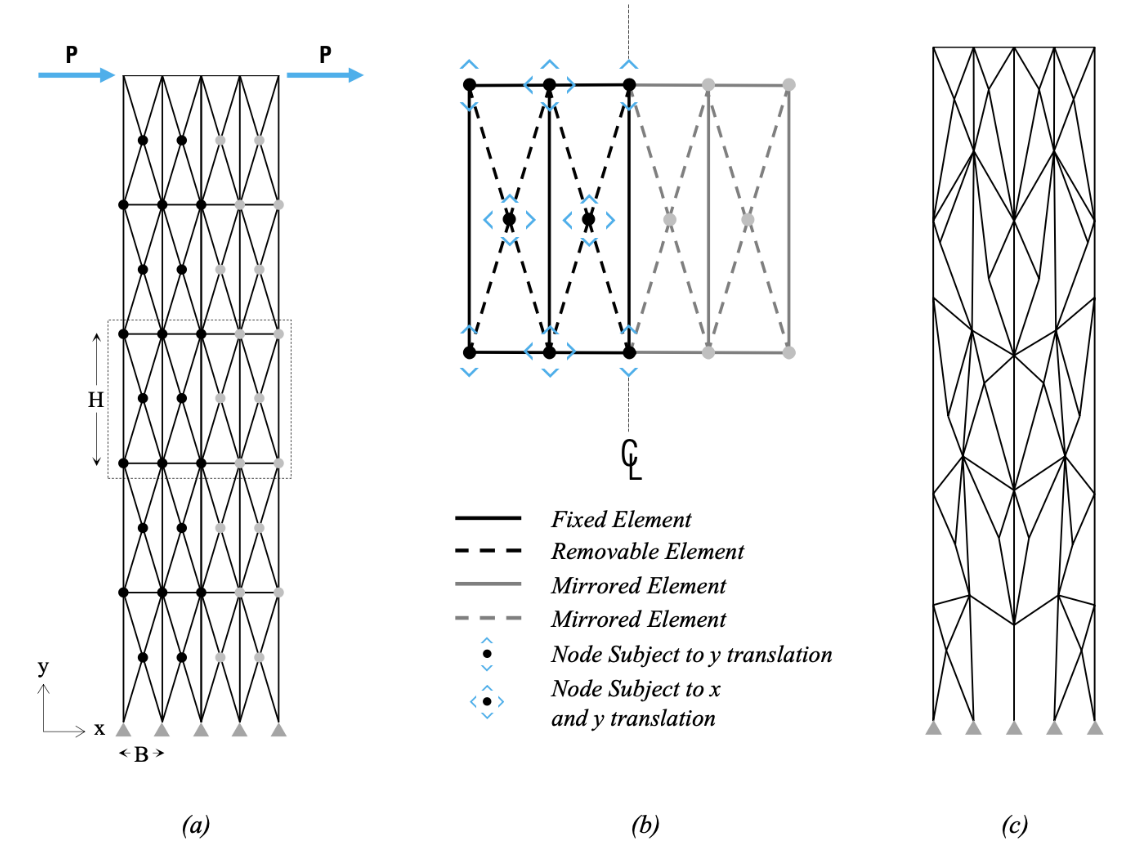


***Figure 2.1:*** *Two-dimensional façade structure subject to geometric and topological variations. The variables shown in this model are randomized to explore the design and objective spaces. (a) Initial structure before modifications are imposed. (b) Variable settings including node translations and members subject to topological modifications. (c) Sample output designs based on variable randomization.*

Figure 3.6: Two-dimensional steel truss façade structure analyzed in [51]

1. Standardized Member Length (SL), by means of which, once calculated the average member length for each design iteration, each member has been penalized based on its difference from the mean;

2. Truck requirements (TR), accounting for length and weight restrictions that would lead to the acquisition of special permits for the shipping phase;

3. Field Connections, both bolted and welded, have been minimized to reduce the number of man hours expended on site for laborers and crane operators;

4. Node Member Connectivity (NMC), aimed at minimizing the number of members framing into a single node;

5. Node Angle Connectivity (NAC), which imposed that each member framing

into the node must have a minimum separation;

6. Cross Section Variation (CSV), aimed at reducing the number of section used.

Regarding the first metric, it has been proposed a practical application of standardizing member length, in which members are grouped into sets of standard lengths in order to improve effectively fabrication and erection procedures. Then, TR involved the application, at first, of length restrictions to the elements needed, leading to the cut of oversized members, and then of weight constraints, in order to count the number of trucks filled and eventually to obtain the minimum one. In this way, enhancing standard shipping, the timing of transportation could be better coordinated with on-site work, yielding construction cost savings and reducing site logistics associated with trucking and oversized load permitting. Depending on the number of splices required to satisfy shipping constraints and the total number of members in the structure, field connections have been evaluated, with the intent of reducing their number. Both NMC and NAC have been used to maximize the accessibility of the laborers to the cast node pads and minimize the number of infeasible connections. The final goal was to improve the speed of construction by reducing connection time in the fabrication and erection phases. Particularly interesting is the the last metric developed, which discouraged high variation in member sizing, which would lead to more complex fabrication and erection processes, especially in the case of non-standard shapes. In an attempt to obtain the least amount of different cross sectional areas, the author has assigned a value to each cross-section to determine the number of unique cross-sections. This has been obtained by multiplying the required diameter, in inches, by ten and adding the member thickness in decimal inches. The final minimized metric was determined based on the percentage of all members that have unique cross sections, so the ratio between the number of unique cross sections divided by the total number of elements. From the output of the analysis, it has been found that the general trends observed implied that there are significant tradeoffs between constructability and structural performance. However, the impact of standardization on weight has to be carefully analysized. In fact, as the number of cross sections in a given structure was decreased, the overall weight of the structure increased, as expected, but this increase is relatively minor in comparison to the significant improvement in constructability. In the reported figure 3.7 it has been shown the case in which the number of different cross-sections in a structure were reduced by a factor of 10, while the structural weight increased by a factor of 2. This implies that remarkable labor and cost savings can be achieved by consolidating cross-sections, while the increase in the cost of material is marginal in comparison.

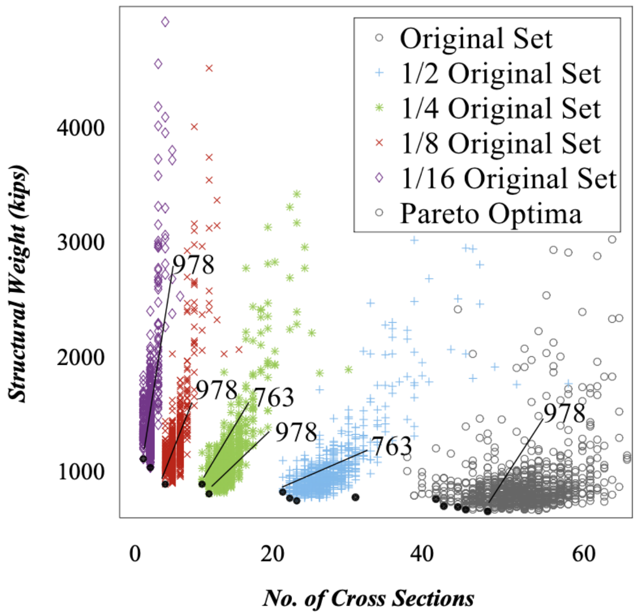


***Figure 3.6:*** *Standardization of cross sections into consolidated sets compared with the structural performance metric, Structural Weight.*

Figure 3.7: Impact of standardization on structural weight [51]

From the experience of the previous studies we can understand how constructability considerations integrated in the design phase will behave as competitive goals with respect to the typical weight minimization one. We can think for example at the complexity topic affecting truss structures, which involves the reduction of the number of nodes and thus leading to longer members. In turn, these elements would have bigger sections to satisfy structural requirements, perhaps implying heavier designs. The same implication would follows the standardization technique, which encourages less diversity in the sections used. However, repetition of members sizes at the cost of some added member weight, can simplifies detailing, fabrication and erection costs. Thus, by means of a simpler and standardized design, we can abate the overall cost, which is generally the most appealing target objective.

# Chapter 4

# Case study 1 - Truss level

After having discussed the basic structural optimization methodologies and constructability difficulties, in the current Chapter we are going to describe the case study on which we have concentrated our investigation. Specifically, we have performed the simultaneous size, shape and topology optimization of steel truss structures, not intended to the most common weight minimization, but developing a new objective function integrated with constructability criteria. At first, we have introduced the truss structure characteristics and employments in civil engineering, as well as how they can be modelled following a parametric design; then we have clarified the design variables considered in the optimization, along with the grouping strategy developed to improve the schematization of the problem. Subsequently the model set-up, the definition of the Objective Function has been discussed, starting from the original hypothesis considered to the final formulation. Finally, from the results comparison of the proposed method and the more common weight minimization, we have highlighted the influence of the additional constructability criteria in the definition of the best individuals. In particular, in this Chapter we have depicted the analysis at the truss level, with the intent to enlarge the point of view, in the following Chapter, towards the scale of a single storey industrial building.

## 4.1 Truss structures

Trusses are made by a configuration of beams, mainly in triangles, that allow to create strong but at the same time lightweight structures. A truss is defined stable if the number of members is just sufficient to prevent distortion of its shape when loaded externally. Specifically, this condition is verified if the equation $m = 2j - 3$ is satisfied, where $j$ is the number of joints and $m$ is the number of members. When the number of members is less than $2j-3$, it would be a deficient or unstable truss. Instead, when the number of members is more than $2j - 3$, the unstable truss is called redundant.

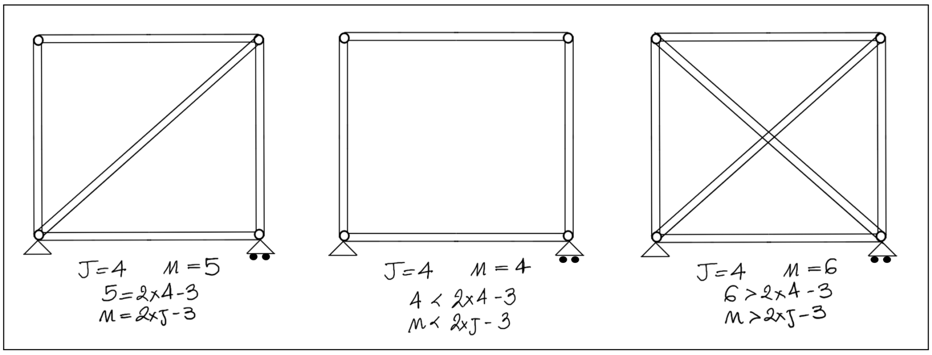


Figure 4.1: Stable and unstable truss configurations: (a) Isostatic (b) Unstable with $m < 2j - 3$ (c) Unstable redundant with $m > 2j - 3$

In a stable truss, the nodes between members are considered as pinned connections, while the external supports are whether hinges or rollers. Moreover, they are able to withstand external loads by developing almost exclusively axial forces, with negligible bending moment and shear force. This is due to the fact that the loads are assumed to be applied only at the nodes, which are supposed to be ideal internal hinges. True pins with free rotation are quite rare in practice. This is mostly due to the comparatively high cost of manufacturing such joints. The joints of a steel truss are nearly always bolted or welded. As a result, bending moments will be transferred to some extent through joints and therefore within the structure. The shape of the joints, on the other hand, is generally such that their capacity to transfer moment is fairly limited. As a result, our assumption frequently leads model behavior to diverge only little from the real one. With reference to the members developing only axial loads, we can use two main approaches to solve a truss structure, which means to calculate the internal forces along each member. Before going into details of such methods, we would like to give a preliminary indication of a truss scheme. If we use the analogy with the Timoshenko beam, the distribution of internal solicitations is intuitive prior to any computation. As for the case of an inflected beam, the upper chord will absorb the compression forces, while the lower chord the tension ones. The magnitude of such internal actions is following simple beam's bending moment diagram, with maximum value in the middle towards zero value at the supports. Vertical and diagonal elements, instead, will absorb the shear actions and they can be in tension and compression alternatively. As before, also their internal force will follow the shear force diagram of a simple supported beam, with higher values at the supports and almost null values in the middle.

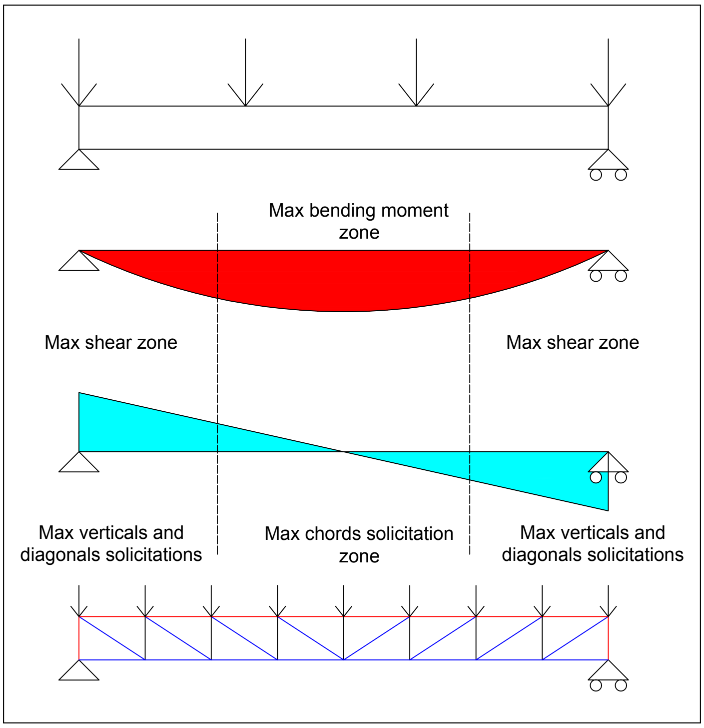


Figure 4.2: Timoshenko beam analogy to have an indication of truss's solicitation distribution

The two rigorous approaches to solve truss structures are the Method of joints and the Method of sections. The former one exploits the equilibrium at each node to retrieve the axial forces along the beam elements. Moreover, the truss is isostatic externally, thus if we know the acting forces, we can calculate the external reactions and then the distribution of the internal forces. An example is reported below, in figure 4.3 to clarify the procedure. Instead, if we are not interested in knowing the axial force in each member but only in specific ones, we can proceed with the Method of sections, also called Ritter's Method. A truss made of triangles is characterized by the property of being cut by an ideal section, which divides the structure in two by passing from only 3 members not joining at the same node. So, we can imagine to divide the truss into two free bodies by passing an imaginary cutting plane through the structure. The cutting plane must, of course, pass through the bar whose force is to be determined. At each point where a bar is cut, the internal force in the bar is applied to the face of the cut as an external load. Although there is no restriction on the number of bars that can be cut, we often use sections that cut three bars since three equations of static equilibrium are available to analyze a free body. For example, if the force in a diagonal bar of a truss with parallel chords is to be computed, we cut a free body by passing a vertical section through the diagonal bar to be analyzed. An equilibrium equation based on summing forces in the y direction will permit us to determine the vertical component of force in the diagonal bar. Instead, if three bars are cut, the force in a particular bar can be determined by extending the forces in the other two bars along their line of action until they intersect. By summing moments about the axis through the point of intersection, we can write an equation involving the third force or one of its components. The previous example is shown also with the resolution obtained by Ritter's Method.

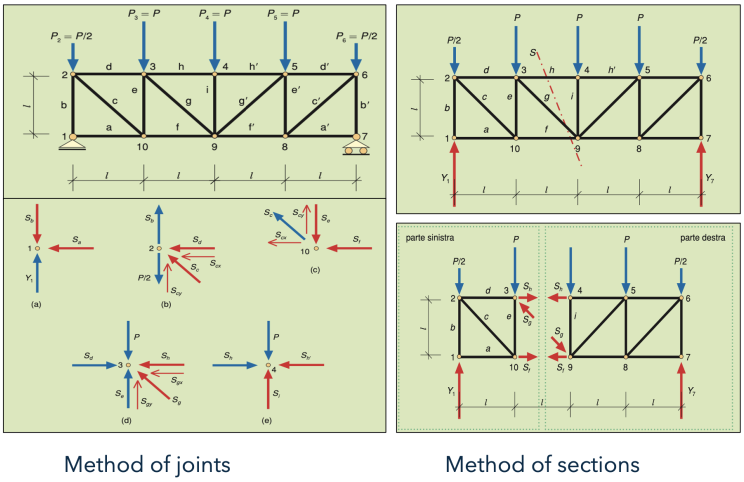


| Member | Tension | Compression |
|---|---|---|
| a,a' | | 0 |
| b,b' | | 2P |
| c,c' | $3/2\sqrt{2}$P | |
| d,d' | | 3/2P |
| e,e' | | 3/2P |
| f,f' | 3/2P | |
| g,g' | $1/2\sqrt{2}$P | |
| h,h' | | 2P |
| i | | P |

Results

Figure 4.3: Methods for truss resolutions - example

From this theoretical introduction to truss structures, now we are going to describe their most common usage in real life applications. In general, truss structures are made of steel or timber, however here we are focusing the attention only on the former ones. In particular, steel is a durable and corrosion-resistant material, making it perfect for usage in outdoor and industrial applications. One of the advantages of steel truss structures is their ability to span long distances without the need for intermediate supports. In fact, they are commonly used in the construction of large buildings such as warehouses, factories and exhibition halls, as well as in the construction of bridges, airports, and other infrastructure projects. They are also used in the construction of roofs, where their strength and rigidity make them ideal for supporting heavy loads and spanning long distances. Trusses are also relatively lightweight compared to other structural systems, which can reduce the overall cost of construction. Moreover, there are many different types of steel truss structures, each one designed to meet specific engineering and architectural requirements. These include Pratt trusses, Warren trusses, Howe trusses, and many others. The type of truss used depends on factors such as the span of the structure, the load-bearing capacity required, besides the aesthetic preferences of the designer. Moreover, the upper chord can be parallel to the lower chord or it can be inclined. For example, in case of roof trusses in areas where snow fall is common, an inclination between 10° to 60° is recommended to drain part of the snow falling from the roof surface.

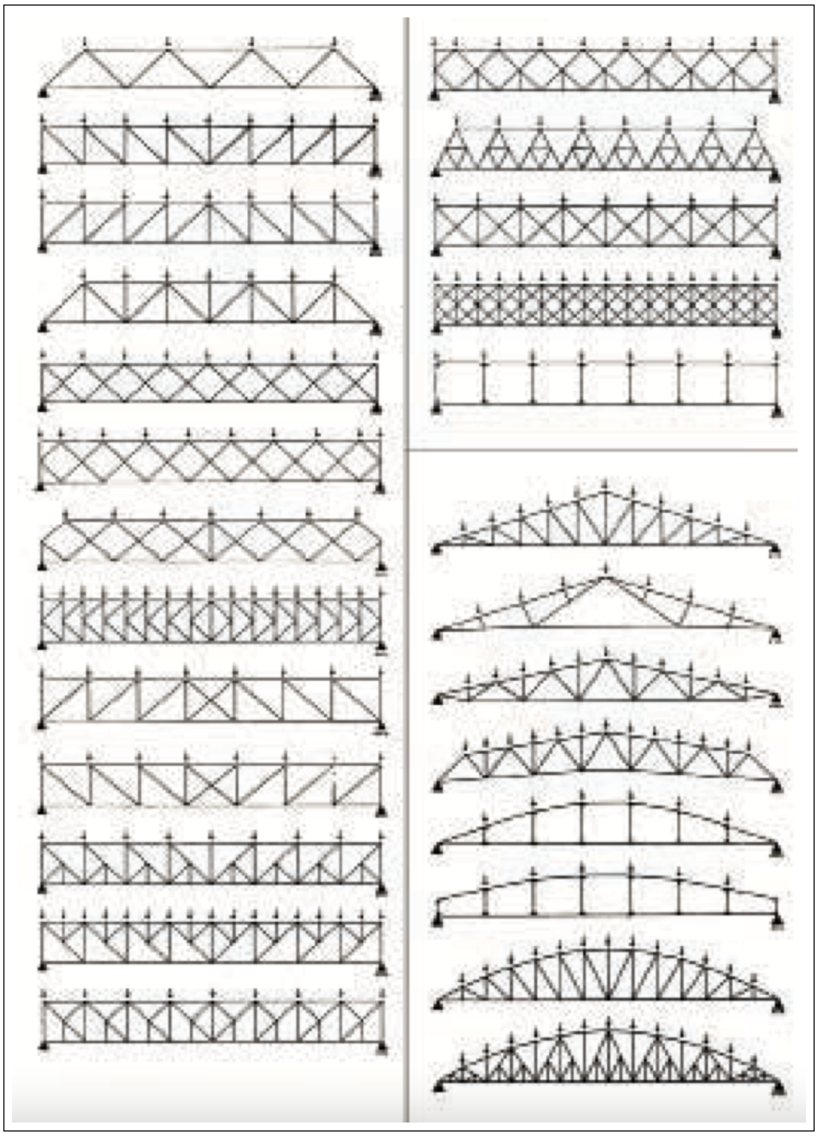

Figure 4.4: Different truss schemes

## 4.2 Parametric Design

The models of the structures studied in the present Thesis have been made following a parametric design approach. The advantage of this technique is that it is very useful for optimization and form finding, because makes it possible to get different versions of a model by varying just input parameters. Parametricism relies on programs, algorithms and computers to manipulate equations for design purposes. The term 'Parametricism', coined in 2008 by Patrik Schumacher, implies that all elements of architecture are becoming parametrically malleable and thus adaptive to each other and to the context. Basically, the relationships between different design elements are established mathematically, and changes made to one of them will automatically affect the others that are connected to it. This allows designers to quickly and easily explore different design options, managing several spatial elements together, and obtaining countless shapes and configurations. Parametric design has become increasingly popular in architecture, industrial design and engineering. It offers numerous advantages over traditional design approaches, including increased efficiency, precision and flexibility. With this approach designers can swiftly create complex and intricate geometries that would be difficult or impossible to achieve using traditional methods. One of the earliest examples of parametric design was the upside down model of churches by Antonio Gaudi. Basically, he created complex vaulted ceilings and arches by suspended weighted strings. By adjusting the position of the weights or the length of the strings, he could change the shape of the catenary arches and, accordingly, the entire model. Later on, the italian Luigi Moretti was the first architect to use the phrase "parametric architecture" in 1939; then, Frei Otto captured the experimental nature of parametric modeling by his "form-finding" activities derived from soap films and paths. In recent decades, parametric modeling has found its way into projects through software packages' scripting interfaces. Examples of such softwares are Grasshopper developed by Robert McNeel&Associates, Bentley Systems' Generative Components, and Revit Autodesk's Dynamo. Zaha Hadid Architects is one of the most widely known architecture firm that brings large-scale parametrically designed buildings to life. The Galaxy SOHO Mall in Beijing, China, is an office, retail, and entertainment complex with almost no visible corners or sharp edges. French architect Jean Nouvel has designed many buildings using parametric design, one of the most notable being the Louvre Abu Dabi. Another example of parametric architecture is Santiago Calatrava's otherworldly design for the World Trade Center Transportation Hub (also known as the Oculus) in New York City. Another name worth mentioning in this framework is the talented italian architect and designer Arturo Tedeschi, also known for its writings about Grasshopper modelling. His works spectrum covers different fields of application, from the traditional architecture, to the industrial design environment (furniture, automotive, installations, products, footwear), where all projects are characterized by extravagant and fashinating shapes.

Figure 4.5: Galaxy SOHO Mall in Beijing by Zaha Hadid

Figure 4.6: World Trade Center Transportation Hub by Santiago Calatrava

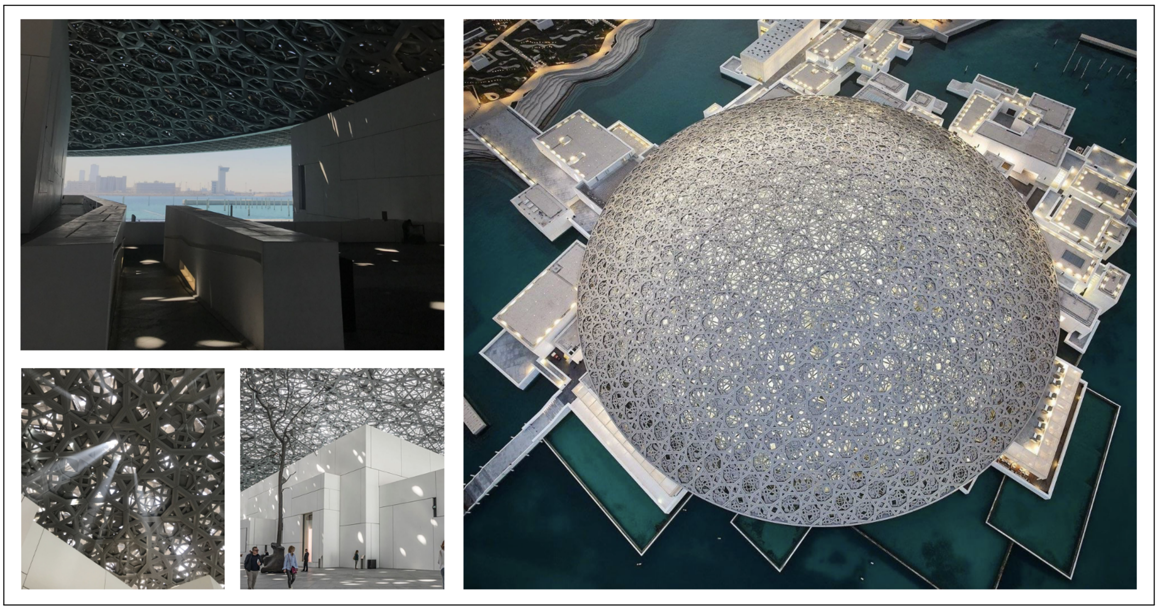

Figure 4.7: Louvre Abu Dhabi by Jean Nouvel

Figure 4.8: Arturo Tedeschi works: HorizON lamp, Ilabo Shoes, Sistema Fessura, The Cloudbridge, from the upper left to bottom right side.

### 4.2.1 Softwares used

The software used in this Thesis to exploit the parametric design principles is Rhinoceros 3D, which includes Grasshopper 3D with Karamba 3D and Octopus plug-ins.

Figure 4.9: Softwares used

- **Rhinoceros 3D**

  It is a 3D modelling tool, commonly used by architects and designers in the early design phase. The software have been developed by McNeel&Associates in 2008. It has been categorized in the CADs software, but it allows to represent very complex form and structures, making it more powerful with respect to AutoCAD software, for example. Rhino uses non-uniform rational b-spline (NURBS), which are mathematical representations of a 3D geometry. NURBS allow to accurately reproduce very complex geometries, from a simple 2D curve to the most challenging 3D shape. Rhino works in parallel with Grasshopper, in fact it allow us to visualize what we are designing in the Grasshopper environment.

- **Grasshopper 3D**

  Grasshopper3D is a visual modelling program, which is able to construct an iterative and interactive design process by modelling objects parametrically. The utility and efficiency of the program is enhanced by the plug-ins contained inside. Specifically, in this Thesis, Karamba3D and Octopus are the main ones used. Focusing on our cases study, this software was very useful to run size, shape and topology optimizations. In fact, by changing the value of the slider component connected to the specific design variable, the software allows to re-create immediately and in a continuously way, several geometries by changing for example cross-sections, number of subdivisions, coordinates of the points, typology of the truss etc.

- **Karamba3D**

  Karamba 3D is a parametric structural analysis tool which is fully embedded into the visual programming environment Grasshopper. It can perform detailed Structural Finite Element Analysis (FEA) for spatial trusses, frames and shell structures. Specifically, in the present Thesis, this Rhino plug-in was used for the structural verification of truss structure in this Chapter and in the following one also for the industrial building. Although it could be less robust than commercial softwares, due to its fast interactivity with Grasshopper, it results more suitable than other FE programs, highly reducing the total amount of computational time. Data are instantly sent from the parametric model created in Grasshopper to Karamba solutor, which subsequently passes the analysis's outputs to the optimizator. In particular, the elements created as simple geometry in Grasshopper are then converted into FEM components and assembled, by indicating the assigned cross-sections, material, joints, supports and loads applied. By means of the "Utilization of elements" component, the structural verification towards buckling requirements can be implemented, according to EN 1993-1-1 included in Eurocode 3 (Design of steel structures - General rules and rules for buildings).

- **Octopus**

  In our Thesis we have not used the more common optimizator Galapagos, but instead we have employed Octopus, developed by Robert Vierlinger and his team, at the University of Applied Arts Vienna. It is a Grasshopper plug-in that enables the solving of a wide range of Multi Objective Optimization

(MOO) issues. In order to find Pareto-optimal solutions, Octopus offers two global metaheuristics methods:

⇒ SPEA2, which stands for "Strength Pareto Evolutionary Algorithm 2"

⇒ Hype Reduction, i.e. "Hypervolume Reduction Algorithm"

Different parameters related to how the algorithm will search for the optimal solutions needs to be set:

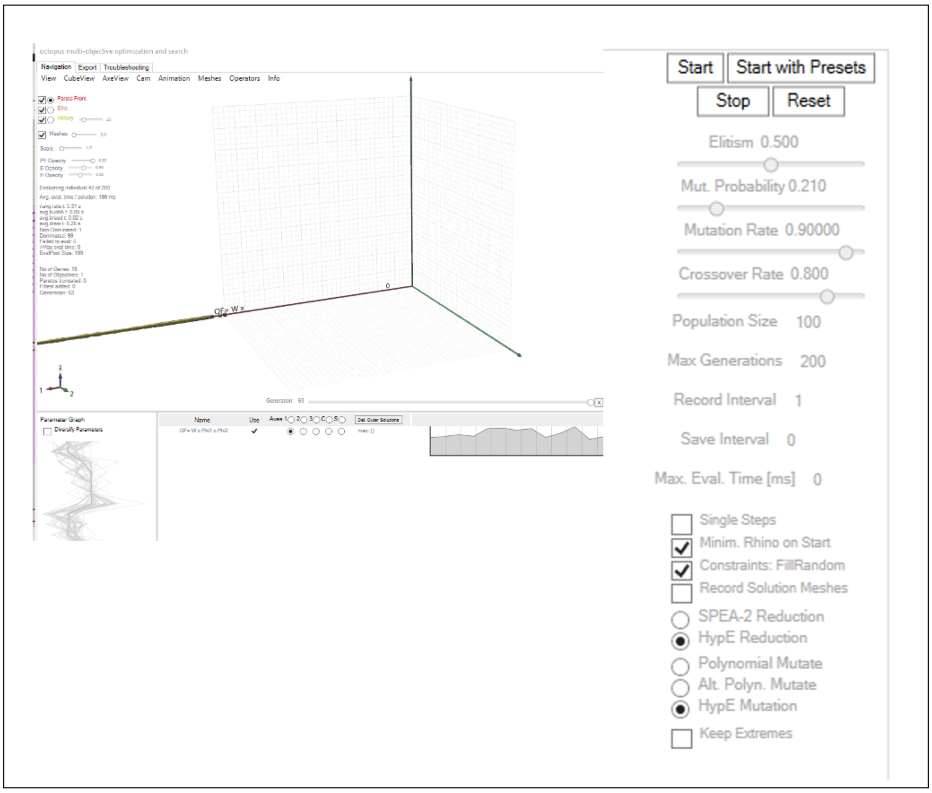


Figure 4.10: Octopus interface

- Elitism gives the percentage of new solutions that are bred out the Elite instead of the entire pool; if high, more local optimization is performed.
- Mut. Probability is the probability of each parameter /gene to become mutated with the 'Mutation Rate'. A low Mutation Rate means little changes to the parameters' values, a high rate means big changes.
- Crossover Rate is the probability of two subsequently generated solutions to exchange parameter values.
- Population Size is the number of solutions per generation. The Elite size is set accordingly, so a total of 2 x Population Size number of solutions are in each generations' pool. This size should be set according to the complexity

of the problem, since a lot of solutions at the same time can maintain a lot of different alternatives.

– Max. Generations is set to zero by default, meaning there is no end to the search. Otherwise Octopus will stop after this number of generations.

– Record Interval is the interval of generations in which a history record is stored.

– Save Interval gives the interval of generations after which the Grasshopper file is saved to prevent data loss when Rhino crashes during search for whatever reason.

Some of those parameters were already mentioned in the Chapter 2 like: Mutuation Probability, Cross-over rate and Elitism. More in details, it is important to appropriately define the population size and maximum number of generations. Both of them are based on the complexity of the problem, in particular a lot of solutions at the same time can maintain several alternatives leading to a more refined optimal solution. In order to start the optimization the algorithm needs to be connected to the different design variables previously defined and to the Objective Function that needs to be minimized.

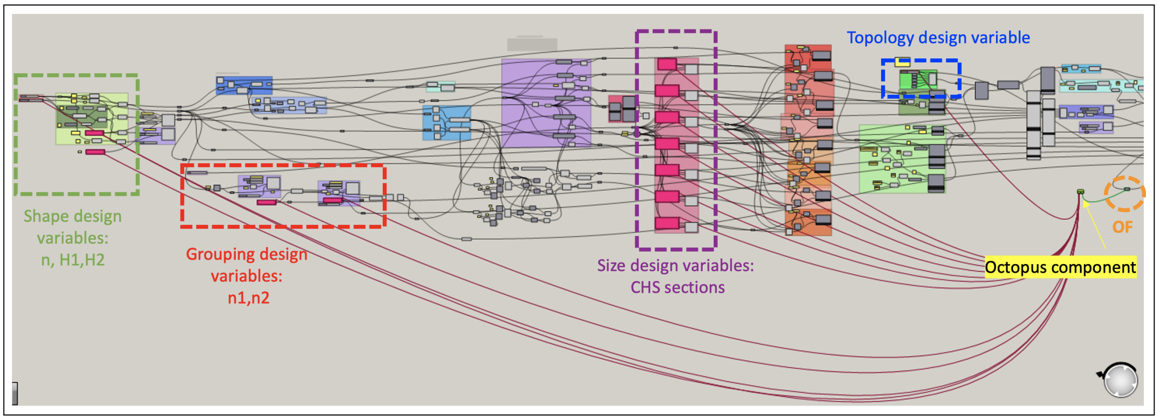


Figure 4.11: Octopus component connected to all the design variables and to the OF

Therefore, the geometry of our structure has been parametrically modelled in Grasshopper. Then, it has been traduced in the FEM elements using the Karamba3D components, assigning the cross-sections, loads and supports. Finally, the design variables and the objective function have been connected to the Octopus optimizator.

## 4.3 Problem overview

As stated before, our intent is to perform a simultaneous size, shape and topology optimization of a steel truss structure. Considering a total span length of 20 meters, we have modelled in a parametric way the truss by creating a first half of the geometry and then exploiting the symmetry with respect to the vertical axis in the middle.

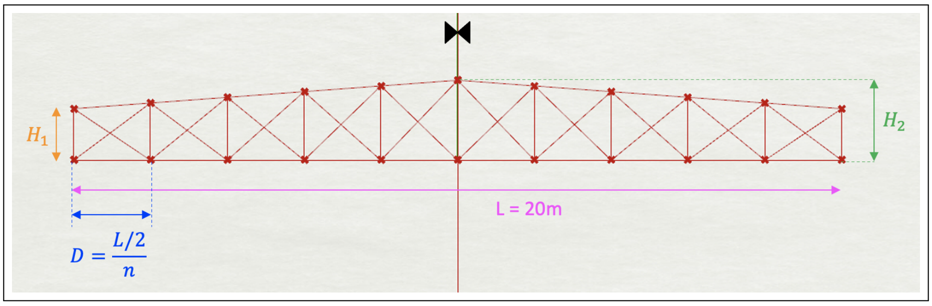


Figure 4.12: Schematic representation of the truss

The shape optimization variables have been identified as the number of subdivisions of half the chords ($n$), along with the heights of the edges ($H_1$) and middle point ($H_2$) of the upper chord. Always considering half geometry, the range in which $n$ can be varied is in between 3 and 10. The upper bound has been set considering a minimum distance between consecutive nodes of 1 meter, while the lower bound accounting for the grouping strategy, explained in the next paragraph 4.4. From a pre-dimensioning of the structure, we have set a range for the height at the edges $H_1$ in between a value of $L/15$ and $L/10$, while the central height $H_2$ ranges between the current value of $H_1$ and a maximum of $L/8$.
Anyways, these variables are not independent one from each other because of geometrical considerations. In fact, the inclination of diagonal members is suggested to be in between 30° and 60° degrees. Therefore, we have imposed the relationship of H1 and H2 as a function of n, combining two conditions:

- Pre-dimensioning rules
  $\frac{L}{15} < H_1 < \frac{L}{10}$
  $H_1 < H_2 < \frac{L}{8}$
- Diagonals inclination in between 30° and 60°
  $D \cdot tan30° < H_i < D \cdot tan60°$, with D equal to the distance between consecutive nodes, computed as $\frac{L/2}{n}$

Depending whether the first of second condition is more stringent than the other, we would obtain a domain for $H_1$ and $H_2$ ranging from minimum and maximum values, according to the following relationships:

| Domain of $H_1$ | Domain of $H_2$ |
|---|---|
| $H_{1,min}$=max($\frac{L}{15}$,$D \cdot tan30°$) | $H_{2,min}$ = max($H_1$,$D \cdot tan30°$) |
| $H_{1,max}$=min($\frac{L}{10}$,$D \cdot tan60°$) | $H_{2,max}$=min($\frac{L}{8}$,$D \cdot tan60°$) |

Table 4.1: Domains definition for $H_1$ and $H_2$ as $H_{i,min} < H_i < H_{i,max}$

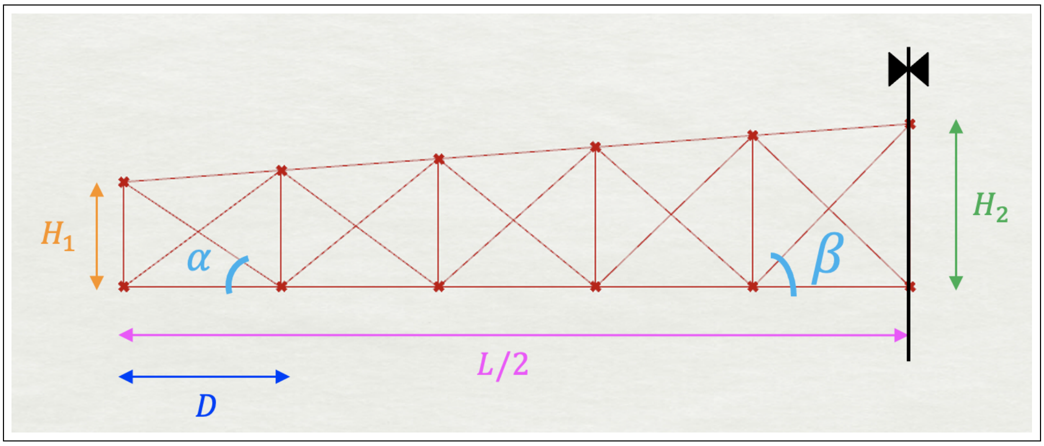


Figure 4.13: Scheme for relationship between n and H1,H2, where $\alpha$ should be at least 30°and $\beta$ maximum value is 60°

Regarding the topology optimization, we have created in Grasshopper five different truss types, namely Vierendeel, Brown, Pratt, Howe and Warren ones. Here below, we have explained their main characteristics and real-life applications:

- VIERENDEEL TRUSS
  This layout of structure was named after the Belgian engineer Arthur Vierendeel, who developed the design in 1896. It is characterized by the absence of diagonal members, without any triangular mesh inside. For this reason, to avoid the instability of the structure, the nodes have to be designed not as pinned connections but fixed ones, in order to guarantee any relative rotation of the members. This is its primary characteristic that sets the Vierendeel apart from other truss layouts. Thus, its cross-sections would be thicker if compared to other typologies with the same span, resulting in heavier designs. Anyhow, it

is widely employed in civil engineering structures, resulting in a more aesthetically pleasing harmonic configuration. For example, it is preferred in presence of windows or open doors, because the exterior envelope remains unobstructed.

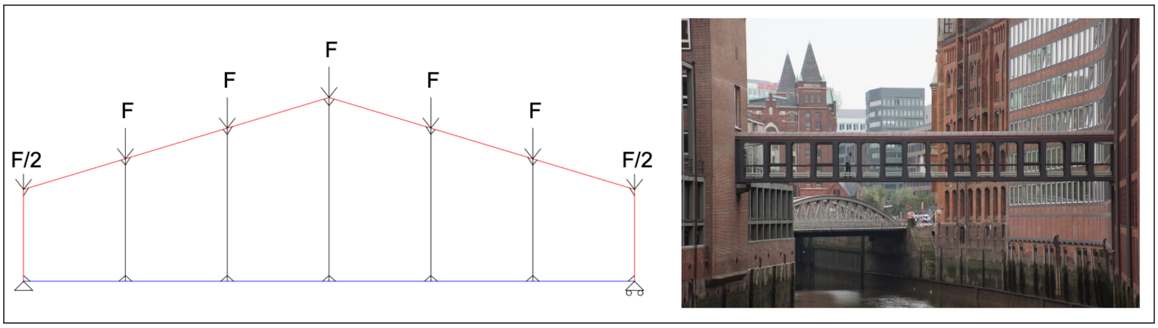


Figure 4.14: Vierendeel truss scheme and application example: AMERON Hotel Speicherstadt footbridge

- PRATT TRUSS

  Pratt truss, first proposed by Thomas Pratt and his son Caleb in 1844, nowadays is one of the most used, allowing long spans to be achieved, ranging from 20 to 100 meters. Also called N-shape, it is made up of vertical and diagonal members that form the 'N' pattern until the central point, where they are inverted. This type of truss is most appropriate for horizontal spans, where the force is predominantly in the vertical direction. Under gravity loads, the vertical members result to be in compression while the diagonals in tension. In this way, a more cost-effective design might be encouraged by giving the diagonal components smaller cross-sections. Besides, since they are in tension, they won't be affected by buckling problems.

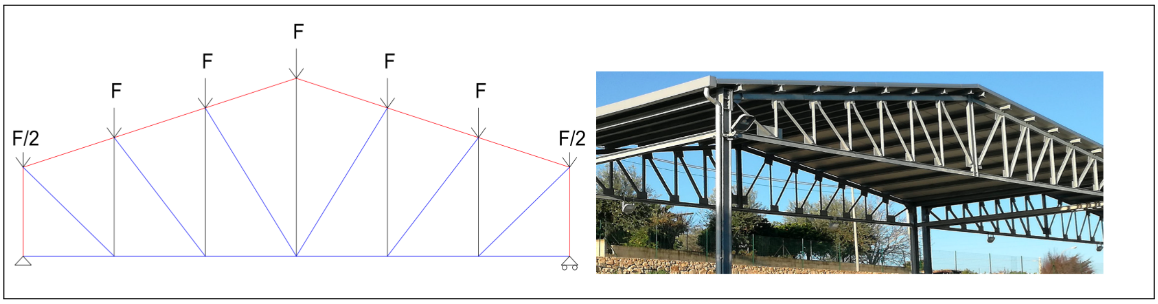


Figure 4.15: Pratt truss scheme and application example (industrial building from "LA META costruzioni Vincenzo Cavallo")

- HOWE TRUSS

  The Howe truss was proposed by William Howe in 1840, four years before the Pratt one. Their configuration is similar, actually specular, because of the orientation of the diagonals. Therefore, under gravitational loads, they are in compression, so buckling verification becomes an issue. Thus, Howe truss is better employed when uplift actions are predominant, which may be the case of open buildings such as aircraft hangers, so that the diagonals can be in tension.

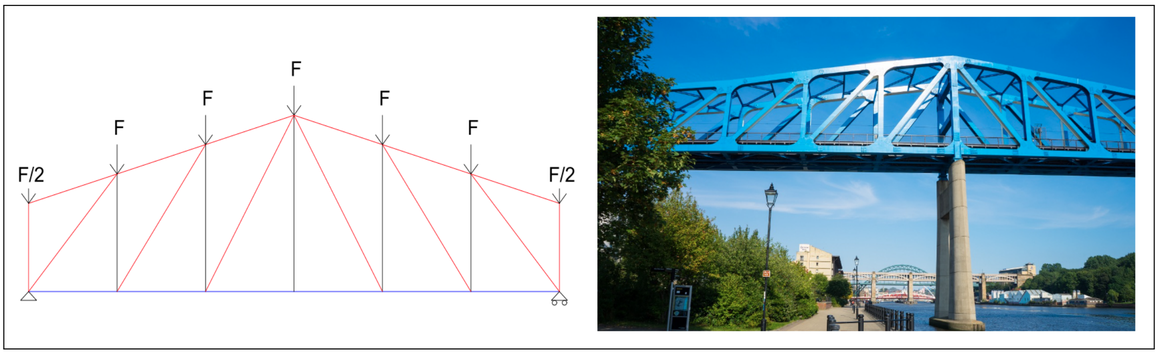


Figure 4.16: Howe truss scheme and application example: Queen Elizabeth II Metro Bridge

- BROWN TRUSS

  The Brown truss has X-shaped diagonals. It is characterized by the fact that one leg of each X is always in tension. More in details, the double diagonals configuration is an hyperstatic truss scheme. This kind of truss is generally employed when we may have an inversion in sign of the actions, like in the case of wind loads or seismic excitations. Of course, this configuration will result in heavier designs even though the single diagonals can have smaller sections.

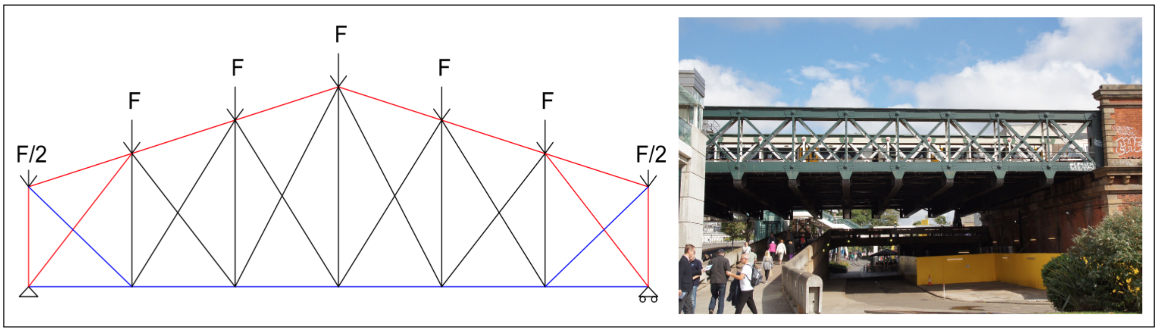


Figure 4.17: Brown truss scheme and application example: Hungerford railway bridge

- WARREN TRUSS

  It is named after the British engineer James Warren, who patented it in 1848, together with Willoughby Theobald Monzani. Its original scheme had a configuration in which the truss members formed a series of equilateral triangles. However, in our analysis, due to the fact that we have an inclined upper chord, the triangles are not equilateral. In fact, there are different version of the Warren truss type, with or without vertical elements, as well as with alternate verticals, with parallel chords or inclined upper chord, with equilateral or isoscele triangles. Looking at the scheme chosen for our investigation, reported in figure 4.18 we can clearly observe that the upper chord is always in compression, while the lower chord in tension. Then, the diagonals have to be distinguished into the descending ones, which are in tension, and ascending ones, which on the contrary are in compression; then once the middle is reached their solicitations are switched. Instead, the additional vertical elements present alternate stresses, in fact, the even ones are in compression, while the odd ones are not stressed. The function of the even vertical elements is to help the distribution of compression actions when long spans are reached. This type of truss is largely employed in civil engineering application thanks to its versatility. In particular, it is often used for steel railway bridges, thus the loads (dead and traffic load) are applied on the deck which distributes the load to the bottom chord.

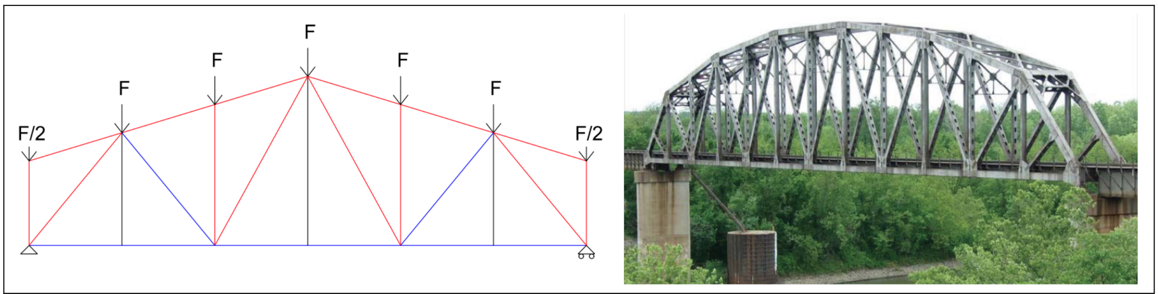


Figure 4.18: Warren truss scheme and application example: BNSF Railroad over Verdigris River

In particular, to switch from one configuration to the other in our optimization, we have created a slider ranging from 0 to 4, in which each number represent a truss type. For example, 0 stands for the Vierendeel one, thus if the topology design variable for the current individual is at 0 value, the configuration analyzed is the Vierendeel one.

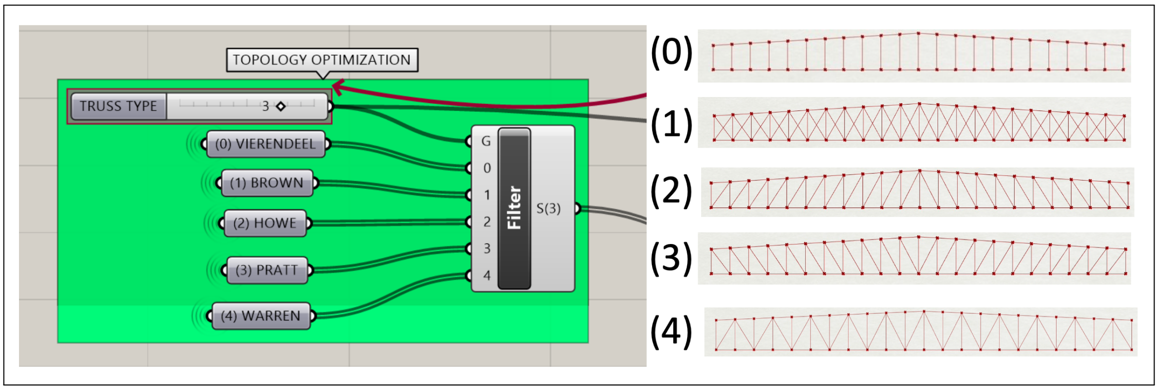


Figure 4.19: Topology optimization design variable

Finally, the size optimization has been carried out by varying the cross-sections of the truss's members. Specifically, we have assigned CHS (circular hollow sections) profiles. In Karamba3D there is a pre-defined catalogue, which has been limited to the first 100 values in order to reduce the computational effort of the optimizer. This reduction has been computed by following the Eurocode 3 specification, in which the general formulation regarding the stability of truss's members can be written as: $N_{Rd} = \frac{A \cdot f_y}{\gamma_m}$. Actually it should be distinguished for tension or compression members, as well as for the different classes of cross-sections, but this was just a preliminary, rough and simplified evaluation.

## 4.4 Grouping strategy

We have just introduced the size design variables, however we have also developed a grouping strategy that involves a further schematization of the problem. The idea was suggested by Gabriele Rosi during our internship at Maffeis Engineering S.p.A. In fact, in real-life structures is not convenient to have different sections for all the members, moreover the real assembly and erection make it possible to install portions of the truss all together. Thus, it follows that a division in macro-areas can be suitable from a practical point of view. Furthermore, we have seen this technique applied to frame structures also during the paper review in Chapter 2, as for example in [36],[25] and [47]. To manage the application of grouping to our truss case, we should always remember about the symmetry with respect to the vertical axis in the middle. First of all, we have distinguished five components of the truss, namely:

1. Lower Chord
2. Upper Chord + External Vertical Structs
3. Internal Vertical Structs
4. Upward-Downward Diagonals
5. Downward-Upward Diagonals

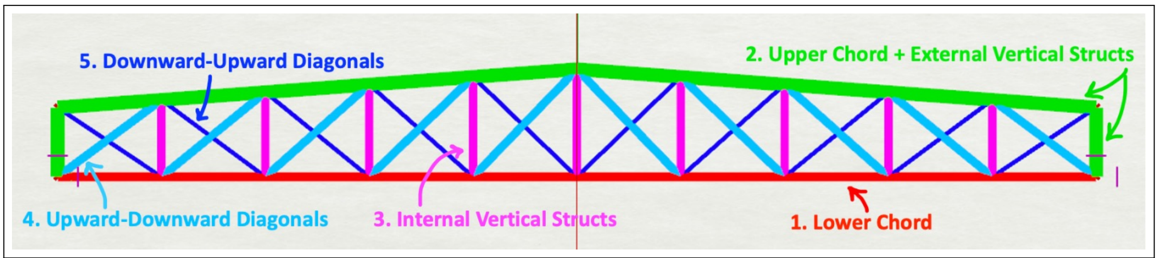


Figure 4.20: Truss's components division

Each component has been in turn divided into three main regions, where in each one the solicitation can be assumed similar. Thus, the grouping strategy consisted into the creation of 3 groups for each component, to which a cross-section is assigned. In more details, if we look at the lower chord's solicitation distribution, it can be highlighted that there are three main points at which the stresses difference is more evident.

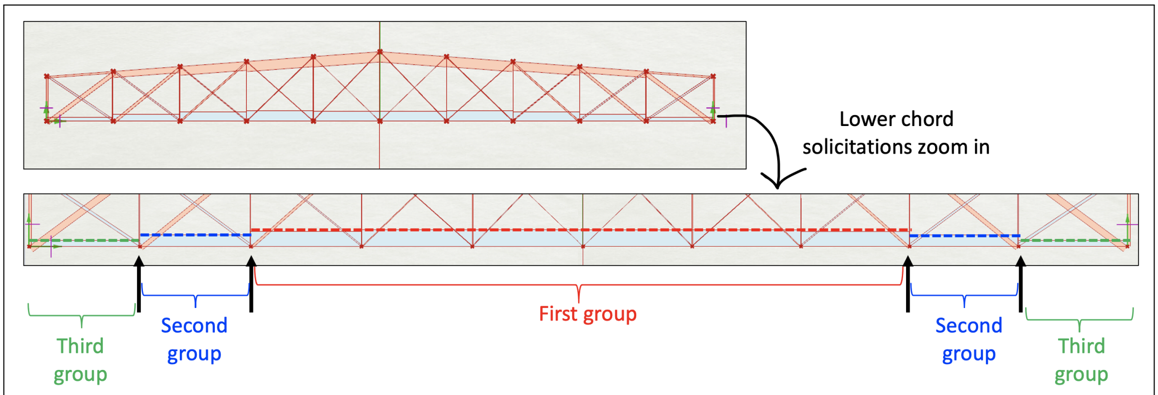


Figure 4.21: Lower chord's solicitation distribution

Exploiting this observation, we have assigned three different cross-sections, one for each group. In fact, if we think to assign a single cross-section to the entire lower chord, it would require the largest one to sustain the highest stresses at the middle, increasing the overall weight of the structure. On the contrary, if we allow the optimizer to choose a different cross-section for each member, the overall structure would result with the lowest weight possible, but with the highest complexity for its construction. In fact, having a high number of different cross-sections is increasing the complexity of fabrication, assembly and erection phases, as well as the overall cost, thus it should not be encouraged. To make a first move towards a balance between the minimization of the cost and the number of different cross-sections used, we have developed the grouping strategy.

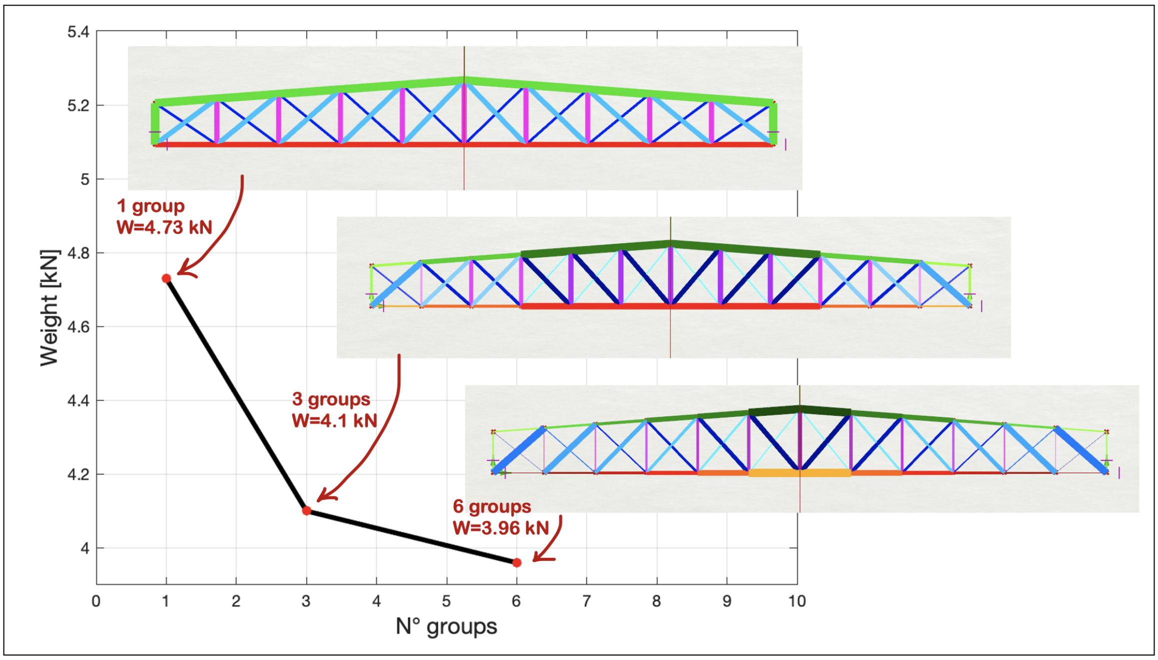


Figure 4.22: Relationship between N°groups and corresponding weight [kN]

Furthermore, the grouping technique has been carried out in a dynamic way. Specifically, the optimizer can manage the group division by changing the point at which we have the passage from one group to the other. To explain the developed approach, we can consider for the sake of simplicity only the lower chord. In particular, let's focus on the case of a truss with a number of subdivisions of the first half equal to 6. If we wanted, for example, to divide the lower chord into 2 groups we would have to identify $n_1$, which is the index of the node at which the lower chord will be divided. Then, in order to actually divide it into 2 groups, not having one of them with zero members, $n_1$ should be a number from 1 to $n - 1 = 5$. From the reported figure 4.23 we have graphically illustrated the meaning of $n_1$.

Then, moving towards our case, if we wnat to divide the lower chord into 3 groups, we should identify two indexes, $n_1$ and $n_2$. In this case $n_1$ would be a value in

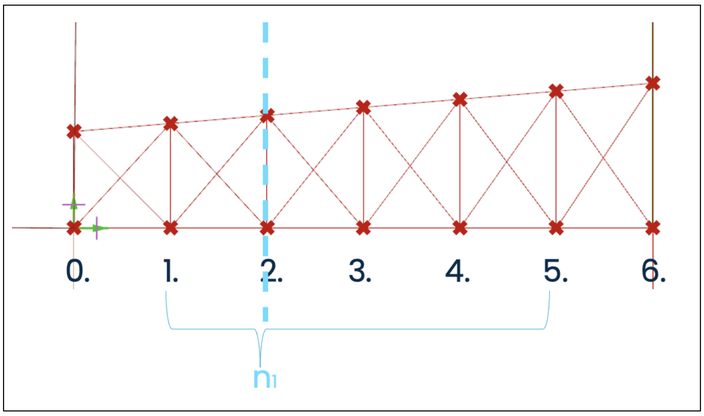


Figure 4.23: Graphical representation of the meaning of $n_1$ variable

between 1 and $n - 2 = 4$, while $n_2$ in between $n_1 + 1$ and $n - 1 = 5$.

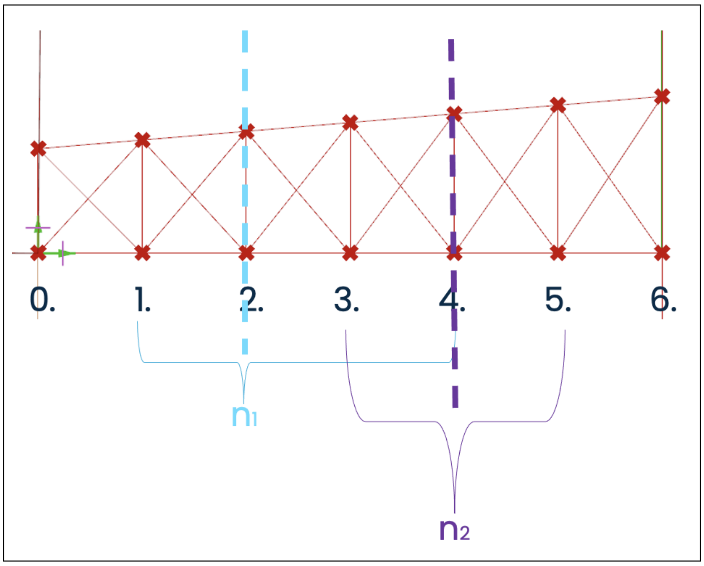


Figure 4.24: Graphical representation of the dynamic grouping strategy with 3 groups

Looking at the figure 4.24, we can see that $n_2$ is establishing the ending node of the first group, while $n_1$ the ending node of the second group.
Following this scheme, we could continue considering all the possible numbers of groups until N°groups = N°subdivisions $n$. However, because of the considerations previously made regarding the actual solicitation distributions and the reduction of the computation effort required for the optimization procedure, we have chosen to subdivide each component into three groups.

## 4.5 Model assembly

Until now we have defined all the most important parameters that are going to govern the analysis. In this subsection, instead, we want to illustrate the procedure followed to assemble the model and how the analysis will be performed. A schematic representation is reported in figure 4.25.

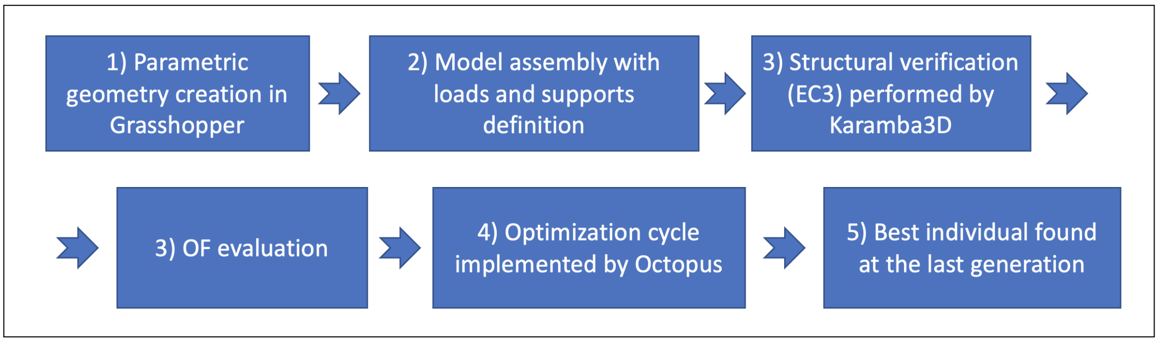


Figure 4.25: Basic procedure flow

Starting from the half geometry creation in the xz plane with the five truss components, by mirroring it with respect to the yz plane, we have completed the truss configuration. At this point, the single line elements, implemented in Grasshopper, have been transformed into beam members by means of Karamba3D components. Therefore, proper cross-sections have to be assigned to them. As said before, the reduced catalogue of CHS profiles has been used, assigning the specific steel S355 material properties. Each component of the truss has been divided by means of the grouping strategy, which is now introduced in the definition of the cross-sections assignment. An example of such procedure has been reported in figure 4.26, to describe how Karamba3D environment works.

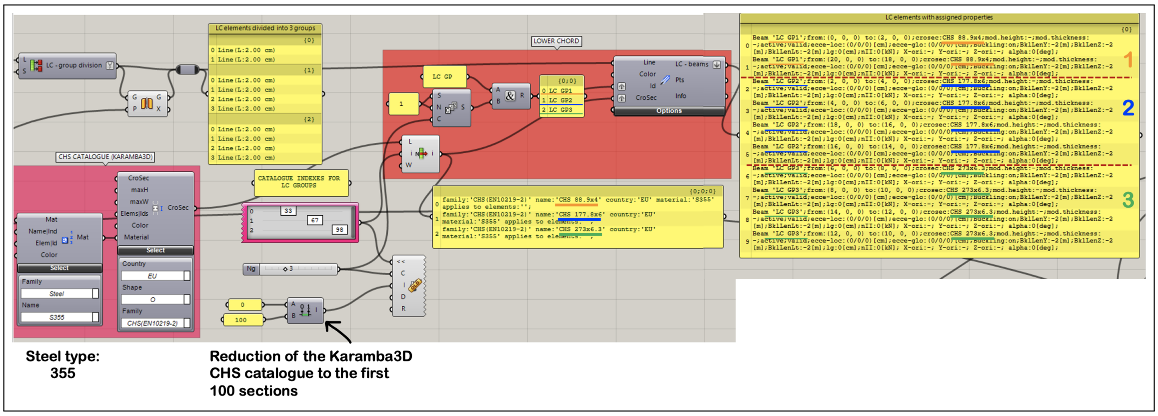


Figure 4.26: 'Line-to-beam' component: example for the Lower Chord elements.

Moreover, loads and supports have to be introduced in the model assembly. Regarding the supports, we have assigned an hinge and a roller to the external nodes of the truss, to make it isostatic externally.

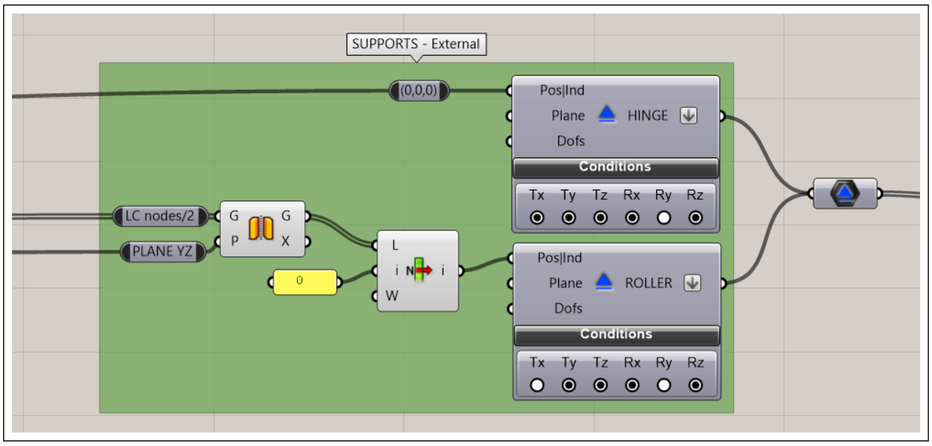


Figure 4.27: Supports set-up in Karamba3D

Then, we have applied to the structure only gravitational loadings, considering the Ultimate Limit State (ULS) combination, according to Eurocode. Unfortunately, in Karamba3D we are not allowed to switch from one combination to the other, therefore we have only used the following one:

$$\gamma_{G1} \cdot G_1 + \gamma_{G2} \cdot G_2 + \gamma_P \cdot P + \gamma_{Q1} \cdot Q_{k1} + \gamma_{Q2} \cdot \psi_0 2 \cdot Q_{k2} + ... \tag{4.1}$$

Where $G_1$, $G_2$ and $Q_{ki}$ are respectively the Permanent structural loads, Permanent non-structural loads and Variable loads. Instead $\gamma$ is a coefficient of amplification that is defined based on the type of the loads. In our case study the following loads have been considered, with their corresponding coefficient of amplification.

| **Type of Load** | **Load Value** | **Coefficient** $\gamma$ |
|---|---|---|
| $G1$ | Own weigth $KN$ | 1.3 |
| $G2$ | $1.471\frac{KN}{m^2}$ | 1.5 |
| $Q_1$ | $0.5\frac{KN}{m^2}$ | 1.5 |

Table 4.2: Vertical loads applied to truss structure

While $G_1$ is automatically applied by Karamba 3D for all the members, $G_2$ and $Q_1$ required the identification of the specific beams on which they will act. In order to apply them to the upper chord of the truss structure, an area of influence should be considered; in our case study an inter-axis of 5 meters is assumed. By multiplying

the Load Value ($G_2$ and $Q_1$), times the inter-axis we will obtain a distributed linear loads in $\frac{KN}{m}$.
Once the model is assembled, the solutor will perform the structural analyses for each configuration and from the output we can implement the Objective Function. In particular, its formulation will be discussed in the next section 4.6, however here we want to summarize the basic flow of our analysis. It must be highlighted the fact that Octopus optimizer works by setting the population size and the number of generations, thus once the optimization has reached the last individual of the last generation it will stop. During each generation, the individuals are created by changing the design variables and imposing the structural verifications according to the Eurocode 3, until the best configuration is obtained. In figure 4.28, a schematic flow chart of our procedure is reported. Specifically, $It$ stands for iteration number, while at STEP 0 the input assumptions regard the fixed 20 m length of the truss, the number of groups equal to 3 and the setting of total number of iterations $It_{max}$ and population size. The resume of the design variables considered in the optimization is reported in the next subsection, in table 4.3.

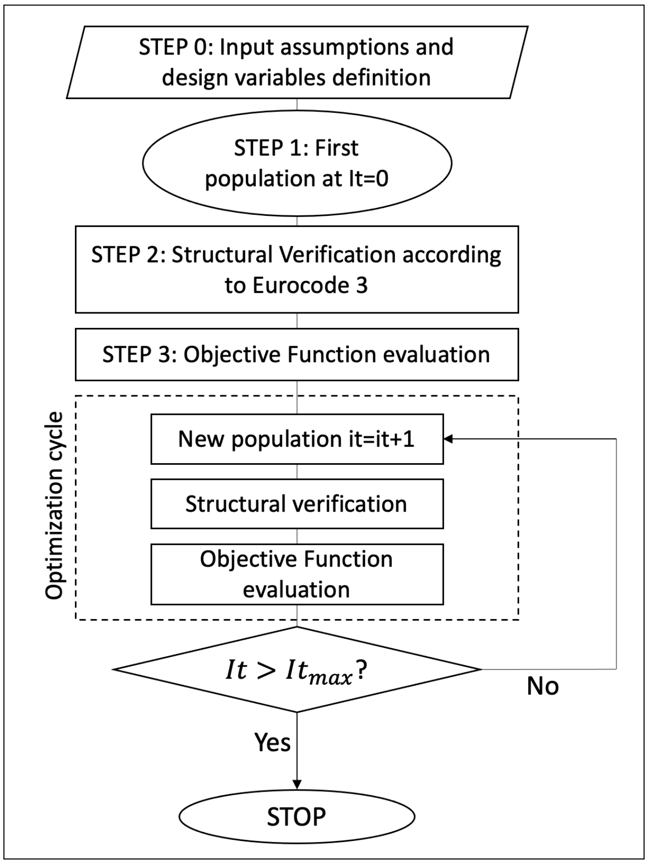


Figure 4.28: Flow chart

## 4.6 Objective function formulation

As stated before, we are going to perform an optimization not simply aimed at the weight minimization, but we are accounting for both structural verifications and constructability issues. To properly formulate our problem, we should define the three main ingredients of the optimization, namely the objective function, the design variables and the constraints applied.
The formulation of our optimization can be expressed as:

$$min\ F(\mathbf{x}) = \rho \sum_{i=1}^{N} (A_i \cdot l_i) \cdot \phi_1(n_{un}) \cdot \phi_2(N_a) \cdot \phi_3(n) \tag{4.2}$$

subjected to

$$\frac{N_{Ed}}{N_{Rd}} \leq 1 \tag{4.3}$$

$$\mathbf{x}_{i,min} < \mathbf{x}_i < \mathbf{x}_{i,max} \tag{4.4}$$

Where:
$N$ is the total number of elements in the truss and $\mathbf{x}$ is the vector of design variables. In the previous sections we have introduced all the $x_i$ involved in the optimization, which are summarized in the table 4.3 below. The four macro-categories of the design variables, i.e. Topology, Layout or Shape definition, Grouping division and Cross-sections assignation, have been distinguished by making use of different colors. Moreover, in the table are reported the lower and upper bound of each $x_i$, specifically in the last column. Their graphical representation has been reported in figure 4.29, where the Brown truss type has been chosen for clearness purposes.

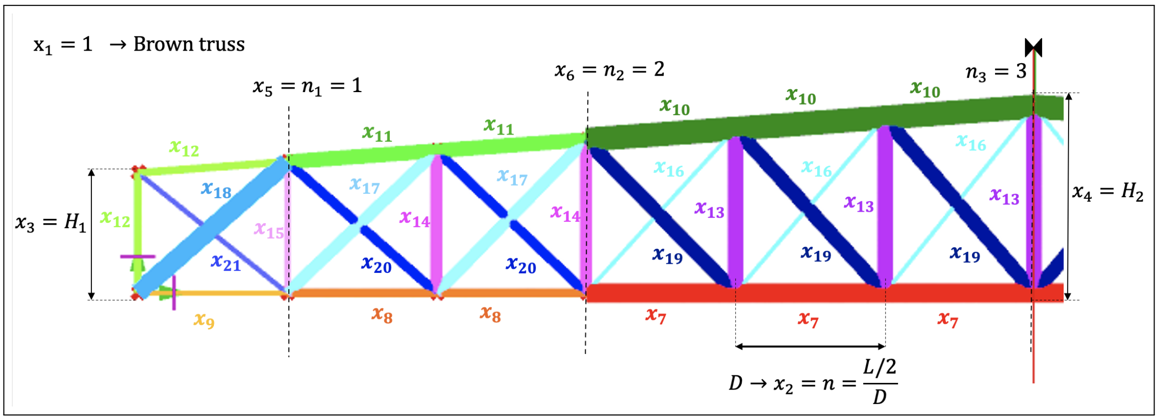


Figure 4.29: Schematic representation of all the design variables

| Design variable | Description | Domain |
|---|---|---|
| $x_1$ | Topology: (0) Vierendeel, (1) Brown, (2) Pratt, (3) Howe, (4) Warren | $0 \div 4$ |
| $x_2 = n$ | Number of subdivisions of half geometry | $3 \div 10$ |
| $x_3 = H_1$ | Heights of upper chord's edges | $H_{1,min} = max(\frac{L}{15}, D \cdot tan30)$<br>$H_{1,max} = min(\frac{L}{10}, D \cdot tan60)$ |
| $x_4 = H_2$ | Heights of upper chord's midpoint | $H_{2,min} = max(H_1, D \cdot tan30)$<br>$H_{2,max} = min(\frac{L}{8}, D \cdot tan60)$ |
| $x_5 = n_1$ | Index at which the third group ends | $1 \div n - 2$ |
| $x_6 = n_2$ | Index at which the second group ends | $n_1 + 1 \div n - 1$ |
| $x_7$<br>$x_8$<br>$x_9$ | 3 sections for the lower chord elements | $0 \div 100$ CHS profiles' index from catalogue |
| $x_{10}$<br>$x_{11}$<br>$x_{12}$ | 3 sections for the upper chord + external vertical structs | $0 \div 100$ CHS profiles' index from catalogue |
| $x_{13}$<br>$x_{14}$<br>$x_{15}$ | 3 sections for the vertical internal structs | $0 \div 100$ CHS profiles' index from catalogue |
| $x_{16}$<br>$x_{17}$<br>$x_{18}$ | 3 sections for the upward-downward diagonals | $0 \div 100$ CHS profiles' index from catalogue |
| $x_{19}$<br>$x_{20}$<br>$x_{21}$ | 3 sections for the downward-upward diagonals | $0 \div 100$ CHS profiles' index from catalogue |

Table 4.3: Design variables where the colors of the cells represent the different categories: blue - Topology; red - Layout definition; green - Grouping division; yellow - Cross-sections assignation.

In equation 4.2, the penalties are respectively:

$$\phi_1 = (1 + K_1 \cdot n_{un}) \tag{4.5}$$

$$\phi_2 = (1 + \Delta) - e^{-\beta \cdot (N_a - \frac{ln\Delta}{\beta})} \tag{4.6}$$

$$\phi_3 = (1+\gamma) - e^{-\alpha\cdot(n-\frac{ln\gamma}{\alpha})} \tag{4.7}$$

All the parameters related to the penalty functions have been calibrated by means of the analysis reported in the next subsections; their resulting values are summarized in table 4.4.

| Parameter | Value |
|---|---|
| $K_1$ | 10 |
| $\Delta$ | 2.70 |
| $\beta$ | 0.1 |
| $\gamma$ | 1.157 |
| $\alpha$ | 0.1 |

Table 4.4: Penalties parameters

With the first penalty 4.5, a constraint referred to element buckling verification is implemented, which is proportional to the number of elements in the unfeasible region, $n_{un}$, and amplified by a coefficient $K_1$. Instead, $\phi_2$ and $\phi_3$, respectively 4.6 and 4.7, are introducing constructability criteria that, once more, encourage the optimization towards heavier designs. In particular, $\phi_2$ is limiting the number of distinct cross-sections used to construct the entire truss ($N_a$). On the other hand, $\phi_3$ tries to reduce the design complexity by lowering the number of subdivisions of the truss, thus the overall number of pieces to be assembled. Both $\phi_2$ and $\phi_3$ have an exponential form, as we can see in the graphical representations below, 4.30.

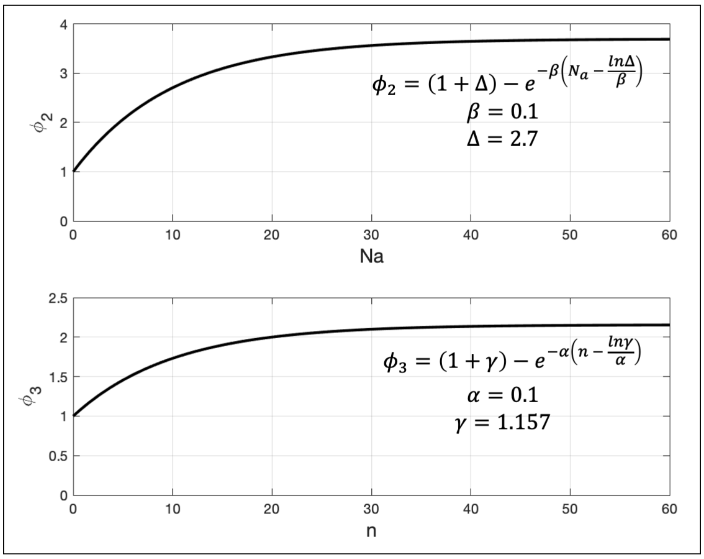


Figure 4.30: $\phi_2$ and $\phi_3$, respectively 4.6 and 4.7

In the following subsections, we are going to illustrate in details the three penalties. It should be highlighted the fact that, in the process of developing the Objective Function, we started by considering at first a simple size minimization, thus allowing the optimizer to vary only from $x_7$ to $x_{21}$ design variables of table 4.3. Then, we integrated also the shape design variables, i.e $x_2$, $x_3$ and $x_4$, as well as the ones regarding the grouping strategy, which are $x_5$ and $x_6$. Once, all the penalties have been tested for the simultaneous size and shape optimization, finally, we included also the topology optimization, thus $x_1$ of 4.3. The reason behind this kind of step analysis is related to the actual influence of the different design variables into the distinct penalty functions. For example, penalty $\Phi_1$ about the structural verification is highly dependent on the size variables, while shape and topology ones are indirectly affecting such requirement. In an analogous way, topology variation is not the main factor that impact the definition of the constructability-based penalties.

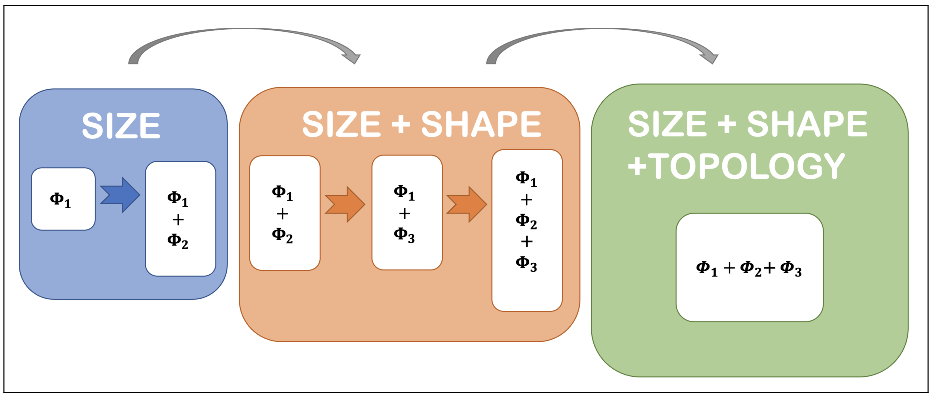


Figure 4.31: Penalties procedure development

### 4.6.1 Penalty $\phi_1 = (1 + K_1 \cdot n_{un})$

One of the main issues with truss structures is buckling instability at the element level. Unfortunately, the standard Karamba3D solutor does not account for such verification, therefore we have included the penalty function $\phi_1$. Specifically, there is a component called "Utilization" that give us the information about the compression buckling requirement satisfaction. In general terms, we can say that the slenderness of members subjected to compression is one of the main aspect to be investigated. Analysing the buckling phenomenon for a simply supported beam, subjected to a pure axial stress, we can state that until the applied load is below a certain treshold, the response of the beam can be reconducted to the form: $\sigma = \frac{P}{A} = E \cdot \varepsilon = \frac{E \cdot \Delta L}{L}$, where $\Delta L$ is the shortening due to the applied load P. However, above a given threshold load, the response of the beam would be affected by a lost of equilibrium, falling to an unstable state. In particular, the stress at which this would happen is called critical load, or Euler's critical load, from Leonardo Eulero (1707-1783) who solved this problem. Its value corresponds to:

$$P_{cr} = \pi^2 \cdot \frac{E \cdot J}{L^2}$$

where

- L=beam length
- $J$=beam inertia moment

To generalize the equation for different situations, the Euler's load can be written as: $P_{cr} = \pi^2 \cdot \frac{E \cdot J}{l_0^2}$, where $l_0$ represent the effective length of the beam against buckling. In particular, $l_0$ depends on the supporting conditions at the beam's edges and the main schemes are reported in figure 4.32.

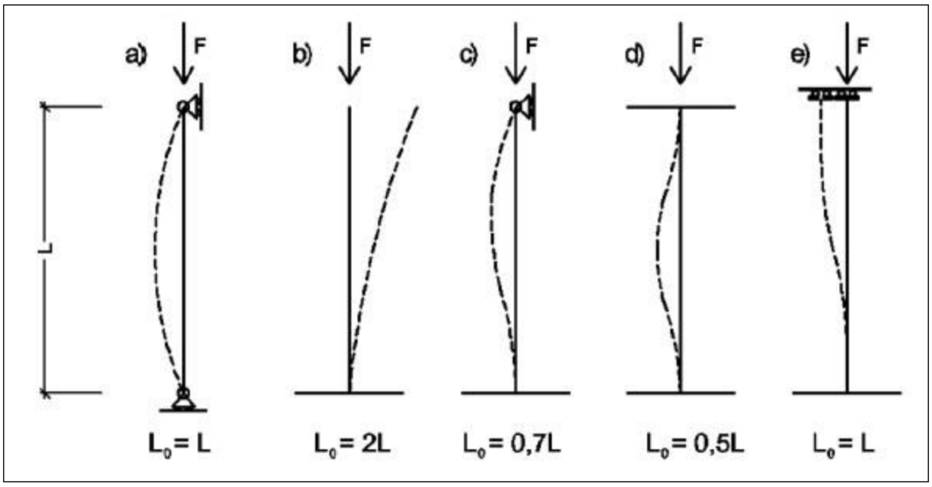


Figure 4.32: Values of buckling effective length for different supporting conditions

Then, to understand in practical terms the influence of the element's slenderness, we can consider the case of two beams of the same material and same section, but with different lengths. An example, taken from [17], is reported in figure 4.33, where the two beams have a square section of 2cm x 2cm, but the first one on the right has a length of 4 cm, while the other one of 40 cm.

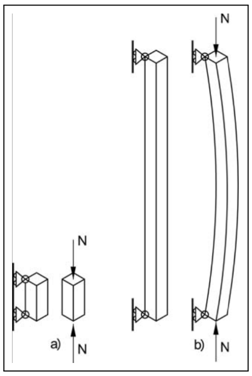


Figure 4.33: Examples of beam's slenderness, taken from [17]

The Euler's critical load for the two cases will be:

$$P_{cr1} = \frac{\pi^2 \cdot E \cdot J}{4cm^2}$$

$$P_{cr2} = \frac{\pi^2 \cdot E \cdot J}{40cm^2}$$

thus in the second case the threshold is 100 times lower, in fact $P_{cr2} = \frac{P_{cr1}}{100}$. If we consider a compressive strength limit in between $P_{cr1}$ and $P_{cr2}$, this means that while in the first case the collapse would be caused by a compression failure, in the second case the collapse would be due to the lost of stability, before the compressive strength limit is reached. Therefore, the slenderness is generally accounted for buckling stability verification and it is defined as:

$$\lambda = \frac{l_0}{\rho}$$

where $\rho = \sqrt{\frac{J}{A}}$ [cm] is the cross-section radius of gyration. Of course, the slenderness depends on the axis we are considering for the J evaluation, thus we would have values referring to x and y axes. According to the Eurocode 3 (section 6.3 - Buckling resistance of members), the verification regarding buckling problem suggest to employ a reductive coefficient $\chi$, which accounts for the Euler's critical load. In particular, $\chi$ determines how much of the compressive stress capacity of a bar can be used before it is assumed to buckle. Given $f_{yd}$ the design compressive strength of steel, it should be satisfied that the acting axial force $N_{Ed}$ is lower or equal than the resistant strength without loss of stability $N_{b,Rd}$. The condition can be written as:

$$N_{Ed} \leq N_{b,Rd}$$

where

$$N_{b,Rd} = \chi \cdot \frac{A \cdot f_{yd}}{\gamma_M}$$

with $\gamma_M$ partial factor of safety for instability resistance, A the beam's section which can be calculated in different ways depending on the sections' class. Instead, the value of $\chi$ is calculated as a function of the beam's slenderness and an imperfection factor $\alpha$. It should be mentioned the fact that an analogous method is followed for the combination of flexural and axial loads, where the compression force along each beam derives from both the actions. In conclusion, from a theoretical point of view, we can state that buckling phenomenon must account for both the elements' slenderness and supporting conditions. In our specific case, all the elements have fixed supports at their ends, but their length is different depending on the cases. Generally, the diagonal members have higher lengths, however in our case with inclined top chord, also the upper chord elements can have significant extent. Of course, we should always remember that buckling is only affecting elements under compression, thus in the case of a Pratt truss, for example, the diagonals are in tension, so buckling is not an issue for them.

Practically speaking, in our analysis we have computed the number of elements with the ratio between the acting stress and buckling strength higher than one. The mathematical formulation can be written as:

$$n_{un} = \sum_{i=1}^{N} n_i$$

where $N$ is the total number of elements in the truss, $n_i$ is a generic member in which $\frac{S_i}{R_i} > 1$, $S_i$ is the acting force along the element and $R_i$ is the resisting force calculated considering the effective buckling length of the beam. This structural constraint has been introduced directly in the formulation of the OF, exploiting the penalty technique. More in details, the number of unfeasible beams, $n_{un}$, has been multiplied by a coefficient $K_1$ in order to amplify this penalization in the evaluation of the OF. The final formulation of $\phi_1$ has been already expressed in 4.5, from which we can observe that if no unfeasible beams are found, $\phi_1$=1, thus no penalization is applied. Whereas, in presence of unfeasible beams it is proportional to their amount.

In particular, the coefficient $K_1$ has been calibrated by performing different analyses by changing its value. If no other penalties are considered, we can see how OF is affected by $\phi_1$ as a function of $n_{un}$ and $K_1$.

| $OF$ | $K_1$ | $n_{un}$ |
|---|---|---|
| $W \cdot (1+1) = 2 \cdot W$ | 1 | 1 |
| $W \cdot (1+10 \cdot 1) = 11 \cdot W$ | 10 | 1 |
| $W \cdot (1+100 \cdot 1) = 101 \cdot W$ | 100 | 1 |

Table 4.5: OF values as a function of $K_1$, for $n_{un}$=1

| $OF$ | $K_1$ | $n_{un}$ |
|---|---|---|
| $W \cdot (1+5) = 6 \cdot W$ | 1 | 5 |
| $W \cdot (1+10 \cdot 5) = 51 \cdot W$ | 10 | 5 |
| $W \cdot (1+100 \cdot 5) = 501 \cdot W$ | 100 | 5 |

Table 4.6: OF values as a function of $K_1$, for $n_{un}$=5

To set $K_1$ we have focused the analysis on a Brown truss size optimization with $n = 6$. In order to simplify the procedure, we have considered the case with only one group, which lowered the computational effort regarding the assignment of different cross-sections to the distinct components. From the results we have concluded that, because there is no evident scattering between the values, it is worthless to adopt a too large value of $K_1$.

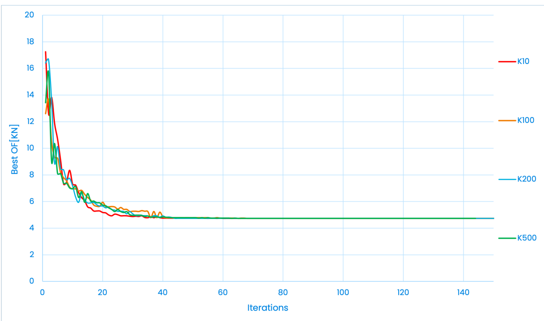


Figure 4.34: Best OF as a function of $K_1$ in the case of $OF = Weight \cdot \phi_1$

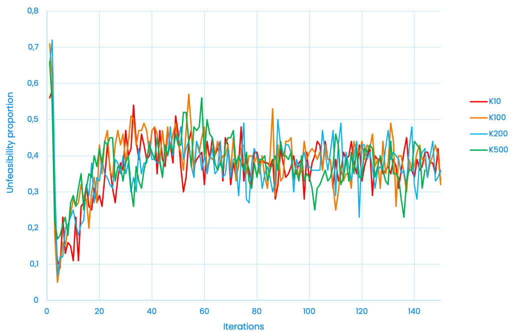


Figure 4.35: Unfeasibility proportion as a function of $K_1$ in the case of $OF = Weight \cdot \phi_1$

In all the cases, the value of the best individual is 4.73125 kN, while the unfeasibility proportion trend is almost the same. In conclusion, the coefficient $K_1$ adopted in the following analyses has been set with a value equal to 10.

### 4.6.2 Penalty $\phi_2 = (1 + \Delta) - e^{-\beta \cdot (N_a - \frac{ln\Delta}{\beta})}$

As briefly mentioned before, by means of the second penalty function we are going to introduce the first constructabiliy criteria in the objective function formulation. It is aimed at reducing the number of different sections ($N_a$) used, in order to simplify the construction of such truss on site, recalling the concepts discussed in the previous chapter 3. It should be noticed that with the grouping strategy, explained in 4.4, we have constrained the problem by defining the maximum number of different cross-sections that can be assigned, i.e. $N_{a,max} = N_{groups} \cdot N_{components}$. In fact, with reference to the case in which each element of the truss has its own cross-section, the grouping technique is already reducing the variability of $N_a$.
For example, dealing with the size optimization of a Brown truss, we know that we would have 5 different components, namely Lower Chord, Upper Chord + External Vertical Structs, Internal Vertical Structs, Upward-Downward Diagonals, Downward-Upward Diagonals. Then, by looking at the distribution of the solicitation for gravitational loadings, we have seen that a reasonable number of groups, which can properly define areas within the structure with similar axial force, is 3. Therefore, we can consider the following fixed parameters:

- Truss lenght = 20 meters
- N°subdivision = 6 x 2 = 12
- N° groups = 3
- N° of possible sections = N°components x N°groups = 5 x 3 = 15

In this specific case, if no grouping and no symmetry were accounted, we would have $N_a = 12 \cdot 4 + 13 = 61$. However, from geometric considerations, we have a symmetric truss thus $N_a = 31$; moreover, exploiting the grouping, $N_a$ is further reduced to 15. Once set the variability domain of $N_a$, now with $\phi_2$ we are imposing a complexity to the algorithm. In practice, we are penalizing the OF adding the condition of finding the lowest weight with the least number of different sections. In fact, as already emphasized in 4.4, the higher $N_a$ value, the lower the weight.
In the definition of the penalty $\phi_2$ we started from a linear formulation, but the results of the preliminary analyses didn't show a clear trend. Therefore, we moved to the exponential form, which has been employed in several researches, like the

ones of Reitman and Hall in [95] and Mu Zhu in [115]. By looking at its equation 4.6, we should highlight the role played by the two variables $\Delta$ and $\beta$:

- $\Delta$ is governing the asymptote at which, for a high number of sections used, we are no longer increasing the penalization;
- $\beta$ is controlling how we reach that asymptote, if faster or in a more gradual way.

In figure 4.36 we can see how, for a fixed $\beta$, the value of $\Delta$ regulates the asymptote; thus for a given value of $N_A$, if $\Delta$ increases, the associated penalty would be higher. On the contrary, in figure 4.37, we can see how fixing $\Delta$, the way in which the asymptote is reached depends on $\beta$; specifically, for lower $\beta$ a more gradual trend is followed.

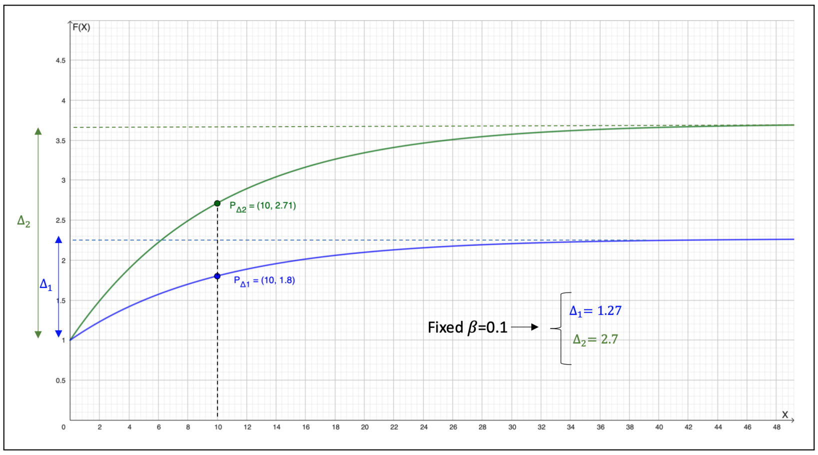


Figure 4.36: Relationship between $\Delta$ and the curve's asymptote

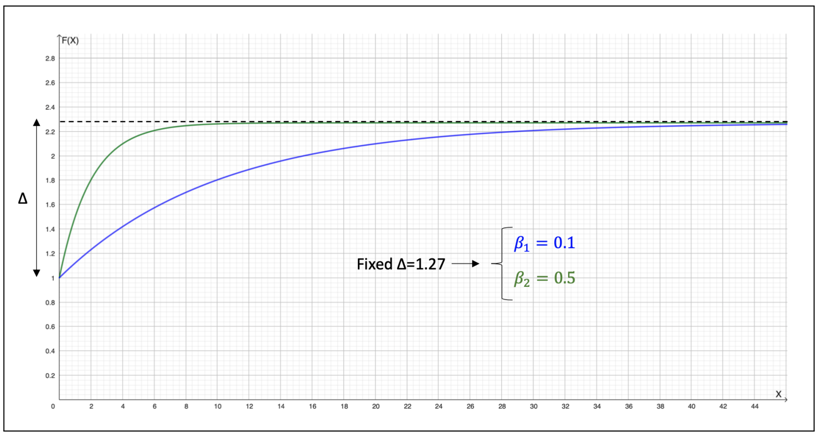


Figure 4.37: Curves with same asymptote, regulated by $\Delta$, but different $\beta$

In order to define the equation that is able to match the issues of our case study, we started from the assessment of a proper $\beta$ value, thus a proper trend. Then, $\Delta$ would be univocally determined once, fixing the chosen $\beta$, the passage through a specific point would be imposed, identifying a suitable penalty level.

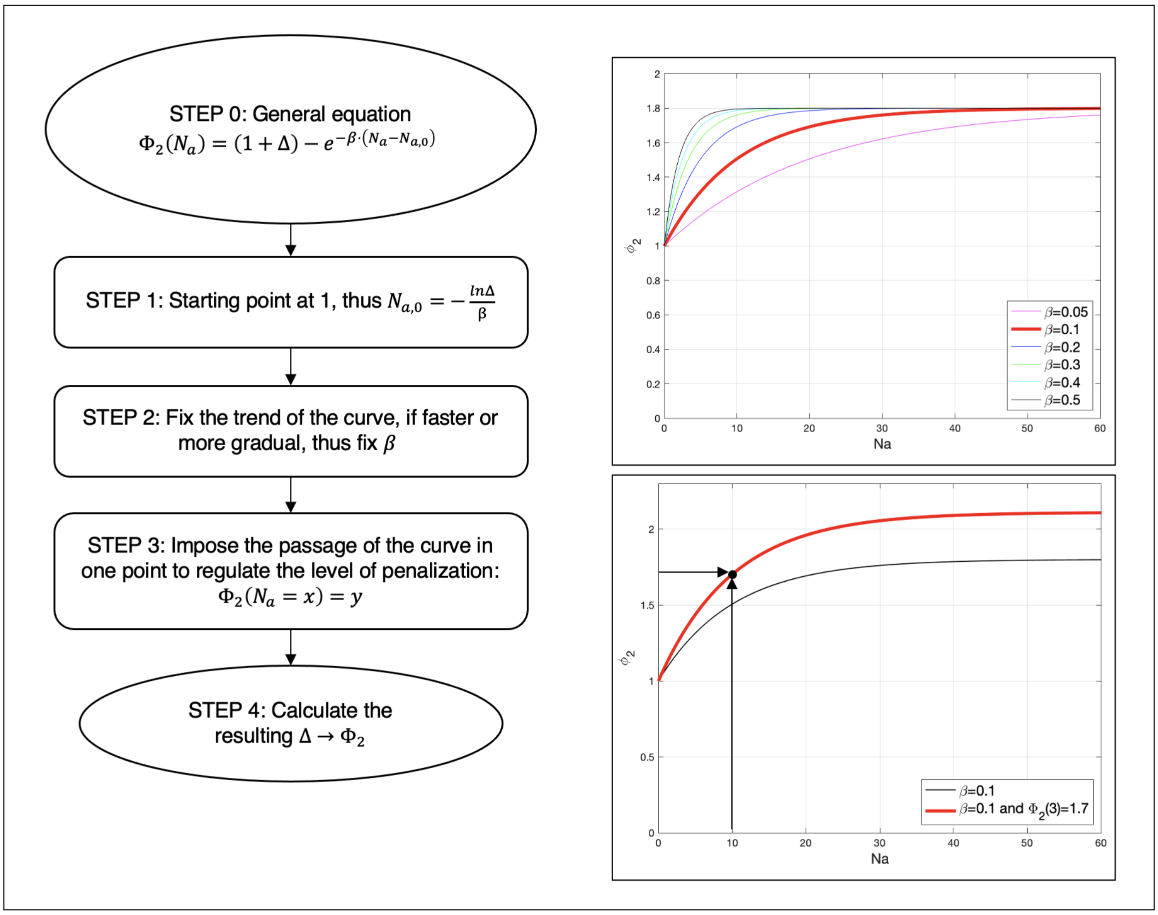


Figure 4.38: Flow chart for determining $\Phi_2$: STEP2 figure on the right and STEP 4 figure on the bottom.

Therefore, for the setting of $\beta$, we need to assume a fixed point in the curve. Precisely:

| **Fixed** | **Variable** | **Resulting** |
|---|---|---|
| **Point in the curve, i.e. penalty level** $\Phi_2(7) = 1.5$ | $\beta$, i.e. curve's trend: 0.1; 0.2; 0.3; 0.5 | $\Delta$, i.e. asymptote height: 0.992; 0.663; 0.569; 0.515 |

Table 4.7: $\beta$ setting procedure

The graph in figure 4.39 shows the defined curves.

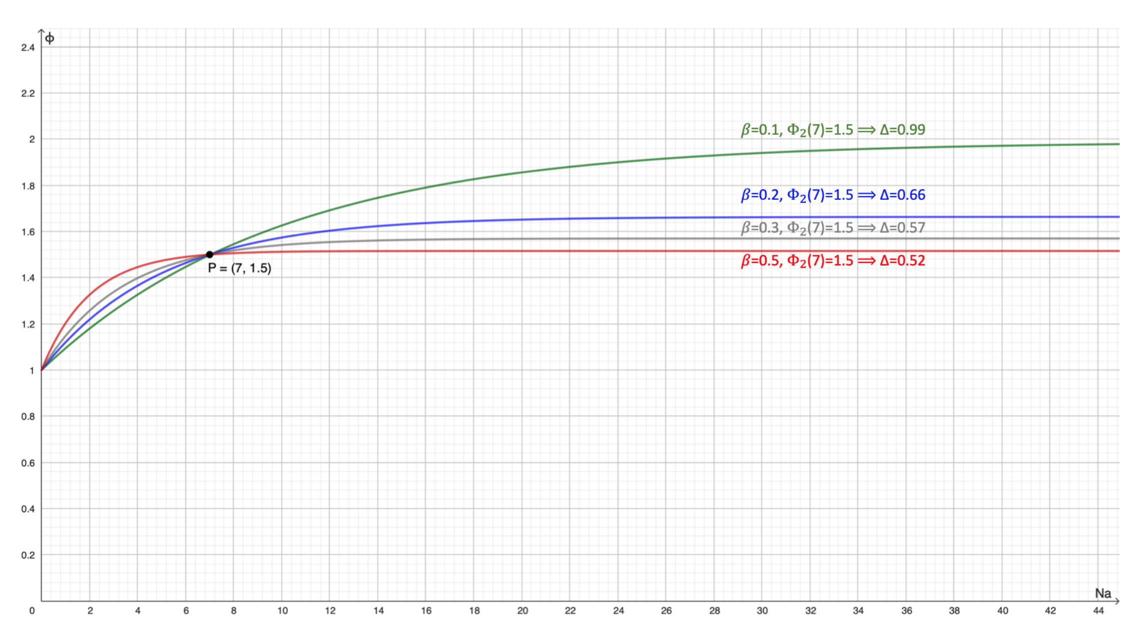


Figure 4.39: Trend of functions for different values of $\beta$

As explained before, by increasing the value of $\beta$, we will reach the asymptote in a faster way (red curve) and, imposed the passage for a fixed point, the value of $\Delta$ decreases. Thus, once the curve reaches a value close enough to that of the asymptote, any further increase in the number of sections won't affect the penalty. By means of table 4.8, let's compare in details the two extreme cases, with $\beta = 0.5$ (red curve) and $\beta = 0.1$ (green curve), having imposed the passage in $\phi_2(7) = 1.5$.

| $N_A$ | $\phi_2(N_a)_{\beta=0.5}$ | Percentage variation | $\phi_2(N_a)_{\beta=0.1}$ | Percentage variation |
|---|---|---|---|---|
| 2 | 1.33 | - | 1.18 | - |
| 3 | 1.4 | 5.26% | 1.26 | 6.77% |
| 4 | 1.45 | 3.57% | 1.33 | 5.55% |
| 5 | 1.47 | 1.37% | 1.39 | 4.51% |
| 6 | 1.49 | 1.36% | 1.45 | 4.31% |
| 7 | 1.5 | 0.67% | 1.5 | 3.44% |
| 8 | 1.51 | 0.66% | 1.55 | 3.33% |
| 9 | 1.51 | 0% | 1.59 | 2.58% |
| 10 | 1.51 | 0% | 1.63 | 2.51% |

Table 4.8: Values of $\phi_2$ with $\beta = 0.5$ and $\beta = 0.1$

The first thing that we can appreciate is that the variability of the penalty, for the same values of $N_a$, is enhanced for the case of $\beta = 0.1$ with respect to the other. For example, for $N_a = 7$ and $N_a = 10$, in the case of $\beta = 0.5$, the OF would consider an increase in weight of about 50% for both the numbers of sections, while in the case of $\beta = 0.1$ it would be amplified by 50% and 63%, respectively. Another important difference when we fix the passage for a specific $N_a$ and we vary the value of $\beta$, is that the corresponding $\Delta$ will change too. In particular, by increasing $\beta$, $\Delta$ decreases, reducing the distance from the origin of the point at which the variability in the results is minimized. With reference to the example previously described, Octopus optimzer has been employed to obtain the best truss configurations for the different $\Phi_2(\beta)$, reported in table 4.9.

| $\beta$ | $\Delta$ | $N_a$ | $Weight[KN]$ |
|---|---|---|---|
| 0.1 | 0.99 | 7 | 4.38 |
| 0.2 | 0.66 | 9 | 4.28 |
| 0.3 | 0.56 | 12 | 4.20 |
| 0.5 | 0.52 | 12 | 4.20 |

Table 4.9: Results considering different $\beta$ values and a fixed penalty of $\phi_2(7) = 1.5$

The same analysis has been carried out imposing the passage in another point, $\phi_2(5) = 1.7$, and testing the same $\beta$ values. The results obtained are summarized in table 4.10.

| $\beta$ | $\Delta$ | $N_a$ | $Weight[KN]$ |
|---|---|---|---|
| 0.1 | 1.779 | 5 | 4.836 |
| 0.2 | 1.1079 | 6 | 4.528 |
| 0.3 | 0.9010 | 8 | 4.305 |
| 0.5 | 0.7626 | 12 | 4.195 |

Table 4.10: Results considering different $\beta$ values and a fixed penalty of $\phi_2(5) = 1.7$

We can appreciate the correlation between the number of sections used and the associated weight of the optimized structure in the two cases, by means of the following graphs 4.40 and 4.41.

Analyzing the data in the tables 4.9 and 4.10, as well as the graphs 4.40 and 4.41, we can conclude that, as expected, the higher $\beta$, the higher the number of sections used, because the algorithm cannot distinguish enough the alteration in the penalty; in turn, the weight would be lower if compared to the case of less $N_a$ used.

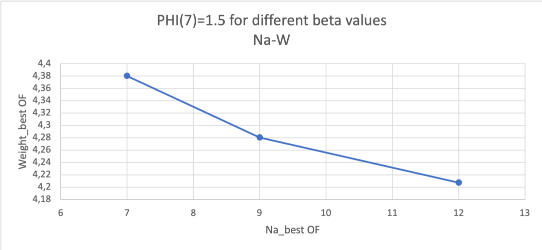


Figure 4.40: Weight of the optimized structure as a function of the $N_a$ assigned, depending on the different $\beta$ used, having imposed $\phi_2(7) = 1.5$

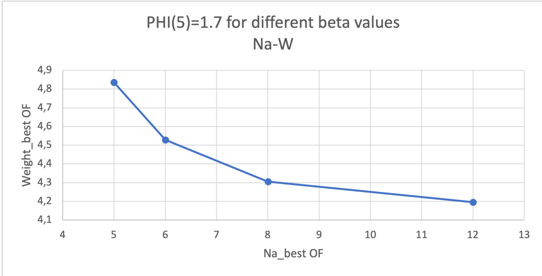


Figure 4.41: Weight of the optimized structure as a function of the $N_a$ assigned, depending on the different $\beta$ used, having imposed $\phi_2(5) = 1.7$

However, our intent is not only in the weight reduction, but in the enhancement of such minimization accounting also for the issues related to high number of different cross-sectional areas used in the same structure. To do so we need to use a lower value of $\beta$.
Summarizing, we should have in mind two basic concepts when we have to deal with the definition of $\beta$. Fixing the passage at a specific point, lower $\beta$ values implies: 1)the asympotote is at a higher y-axis value, because $\Delta$ is higher, and 2)to reach it, the curve has a more gradual trend, thus the scattering of the penalty values is enhanced.

From the previous considerations we have decided to work with a $\beta = 0.1$. Then the curve will be identified if a specific point would be imposed, thus specific x-coordinate, $N_a$, and y-coordinate, $\phi_2$. To study the influence of this penalty in the evaluation of the best individual, we have analyzed different levels of penalization. They could be achieved in a dual way: or, fixing a y-coordinate, we vary $N_a$, or, vice-versa, fixing the x-coordinate, the $\phi_2$ value is changed. Focusing on the first procedure, we have defined three level of penalties:

| | Level | $N_a$ imposed |
|---|---|---|
| Fixed $\beta = 0.1$ and $\Phi_2 = 1.7$ | LOW | 7 |
| | MEDIUM | 5 |
| | HIGH | 3 |

Table 4.11: Different level of penalty for fixed $\beta$

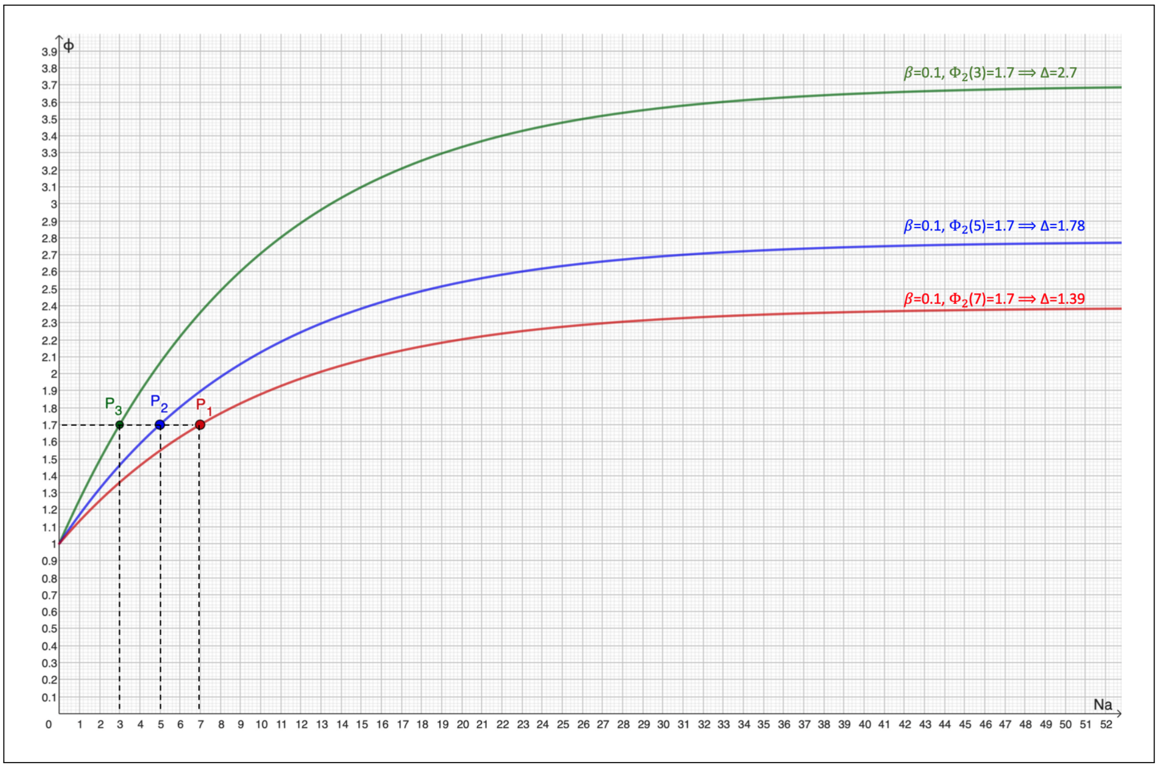


Figure 4.42: Trend of $\phi_2$, with $\beta = 0.1$, fixing the same penalty(1.7) at different $N_a$

To better comprehend the influence of the degree of penalization imposed in the three cases, let's consider how the OF would be affected if, for example, we use $N_a = 8$ different sections. The green curve will imply a penalization of such choice of about 25.25% more than the blue curve and almost 40% more than the red one. Precisely, we would obtain the values reported in table 4.12.

| Penalty | $N_a$ | $\phi_2(N_a)$ | Percentage variation |
|---|---|---|---|
| $f(3) = 1.7$ | 8 | 2.48 | - |
| $f(5) = 1.7$ | 8 | 1.98 | 25.25% |
| $f(7) = 1.7$ | 8 | 1.77 | 11.86% |

Table 4.12: Obtained penalties at the same $N_a = 8$

Now we can analyze the results of the optimizations, for the specific low, medium and high penalties, looking at the outcomes reported in the table 4.13.

| Penalty | $\Delta$ | $N_a$ | $Weight[KN]$ |
|---|---|---|---|
| $f(3) = 1.7$ | 2.701 | 4 | 5.15 |
| $f(5) = 1.7$ | 1.779 | 5 | 4.83 |
| $f(7) = 1.7$ | 1.3905 | 6 | 4.51 |

Table 4.13: Results for HIGH, MEDIUM and LOW penalty

As expected, the higher the penalization, the lower will be the number of sections used for the optimized configuration. It's important to underline that if $N_a$ of the best individual reduces, the weight will increase, following a trend like the one in the graph 6.6. Due to the fact that our final objective is to get a truss structure with both minimum weight and number of cross sections, a balance should be found.

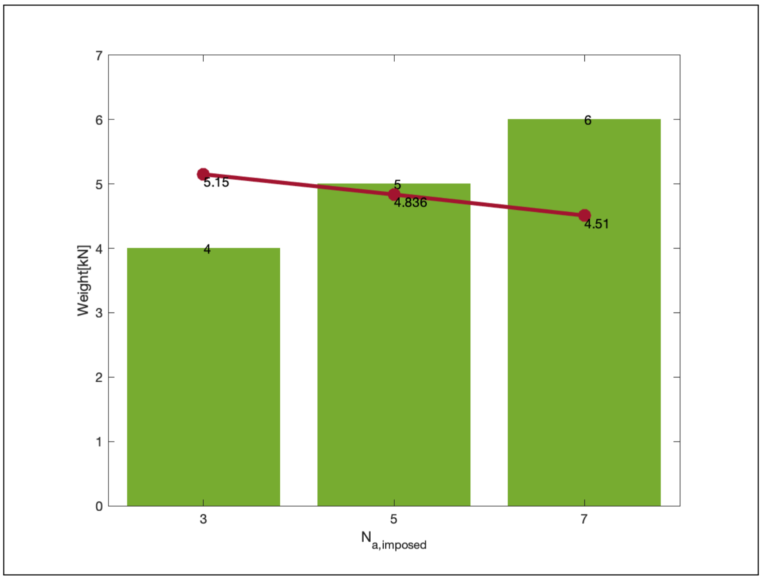


Figure 4.43: Trend of Na and Weight found by the optimizer for different levels of penalty, fixed $\beta = 0.1$

To play with the degree of penalization, instead of varying the $N_a$ at which we impose the passage of the curve, we can act by fixing it and increase the ordinate of the point, thus the corresponding $\phi_2$ value. Therefore, we decided to keep $N_a = 3$ because from the previous analyses it gave the best outcomes. Then, we have studied the responses considering:

$$N_a = 3 \Rightarrow \begin{cases} \phi_2 = 1.5 \\ \phi_2 = 1.7 \end{cases}$$

In the graph 4.44 we can see the specific curves:

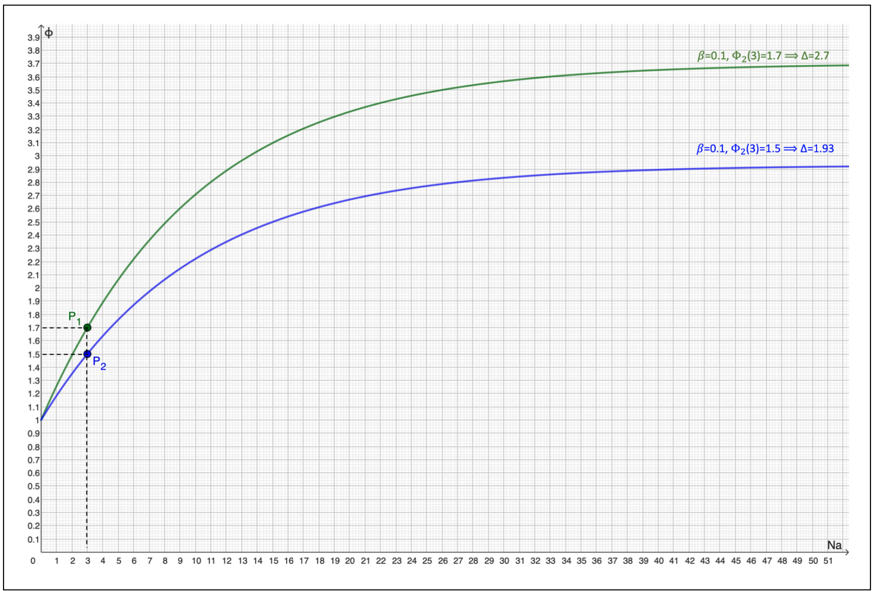


Figure 4.44: Trend of curves for the two different penalty values with $N_a = 3$

The application of these two penalties will result in the truss's configurations reported in tables 4.14, 4.15 and 4.16.

| Penalty | $\Delta$ | $N_a$ | $Weight[KN]$ |
|---|---|---|---|
| $f(3) = 1.5$ | 1,92 | 6 | 4.835 |
| $f(3) = 1.7$ | 2.7 | 4 | 5.150 |

Table 4.14: Results for HIGH penalty

| Penalty | $\Delta$ | $N_a$ | $Weight[KN]$ |
|---|---|---|---|
| $f(5) = 1.5$ | 1,27 | 6 | 4.510 |
| $f(5) = 1.7$ | 1.77 | 5 | 4.836 |

Table 4.15: Results for MEDIUM penalty

| Penalty | $\Delta$ | $N_a$ | $Weight[KN]$ |
|---|---|---|---|
| $f(7) = 1.5$ | 0,929 | 7 | 4.380 |
| $f(7) = 1.7$ | 1.39 | 6 | 4.510 |

Table 4.16: Results for LOW penalty

In conclusion, we have seen how this penalty function works and how it can be set for specific needs. Until now, we have illustrated how this penalty function works in the size optimization framework. In fact, it is directly influencing the size design variables, i.e. the cross-sections. However, in the chapter 5, we are going to explain how $\phi_2$ will perform in combination with $\phi_3$ and with the additional shape and topology design variables.

### 4.6.3 Penalty $\phi_3 = (1+\gamma) - e^{-\alpha\cdot(n-\frac{ln\gamma}{\alpha})}$

While with the second penalty we have encouraged a simplified design by lowering the number of sections used, pursuing a standardization of the elements, this objective has been tackled in a different way by means of the third penalty. Here, the complexity has been reduced by accounting for the number of subdivisions of the truss. In fact, increasing $n$ values lead to higher number of elements, as well as more and more connections to be made to link the truss's components. Also in this case we have adopted an exponential formulation, as reported in 4.7, increasing the penalization of the objective function for higher $n$ values. As in $\phi_2$, here $\gamma$ and $\alpha$ have the same influence in the curve's setting as $\delta$ and $\beta$, respectively. Therefore, in their identification we have exploited the results of the previous penalty, so a value of $\alpha = 0.1$ has been chosen. In this way the trend of the curve has been fixed. Then $\gamma$ has been obtained, as it was for $\Delta$, by fixing a specific point in the curve. In order to have a good response from the optimizer to such penalization, we have imposed the passage in $\phi_3(3) = 1.3$. In particular, the values of the resulting $\phi_3$ are summarized in the following table 4.17.

| $N_A$ | $\phi_3(n)_{\beta=0.1}$ |
|---|---|
| 3 | 1.3 |
| 4 | 1.38 |
| 5 | 1.46 |
| 6 | 1.52 |
| 7 | 1.58 |
| 8 | 1.64 |
| 9 | 1.69 |
| 10 | 1.73 |

Table 4.17: Values of $\phi_3$ with $\beta = 0.1$

However, in the problem's setting we should account also for another factor related to $n$. In fact, too low $n$ values imply structural problems, because the distance between consecutive nodes increases, thus buckling instability can be favoured. Therefore, we have introduced also a limiting domain where the algorithm can search for the optimal solution. In particular, for our case study of a 20 meters span truss, we have limited $n$ in between 3 and 10. The lower bound has been defined accounting for the structural performance just explained, as well as the grouping strategy. Whereas, the upper bound has been set considering a minimum element length of 1 meter. Now, the algorithm has been encouraged to reduce the complexity, finding a balance with the penalty $phi_1$ about buckling stability requirements.

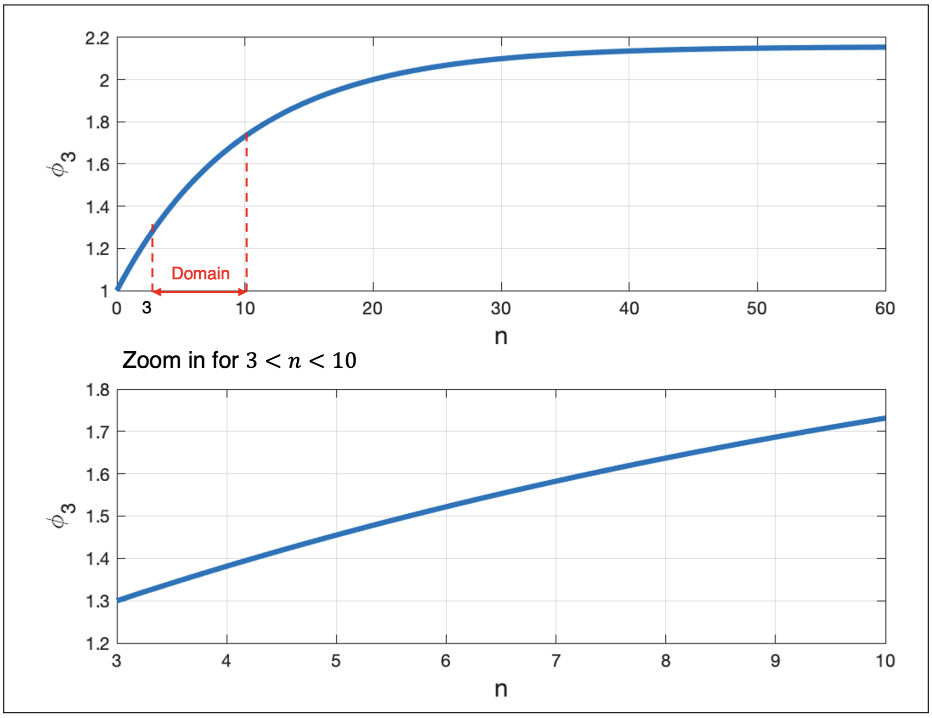


Figure 4.45: Resulting $\Phi_3$ with a zoom in of the curve in the domain of $n$

It should be stressed the nature of this third penalty, which is directly affecting the shape design variables of the problem. Therefore, we have tested $\phi_3$ without considering $\phi_2$, in order to see how the best individual would be chosen. In the chapter 5.8, we are going to show the results in the case of:

- $OF = W \cdot \phi_1 \cdot \phi_3$ for size and shape optimization
- $OF = W \cdot \phi_1 \cdot \phi_2 \cdot \phi_3$ for size and shape optimization
- $OF = W \cdot \phi_1 \cdot \phi_2 \cdot \phi_3$ for size, shape and topology optimization

# Chapter 5

# Results - Truss level

## 5.1 Size optimization

We started our investigation from a simple size optimization, therefore only the design variables from $x_7$ to $x_{21}$ of table 4.3 (yellow section) have been considered. In this instance, due to the fact that we are not varying the shape and topology design variables, we have fixed the following parameters:

- Brown truss type $x_1 = 1$
- Number of subdivisions of half the geometry $x_2 = n = 6$
- External height of the upper chord $x_3 = H_1 = 1.33m$, which is equal to $L/15$
- Middle height of the upper chord $x_4 = H_2 = 2.5m$, which is equal to $L/8$
- Indexes of the grouping division $x_5 = n_1 = 2$ and $x_6 = n_2 = 2$

The following subsections are going to illustrate the results for the cases in which we have introduced step by step the penalty functions. We started by analyzing how the first penalty works and then we tested also the second one. The third penalty has not been considered in the size optimization environment because it is related to the variation of the coordinates of the nodes. Furthermore, we have performed a preliminary simple weight minimization, for comparison purposes. However, the optimized structure resulted to be characterized by the same cross-section (CHS 21.3x2) for all the members. By looking at the maximum compressive load, of about 280 kN, we can conclude that it won't be sustained by the buckling resistance provided by the section assigned. Therefore, the first penalty function is essential for the structural stability of the truss, so the comparison of the different cases will be done referring to the case of $\Phi_1$ only.

### 5.1.1 Size - Case A: $\Phi_1$

The Objective Function in this case is simply:

$$min\ F(\mathbf{x}) = \rho \sum_{i=1}^{N} (A_i \cdot l_i) \cdot \phi_1(n_{un})$$

The resulting optimized structure is reported in figure 5.1.

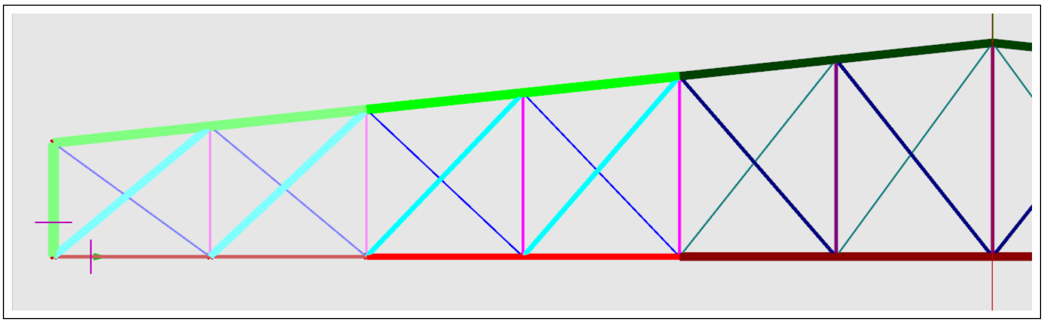

Figure 5.1: Size - Case A: Configuration of the optimized truss

In particular, in the table 5.1 are summarized the cross-sections used in the specific truss, while in table 5.2 its main characteristics.

| | CHS 1°group | CHS 2°group | CHS 3°group |
|---|---|---|---|
| **Lower Chord** | 101.6x2 | 76.1x2.5 | 42.4x3 |
| **Upper Chord + Ext. Vert. Structs** | 101.6x4 | 114.3x3 | 114.3x2.5 |
| **Int. Vert. Structs** | 42.4x2 | 33.7x2 | 21.3x2 |
| **Upward-Downward Diagonals** | 21.3x2 | 60.3x2 | 88.9x2 |
| **Downward-Upward Diagonals** | 42.4x2 | 21.3x2 | 21.3x3 |

Table 5.1: Size - Case A: Cross-sections of the optimized truss

| Best OF | Weight [kN] | $N_a$ |
|---|---|---|
| 4.162 | 4.162 | 12 |

Table 5.2: Size - Case A: Main features of the optimized truss

Then we have reported the charts about the best individual found at each iteration, as well as its weight, number of sections used and the unfeasibility proportion throughout the optimization.

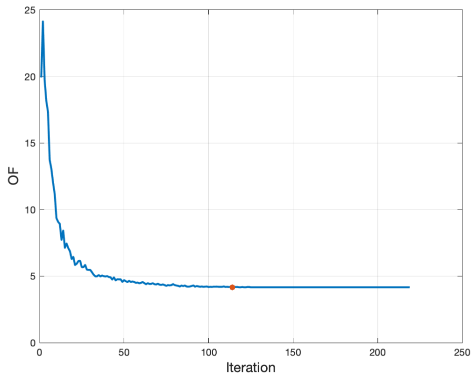


Figure 5.2: Size - Case A: Best individual - Iteration

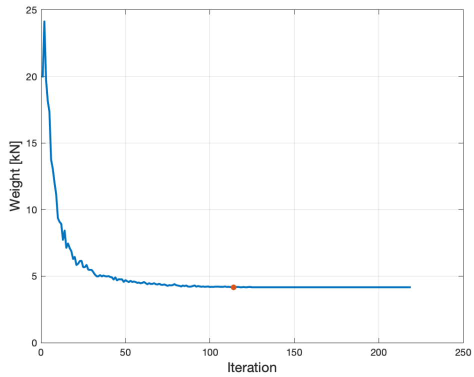


Figure 5.3: Size - Case **A**: Weight of best individual at each iteration

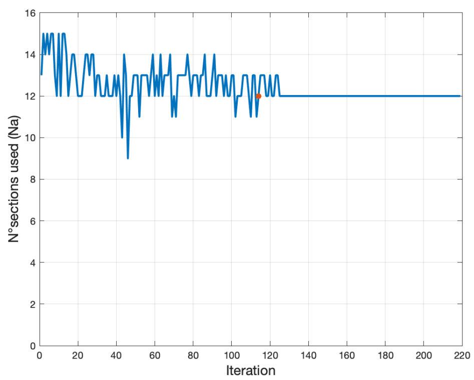


Figure 5.4: Size - Case A: $N_a$ of best individual at each iteration

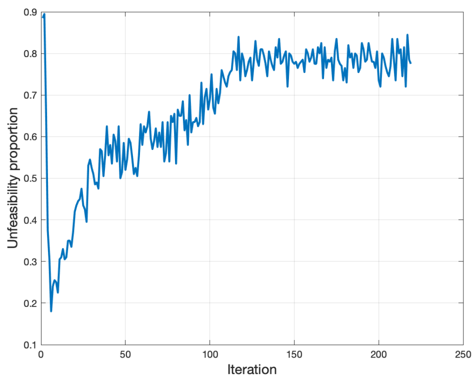


Figure 5.5: Size - Case A: Unfeasibility proportion

As we can see, the value of the best OF and its corresponding weight are the same, meaning that no unfeasible individual has been chosen. This demonstrate the validity of the coefficient $K_1$ chosen. We have decided to illustrate also how the number of section used are employed when the second penalty is not present, to show in the next case how it will influence the objective function. We should highlight the meaning of the unfeasibility proportion chart, which gives an estimation of the % of unfeasible individuals created at each generation. It depends on the internal set-up of the algorithm inside Octopus package, regarding the selection, crossover and mutation operators.

### 5.1.2 Size - Case B: $\Phi_1$+$\Phi_2$

The Objective Function in this case is

$$minF(\mathbf{x}) = \rho \sum_{i=1}^{N} (A_i \cdot l_i) \cdot \phi_1(n_{un}) \cdot \phi_2(N_a)$$

The resulting best individual found by Octopus is the following one:

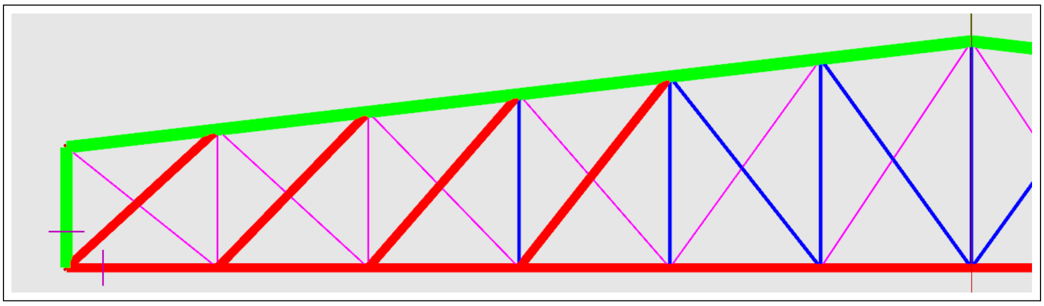

Figure 5.6: Size - Case B: Configuration of the optimized truss

| | CHS 1°group | CHS 2°group | CHS 3°group |
|---|---|---|---|
| **Lower Chord** | 101.6x2 | 101.6x2 | 101.6x2 |
| **Upper Chord + Ext. Vert. Structs** | 139.7x3 | 139.7x3 | 139.7x3 |
| **Int. Vert. Structs** | 42.4x2.5 | 42.4x2.5 | 21.3x2 |
| **Upward-Downward Diagonals** | 21.3x2 | 101.6x2 | 101.6x2 |
| **Downward-Upward Diagonals** | 41.4x2.5 | 21.3x2 | 21.3x2 |

Table 5.3: Size - Case B: Cross-sections of the optimized truss

| Best OF | Weight [kN] | $N_a$ |
|---|---|---|
| 9.747624 | 5.156383 | 4 |

Table 5.4: Size - Case B: Main features of the optimized truss

It can be immediately observed how the optimized configuration is different from the previous case. A single cross-section has been assigned for each chord, while the external upward-downward diagonals present the same section of the lower chord. For the internal vertical structs elements and the remaining diagonals, other two smaller cross-sections are used. The total weight in this optimization is 5.16 kN, obviously higher with respect to the former of about 4.162 kN. This gained amount of weight is counterbalanced by a huge loss in variability of cross-sections used, from 12 to only 4. The charts about the best individual at each generation, as well as its corresponding weight and $N_a$ are reported below, together with the unfeasibility proportion.

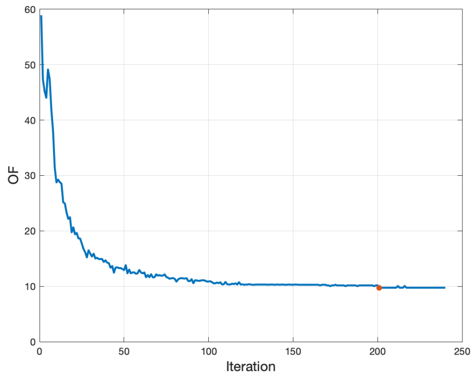


Figure 5.7: Size - Case B: Best individual - Iteration

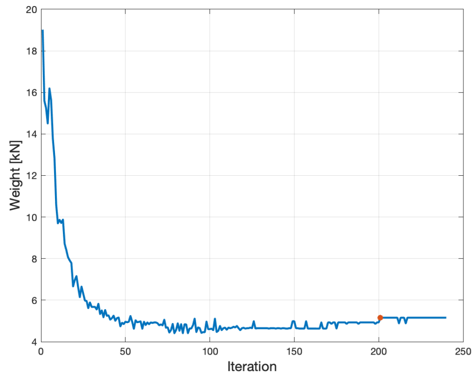


Figure 5.8: Size - Case B: Weight of best individual at each iteration

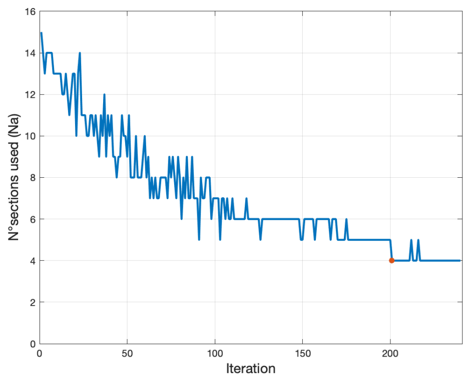


Figure 5.9: Size - Case B: $N_a$ of best individual at each iteration

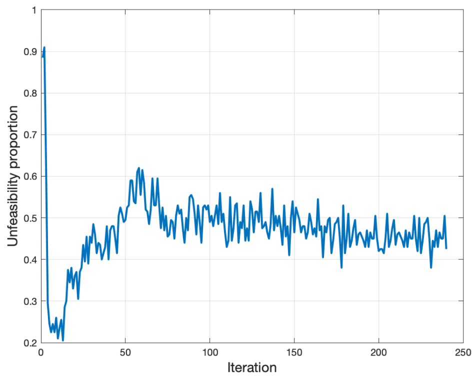


Figure 5.10: Size - Case B: Unfeasibility proportion

As in the previous case, the unfeasibility proportion chart 5.10 shows how the algorithm is always guaranteeing a % of feasible individuals at each iteration while trying to refining the optimization.

## 5.2 Size and shape optimization

In this section we are going to consider both the size design variables, i.e. from $x_7$ to $x_{21}$ of table 4.3 (yellow section), as well as the shape ones, namely $x_2$, $x_3$ (red section) and $x_4$, and the ones related to the grouping division, i.e. $x_5$ and $x_6$ (green section). The only fixed parameter is the type of truss, that once again is the Brown one. Starting from the OF with only $\Phi_1$, we are going to see how the introduction of the other two penalties is affecting the final result. Moreover, we are going to highlight the differences with the previous simple size optimization cases.

### 5.2.1 Size & Shape - Case A: $\Phi_1$

We have considered the same objective function 5.1.1. The resulting best individual found by Octopus is the following one:

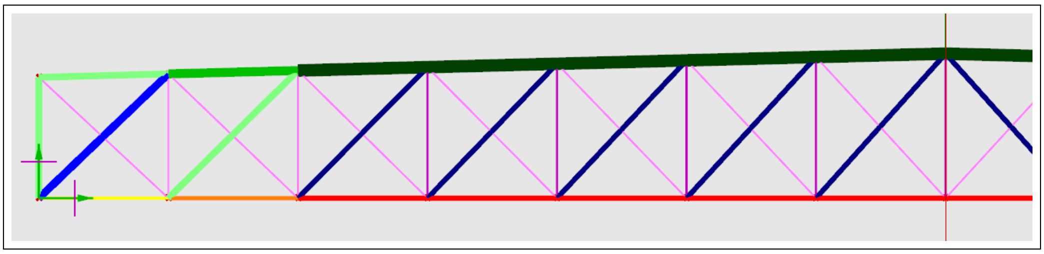

Figure 5.11: Size & Shape - Case A: Configuration of the optimized truss

| | CHS 1°group | CHS 2°group | CHS 3°group |
|---|---|---|---|
| **Lower Chord** | 60.3x5 | 48.3x3 | 33.7x2 |
| **Upper Chord + Ext. Vert. Structs** | 139.7x3 | 101.6x2.5 | 76.1x2 |
| **Int. Vert. Structs** | 26.9x2 | 21.3x2 | 21.3x2 |
| **Upward-Downward Diagonals** | 60.3x2.5 | 76.1x2 | 88.9x2 |
| **Downward-Upward Diagonals** | 21.3x2 | 21.3x2 | 21.3x2 |

Table 5.5: Size & Shape - Case A: Cross-sections of the optimized truss

| **Best OF** | **Weight [kN]** | $N_a$ | $n$ | $H_1$ | $H_2$ | $n_1$ | $n_2$ | $n_3$ |
|---|---|---|---|---|---|---|---|---|
| 4.3992 | 4.3392 | 10 | 7 | 1.33 | 1.59 | 1 | 1 | 5 |

Table 5.6: Size & Shape - Case A: Main features of the optimized truss

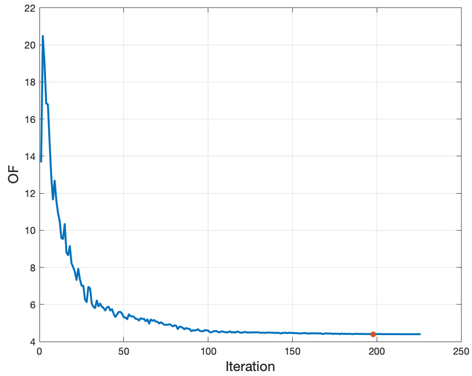


Figure 5.12: Size & Shape - Case A: Best individual - Iteration

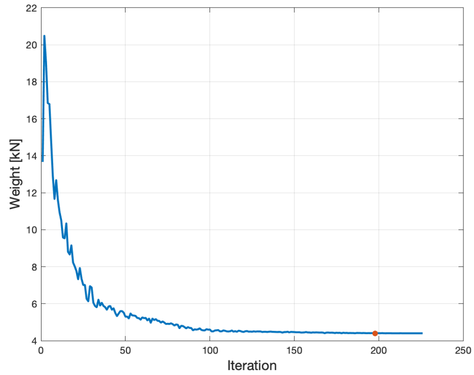


Figure 5.13: Size & Shape - Case A: Weight of best individual at each iteration

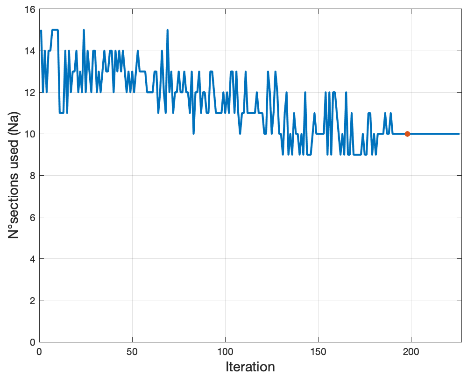


Figure 5.14: Size & Shape - Case A: $N_a$ of best individual at each iteration

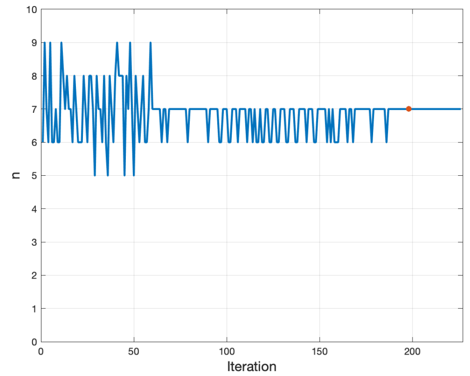


Figure 5.15: Size & Shape - Case A: $n$ of best individual at each iteration

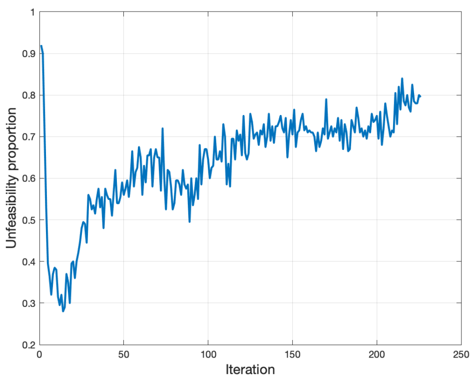


Figure 5.16: Size & Shape - Case A: Unfeasibility proportion

From the charts 5.12 and 5.13, we can see that even if the number of design variables is rised the coefficient $K_1$ set at 10 is still working properly. Regarding the grouping division, we can see that the indexes $n_1$ and $n_2$ are fixing the two external elements to be in single groups, while the central part is unified. The optimal number of subdivisions is set at 7, while the number of sections used is 10. In the following analyses we are going to see how the complexity will be minimized, in favour of slight increases in weights.

### 5.2.2 Size & Shape - Case B: $\Phi_1$+$\Phi_2$

We have considered the same objective function of 5.1.2. The resulting best individual found by Octopus is the following one:

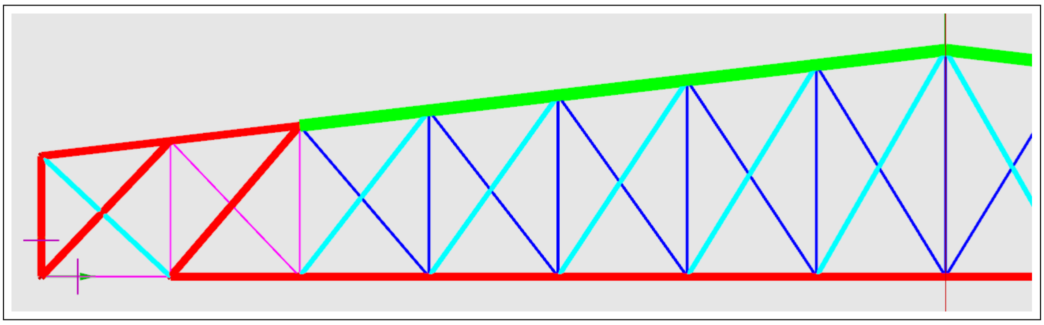

Figure 5.17: Size & Shape - Case B: Configuration of the optimized truss

| | CHS 1°group | CHS 2°group | CHS 3°group |
|---|---|---|---|
| **Lower Chord** | 88.9x3 | 88.9x3 | 21.3x2 |
| **Upper Chord + Ext. Vert. Structs** | 139.7x3 | 139.7x3 | 88.9x3 |
| **Int. Vert. Structs** | 33.7x2 | 21.3x2 | 21.3x2 |
| **Upward-Downward Diagonals** | 60.3x2 | 88.9x3 | 88.9x3 |
| **Downward-Upward Diagonals** | 33.7x2 | 21.3x2 | 60.3x2 |

Table 5.7: Size & Shape - Case B: Cross-sections of the optimized truss

| **Best OF** | **Weight [kN]** | $N_a$ | $n$ | $H_1$ | $H_2$ | $n_1$ | $n_2$ | $n_3$ |
|---|---|---|---|---|---|---|---|---|
| 10.08232 | 4.8887 | 5 | 7 | 1.33 | 1.72 | 1 | 1 | 5 |

Table 5.8: Size & Shape - Case B: Main features of the optimized truss

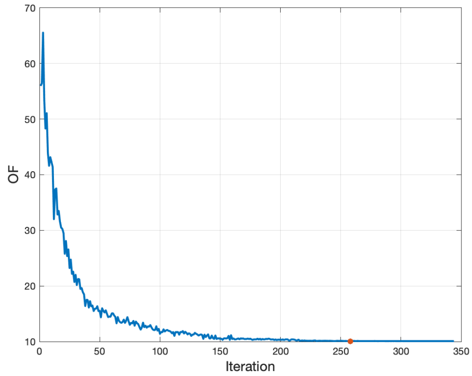


Figure 5.18: Size & Shape - Case B: Best individual - Iteration

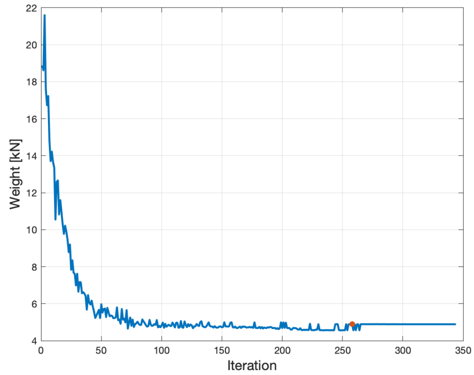


Figure 5.19: Size & Shape - Case B: Weight of best individual at each iteration

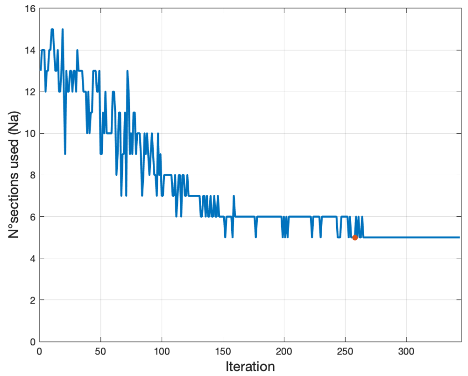


Figure 5.20: Size & Shape - Case B: $N_a$ of best individual at each iteration

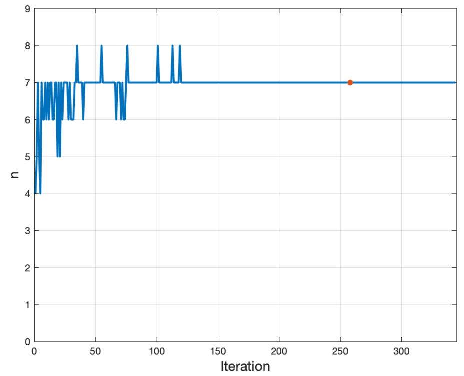


Figure 5.21: Size & Shape - Case B: $n$ of best individual at each iteration

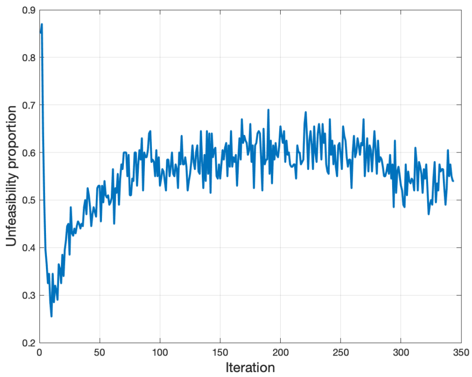


Figure 5.22: Size & Shape - Case B: Unfeasibility proportion

Comparison with the size and shape optimization case, where only $\Phi_1$ were considered: lowered variability in number of sections used, from 10 to 5; same $n$, $n_1$ and $n_2$; weight increase of about 13%.
Comparison with the analogous case in the size environment: weight reduction of about 5%; slight increase in $N_a$, from 4 to 5; 7 subdivisions instead of the fixed 6 of before; same $H_1$, while $H_2$ passes from 2.5m to 1.72m.

### 5.2.3 Size & Shape - Case C: $\Phi_1$+$\Phi_3$

The Objective Function in this case is:

$$minF(\mathbf{x}) = \rho \sum_{i=1}^{N} (A_i \cdot l_i) \cdot \phi_1(n_{un}) \cdot \phi_3(n)$$

The resulting best individual found by Octopus is the following one:

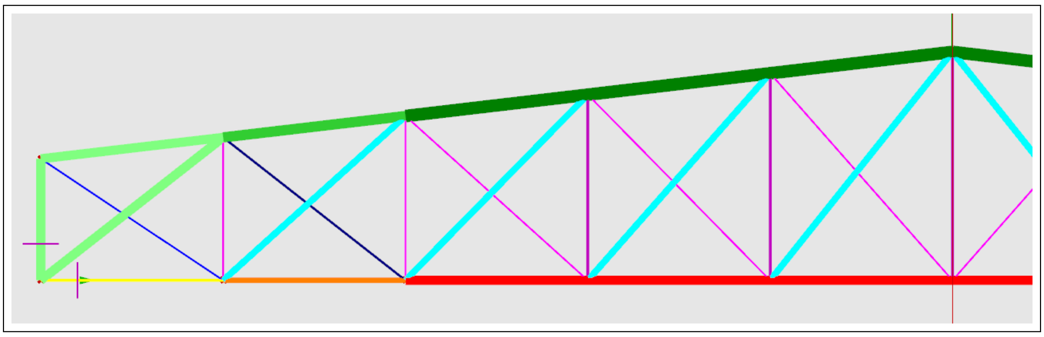

Figure 5.23: Size & Shape - Case C: Configuration of the optimized truss

| | CHS 1°group | CHS 2°group | CHS 3°group |
|---|---|---|---|
| **Lower Chord** | 101.6x2.5 | 60.3x3 | 33.7x2.5 |
| **Upper Chord + Ext. Vert. Structs** | 139.7x3 | 114.3x3 | 101.6x2 |
| **Int. Vert. Structs** | 33.7x2 | 21.3x2 | 21.3x2 |
| **Upward-Downward Diagonals** | 76.1x2 | 76.1x2 | 101.6x2 |
| **Downward-Upward Diagonals** | 21.3x2 | 26.9x2 | 21.3x2.5 |

Table 5.9: Size & Shape - Case C: Cross-sections of the optimized truss

| **Best OF** | **Weight [kN]** | $N_a$ | $n$ | $H_1$ | $H_2$ | $n_1$ | $n_2$ | $n_3$ |
|---|---|---|---|---|---|---|---|---|
| 6.148 | 4.224 | 11 | 5 | 1.33 | 1.81 | 1 | 1 | 3 |

Table 5.10: Size & Shape - Case C: Main features of the optimized truss

We can recognize the effectiveness of this third penalty, highlighting the abatement of $n$ down to 5. In particular, looking at the following chart 5.27 we can see that this value has been found just at the beginning, while in the remaining iterations the other design variables have been varied. The resulting weight is far less than case B, of about 16%. However, in terms of overall complexity, case B was slightly better.

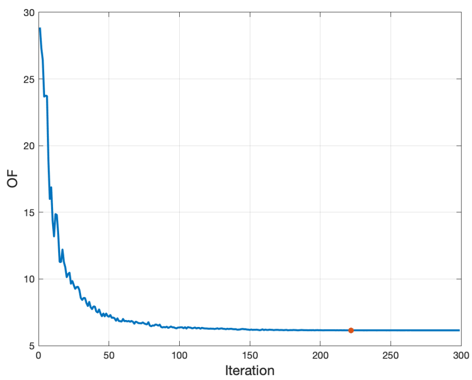


Figure 5.24: Size & Shape - Case C: Best individual - Iteration

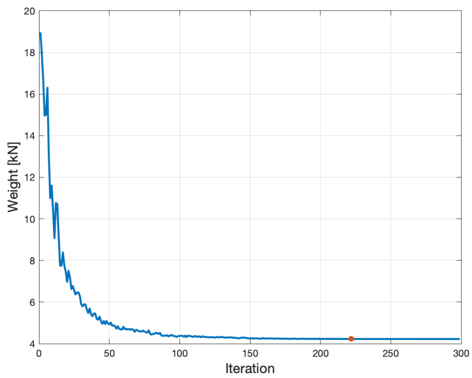


Figure 5.25: Size & Shape - Case C: Weight of best individual at each iteration

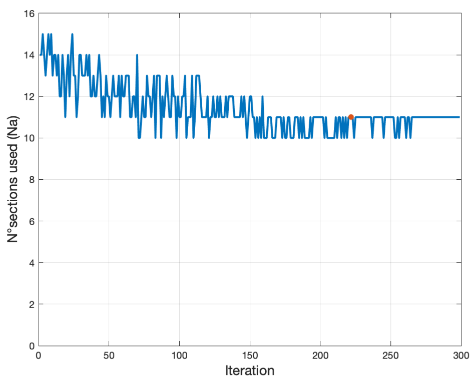


Figure 5.26: Size & Shape - Case C: $N_a$ of best individual at each iteration

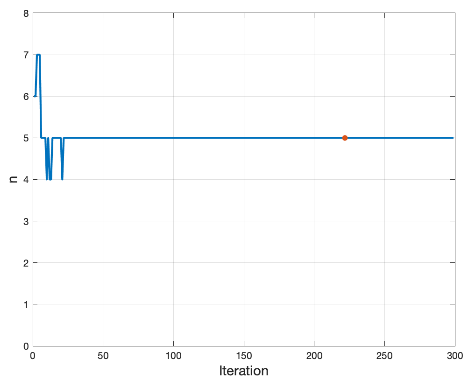


Figure 5.27: Size & Shape - Case C: $n$ of best individual at each iteration

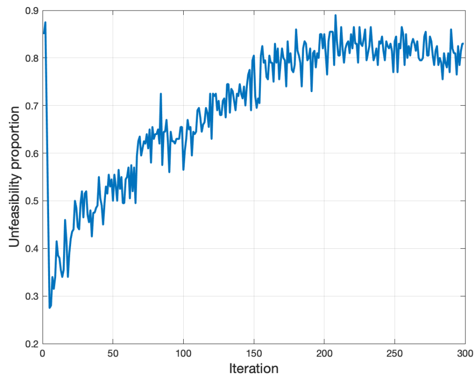


Figure 5.28: Size & Shape - Case C: Unfeasibility proportion

### 5.2.4 Size & Shape - Case D: $\Phi_1+\Phi_2+\Phi_3$

Finally, the Objective Function in this case is the one with all the penalty functions:

$$\rho\sum_{i=1}^{N}(A_i \cdot l_i)\cdot\phi_1(n_{un})\cdot\phi_2(N_a)\cdot\phi_3(n)$$

The resulting best individual found by Octopus is the following one:

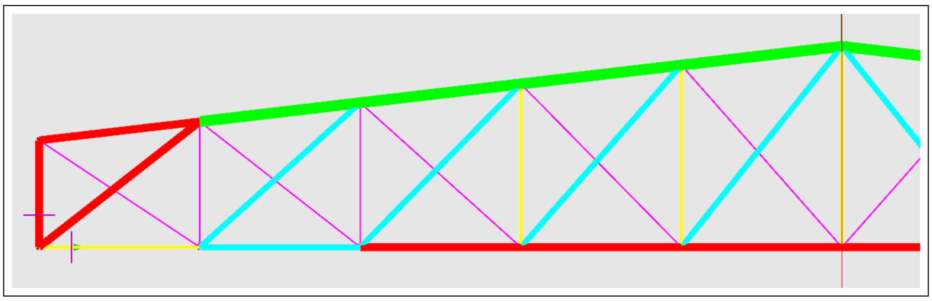

Figure 5.29: Size & Shape - Case D: Configuration of the optimized truss

Its corresponding cross-sections are reported in table 5.11, where only 5 different values are assigned. In table 5.12, the main characteristics of the optimized configuration are summarized. A good balance in terms of complexity and weight minimization has been found. In fact, in this last case where the three penalty functions work simultaneously, we can see how the optimized feasible truss is characterized by a low complexity both in terms of $N_a$ and $n$. Moreover, the resulting weight is one of the best gained so far. It is 2.5% lower than the case A, where only $\Phi_1$ were accounted, 14% lower than case B, where $\Phi_1$ and $\Phi_2$ were combined, and less than

2% higher than case C, where the first and third penalties appeared in the OF.

| | **CHS 1°group** | **CHS 2°group** | **CHS 3°group** |
|---|---|---|---|
| **Lower Chord** | 101.6x2 | 76.1x2 | 42.4x2 |
| **Upper Chord + Ext. Vert. Structs** | 139.7x3 | 139.7x2 | 101.6x2 |
| **Int. Vert. Structs** | 42.4x2 | 21.3x2 | 21.3x2 |
| **Upward-Downward Diagonals** | 76.1x2 | 76.1x2 | 101.6x2 |
| **Downward-Upward Diagonals** | 21.3x2 | 21.3x2 | 21.3x2 |

Table 5.11: Size & Shape - Case D: Cross-sections of the optimized truss

| **Best OF** | **Weight [kN]** | $N_a$ | $n$ | $H_1$ | $H_2$ | $n_1$ | $n_2$ | $n_3$ |
|---|---|---|---|---|---|---|---|---|
| 12.8858 | 4.2934 | 5 | 5 | 1.39 | 2.28 | 1 | 1 | 3 |

Table 5.12: Size & Shape - Case D: Main features of the optimized truss

Here below we have reported the usual chart related to the main parameters varied among the iterations. As in case C, the optimal number of subdivisions has been found in the early stages of the optimization. Instead, the number of different cross-sections used has a more gradual trend. The unfeasibility proportion chart is always showing how Octopus is always creating a high number of unfeasible individuals at each iteration, in order to refine the analysis, while maintaining a sufficient number of feasible ones.

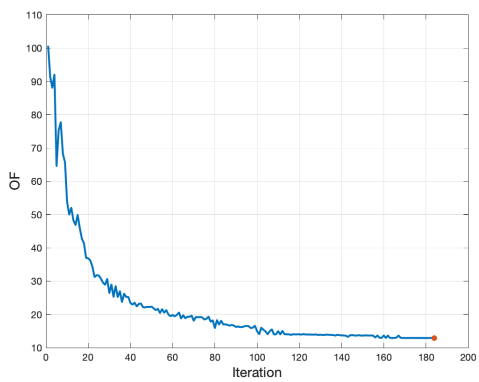


Figure 5.30: Size & Shape - Case D: Best individual - Iteration

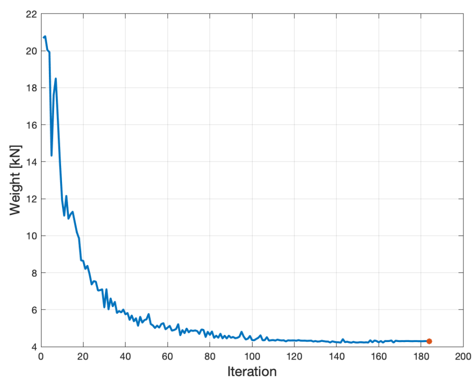


Figure 5.31: Size & Shape - Case D: Weight of best individual at each iteration

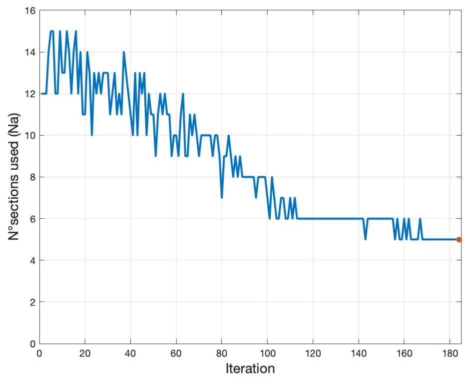


Figure 5.32: Size & Shape - Case D: $N_a$ of best individual at each iteration

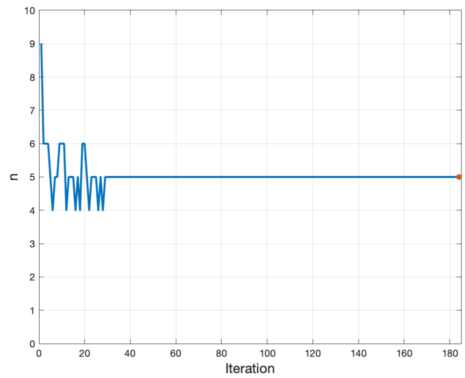


Figure 5.33: Size & Shape - Case D: $n$ of best individual at each iteration

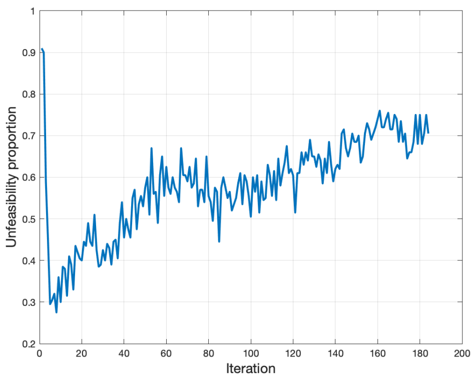


Figure 5.34: Size & Shape - Case D: Unfeasibility proportion

## 5.3 Size, shape and topology optimization

In this last section, we have directly performed the optimization comprehensive of all the design variables, now including $x_1$. The novelty with respect to the previous case relies, in fact, in the topology slider that can choose between five different truss configurations.

### 5.3.1 Size, Shape & Topology: $\Phi_1(n_{un})+\Phi_2(N_a)+\Phi_3(n)$

The Objective Function is the same of the previous case, i.e

$$\rho \sum_{i=1}^{N} (A_i \cdot l_i) \cdot \phi_1 \cdot \phi_2 \cdot \phi_3$$

The resulting best individual found by Octopus is the following one:

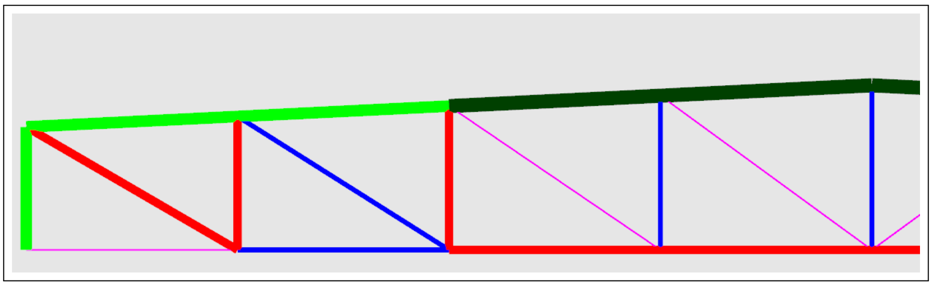

Figure 5.35: Size, Shape & Topology: Configuration of the optimized truss

| | **CHS 1°group** | **CHS 2°group** | **CHS 3°group** |
|---|---|---|---|
| **Lower Chord** | 101.6x2 | 60.3x2 | 21.3x2 |
| **Upper Chord + Ext. Vert. Structs** | 168.3x3 | 139.7x3 | 139.7x3 |
| **Int. Vert. Structs** | 60.3x2 | 101.6x2 | 101.6x2 |
| **Downward-Upward Diagonals** | 21.3x2 | 60.3x2 | 101.6x2 |

Table 5.13: Size, Shape & Topology: Cross-sections of the optimized truss

| **Best OF** | **Weight [kN]** | $N_a$ | $n$ | $H_1$ | $H_2$ | $n_1$ | $n_2$ | $n_3$ |
|---|---|---|---|---|---|---|---|---|
| 12.4295 | 4.3627 | 5 | 4 | 1.7 | 2.38 | 1 | 1 | 2 |

Table 5.14: Size, Shape & Topology: Main features of the optimized truss

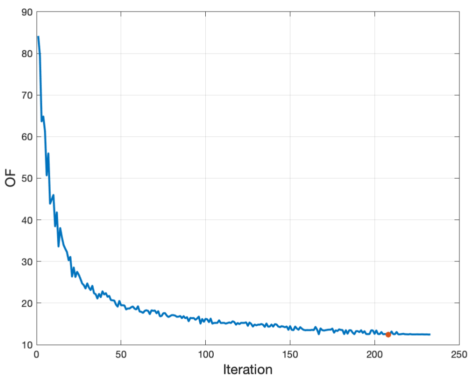


Figure 5.36: Size, Shape & Topology: Best individual - Iteration

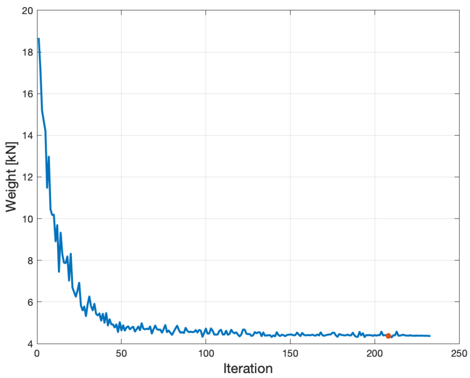


Figure 5.37: Size, Shape & Topology: Weight of best individual at each iteration

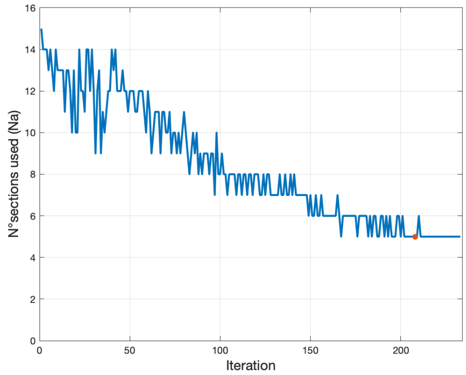


Figure 5.38: Size, Shape & Topology: $N_a$ of best individual at each iteration

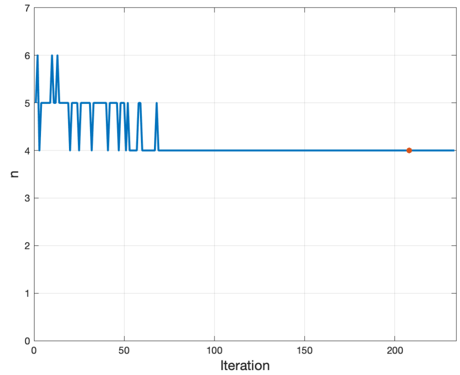


Figure 5.39: Size, Shape & Topology: $n$ of best individual at each iteration

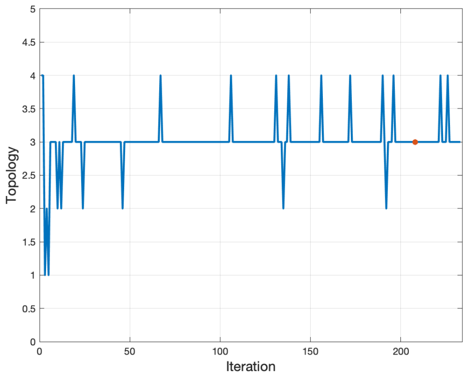


Figure 5.40: Size, Shape & Topology: Topology of best individual at each iteration

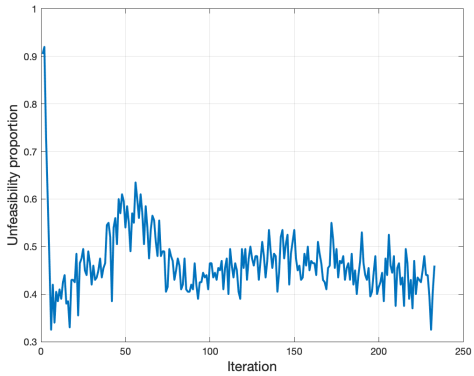


Figure 5.41: Size, Shape & Topology: Unfeasibility proportion

From table 5.13 we can see the CHS cross-sections assigned to each element. Also in this case a balance between complexity and weight of the truss structure has been found, as can be observed from table 5.14. However, the most important consideration that can be drawn from the results refers to the topology selected by the optimizer, which is Pratt one. As a matter of fact, it should be expected due to the fact that we have considered only gravitational loadings. In Pratt trusses, as explained in Chapter 4, the diagonal members, which are the longest ones, are in tension and not in compression, thus they won't require additional by buckling instability verifications.

## 5.4 Discussion and final considerations

In the cases in which the Objective Function included all the penalties, i.e. $\phi1$, $\phi2$ and $\phi3$, we have tested the robustness of the algorithhm by performing the same analysis twenty times. Specifically, it was done for 'Size & Shape - Case D', described in Section 5.2.4, which deals with a size and shape optimization, as well as for 'Size, Shape & Topology' discussed in Section 5.3.1.

**Results for 'Size & Shape - Case D: $\Phi_1$+$\Phi_2$+$\Phi_3$'**

In the table 5.15 the results of all the optimization performed are summarized. In particular, they have been sorted from the smallest to the largest in terms of best objective function.

| **Best OF** | **Weight [kN]** | $N_a$ | $n$ | $H_1$ | $H_2$ | $n_1$ | $n_2$ | $n_3$ |
|---|---|---|---|---|---|---|---|---|
| 12.885 | 4.293 | 5 | 5 | 1.39 | 2.28 | 1 | 1 | 3 |
| 13.259 | 4.820 | 4 | 5 | 1.54 | 1.8 | 1 | 1 | 3 |
| 13.290 | 4.831 | 4 | 5 | 1.54 | 2.25 | 1 | 1 | 3 |
| 13.512 | 5.175 | 4 | 4 | 1.47 | 1.65 | 1 | 1 | 2 |
| 13.817 | 4.603 | 5 | 5 | 1,44 | 1,8 | 1 | 1 | 3 |
| 13.869 | 4.621 | 5 | 5 | 1.45 | 1.82 | 1 | 1 | 3 |
| 13.976 | 5.352 | 4 | 4 | 1.45 | 1.59 | 1 | 1 | 2 |
| 14.035 | 4.471 | 5 | 6 | 1.67 | 2.43 | 1 | 1 | 4 |
| 14.043 | 4.881 | 4 | 6 | 1.33 | 1.61 | 1 | 1 | 4 |
| 14.176 | 4.927 | 4 | 6 | 1.38 | 2.07 | 1 | 1 | 4 |
| 14.247 | 4.747 | 5 | 5 | 1.76 | 1.78 | 1 | 1 | 3 |
| 14.353 | 5.037 | 5 | 4 | 1.36 | 2.01 | 1 | 1 | 2 |
| 14.364 | 5.041 | 5 | 4 | 1.47 | 1.58 | 1 | 1 | 2 |
| 14.401 | 4.798 | 5 | 5 | 1.33 | 2.07 | 1 | 1 | 3 |
| 14.595 | 5.123 | 5 | 4 | 1.34 | 2.21 | 1 | 1 | 2 |
| 14.782 | 5.188 | 5 | 4 | 1.33 | 1.77 | 1 | 1 | 2 |
| 15.085 | 4.922 | 6 | 4 | 1.45 | 2.5 | 1 | 1 | 2 |
| 15.121 | 5.307 | 5 | 4 | 1.59 | 1.63 | 1 | 1 | 2 |
| 15.372 | 5.016 | 6 | 4 | 1.44 | 2.5 | 1 | 1 | 2 |
| 15.549 | 5.457 | 5 | 4 | 1.33 | 1.55 | 1 | 1 | 2 |

Table 5.15: Results of the best individual of each optimization for 'Size & Shape - Case D: $\Phi_1$+$\Phi_2$+$\Phi_3$'

In addition, in table 5.16, we have reported the Best, Worst and Mean values, as well as the Standard Deviation of the OF. More in details, the best value corresponds to the minimum OF, while the worst value to the maximum OF.

| Best | Worst | Mean | Standard Deviation |
|---|---|---|---|
| 12.885 | 15.549 | 14.236 | 0.713 |

Table 5.16: Best, Worst, Mean and Standard deviation related to the OF values of 'Size & Shape - Case D: $\Phi_1+\Phi_2+\Phi_3$'

**Results for 'Size, Shape & Topology: $\Phi_1+\Phi_2+\Phi_3$'**

In table 5.17 the results of every optimization have been summarized and sorted from the smallest to the largest in terms of Best OF; while in table 5.18, Best (min), Worst (max), Mean and Standard Deviation have been reported.

| Best OF | Weight [kN] | $N_a$ | $n$ | $H_1$ | $H_2$ | $n_1$ | $n_2$ | $n_3$ | Topology |
|---|---|---|---|---|---|---|---|---|---|
| 12.429 | 4.362 | 5 | 4 | 1.7 | 2.38 | 1 | 1 | 2 | PRATT |
| 12.435 | 4.143 | 5 | 5 | 1.53 | 1.96 | 1 | 1 | 3 | PRATT |
| 12.598 | 4.379 | 4 | 6 | 1.33 | 1.79 | 1 | 1 | 4 | PRATT |
| 12.604 | 4.424 | 5 | 4 | 1.97 | 2.39 | 1 | 1 | 2 | PRATT |
| 12.728 | 4.467 | 5 | 4 | 1.33 | 1.92 | 1 | 1 | 2 | PRATT |
| 12.776 | 4.644 | 4 | 5 | 1.55 | 1.85 | 1 | 1 | 3 | HOWE |
| 12.853 | 4.282 | 5 | 5 | 1.38 | 2.17 | 1 | 1 | 3 | PRATT |
| 12.876 | 4.202 | 6 | 4 | 1.57 | 2.24 | 1 | 1 | 2 | PRATT |
| 12.881 | 4.683 | 4 | 5 | 1.59 | 1.85 | 1 | 1 | 3 | HOWE |
| 13.069 | 4.587 | 5 | 4 | 1.33 | 1.86 | 1 | 1 | 2 | PRATT |
| 13.081 | 4.358 | 5 | 5 | 1.42 | 1.94 | 1 | 1 | 3 | PRATT |
| 13.144 | 4.613 | 5 | 4 | 1.34 | 2.06 | 1 | 1 | 2 | WARREN |
| 13.173 | 4.623 | 5 | 4 | 1.38 | 1.95 | 1 | 1 | 2 | PRATT |
| 13.182 | 4.392 | 5 | 5 | 1.37 | 1.85 | 1 | 1 | 3 | PRATT |
| 13.317 | 4.125 | 6 | 5 | 1.56 | 2.05 | 2 | 1 | 3 | PRATT |
| 13.389 | 4.699 | 5 | 4 | 1.46 | 1.68 | 1 | 1 | 2 | PRATT |
| 13.480 | 4.731 | 5 | 4 | 1.76 | 2.48 | 1 | 1 | 2 | PRATT |
| 13.777 | 4.590 | 5 | 5 | 1.33 | 1.84 | 1 | 1 | 3 | HOWE |
| 14.565 | 4.512 | 6 | 5 | 1.35 | 2.15 | 1 | 1 | 3 | HOWE |

Table 5.17: Results of the best individual of each optimization for 'Size, Shape & Topology: $\Phi_1+\Phi_2+\Phi_3$'

| Best | Worst | Mean | Standard Deviation |
|---|---|---|---|
| 12.429 | 14.565 | 13.072 | 0.509 |

Table 5.18: Best, Worst, Mean and Standard deviation related to the OF values of 'Size, Shape & Topology: $\Phi_1+\Phi_2+\Phi_3$'

Analyzing the results of both cases there is a slight variability among the optimized individuals. In order to obtain more refined results, the same analysis should be performed at least 50 times.

**Results of best individual for each case**

Summarizing the results obtained for all the cases tested, we can refer to table 5.19.

| | **Best OF** | **W[kN]** | $N_a$ | $n$ | $H_1$ | $H_2$ | $n_1$ | $n_2$ | $n_3$ |
|---|---|---|---|---|---|---|---|---|---|
| Size - case **A**: $\Phi_1$ | 4.162 | 4.162 | 12 | 6 | 1.33 | 2.5 | 2 | 2 | 2 |
| Size - case **B**: $\Phi_1+\Phi_2$ | 9.748 | 5.156 | 4 | 6 | 1.33 | 2.5 | 2 | 2 | 2 |
| Size & Shape - Case **A**: $\Phi_1$ | 4.399 | 4.399 | 10 | 7 | 1.33 | 1.59 | 1 | 1 | 5 |
| Size & Shape - Case **B**: $\Phi_1+\Phi_2$ | 10.082 | 4.889 | 5 | 7 | 1.33 | 1.72 | 1 | 1 | 5 |
| Size & Shape - Case **C**: $\Phi_1+\Phi_3$ | 6.148 | 4.224 | 11 | 5 | 1.33 | 1.81 | 1 | 1 | 3 |
| Size & Shape - Case **D**: $\Phi_1+\Phi_2+\Phi_3$ | 12.886 | 4.293 | 5 | 5 | 1.39 | 2.28 | 1 | 1 | 3 |
| Size, Shape & Topology: $\Phi_1+\Phi_2+\Phi_3$ | 12.429 | 4.363 | 5 | 4 | 1.7 | 2.38 | 1 | 1 | 2 |

Table 5.19: Results of the cases tested; in red the parameters fixed in the size analyses.

Due to the fact that the objective function are not comparable with one another, with the exception of the last two rows, we can analyze the resulting weights. The minimum value is obtained in the optimization denoted as 'Size - Case A: $\Phi_1$'. It is interesting the fact that it is associated with the highest number of different cross-sections used. On the contrary, the heavier design has been found for the analysis denoted as 'Size - Case B: $\Phi_1+\Phi_2$', where the second penalty function has been integrated. Once again, we should underline the fact that it is the case in which the lowest number of sections used has been employed. Therefore, we can observe that the complexity in terms of $N_a$ is the one that influence the most the weight of the optimized structure. On the other hand, we can also state that the third penalty function, thus the complexity in terms of number of subdivision, is working fine when combined with the first two. In fact, from 'Size & Shape - Case C: $\Phi_1+\Phi_3$'

and 'Size & Shape - Case D: $\Phi_1+\Phi_2+\Phi_3$', $n$ is stable at 5.

Another important observation is that, for the specific analysis considered with gravitational loads only, the optimized configuration is always characterized by $n_1 = n_2 = 1$. This means that the outer elements of each component have different sections, while the internal part is unifed with the same cross-section.

For future development in this field, it would be interesting to employ a different grouping division, thus using two different indexes, for each component. For sure this would increase the computational effort because the design variables associated to the indexes are going to pass from 2 to $N^o of component \cdot 2$. However, it could be useful to discriminate among the different components and to refine the analysis, in order to see how the solicitation distribution would be optimized.

# Chapter 6

# Case study 2 - Industrial building level

The analysis illustrated so far was limited to the level of the truss element, however our scope is to fit such theoretical procedure to a large scale structure. Due to the great employment of truss structures in industrial buildings, we have decided to explore this type of construction. Thus, in the present Chapter we are going to parametrically model and optimize the building under study, following the scheme of the previous case study. We are going to stress the main differences and analogies with the analysis at the truss level and how our objective function can work in a larger and more challenging environment.

## 6.1 Parametric modelling

Also in this instance we have exploited the power of parametric design to create the geometry of our structure using Grasshopper. In fact, the design is composed by a repetition of specific modules at a distance $s$, which stands for spacing, that will be an indirect variable of the problem. Specifically, our aim is to optimize the number of modules, which can be seen as the ratio of half the length and the spacing. Looking at the schematic representation of the overall geometry in figure 6.1, we can see that the modules consist of the truss system with the two columns at the outer sides. In particular, the truss system is the same of the previous case study, while the height of the columns has been set equal to 5 meters. Actually the external vertical structs of the truss are now removed and replaced by the column which rise up to the upper chord nodes.

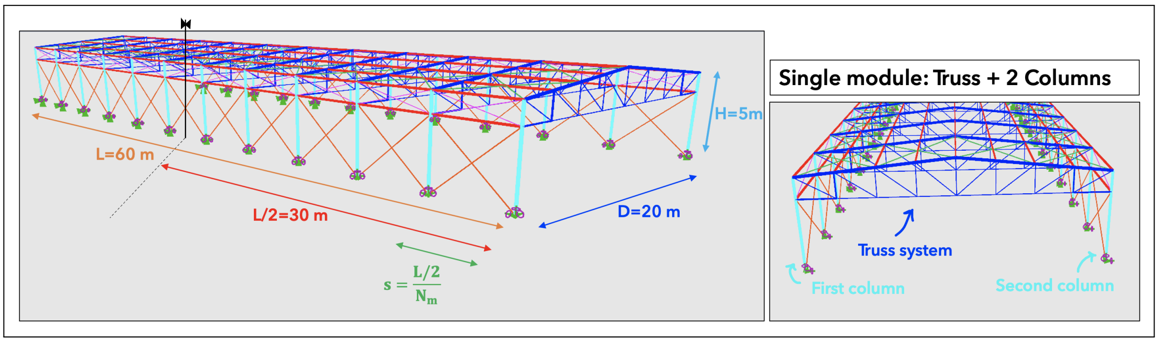


Figure 6.1: Industrial building general scheme with modules

Therefore, fixing the entire extent of the structure, which has been set equal to 60 meter, these modules can be denser or more widely spaced. Going into the details of the geometric modelling, we have started from the definition of the origin point in the middle of the structure, in order to take advantage of the symmetry with respect to the xz plane. Actually, we have the symmetry also with respect to the yz plane, however it cannot be exploited due to the presence of lateral load too. Hence, the geometry has been created in the first half, considering half portion of the entire horizontal development of 60 meters on the y-axis. Then, it has been mirrored with respect to xz plane. For this reason, the design variable related to the number of modules $N_m$ is referred to half geometry. Let's now focus on the actual model creation in Grasshopper. First of all, we should distinguish the main components of the industrial building:

- **Truss system**, distinguished in the five components seen in 4.4, i.e. Lower Chord, Upper Chord, Internal Vertical Structs, Upward-Downward Diagonals, Downward-Upward Diagonals;
- **Columns**;
- **Purlins or Secondary beams**;
- **Roof bracings**;
- **Vertical bracings type 1**, which are the upper ones;
- **Vertical bracings type 2**, the lower ones.

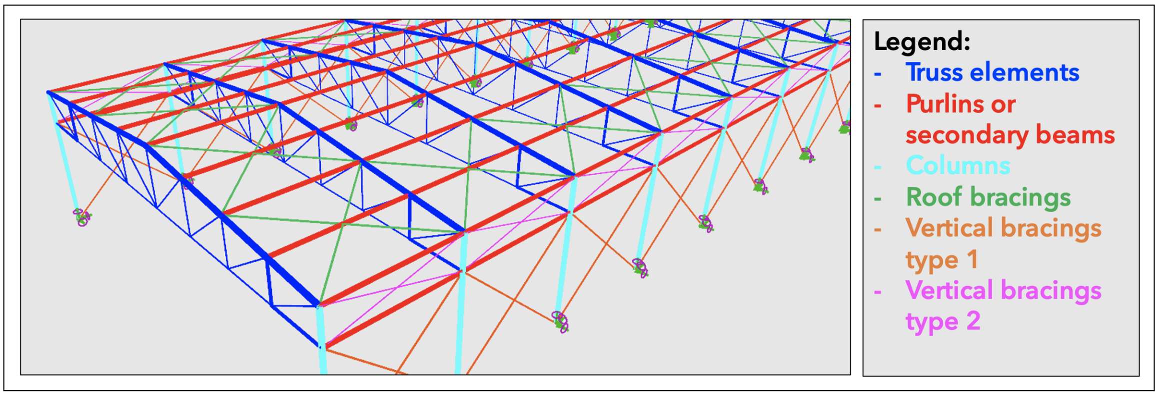


Figure 6.2: Industrial building's components

In the reported figure 6.2, we can easily recognize them thanks to the different colors used. Another important feature of the overall geometry is the presence of the symmetric scheme of the roof bracing systems, which are present at the edges of the structure and in the middle, regardless the spacing used. Hence, we have started the geometry by creating the first module, located at a distance of $s/2$ in y-direction from the origin. Then, to have a symmetric configuration of the roof bracings, we have imposed that in its half there will be at least two more modules. In this way we have fixed the lower bound of $N_m$ equal to 3, that in turn leads to a spacing value of 12 meters, according to the equations 6.1, 6.2 and 6.3. It has been found considering the following geometric relationships, represented graphically in figure 6.3.

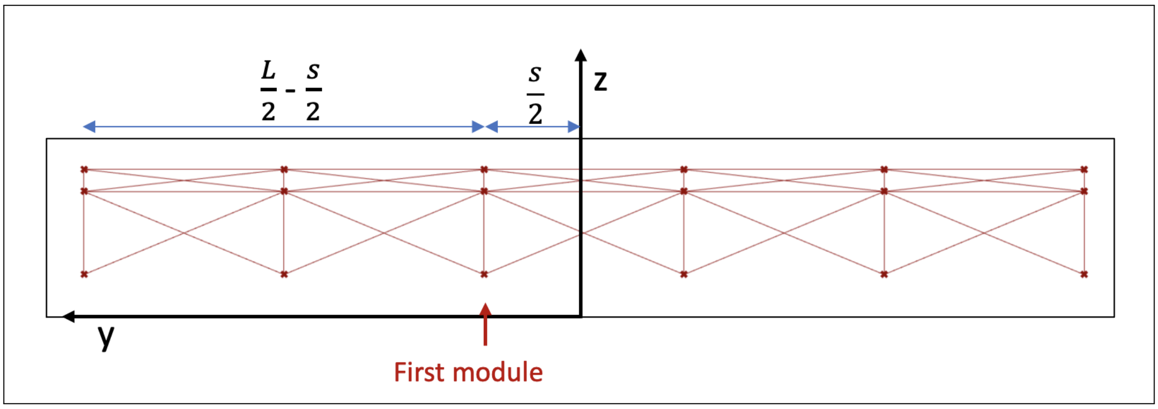


Figure 6.3: Geometrical relationships for $N_m$ domain definition

$$\frac{L}{2} - \frac{s}{2} = (N_m - 1) \cdot s \tag{6.1}$$

which leads to

$$N_m = \frac{\frac{L+s}{2}}{s} \tag{6.2}$$

and

$$s = \frac{\frac{L}{2}}{N_m - \frac{1}{2}} \tag{6.3}$$

Instead, the upper limit of $N_m$ has been set by imposing a minimum spacing of 4 meters, thus obtaining $N_{m,max} = 8$. In the reported figure 6.4, we can see how these extreme $N_m$ values influence the overall configuration.

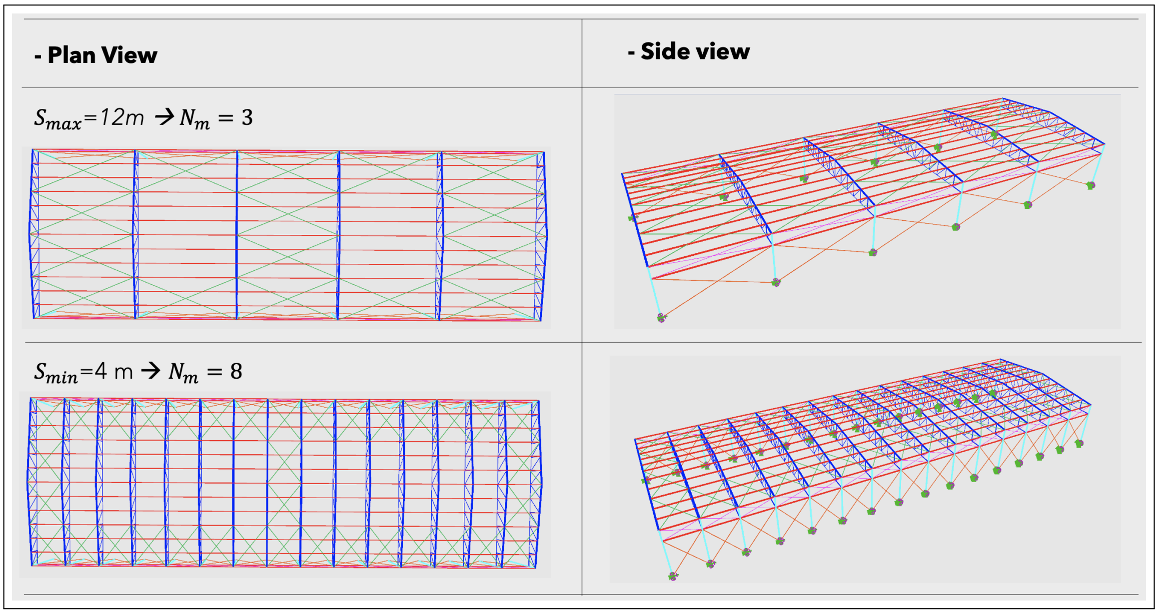


Figure 6.4: $N_m$ limiting configurations

The vertical bracings, both type 1 and 2, are covering the entire length in the y-direction. The roof bracing, instead, as said, are distributed symmetrically along the plan of the structure. However, it should be mentioned that, looking at their distribution with respect to the upper chord nodes, they will cover a span length of one quarter of the entire truss of 20 meters, no matter the value of $n$. It has been done to avoid the integration of the industrial building complexity, so their number will be fixed during the optimization. Then, for what regard the secondary beams, they are created by connecting the nodes of the upper chord from one module to the other. In this way the geometric modelling has been created.

### 6.1.1 Elements cross-section

Now, we have to transform it into actual beam elements, as we have done for the truss, using Karamba3D. Precisely, the grouping and cross-sections assignment of the truss system has been performed exactly as before. Instead, the other components have been simply assigned with specific cross-section profiles, namely:

- **Columns** → HEA section, which stands for European wide flange beam section;
- **Purlins** → IPE section, i.e. European I-section beam with parallel flanges;
- **Bracings** → ROPE sections

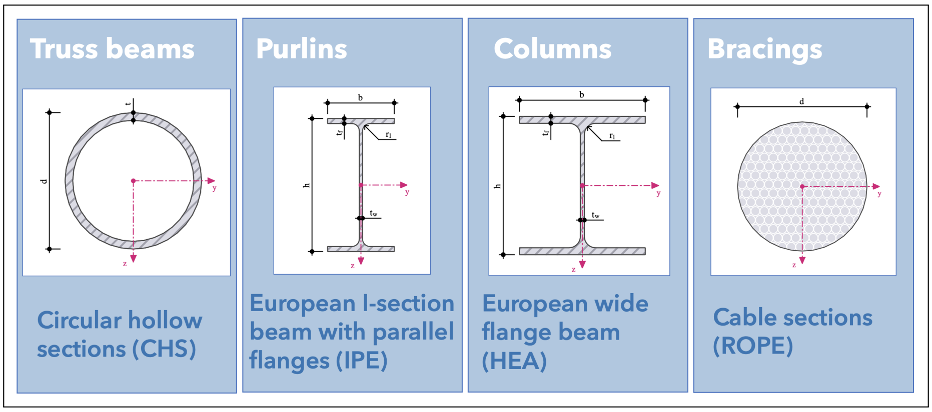


Figure 6.5: Industrial building's elements sections

### 6.1.2 Loads

In this section the loads applied to the large span building are evaluated and properly described. As said in chapter 4.5, Karamba 3D can consider only one combination of loads, therefore, also in this case, the Ultimate Limit State (ULS) analysis has been considered. In contrast to the case study at the truss level, where only gravity loads were applied to the structure, here both gravitational and horizontal loads were taken into consideration. Therefore, the following combination have been employed:

$$\gamma_{G1} \cdot G_1 + \gamma_{G2} \cdot G_2 + \gamma_P \cdot P + \gamma_{Q1} \cdot Q_{k1} + \gamma_{Q2} \cdot \psi_{02} \cdot Q_{k2} + \gamma_{Q3} \cdot \psi_{03} \cdot Q_{k3} + ... \quad (6.4)$$

- **Gravity loads**

  Regarding the gravitational loadings, the following ones have been evaluated:

1. **Permanent Structural, or Dead, Load** $(G_1)$

   The Dead Load is simply the self-weight of all the components of the structure. In Karamba3D it is computed automatically, so we have simply applied the coefficient of the load combination considered.

2. **Permanent Non-Structural Load** $(G_2)$

   The Permanent Non-Structural Load, i.e. $G_2$, is referred to the corrugated sheet, which is the material used to cover the roof of the building. In particular, it is useful to distribute loads on bottom purlins.

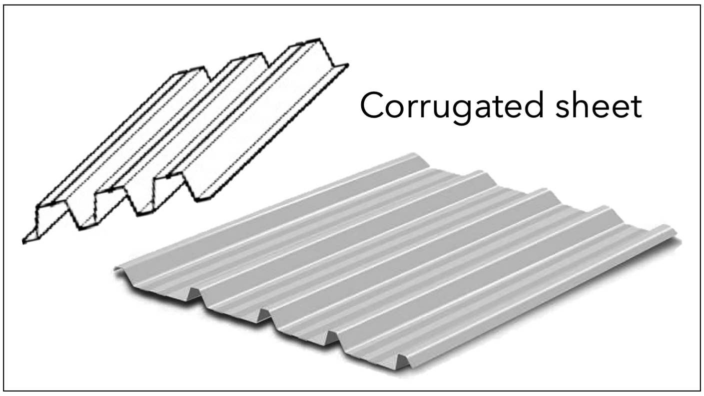


Figure 6.6: Corrugated sheet

   The standard load considered for the corrugated sheet is $0.05 kN/m^2$, which has to be multiplied by the length of influence. The evaluation of the area of influence will be depicted at the end on this section.

3. **Maintenance Load** $(q_k)$

   In order to define the value of $q_k$ we should refer to the indications provided by the Eurocode. In particular, the roof of our building, where the loads is going to be applied, belongs to the category H. Specifically, this category is referred to the covers accessible only for maintenance, which match with our case study. The value recommend by the Eurocode is $q_k = 0.4\frac{KN}{m^2}$, however, the Code specifies that it can be changed, according to the National Annex. Due to the fact that we are assuming the location of our building in Turin (Italy), the National Code we need to refer to is "Norme tecniche per le costruzioni" (NTC2018). Looking at the chapter 3.1 "Opere civili e industriali" and specifically the sub-section 3.1.4 "Sovraccarichi" from table 3.1.II in figure 6.7, the correct value is $q_k = 0.5\frac{KN}{m^2}$.

**Tabella 3.1.II** – *Valori dei carichi d'esercizio per le diverse categorie di edifici*

| Cat. | Ambienti | $q_k$ [kN/m$^2$] | $Q_k$ [kN] | $H_k$ [kN/m] |
|---|---|---|---|---|
| A | **Ambienti ad uso residenziale.** Sono compresi in questa categoria i locali di abitazione e relativi servizi, gli alberghi. (ad esclusione delle aree suscettibili di affollamento) | 2,00 | 2,00 | 1,00 |
| B | **Uffici.** | | | |
| | Cat. B1 Uffici non aperti al pubblico | 2,00 | 2,00 | 1,00 |
| | Cat. B2 Uffici aperti al pubblico | 3,00 | 2,00 | 1,00 |
| C | **Ambienti suscettibili di affollamento** | | | |
| | Cat. C1 Ospedali, ristoranti, caffè, banche, scuole | 3,00 | 2,00 | 1,00 |
| | Cat. C2 Balconi, ballatoi e scale comuni, sale convegni, cinema, teatri, chiese, tribune con posti fissi | 4,00 | 4,00 | 2,00 |
| | Cat. C3 Ambienti privi di ostacoli per il libero movimento delle persone, quali musei, sale per esposizioni, stazioni ferroviarie, sale da ballo, palestre, tribune libere, edifici per eventi pubblici, sale da concerto, palazzetti per lo sport e relative tribune | 5,00 | 5,00 | 3,00 |
| D | **Ambienti ad uso commerciale.** | | | |
| | Cat. D1 Negozi | 4,00 | 4,00 | 2,00 |
| | Cat. D2 Centri commerciali, mercati, grandi magazzini, librerie… | 5,00 | 5,00 | 2,00 |
| E | **Biblioteche, archivi, magazzini e ambienti ad uso industriale.** | | | |
| | Cat. E1 Biblioteche, archivi, magazzini, depositi, laboratori manifatturieri | ≥ 6,00 | 6,00 | 1,00* |
| | Cat. E2 Ambienti ad uso industriale, da valutarsi caso per caso | — | — | — |
| F-G | **Rimesse e parcheggi.** | | | |
| | Cat. F Rimesse e parcheggi per il transito di automezzi di peso a pieno carico fino a 30 kN | 2,50 | 2 x 10,00 | 1,00** |
| | Cat. G Rimesse e parcheggi per transito di automezzi di peso a pieno carico superiore a 30 kN: da valutarsi caso per caso | — | — | — |
| H | **Coperture e sottotetti** | | | |
| | Cat. H1 Coperture e sottotetti accessibili per sola manutenzione | 0,50 | 1,20 | 1,00 |
| | Cat. H2 Coperture praticabili | secondo categoria di appartenenza | | |
| | Cat. H3 Coperture speciali (impianti, eliporti, altri) da valutarsi caso per caso | — | — | — |

Figure 6.7: Table 3.1.II of NTC2018 to define the load $q_k$

4. **Snow Load** ($q_s$)

Based on the building's position, the snow load is assessed and, as it was previously said, Turin's location has been taken into account. The general formulation for the snow pressure, according to the Eurocode, is:

$$q_s = q_{sk} \cdot \mu_i \cdot C_E \cdot C_T \tag{6.5}$$

Where:

- $q_{sk}$ is the characteristic value of the snow load on the ground. In order to determine its value, we should refer to the national annex NTC2018. It depends on climate conditions and local exposure of the zone considered and it is correlated with the altitude. It can be computed according to the equation $q_{sk} = 1.39 \cdot (1 + (\frac{a_s}{728})^2)$, where $a_s$ is the elevation above sea level. Specifically, Turin is at 239 meters above the sea level, thus we obtain a value of $q_{sk} = 1.539 \frac{KN}{m^2}$.
- $\mu_i$ is a shape coefficient related to the inclination of the roof. It varies according to the reported table 6.1:

| Shape coefficient | $0° \leq \alpha \leq 30°$ | $30° \leq \alpha \leq 60°$ | $\alpha \geq 60°$ |
|---|---|---|---|
| $\mu_1$ | 0.8 | $0.8 \cdot \frac{(60-\alpha)}{30}$ | 0.0 |

Table 6.1: Values of shape coefficient $\mu_i$ based on the inclination of the roof

In our building the inclination of the roof is lower than 30°, therefore $\mu_i = 0.8$.

- $C_E$ is the exposure coefficient and it is always related to the zone where the building is located. For our case, a value equal to 1 is assigned, due to the fact that there is not a significant removal of snow on building produced by the wind.
- $C_T$ is the thermal coefficient and it is usually assumed equal to 1.

The final value of the snow load is: $q_s = 1.23\frac{KN}{m^2}$

Before going into the details of the other class of actions considered, i.e. the lateral ones, we would like to explain how the above mentioned vertical actions have been applied. With the exception of the Dead Load $G_1$, that is automatically considered by the software, for the other ones, the area of influence of such loads has to be identified. $G_2$, $q_k$, as well as $q_s$ are applied on the purlins and their area of influence is a function of their relative distance. In the following figure 6.8, a schematic representation is reported.

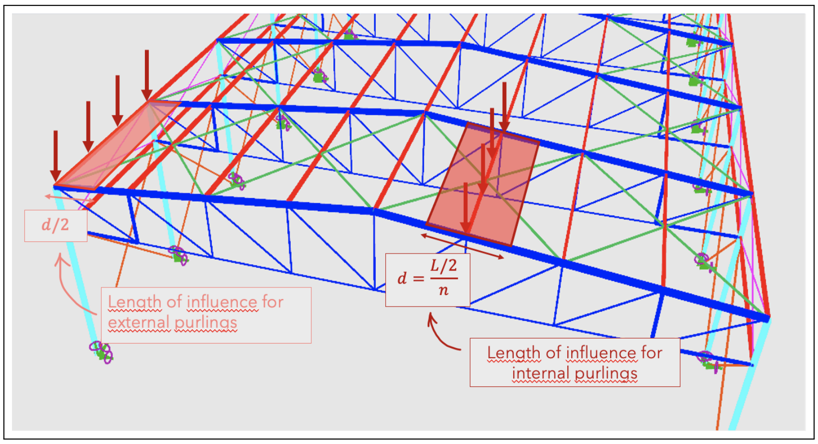


Figure 6.8: Lenght of influence for internal and external purlins

As we can see, there is a difference between the length of influence for internal and external purlins, which are both function of the distance between the upper chord's node. Specifically, the values considered in our analysis are function of the design variable $n$. Finally, the unitary length loads to be applied on the purlins are computed as the just explained pressure values, multiplied by the length of influence, resulting in $kN/m$.

- **Lateral loads**

1. **Wind Load (p)**

   Wind is the movement of air masses characterised by a velocity field that fluctuates randomly in time and space. It exerts aerodynamic actions on whole structures or on individual structural components. Wind load act as a lateral pressure on the external surface of the large span building. As said for the other loads, Eurocode suggests to refer to the National Annex to determine wind pressure.

   Referring to the chapter 3.3 of NTC2018, the pressure exerted by the wind is:

$$p = q_b \cdot c_e \cdot c_p \cdot c_d \tag{6.6}$$

   Where:

   – $q_b$ is the reference kinethic pressure evaluated as:

$$q_b = \frac{1}{2} \cdot \rho \cdot v_b^2 \tag{6.7}$$

   Specifically, $\rho$ is the air density equal to $1.25 \frac{kg}{m^3}$, while $v_b$ is the wind velocity and it depends on the location of the building. NTC2018 in the section 3.3.1 provides the table illustrated in figure 6.9 with the values of $v_b$:

| Zone | Description | $v_{b,0}$[m/s] | $a_0$[m] | $k_a$[1/s] |
|---|---|---|---|---|
| 1 | Valle d'Aosta, Piedmont, Lombardy, Trentino Alto Adige, Veneto, Friuli Venezia Giulia (excluding the province of Trieste) | 25 | 1000 | 0.010 |
| 2 | Emilia Romagna | 25 | 750 | 0.015 |
| 3 | Tuscany, Marche, Umbria, Lazio, Abruzzo, Molise, Puglia, Campania, Basilicata, Calabria, (excluding the province of Reggio Calabria) | 27 | 500 | 0.020 |
| 4 | Sicilia e provincia Reggio Calabria | 28 | 500 | 0.020 |
| 5 | Sardinia (east of the straight-line connecting Cape Teulada with the island of Maddalena) | 28 | 750 | 0.015 |
| 6 | Sardinia (area to the west of the straight-line connecting Cape Teulada with the island of Maddalena) | 28 | 500 | 0.020 |
| 7 | Liguria | 28 | 1000 | 0.015 |
| 8 | Province of Trieste | 30 | 1500 | 0.010 |
| 9 | Islands (with the exception of Sicily and Sardinia) and open sea | 31 | 500 | 0.020 |

Figure 6.9: Table 3.3.I of NTC2018 to define the $v_b$, $a_0$ and $k_a$

   Turin is in zone 1 so the final value of $q_b$ is $0.391 \frac{KN}{m^2}$ according to equation 6.7.

– $C_e$ is the exposure coefficient, which has the following expression:

$$c_e(z) = k_r^2 \cdot c_t \cdot ln(\frac{z}{z_0}) \cdot [7 + c_t \cdot ln(\frac{z}{z_0})] \quad for \quad z \geq z_{min} \tag{6.8}$$

$$c_e(z) = c_e(z_{min}) \quad for \quad z < z_{min} \tag{6.9}$$

In particular $k_r$ is the class of roughness and we need to refer to table 3.3.III of NTC2018 reported in figure 6.10.

**Tab. 3.3.III** - *Classi di rugosità del terreno*

| Classe di rugosità del terreno | Descrizione |
|---|---|
| A | Aree urbane in cui almeno il 15% della superficie sia coperto da edifici la cui altezza media superi i 15 m |
| B | Aree urbane (non di classe A), suburbane, industriali e boschive |
| C | Aree con ostacoli diffusi (alberi, case, muri, recinzioni,....); aree con rugosità non riconducibile alle classi A, B, D |
| D | a) Mare e relativa fascia costiera (entro 2 km dalla costa); b) Lago (con larghezza massima pari ad almeno 1 km) e relativa fascia costiera (entro 1 km dalla costa) c) Aree prive di ostacoli o con al più rari ostacoli isolati (aperta campagna, aeroporti, aree agricole, pascoli, zone paludose o sabbiose, superfici innevate o ghiacciate, ....) |

Figure 6.10: Table 3.3.III of NTC2018 to define the class of roughness

Due to the fact that our structure is an industrial building, a class of roughness 'B' is assigned.

The next step concerns the definition of the exposure category, referring to the table shown in figure 6.11 provided by the National code.

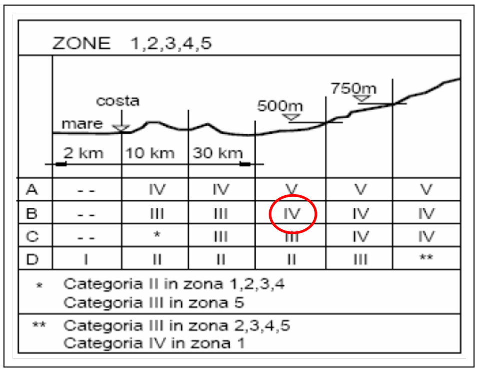


| | | | | | | |
|---|---|---|---|---|---|---|
| A | - - | IV | IV | V | V | V |
| B | - - | III | III | IV | IV | IV |
| C | - - | * | III | III | IV | IV |
| D | I | II | II | II | III | ** |

* Categoria II in zona 1,2,3,4
Categoria III in zona 5

** Categoria III in zona 2,3,4,5
Categoria IV in zona 1

Figure 6.11: Table 3.3.III of NTC2018 to define the exposure coefficient

For our case study the exposure coefficient is IV.

Finally, from table 3.3.II of NTC2018 6.12, based on the site exposure coefficient (IV) previosuly evaluated, all the terms contained in equation 6.8 can be determined.

| Site exposure category | $k_r$ | $z_0$ [m] | $z_{min}$ [m] |
|---|---|---|---|
| I | 0,17 | 0,01 | 2 |
| II | 0,19 | 0,05 | 4 |
| III | 0,20 | 0,10 | 5 |
| IV | 0,22 | 0,30 | 8 |
| V | 0,23 | 0,70 | 12 |

Figure 6.12: Table 3.3.II of NTC2018 to define $k_r$, $z_0$ and $z_{min}$

The final value of $c_e$ is 1.55 .

- $c_p$ is the shape coefficient, which is related to the inclination of the roof $\alpha$. The image below 6.13 illustrates how the coefficient should be considered in the evaluation of the wind pressure acting on the different structural elements, according to the Code.

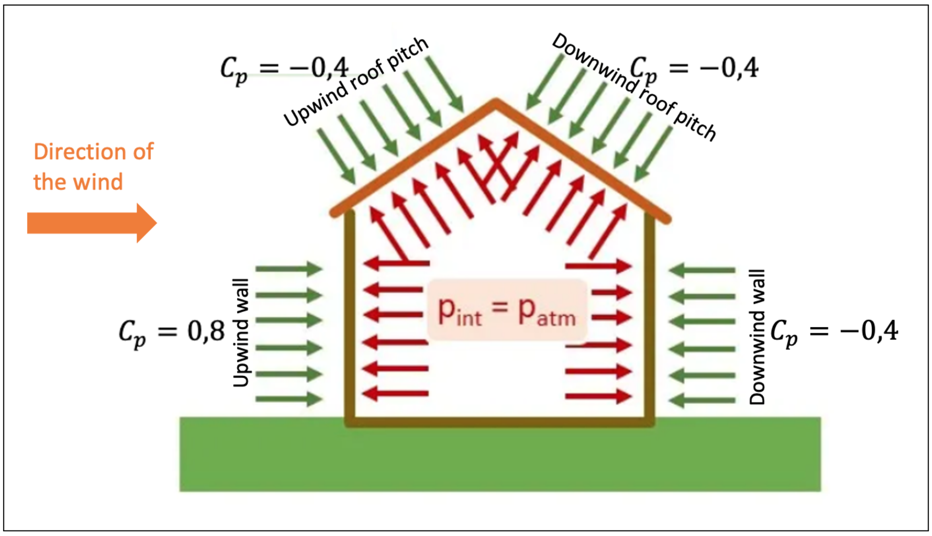


Figure 6.13: Values of shape coefficient $c_p$

- $c_d$ is the dynamic coefficient, which is generally set equal to 1 in buildings with an height lower than 80 meters.

Once $v_b$, $c_t$, $c_p$ and $c_e$ have been properly defined, the final wind pressure acting on the large span building is given. The following table 6.2 contains the values of the wind pressures $p$, evaluated according to the equation 6.6:

| | $c_p$ | $p[\frac{KN}{m^2}]$ |
|---|---|---|
| **Upwind wall** | 0.8 | 0.48 |
| **Downwind wall** | -0.4 | -0.24 |
| **Upwind roof pitch** | -0.4 | -0.24 |
| **Downwind roof pitch** | -0.4 | -0.24 |

Table 6.2: Wind pressure $p$ values for the different $c_pe$

It's important to clarify that we have taken into account only the external pressure caused by the wind. This is due to the assumption that the building has no openings and it can be considered as an airtight construction, 'costruzione stagna', according to NTC2018. Nevertheless, if we would like to consider any openings, it would be necessary to consider the coefficient $c_{pi}$ referred to an internal pressure. Specifically, the value of $c_{pi}$ will vary based on the area covered by the openings; for example if less than 1\3 of the total area, a value of $c_{pi} = \pm 0.2$ should be considered. As illustrated in figure 6.13, the internal pressure is represented by the red arrows and is going to act in the opposite way with respect the external one.
Regarding the application of the wind load, as already discussed for the vertical actions, a correct area of influence should be properly defined. Particularly, wind pressure has been applied only to purlins, normal to their development considering the same scheme shown in figure 6.8, while for columns, along x-direction, as illustrated in the following figure 6.14:

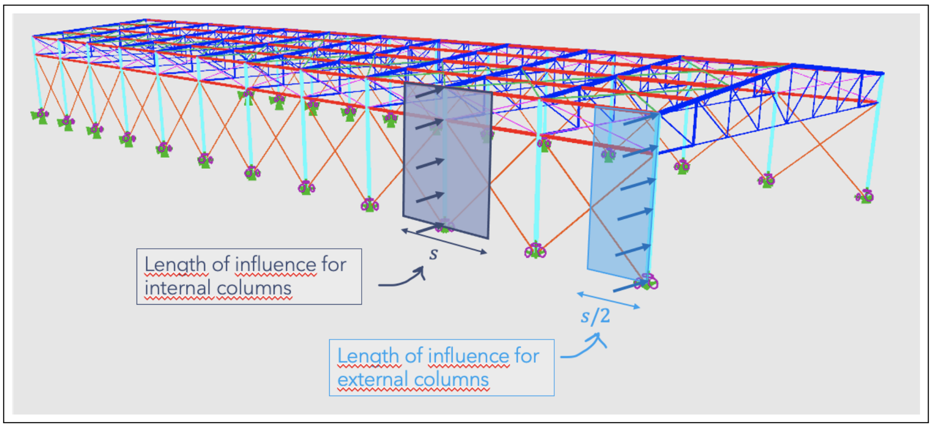


Figure 6.14: Lenght of influence for internal and external columns

Once all the loads, both vertical and horizontal, are properly evaluated, the next step is to assign the coefficients of the load combination to each of them.
Unfortunately there is only one load combination that can be defined in Karamba 3D, therefore we have considered the heaviest one. In particular, we have chosen as dominant variable load the Maintenance Load $q_k$ in order to be able to maximize the bending moment. In turn, the Snow load and the Wind action have been accounted as secondary variable loads with the proper $\psi_{0j}$ coefficient. Referring to the ULS equation 6.4 and tables 2.5.I, 2.6.I of NTC2018 in figure 6.15 provided by the national annex NTC2018, the following coefficients have been applied, as reported in table 6.3:

**Tab. 2.6.I** – *Coefficienti parziali per le azioni o per l'effetto delle azioni nelle verifiche SLU*

| | | Coefficiente $\gamma_F$ | EQU | A1 | A2 |
|---|---|---|---|---|---|
| Carichi permanenti $G_1$ | Favorevoli | $\gamma_{G1}$ | 0,9 | 1,0 | 1,0 |
| | Sfavorevoli | | 1,1 | 1,3 | 1,0 |
| Carichi permanenti non strutturali $G_2$[(1)] | Favorevoli | $\gamma_{G2}$ | 0,8 | 0,8 | 0,8 |
| | Sfavorevoli | | 1,5 | 1,5 | 1,3 |
| Azioni variabili Q | Favorevoli | $\gamma_{Qi}$ | 0,0 | 0,0 | 0,0 |
| | Sfavorevoli | | 1,5 | 1,5 | 1,3 |

[(1)] Nel caso in cui l'intensità dei carichi permanenti non strutturali o di una parte di essi (ad es. carichi permanenti portati) sia ben definita in fase di progetto, per detti carichi o per la parte di essi nota si potranno adottare gli stessi coefficienti parziali validi per le azioni permanenti.

**Tab. 2.5.I** – *Valori dei coefficienti di combinazione*

| Categoria/Azione variabile | $\psi_{0j}$ | $\psi_{1j}$ | $\psi_{2j}$ |
|---|---|---|---|
| Categoria H - Coperture accessibili per sola manutenzione | 0,0 | 0,0 | 0,0 |
| Categoria I – Coperture praticabili | da valutarsi caso per caso | | |
| Categoria K – Coperture per usi speciali (impianti, eliporti, ...) | | | |
| Vento | 0,6 | 0,2 | 0,0 |
| Neve (a quota ≤ 1000 m s.l.m.) | 0,5 | 0,2 | 0,0 |
| Neve (a quota > 1000 m s.l.m.) | 0,7 | 0,5 | 0,2 |
| Variazioni termiche | 0,6 | 0,5 | 0,0 |

Figure 6.15: Table 2.6.I and 2.5.I of NTC2018 to define the load's coefficient

| Load Type | Load Name | Load Value $[\frac{KN}{m^2}]$ | $\gamma$ | $\psi$ |
|---|---|---|---|---|
| Dead Load | G1 | Structure weigth | 1.3 | - |
| Perm. Non-struct. Load | G2 | 0.05 | 1.5 | - |
| Maintanance Load | $q_k$ | 0.5 | 1.5 | - |
| Snow Load | $q_s$ | 1.23 | 1.5 | 0.5 |
| Wind Load | $p$ | Depends on $c_p$ | 1.5 | 0.6 |

Table 6.3: Summary of loads applied to the building and their relative value and coefficient

### 6.1.3 Supports

Both internal and external constraints have been utilized for the large span construction. Specifically, the base points of the columns were fixed to the ground, preventing any translational and rotational motions. Regarding the internal ones, Karamba 3D automatically applies rigid links between all the structural elements.

## 6.2 Objective Function Formulation

The optimization carried out for the industrial building application takes its origin from the formulation of the simple truss, which has been slightly modified to better fit this case study. First of all, we should start by the definition of the design variables involved. In fact, with respect to the previous ones, reported in table 4.3, six additional design variables have been introduced. Specifically, the cross-sections of the structural members added, i.e. columns, purlins and bracings, distinguished into 1 roof bracing and 2 types of vertical ones, have been integrated with the former size variables of the truss. Moreover, a shape design variable related to the spatial configuration of the structure has been added, namely the number of modules of one half ($N_m$). The final number of design variable considered is 27 and the additional ones are summarized in table 6.4.

| **Design variable** | **Description** | **Domain** |
|---|---|---|
| $x_{22}$ | Numbers of modules in one half | $3 \div 8$ |
| $x_{23}$ | Column HEA cross-section | $0 \div 23$ profiles' index from catalogue |
| $x_{24}$ | Purlin IPE cross-section | $0 \div 17$ profiles' index from catalogue |
| $x_{25}$ | Roof bracing ROPE PV cross-section | $0 \div 24$ profiles' index from catalogue |
| $x_{26}$ | Vertical bracing type 1 ROPE PV cross-section | $0 \div 24$ profiles' index from catalogue |
| $x_{27}$ | Vertical bracing type 1 ROPE PV cross-section | $0 \div 24$ profiles' index from catalogue |

Table 6.4: Design variables where the colors of the cells represent the different categories: purple - Global layout definition; orange - Additional size design variables

Once clarified all the parameters involved in the optimization, it can be easier to understand the aim of this analysis. In fact, the simultaneous size, shape and topology optimization of the truss, composing the modules of the industrial building, will be carried out, in parallel with the size and shape optimization at the larger scale. The cross-sections of the additional elements are going to be minimized, still satisfying the structural verification, while the spacing between the modules is going to be adjusted at each iteration. To be more clear, the shape optimization at the industrial building level is going to be performed only varying the number of modules present.

Focusing on the Objective Function formulation, it is the same as the one used for the analysis on the truss structure, explained in section 4.6 with the equation 4.2:

$$min\ F(\mathbf{x}) = \rho \sum_{i=1}^{N} (A_i \cdot l_i) \cdot \phi_1(n_{un}) \cdot \phi_2(N_a) \cdot \phi_3(n)$$

While the first penalty related to buckling instability verification is now enlarged to all the elements, the other two penalties regarding the design simplification are not working in the general framework. In fact, the constructability criteria embedded in $\phi_2$ and $\phi_3$ are going to act only on the truss components and, in particular, to the number of sections used ($N_a$) and to the number of subdivisions of the chords ($n$), respectively. In this way the complexity is going to be studied only at the truss level, making it possible to analyse the validity of the previous considerations. As a result, we can effectively appreciate the discoveries of the truss level optimization of Chapter 4, in a more challenging scenario. In particular, this is the reason why we have fixed the number of roof bracings regardless $n$, in order to avoid a higher complexity.

## 6.3 Results - Industrial building level

In this section the results of the industrial building optimizations have been summarized. The analysis has been performed 15 times in order to obtain more refined results and to test how the algorithm works in this second case study. In the following table 6.5, the results are sorted from the smallest to the largest in terms of best objective function.

| **Best OF** | **Weight [kN]** | $N_a$ | $n$ | $H_1$ | $H_2$ | $n_1$ | $n_2$ | $n_3$ | $N_m$ | **Topology** |
|---|---|---|---|---|---|---|---|---|---|---|
| 775,427 | 330,228 | 3 | 4 | 2 | 2,17 | 1 | 1 | 1 | 7 | HOWE |
| 790,020 | 336,442 | 3 | 4 | 2 | 2 | 1 | 1 | 1 | 7 | HOWE |
| 885,230 | 339,024 | 4 | 4 | 2 | 2 | 2 | 1 | 1 | 7 | HOWE |
| 888,228 | 340,172 | 4 | 4 | 1,99 | 2,07 | 1 | 1 | 1 | 7 | HOWE |
| 894,320 | 342,505 | 4 | 4 | 1,99 | 2,01 | 1 | 1 | 1 | 7 | HOWE |
| 932,095 | 396,947 | 3 | 4 | 1,94 | 2,01 | 2 | 1 | 1 | 6 | WARREN |
| 937,174 | 399,110 | 3 | 4 | 2 | 2,43 | 1 | 1 | 1 | 6 | HOWE |
| 964,094 | 369,228 | 4 | 4 | 1,54 | 1,64 | 1 | 1 | 1 | 7 | HOWE |
| 967,429 | 370,505 | 4 | 4 | 1,67 | 1,67 | 2 | 1 | 1 | 6 | HOWE |
| 974,337 | 341,988 | 5 | 4 | 2 | 2,1 | 2 | 1 | 1 | 7 | HOWE |
| 983,096 | 376,505 | 4 | 4 | 1,97 | 1,99 | 1 | 1 | 1 | 8 | PRATT |
| 1014,911 | 356,229 | 5 | 4 | 1,68 | 1,87 | 1 | 2 | 1 | 8 | HOWE |
| 1023,262 | 391,888 | 4 | 4 | 2 | 2,31 | 1 | 2 | 1 | 7 | WARREN |
| 1036,499 | 396,957 | 4 | 4 | 2 | 2 | 1 | 2 | 1 | 7 | PRATT |
| 1042,326 | 399,189 | 4 | 4 | 1,96 | 2,16 | 1 | 1 | 1 | 6 | PRATT |

Table 6.5: Results of the best individual of each optimization for the Industrial building

Analyzing the results, several considerations can be drawn. First of all, focusing on the last column 'Topology', the variability in the optimal solution can be highlighted. In fact, the Howe truss is the most chosen one, however sometimes the optimizer prefers also Pratt and Warren. Due to that, we have distinguished the results for the different typology, i.e. Howe 6.6, Warren 6.8 and Pratt 6.10. We should recall the fact that, because of the limit to only one load combination imposed by Karamba3D, we have been able to apply the wind action only from left to right. Therefore, this has influenced the final configuration of the truss systems.
Here below the results of the optimizations with Howe truss as optimal solution are reported in table 6.6.

| Best OF | Weight [kN] | $N_a$ | $n$ | $H_1$ | $H_2$ | $n_1$ | $n_2$ | $n_3$ | $N_m$ | Topology |
|---|---|---|---|---|---|---|---|---|---|---|
| 775,427 | 330,228 | 3 | 4 | 2 | 2,17 | 1 | 1 | 2 | 7 | HOWE |
| 790,02 | 336,442 | 3 | 4 | 2 | 2 | 1 | 1 | 2 | 7 | HOWE |
| 885,23 | 339,024 | 4 | 4 | 2 | 2 | 2 | 1 | 1 | 7 | HOWE |
| 888,228 | 340,172 | 4 | 4 | 1,99 | 2,07 | 1 | 1 | 2 | 7 | HOWE |
| 894,32 | 342,505 | 4 | 4 | 1,99 | 2,01 | 1 | 1 | 2 | 7 | HOWE |
| 937,174 | 399,11 | 3 | 4 | 2 | 2,43 | 1 | 1 | 2 | 6 | HOWE |
| 964,094 | 369,228 | 4 | 4 | 1,54 | 1,64 | 1 | 1 | 2 | 7 | HOWE |
| 967,429 | 370,505 | 4 | 4 | 1,67 | 1,67 | 2 | 1 | 1 | 6 | HOWE |
| 974,337 | 341,988 | 5 | 4 | 2 | 2,1 | 2 | 1 | 1 | 7 | HOWE |
| 1014,911 | 356,229 | 5 | 4 | 1,68 | 1,87 | 1 | 2 | 1 | 8 | HOWE |

Table 6.6: Results of the best individual for Industrial building with Howe truss

In the table below 6.7 also the Best, Worst and Mean values, as well Standard Devation of the OF are reported. Specifically, the best value is related to the minimum OF value, while the worst to the maximum one.

| Best | Worst | Mean | Standard Deviation |
|---|---|---|---|
| 775.427 | 1014.911 | 909.117 | 78.83 |

Table 6.7: Best, Worst, Mean and Standard deviation related to the OF values of the optimized Industrial building with Howe truss

Focusing on the best optimized individuals with Howe truss and referring to table 6.6, there is still some variability in the results and this is mainly due to the high number of design variables that the optimizer have to manage.

More in detail starting from the OF values the minimum one is obtained reducing the complexity at truss level, as expected. In fact lowering the values of $N_a$ and $n$ the best individual is found. However, regarding $N_a$, looking at all the results, there isn't a clear trend, in fact it varies from 3 to 5. On the contrary, the number of subdivisions $n$ is stable at 4. About weight values of the optimized individuals, a narrow range of results can be observed, in fact it fluctuates between $330KN$ and $356KN$. With respect to the case study 1, in which the weight increased when $N_a$ and $n$ decreased, here the total weight of the structure cannot be directly related to the complexity of truss structure. As a matter of fact, now there are many other structural elements that contribute to the weight final value.

Moving to the column of the table referred to the values of $N_m$, the number of modules, and keeping in mind that it ranges between 3 and 8, we can state that the

optimizer mainly prefers to work with more modules, from 6 to 8. This choice is justified by the fact that if the spacing is widened, resulting in a lower $N_m$ value, heavier section are necessary. Furthermore, the algorithm is not directly guided in the selection of $N_m$.
Regarding the geometric layout, i.e. $H_1$ and $H_2$ values, there is almost a clear trend. Specifically, fixing $n = 4$, the allowable ranges for the two parameter are $1.44 < H_1 < 2$ and $H_1 < H_2 < 2.5$. Looking at the results, we can see that the values assigned to the optimized structures vary in these limits: $1.54 < H_1 < 2$ and $1.64 < H_2 < 2.43$.
A final consideration can be made about the values assigned to the index $n_i$ in the definition of the grouping. Index $n_2$ is almost fixed at 1, with the exception of the last best individual that is also the worst in our set. Instead, $n_1$ and $n_3$ vary between 1 and 2. Perhaps if we could perform a higher number of analysis it would be possible to establish a more stable trend.
Here below the tables summarizing the results of the remaining typologies, i.e. Warren and Pratt ones, have been reported.

| **Best OF** | **Weight [kN]** | $N_a$ | $n$ | $H_1$ | $H_2$ | $n_1$ | $n_2$ | $n_3$ | $N_m$ | **Topology** |
|---|---|---|---|---|---|---|---|---|---|---|
| 932,095 | 396,947 | 3 | 4 | 1,94 | 2,01 | 2 | 1 | 1 | 6 | WARREN |
| 1023,262 | 391,888 | 4 | 4 | 2 | 2,31 | 1 | 2 | 1 | 7 | WARREN |

Table 6.8: Results of the best individual for Industrial building with Warren truss

| **Best** | **Worst** | **Mean** | **Standard Deviation** |
|---|---|---|---|
| 932,095 | 1023,262 | 932,095 | 63,008 |

Table 6.9: Best, Worst, Mean and Standard deviation related to the OF values of Industrial building with Warren truss

The Warren truss has been chosen only twice out of the 15 optimizations, therefore we cannot make an analysis as detailed as the one referred to the Howe truss. However, looking at tables 6.8 and 6.9, first of all, we can say that the best objective function value is much higher than the best of the Howe configuration. It is interesting the fact that also in this case $n$ is always stable at 4, proving that the penalty $\Phi_3$ is guiding effectively the algorithm. All the other parameters are different in the two individuals, but recall a little bit the values of the Howe case.

| **Best OF** | **Weight [kN]** | $N_a$ | $n$ | $H_1$ | $H_2$ | $n_1$ | $n_2$ | $n_3$ | $N_m$ | **Topology** |
|---|---|---|---|---|---|---|---|---|---|---|
| 983,096 | 376,505 | 4 | 4 | 1,97 | 1,99 | 1 | 1 | 2 | 8 | PRATT |
| 1036,499 | 396,957 | 4 | 4 | 2 | 2 | 1 | 2 | 1 | 7 | PRATT |
| 1042,326 | 399,189 | 4 | 4 | 1,96 | 2,16 | 1 | 1 | 2 | 6 | PRATT |

Table 6.10: Results of the best individual for Industrial building with Pratt truss

| **Best** | **Worst** | **Mean** | **Standard Deviation** |
|---|---|---|---|
| 983,096 | 1042,326 | 1020,640 | 32,644 |

Table 6.11: Best, Worst, Mean and Standard deviation related to the OF values of Industrial building with Pratt truss

Looking at the Pratt optimized trusses, we have now three individuals out of the total 15 ones. The best OF is in between the two previously analyzed cases, however the difference with the Howe case is significant. In this case, both $N_a$ and $n$ are fixed at the same value in all the three optimized structures, while a variability in all the other parameter is visible.
Once all the outcomes have been introduced and examined, let's now focus on the best individual among the 15 analysis summarized in table 6.5.
The resulting best industrial building is characterized by truss systems belonging to the Howe category and the overall configuration is the following one:

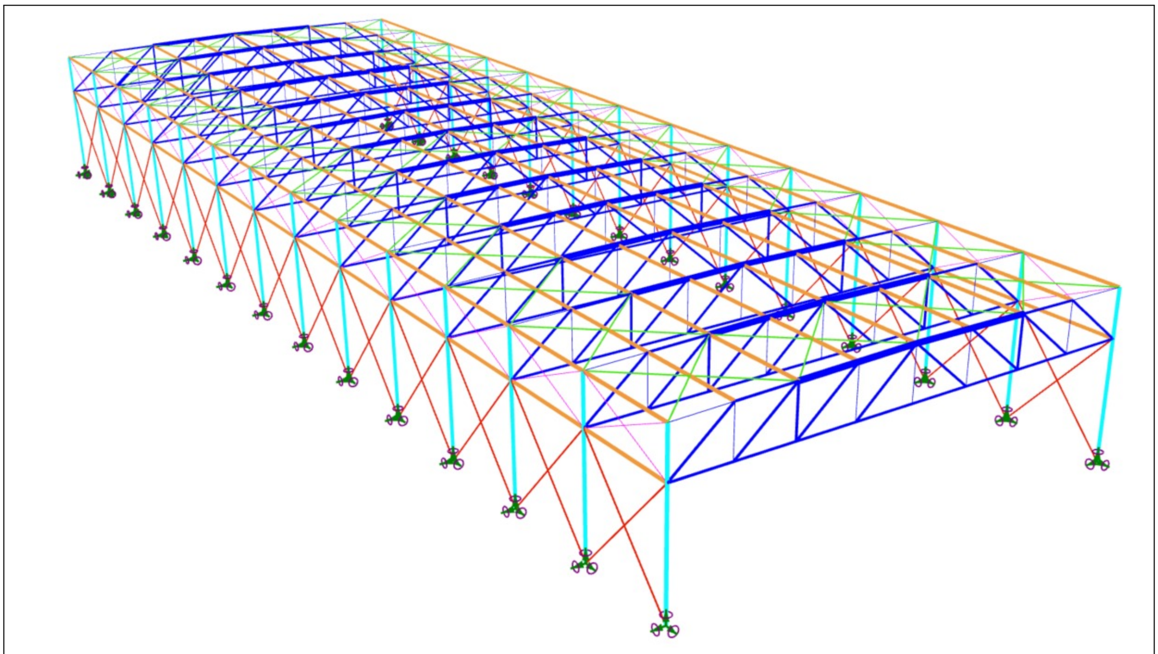

Figure 6.16: Configuration of the optimized Industrial building

| **Best OF** | **Weight [kN]** | $N_a$ | $n$ | $H_1$ | $H_2$ | $n_1$ | $n_2$ | $n_3$ | $N_m$ |
|---|---|---|---|---|---|---|---|---|---|
| 775.427 | 330.228065 | 3 | 4 | 2 | 2.17 | 1 | 1 | 2 | 7 |

Table 6.12: Best Individual of the optimized Industrial Building

The figure below 6.17 is showing the optimized truss and the groups subdivision of the different components:

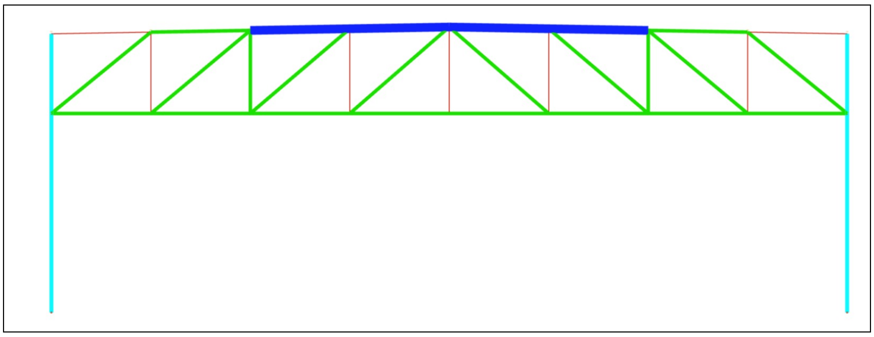

Figure 6.17: Configuration of the Howe truss in the optimized Industrial building

In the tables 6.13 and 6.14 the cross-sections assigned to all the structural members are reported:

| | **CHS 1°group** | **CHS 2°group** | **CHS 3°group** |
|---|---|---|---|
| **Lower Chord** | 88.9x2.5 | 88.9x2.5 | 88.9x2.5 |
| **Upper Chord** | 219.1x6 | 88.9x2.5 | 21.3x2 |
| **Int. Vert. Structs** | 21.3x2 | 88.9x2.5 | 21.3x2 |
| **Upward-Downward Diagonals** | 88.9x2.5 | 88.9x2.5 | 88.9x2.5 |

Table 6.13: Cross-sections of the optimized truss in the Industrial building

| **Structural Elements** | **Cross Section Type** |
|---|---|
| Columns | HEA 100 |
| Purlins | IPE 120 |
| Roof Bracings | Rope PV 300 |
| Vertical Bracings 1 | Rope PV 40 |
| Vertical Bracings 2 | Rope PV 360 |

Table 6.14: Cross-sections of the structural elements in the Industrial building

Now the charts about the main parameters of the best individual at each iteration have been reported.

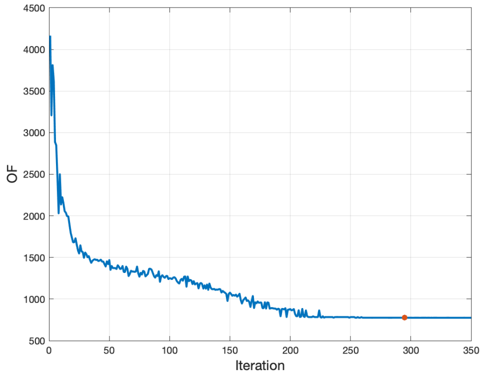


Figure 6.18: Best individual at each iteration

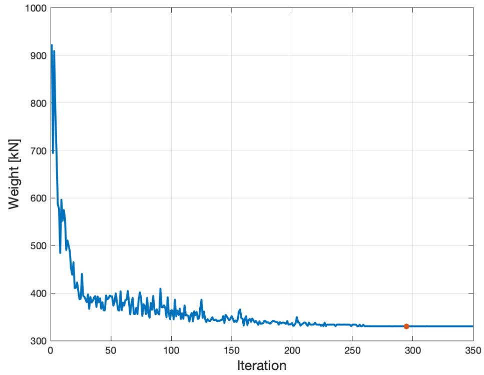


Figure 6.19: Weight of best individual at each iteration

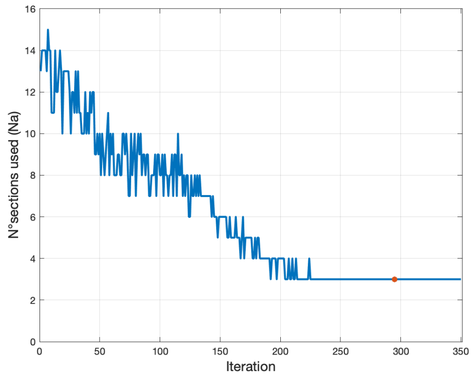


Figure 6.20: $N_a$ of best individual at each iteration

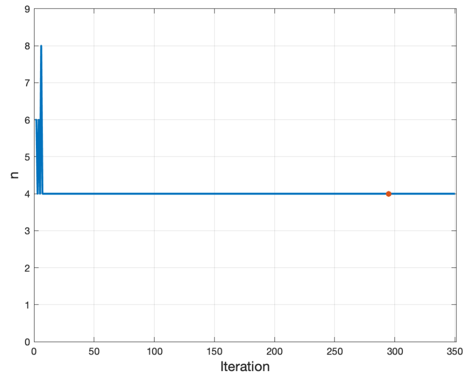


Figure 6.21: $n$ of best individual at each iteration

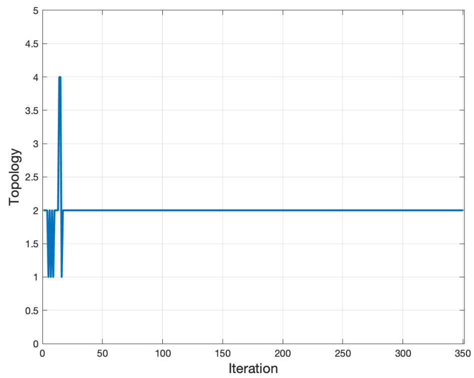


Figure 6.22: Topology of best individual at each iteration

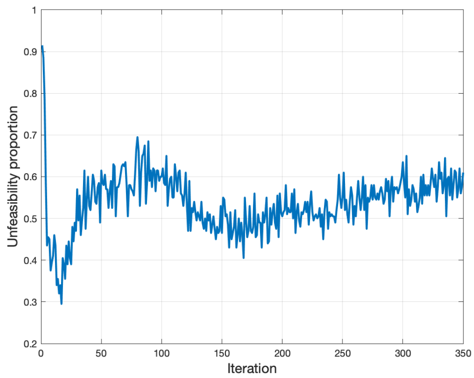


Figure 6.23: Unfeasability proportion

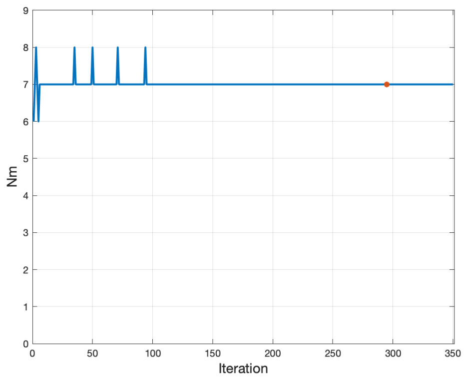


Figure 6.24: $N_m$ of best individual at each iteration

From chart of 6.20 and 6.21 we can appreciate how the penalty $\phi 2$ and $\phi 3$ are still working in the correct manner. Specifically, the complexity related to $N_a$ has been further reduced, in fact the final value of different cross-section used is 3. We can highlight the fact that with $\phi 2$ we are guiding the algorithm to refine the analysis and choose lower $N_a$ values, as visible in 6.20. Instead, for the topology 6.22 as well as for $N_m$ 6.24, with our objective function we have not leading the optimization toward a specific condition. In fact, the optimizer after few iterations begins to stagnate in the same solution. This is due to the fact that is free to choose any solution because no penalty is influencing the optimal final value.

Let's see in details the structural features of the optimized structure. In particular, in figure 6.25 it has been reported the axial force diagram of the all structure. It is clearly visible that the Axial Stress is pronounced for the trusses components and for columns. In particular, in the Howe truss, Lower Chord and Vertical elements work in tension, while the beams of the Upper Chord and Diagonal are compressed, as well as the columns of the industrial building. Instead, in figure 6.26 it is clearly visible the bending moment diagrams affecting the purlin elements.
In addition, in 6.27 the displacements of the different structural elements has been reported. We should highlight the fact that the analysis has been performed considering Ultimate Limit States, therefore no restriction on the vertical displacements has been imposed. In particular, the highest displacement affecting the central part of the structure is lower of 8 cm.

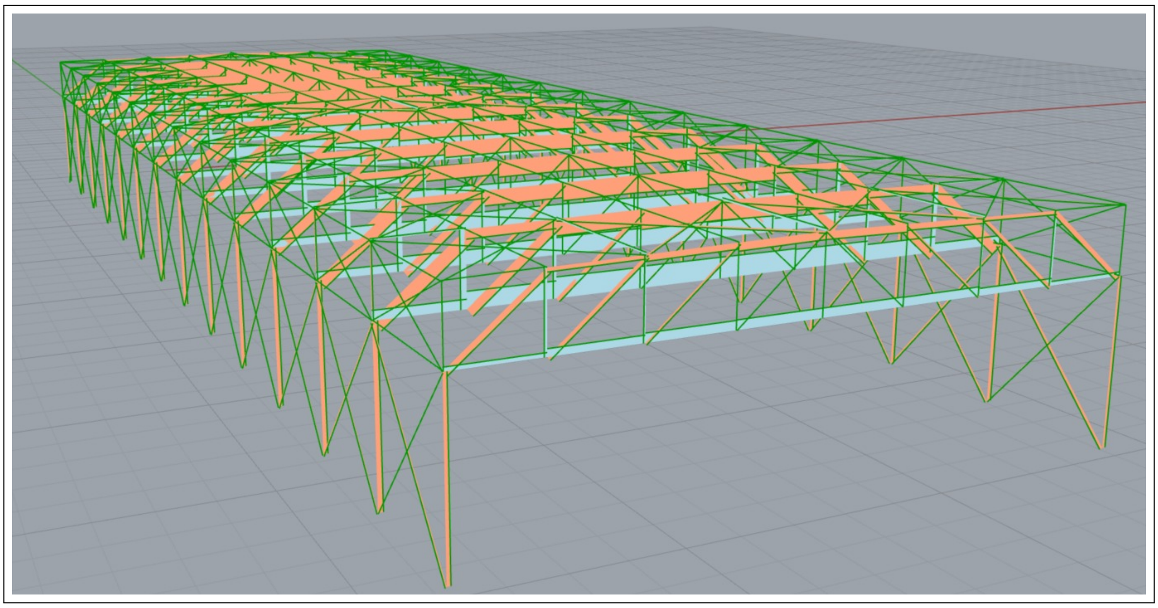

Figure 6.25: Axial force diagram. In orange the compressed elements, in blue the tension one

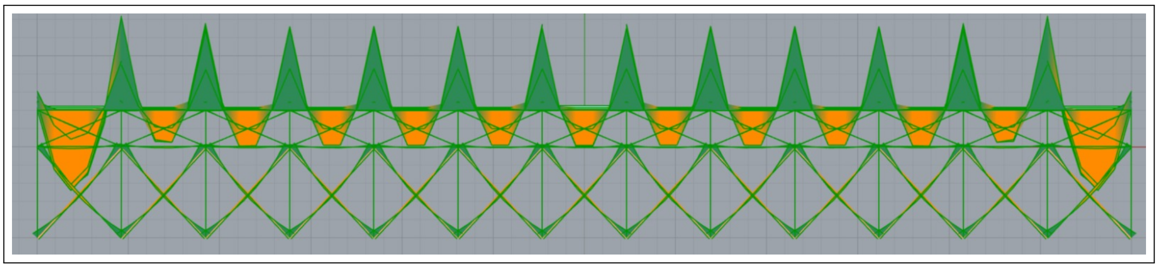

Figure 6.26: Bending moment diagram. In orange the negative values, in green the positive one

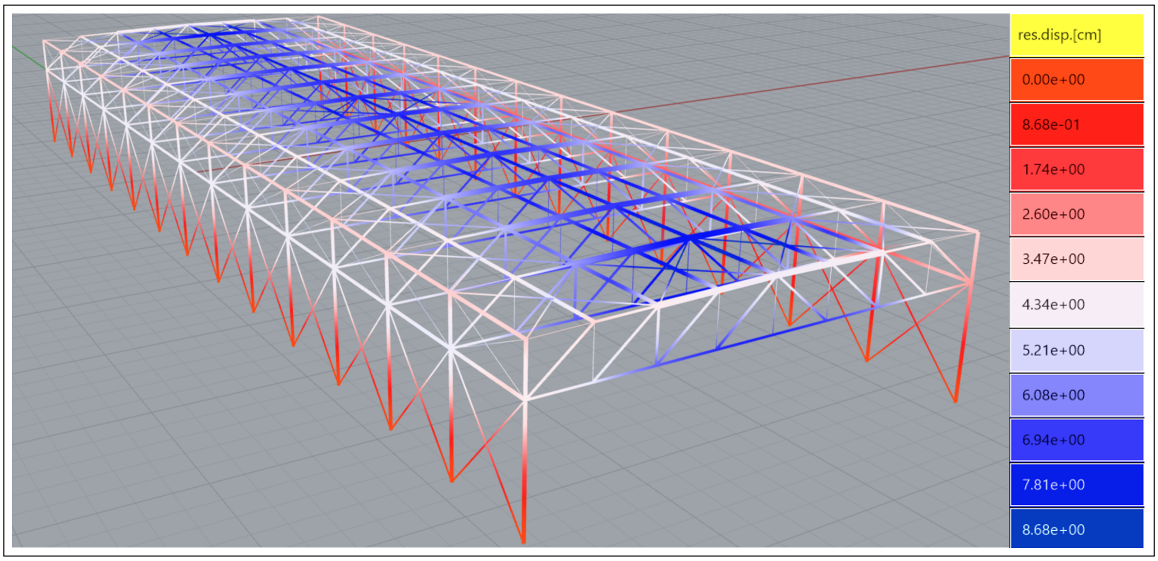


Figure 6.27: Displacements and related legend of the Industrial building

# Chapter 7

# Discussions and final considerations

In this Thesis we have seen the applicability of the proposed objective function for simpler and more challenging truss structures. It has been stresses the importance of constructability considerations together with a weight minimization, aimed at finding a simplified and standardized design. Ranging from a simple size optimization to a simultaneous size, shape and topology one, we have studied the single penalty functions introduced, how they work and how they can be calibrated according to the specific needs. Starting from the truss level analysis, we originally expected to obtain higher weights for lower design complexity, in fact a balance between these aspects has been found for the optimized structures. Moreover, for what regard the case in which the topology slider has been considered as design variable too, the Pratt configuration has been chosen. This was, once again, expected because, for gravitational loads only, in this type of truss the longer diagonal elements work in tension, thus avoiding further verifications for compressive states. On the contrary, in the Howe truss, for example, the diagonals are in compression thus it should be avoided. The most challenging task was to understand the calibration of the parameters employed in each single penalty. Specific trends have been identified and recommendations on possible changes have been provided.

Then, in the passage from the truss level to the one of the industrial building, the most important modifications have been highlighted. In particular, the additional design variables were mainly related to the cross-sections employed for the new structural elements and the one linked to the spacing of the different modules. For this

second case study, the objective function has been applied with a simple alteration regarding the buckling structural verification, which is now testing all the elements. Constructability considerations, instead, have not been enlarged to the global level, but remain at the truss one. This is evident, for example, in the variability of $N_m$ in the optimized structures, visible in table 5.8. In fact, the algorithm is not encouraged towards a reduction of $N_m$, which in turn could lead to a decrease in the overall number of pieces, connections and so on. Therefore, a possible enhancement of the reported study could be the generalization of the complexity, including the number of modules as a parameter in the OF, analogous to $n$ in the third penalty. In a similar way to $n$, in fact, low $N_m$ values imply heavier sections, thus from an economical point of view it is not straightforward if it would be advantageous or not. Furthermore, it would be extremely interesting the outcomes of this double simplification of the design, in order to be able to understand if the optimization would promote a more complex truss system with low $N_m$, thus lower number of modules, trusses and thus pieces, or vice versa. In other words, it would be more important the truss complexity or the global one? Moreover, a further global parameter of the complexity can be identified in the variation of the roof bracings as a function of the truss chord's nodes. In fact, as stated before, their configuration has been fixed, but the inclusion of their pattern variability in the objective function could enhance the dual design streamlining.
Another significant finding from the analyses is that the algorithm is not sufficiently guided in the topology identification. In fact, in our optimization, Octopus is free to assign any possible type of configuration, without a specific encouragement towards a specific one. Most of the time, it is able to retrieve the one that reduces the number of pieces, that in turn abate the OF value, however there could be a more stable trend. Therefore, we could consider introducing a gradual exploration in the algorithm. Specifically, it should be improved at the beginning in order to find the best one, and then reduced to lessen the computational effort.
Another future investigation could be the optimization of the cross-sections profiles, thus obtaining the best one for each specific component. In fact, we know that for the truss elements it could be convenient to employ I-shaped or H-shaped profiles, as well as UPN or L-shaped ones. In any case, the optimization of the profiles should be aimed at finding feasible connections between the components.
Furthermore, we suggest to expand the analysis considering other load combinations. The limit imposed by Karamba3D of a single load combination can be overcomed

in different ways. In Grasshopper environment there are plug-ins that allow to solve the structural analysis using external solutors, like SAP2000. In this way, multiple load combinations can be taken into account. The main drawback in such procedure would be the increase of the computational time, however it would result in a more comprehensive analysis.

# Bibliography


[1] Adeli, H., and Cheng, N.-T. Integrated genetic algorithm for optimization of space structures. *Journal of Aerospace Engineering 6*, 4 (1993), 315–328.

[2] Al-Salloum, Y., and Almusallam, T. Optimality and safety of rigidly- and flexibly-jointed steel frames. *Journal of Constructional Steel Research 35*, 2 (1995), 189–215.

[3] Albadr, M. A., Tiun, S., Ayob, M., and Al-Dhief, F. Genetic algorithm based on natural selection theory for optimization problems. *Symmetry 12*, 11 (2020), 1758.

[4] Anderson, S., Fisher, D., and Gupta, V. *Total Constructability Management: A Process-oriented Framework.* Project Management Institute, 1995.

[5] Apostolakis, G. Optimal evolutionary seismic design of three-dimensional multistory structures with damping devices. *Journal of Structural Engineering 146*, 10 (2020), 04020205.

[6] Arditi, D., Elhassan, A., and Toklu, Y. C. Constructability analysis in the design firm. *Journal of construction engineering and management 128*, 2 (2002), 117–126.

[7] Artar, M. Optimum design of braced steel frames via teaching learning based optimization. *Steel and Composite Structures 22*, 4 (2016), 733–744.

[8] Artar, M., and Daloglu, A. T. Optimum design of steel frames with semi-rigid connections and composite beams. *Structural engineering and mechanics: An international journal 55*, 2 (2015), 299–313.

[9] Artar, M., and Daloglu, A. T. Optimum design of steel space frames with composite beams using genetic algorithm. *Steel and Composite Structures 19*, 2 (2015), 503–519.

[10] Azad, S. K., Bybordiani, M., Azad, S. K., and Jawad, F. K. Simultaneous size and geometry optimization of steel trusses under dynamic excitations. *Structural and Multidisciplinary Optimization 58* (2018), 2545–2563.

[11] Baghdadi, A., Heristchian, M., and Kloft, H. Connections placement optimization approach toward new prefabricated building systems. *Engineering Structures 233* (2021), 111648.

[12] Bagherinejad, M. H., and Haghollahi, A. Topology optimization of steel plate shear walls in the moment frames. *Steel and Composite Structures 29*, 6 (2018), 767–779.

[13] Balling, R. J. Optimal steel frame design by simulated annealing. *Journal of structural Engineering 117*, 6 (1991), 1780–1795.

[14] Banihashemian, S. S., and Adibnia, F. A novel robust soft-computed range-free localization algorithm against malicious anchor nodes. *Cognitive Computation 13*, 4 (2021), 992–1007.

[15] Beghini, L. L., Beghini, A., Katz, N., Baker, W. F., and Paulino, G. H. Connecting architecture and engineering through structural topology optimization. *Engineering Structures 59* (2014), 716–726.

[16] Camp, C. V., and Farshchin, M. Design of space trusses using modified teaching–learning based optimization. *Engineering Structures 62* (2014), 87–97.

[17] CATTA, G. Sperimentazione su travi reticolari in scala ridotta: un ausilio alla didattica.

[18] Cheng, F. Y., and Juang, D. Recursive optimization for seismic steel frames. *Journal of Structural Engineering 115*, 2 (1989), 445–466.

[19] Cheng, J. Optimum design of steel truss arch bridges using a hybrid genetic algorithm. *Journal of Constructional Steel Research 66*, 8-9 (2010), 1011–1017.

[20] Choi, S.-H., and Kim, S.-E. Optimal design of steel frame using practical nonlinear inelastic analysis. *Engineering Structures 24*, 9 (2002), 1189–1201.

[21] Choi, S. W., Kim, Y., Lee, J., Hong, K., and Park, H. S. Minimum column-to-beam strength ratios for beam–hinge mechanisms based on multi-objective seismic design. *Journal of Constructional Steel Research 88* (2013), 53–62.

[22] Coello, C., and Christiansen, A. D. Multiobjective optimization of trusses using genetic algorithms. *Computers & Structures 75*, 6 (2000), 647–660.

[23] Csébfalvi, A. Optimal design of frame structures with semi-rigid joints. *Periodica Polytechnica Civil Engineering 51*, 1 (2007), 9–15.

[24] Daloglu, A. T., Artar, M., Özgan, K., and Karakas, A. İ. Optimum design of steel space frames including soil-structure interaction. *Structural and Multidisciplinary Optimization 54*, 1 (2016), 117–131.

[25] Dehghani, S., Vosoughi, A., and Banan, M. R. The effects of rehabilitation objectives on near optimal trade-off relation between minimum weight and maximum drift of 2d steel x-braced frames considering soil-structure interaction using a cluster-based nsga ii. *Structural and Multidisciplinary Optimization 59* (2019), 1703–1722.

[26] Dhingra, A. K., and Lee, B. A genetic algorithm approach to single and multiobjective structural optimization with discrete–continuous variables. *International Journal for Numerical Methods in Engineering 37*, 23 (1994), 4059–4080.

[27] Doğan, E., Şeker, S., and andCelalettin Kozanoğlu, M. P. S. Investigating the effect of joint behavior on the optimum design of steel frames via hunting search algorithm. *Advanced Steel Construction 14*, 2 (2018), 166–183.

[28] El Majdoubi, O., Abdoun, F., Rafalia, N., and Abdoun, O. Artificial intelligence approach for multi-objective design optimization of composite structures: parallel genetic immigration. *International Journal 9*, 3 (2020).

[29] Elvin, A., and Strydom, J. Optimizing the design of tall buildings using the principle of virtual work: The effect of semi rigid connections. *International Journal of Steel Structures 21* (2021), 1–21.

[30] Erbatur, F., and Al-Hussainy, M. Optimum design of frames. *Computers & structures 45*, 5-6 (1992), 887–891.

[31] Fathizadeh, S., Vosoughi, A., and Banan, M. R. Considering soil–structure interaction effects on performance-based design optimization of moment-resisting steel frames by an engineered cluster-based genetic algorithm. *Engineering Optimization 53*, 3 (2021), 440–460.

[32] Feng, T.-T., Arora, J., and Haug Jr, E. Optimal structural design under dynamic loads. *International Journal for Numerical Methods in Engineering 11*, 1 (1977), 39–52.

[33] Fu, J., Wu, J., Dong, C., Xu, A., and Pi, Y.-L. Optimization design of large span portal-rigid steel frame with tapered sections under wind-induced drift constraint. *Engineering Structures 194* (2019), 396–405.

[34] Gandomi, A. H., Talatahari, S., Yang, X.-S., and Deb, S. Design optimization of truss structures using cuckoo search algorithm. *The structural design of tall and special buildings 22*, 17 (2013), 1330–1349.

[35] Ghasemof, A., Mirtaheri, M., and Mohammadi, R. K. A new swift algorithm for bi-objective optimum design of steel moment frames. *Journal of Building Engineering 39* (2021), 102162.

[36] Gholizadeh, S., Davoudi, H., and Fattahi, F. Design of steel frames by an enhanced moth-flame optimization algorithm. *Steel Compos Struct 24*, 1 (2017), 129–140.

[37] Gholizadeh, S., and Fattahi, F. Optimum design of steel structures for earthquake loading by grey wolf algorithm.

[38] Gholizadeh, S., and Milani, A. Optimal performance-based design of steel frames using advanced metaheuristics.

[39] Gholizadeh, S., and Milany, A. An improved fireworks algorithm for discrete sizing optimization of steel skeletal structures. *Engineering Optimization 50*, 11 (2018), 1829–1849.

[40] Gholizadeh, S., and Moghadas, R. K. Performance-based optimum design of steel frames by an improved quantum particle swarm optimization. *Advances in Structural Engineering 17*, 2 (2014), 143–156.

[41] Gholizadeh, S., and Poorhoseini, H. Seismic layout optimization of steel braced frames by an improved dolphin echolocation algorithm. *Structural and Multidisciplinary Optimization 54* (2016), 1011–1029.

[42] Habibi, A., Saffari, H., and Izadpanah, M. Optimal lateral load pattern for pushover analysis of building structures. *Steel Compos Struct 32*, 1 (2019), 67–77.

[43] Hajirasouliha, I., and Moghaddam, H. New lateral force distribution for seismic design of structures. *Journal of Structural Engineering 135*, 8 (2009), 906–915.

[44] Hajirasouliha, I., Pilakoutas, K., and Moghaddam, H. Topology optimization for the seismic design of truss-like structures. *Computers & structures 89*, 7-8 (2011), 702–711.

[45] Haque, M. Optimal design of plane frames by the complex method. In *Advances and Trends in Structures and Dynamics*. Elsevier, 1985, pp. 451–456.

[46] Hasançebi, O., and Azad, S. K. Adaptive dimensional search: a new metaheuristic algorithm for discrete truss sizing optimization. *Computers & Structures 154* (2015), 1–16.

[47] Hasançebi, O., and Azad, S. K. Discrete sizing of steel frames using adaptive dimensional search algorithm. *Periodica Polytechnica Civil Engineering 63*, 4 (2019), 1062–1079.

[48] Hasançebi, O., and DOGANB, E. Evaluation of topological forms for weight effective optimum design of single-span steel truss bridges.

[49] Hassanzadeh, A., and Gholizadeh, S. Collapse-performance-aided design optimization of steel concentrically braced frames. *Engineering Structures 197* (2019), 109411.

[50] Hayalioglu, M., and Saka, M. Optimum design of geometrically nonlinear elastic-plastic steel frames with tapered members. *Computers & structures 44*, 4 (1992), 915–924.

[51] Horn, A. *Integrating constructability into conceptual structural design and optimization.* PhD thesis, Massachusetts Institute of Technology, 2015.

[52] Hsu, Y.-L. A review of structural shape optimization. *Computers in Industry 25*, 1 (1994), 3–13.

[53] Jakiela, M. J., Chapman, C., Duda, J., Adewuya, A., and Saitou, K. Continuum structural topology design with genetic algorithms. *Computer Methods in Applied Mechanics and Engineering 186*, 2-4 (2000), 339–356.

[54] Kapoor, M., and Rao, J. Optimum aseismic design of multistorey steel frames. *Engineering optimization 11*, 3-4 (1987), 339–353.

[55] Karimi, F., and Vaez, S. R. H. Two-stage optimal seismic design of steel moment frames using the lrfd-pbd method. *Journal of Constructional Steel Research 155* (2019), 77–89.

[56] Kaveh, A., and Abbasgholiha, H. Optimum design of steel sway frames using big bangbig crunch algorithm.

[57] Kaveh, A., and Farhadmanesh, M. Optimal seismic design of steel plate shear walls using metaheuristic algorithms. *Periodica Polytechnica Civil Engineering 63*, 1 (2019), 1–17.

[58] Kaveh, A., and Farhoudi, N. Layout optimization of braced frames using differential evolution algorithm and dolphin echolocation optimization. *Periodica Polytechnica Civil Engineering 59*, 3 (2015), 441–449.

[59] Kaveh, A., and Farhoudi, N. Dolphin monitoring for enhancing metaheuristic algorithms: Layout optimization of braced frames. *Computers & Structures 165* (2016), 1–9.

[60] Kaveh, A., and Ghazaan, M. I. A comparative study of cbo and ecbo for optimal design of skeletal structures. *Computers & Structures 153* (2015), 137–147.

[61] Kaveh, A., Hamedani, K. B., Hosseini, S. M., and Bakhshpoori, T. Optimal design of planar steel frame structures utilizing meta-heuristic optimization algorithms. In *Structures* (2020), vol. 25, Elsevier, pp. 335–346.

[62] Kaveh, A., Kabir, M. Z., and Bohlool, M. Optimal design of multi-span pitched roof frames with tapered members. *Periodica Polytechnica Civil Engineering 63*, 1 (2019), 77–86.

[63] Kaveh, A., and Mahdavi, V. Colliding bodies optimization for size and topology optimization of truss structures. *Structural Engineering and Mechanics 53*, 5 (2015), 847–865.

[64] Kaveh, A., Mahdipour Moghanni, R., and Javadi, S. Chaotic optimization algorithm for performance-based optimization design of composite moment frames. *Engineering with Computers* (2021), 1–13.

[65] Kaveh, A., Shojaei, I., Gholipour, Y., and Rahami, H. Seismic design of steel frames using multi-objective optimization. *Struct. Eng. Mech 45*, 2 (2013), 211–232.

[66] Khan, S. *Constructability: A Tool for Project Management.* CRC Press, 2018.

[67] Korkmaz, K., and El-Gafy, M. Structural optimization assessment for steel structures. *J Steel Struct Constr 4*, 147 (2018), 2472–0437.

[68] Lagaros, N. D., Psarras, L. D., Papadrakakis, M., and Panagiotou, G. Optimum design of steel structures with web openings. *Engineering structures 30*, 9 (2008), 2528–2537.

[69] Liu, Q., and Paavola, J. An optimization procedure for seismic design of steel frames for multi-performance and multi-hazard levels. *Advances in Structural Engineering 18*, 1 (2015), 59–74.

[70] Lv, Y., Li, Z.-X., Xu, L.-H., and Ding, Y. Equivalent seismic performance optimization of steel structures based on nonlinear damage analysis. *Advances in Structural Engineering 18*, 7 (2015), 941–958.

[71] Machaly, E. Optimum weight analysis of steel frames with semirigid connections. *Computers & structures 23*, 4 (1986), 461–474.

[72] Machaly, E. Optimum weight analysis of steel grid bridges. *Computers & structures 23*, 5 (1986), 575–586.

[73] Mansouri, S. F., and Maheri, M. R. Performance-based seismic design of steel frames using constraint control method. *Advances in Structural Engineering 22*, 12 (2019), 2648–2661.

[74] McKinstray, R., Lim, J. B., Tanyimboh, T. T., Phan, D. T., and Sha, W. Optimal design of long-span steel portal frames using fabricated beams. *Journal of Constructional Steel Research 104* (2015), 104–114.

[75] Mei, L., and Wang, Q. Structural optimization in civil engineering: a literature review. *Buildings 11*, 2 (2021), 66.

[76] Memari, A., and Madhkhan, M. Optimal design of steel frames subject to gravity and seismic codes' prescribed lateral forces. *Structural optimization 18*, 1 (1999), 56–66.

[77] Moghaddam, H., and Hajirasouliha, I. Toward more rational criteria for determination of design earthquake forces. *International Journal of Solids and Structures 43*, 9 (2006), 2631–2645.

[78] Moghaddam, H., and Hajirasouliha, I. Optimum strength distribution for seismic design of tall buildings. *The Structural Design of Tall and Special Buildings 17*, 2 (2008), 331–349.

[79] Moghaddam, H., Hajirasouliha, I., and Doostan, A. Optimum seismic design of concentrically braced steel frames: concepts and design procedures. *Journal of Constructional Steel Research 61*, 2 (2005), 151–166.

[80] Moghaddam, H., Hajirasouliha, I., and Gelekolai, S. M. H. Performance-based seismic design of moment resisting steel frames: Adaptive optimisation framework and optimum design load pattern. In *Structures* (2021), vol. 33, Elsevier, pp. 1690–1704.

[81] Mohammadi, R. K., and Sharghi, A. H. On the optimum performance-based design of eccentrically braced frames. *Steel Compos. Struct 16*, 4 (2014), 357–374.

[82] Mojtabaei, S. M., Hajirasouliha, I., and Ye, J. Optimisation of cold-formed steel beams for best seismic performance in bolted moment connections. *Journal of Constructional Steel Research 181* (2021), 106621.

[83] Moradi, S., and Alam, M. S. Multi-criteria optimization of lateral load-drift response of posttensioned steel beam-column connections. *Engineering structures 130* (2017), 180–197.

[84] O'Connor, J. T., Rusch, S. E., and Schulz, M. J. Constructability concepts for engineering and procurement. *Journal of Construction Engineering and Management 113*, 2 (1987), 235–248.

[85] Ohsaki, M., Iwatsuki, O., and Watanabe, H. Seismic response of building frames with flexible base optimized for reverse rocking response. *Engineering structures 74* (2014), 170–179.

[86] Oskouei, A. V., Fard, S. S., and Aksogan, O. Using genetic algorithm for the optimization of seismic behavior of steel planar frames with semi-rigid connections. *Structural and multidisciplinary optimization 45* (2012), 287–302.

[87] Palizzolo, L., Benfratello, S., and Tabbuso, P. Discrete variable design of frames subjected to seismic actions accounting for element slenderness. *Computers & Structures 147* (2015), 147–158.

[88] Pan, J., and Wang, D.-y. Topology optimization of truss structure with fundamental frequency and frequency domain dynamic response constraints. *Acta Mechanica Solida Sinica 19* (2006), 231–240.

[89] Pasquire, C., and Gibb, A. Considerations for assessing the benefits of standardisation and pre-assembly in construction (the findings of a pilot study). In *report to CIBSE Seminar on Standardisation in the Design and Construction of Building Services Installations* (1999), vol. 26.

[90] Paulson Jr, B. Designing to reduce construction costs. *Journal of the Construction Division 102*, C04 (1976).

[91] Phan, D. T., Lim, J. B., Tanyimboh, T. T., and Sha, W. An efficient genetic algorithm for the design optimization of cold-formed steel portal frame buildings.

[92] Phan, D. T., Mojtabaei, S. M., Hajirasouliha, I., Ye, J., and Lim, J. B. Coupled element and structural level optimisation framework for cold-formed steel frames. *Journal of Constructional Steel Research 168* (2020), 105867.

[93] Pulaski, M. H., and Horman, M. J. Organizing constructability knowledge for design. *Journal of construction engineering and management 131*, 8 (2005), 911–919.

[94] Qiao, S., Han, X., Zhou, K., and Ji, J. Seismic analysis of steel structure with brace configuration using topology optimization. *Steel and Composite Structures 21*, 3 (2016), 501–515.

[95] Reitman, M. I., and BRENT HALL, W. Optimal structural standardization. *Engineering Optimization+ A35 16*, 2 (1990), 109–128.

[96] Rozvany, G. I. A critical review of established methods of structural topology optimization. *Structural and multidisciplinary optimization 37* (2009), 217–237.

[97] RUBY, D. I. *Constructability of structural steel buildings*. American Institute of Steel Construction, 2008.

[98] RUSSELL, J. S., SWIGGUM, K. E., SHAPIRO, J. M., AND ALAYDRUS, A. F. Constructability related to tqm, value engineering, and cost/benefits. *Journal of performance of constructed facilities 8*, 1 (1994), 31–45.

[99] SAFARI, D., AND MAHERI, M. R. Genetic algorithm search for optimal brace positions in steel frames. *J Adv Conc Des 2*, 4 (2006), 400–415.

[100] SAKA, M. Optimum design of steel frames with stability constraints. *Computers & structures 41*, 6 (1991), 1365–1377.

[101] SAKA, M. Optimum design of pitched roof steel frames with haunched rafters by genetic algorithm. *Computers & structures 81*, 18-19 (2003), 1967–1978.

[102] SAKA, M., AND HAYALIOGLU, M. Optimum design of geometrically nonlinear elastic-plastic steel frames. *Computers & structures 38*, 3 (1991), 329–344.

[103] SCHOLZ, H., AND FALLER, G. A micro-computer program for the elastic-plastic analysis and optimum design of plane frames. *Computers & structures 24*, 6 (1986), 941–947.

[104] SENARATNA, N. I. Genetic algorithms: The crossover-mutation debate. *Degree of Bachelor of Computer Science of the University of Colombo* (2005).

[105] SOTIROPOULOS, S., AND LAGAROS, N. D. Optimum topological bracing design of tall steel frames subjected to dynamic loading. *Computers & Structures 259* (2022), 106705.

[106] STROMBERG, L. L., BEGHINI, A., BAKER, W. F., AND PAULINO, G. H. Topology optimization for braced frames: combining continuum and beam/-column elements. *Engineering Structures 37* (2012), 106–124.

[107] TAJS-ZIELIŃSKA, K., AND BOCHENEK, B. Topology optimization-engineering contribution to architectural design. In *IOP Conference Series: Materials Science and Engineering* (2017), vol. 245, IOP Publishing, p. 082057.

[108] TALATAHARI, S., GANDOMI, A. H., YANG, X.-S., AND DEB, S. Optimum design of frame structures using the eagle strategy with differential evolution. *Engineering Structures 91* (2015), 16–25.

[109] TANGARAMVONG, S., AND TIN-LOI, F. Optimal performance-based rehabilitation of steel frames using braces. *Journal of Structural Engineering 141*, 10 (2015), 04015015.

[110] TANTELY, J. S., AND HE, Z. Collapse safety margin-based design optimization of steel structures with concentrically braced frames. *Adv. Steel Constr. 15*, 2 (2019), 137–144.

[111] Thevendran, V., Gupta, N. D., and Tan, G. Minimum weight design of multi-bay multi-storey steel frames. *Computers & structures 43*, 3 (1992), 495–503.

[112] Wang, F., and Chan, S. L. Optimization and sensitivity analysis of space frames allowing for large deflection. *Engineering structures 28*, 10 (2006), 1395–1406.

[113] Wong, F. W., Lam, P. T., Chan, E. H., and Wong, F. K. Factors affecting buildability of building designs. *Canadian Journal of Civil Engineering 33*, 7 (2006), 795–806.

[114] Xu, L.-H., Xiao, S.-J., Wu, Y.-W., and Li, Z.-X. Seismic failure mode identification and multi-objective optimization for steel frame structure. *Advances in Structural Engineering 21*, 13 (2018), 2005–2017.

[115] Zhu, M. *Topology optimization of frame structures: Design For constructability and stochastic dynamic loads.* PhD thesis, Johns Hopkins University, 2015.